DESIGN AND DEVELOPMENT OF DNA BIOSENSORS BASED ON SILVER NANOCLUSTERS AND HYBRIDISATION CHAIN REACTION

WONG ZHENG WEI

Thesis submitted to the University of Nottingham
for the degree of Doctor of Philosophy

2022

Abstract

Biosensors that couple hybridisation chain reaction amplification and fluorogenic silver nanoclusters (HCR-AgNCs) have the potential to enable simple and cost-effective detection of target analytes. These biosensors feature non-enzymatic amplification at mild conditions with a strong label-free fluorescence response. Whilst the proof-of-concept of these sensors have been promising, the design and developmental stages of HCR-AgNCs biosensors remain a challenge due to the lack of studies within the field itself.

The primary aim of this thesis was to design and develop new HCR-AgNCs biosensors for specific detection of short nucleic acid sequences (*i.e.,* DNA and microRNA (miR)). To achieve this, three novel HCR-AgNCs biosensors were developed by designing DNA probes with assistance of computational software, then validated *via* lab-based experiments such as feasibility tests, condition optimisation, as well as performance analysis in both buffer and complex samples.

A ratiometric fluorescence HCR-AgNCs biosensor was first developed for miR detection, where emission of AgNCs changed from red to yellow in the absence and presence of miR-155. The ratiometric analysis has reduced the possibility of false measurement and increased the sensitivity of the assay, with limit of detection (LOD) measured at 1.18 fM. In the next study, a HCR biosensor was integrated with an externalised AgNCs probes *via* an 'end-to-end cluster transfer' mechanism, for DNA detection. This strategy simplified the designing process of DNA hairpins, ensured HCR predictability, and formed specific AgNCs species. In addition, the HCR-AgNCs biosensor exhibited high sensitivity towards the DNA target, with qualitative LOD at 1 pM and quantitative LOD at 3.35 fM. In the final study, magnetic-assistance was integrated into a ratiometric fluorescence HCR-AgNCs biosensor for the detection of miR-144-3p. The addition of magnetic beads (MBs) into the HCR-AgNCs biosensor facilitated a quick extraction and direct analysis of miR-144-3p, with LOD measured at 4.88 fM and satisfactory detection in raw human serum sample.

The overall findings from these works conclude that by carefully designing the DNA probes used to construct HCR-AgNCs, one can develop a functional and stable HCR-AgNCs biosensor without overcomplicating the detection process. Besides that, the concept of proximity-dependent AgNCs, introduced in each of the proposed biosensors, addressed

some of the practical limitations posed by conventional HCR-AgNCs biosensors. Moreover, the implementation of different sensing mechanism and modifications (*i.e.*, externalisation of AgNCs and MBs addition) in these studies highlight the versatility of HCR-AgNCs assays for different applications.

Ultimately, the design and development efforts of HCR-AgNCs biosensors in this work can inspire further insights and research into this class of biosensors and facilitate extensive biosensing applications in the field of clinical diagnostics and beyond.

Acknowledgements

First and foremost, I would like to extend my sincerest thanks to my supervisor, Dr. New Siu Yee. Throughout my PhD, she has always exuded remarkable knowledge, enthusiasm, and professionalism, that I have found inspiring. This thesis would not have been completed without the freedom that she has given me, while at the same time always being available for discussion and guidance. Likewise, I am grateful for her scientific intuition, time, and support, especially during my write-up (*i.e.,* publications and this thesis), applications (*i.e.,* grant and award), and conference presentations (*i.e.,* material preparation and mock rounds).

I am grateful for the encouragement and support that I have received from diverse individuals over the past few years: (i) my co-supervisors Dr. Valerie Shang, Dr. Lee Mei Kee and Dr. Ng Jeck Fei; (ii) Dr. Aliana for her support and facilitating the process of obtaining some research materials; (iii) Dr. Wang Zhiyi and Dr. Chia Chin Hua for their advice and suggestions on magnetic work; (iv) Prof. Hou Yanglong for hosting my research attachment at Peking University; (v) Dr. David Zhang for his guidance on kinetic studies with NABLAB software; (vi) Dr. Lee Shi Ting for her mentorship and pep talks that got me into the right mindset at the early stage of my PhD; and (vii) Sue Siao Yi who taught me the ways to easily 'access' all the essential software that I am using now. I would also like to thank the lab technicians, administration, and colleagues at University of Nottingham Malaysia (UNM). I acknowledge the analytical teams at MIMOS and Monash University for putting up with my last-minute scheduling and giving me the opportunities to run trials for my samples.

In addition, I would like to acknowledge the different funding bodies that made the work in this thesis possible: (i) Fundamental Research Grant Scheme (FRGS) and the Taylor's Research Grant for financially supporting the research work described in this thesis; (ii) UNM's Faculty of Science and Engineering for the scholarship to pursue my doctorate degree; and (iii) UNM's Graduate School for the International Research Collaboration Award with a 2-month research attachment at Peking University.

The COVID-19 pandemic significantly affected my research progress since 2020. Although the multiple nationwide lockdowns have hindered my experimental work and disrupted my research plans, the pandemic has given me the much-needed motivation to complete my research work. During this period, I was able to grow professionally (*i.e.,*

networking at online events), improve my skills (*i.e.*, online courses and workshops) and increase the impact of my research (*i.e.*, virtual conferences, symposiums, and forums). That said (ironically), I acknowledge the pandemic as being a critical motivator for me to complete my research work and this thesis, by any means necessary.

Finally, I am thankful for the backbone of support that I have received from my family and friends. I would like to express my utmost gratitude to my parents for their never-ending patience, support and understanding over the past few years. Last but not least, this journey would not have been possible without the encouragement and love from my partner. She was the one who convinced me to pursue a doctorate degree and has supported me thenceforth without doubt. Having said that, I will be eternally grateful for all that we have gone through together during this journey.

Once again, I would like to thank everybody who has made the past four years more than just a thesis; a life-changing experience.

List of Abbreviations

ΔG	free energy
λ_{EX}	excitation wavelength
λ_{EM}	emission wavelength
1^o	primary
2^o	secondary
A	adenine
AFM	atomic force microscopy
Ag^+	silver ions
AgNCs	silver nanoclusters
AGR2	anterior gradient protein 2 homolog
ATP	adenosine triphosphate
bp	base-pair
C	cytosine
^oC	degree Celsius
C1	capture 1
C2	capture 2
C3	capture 3
CuNCs	copper nanoclusters
DNA	deoxyribonucleic acid
dsDNA	double stranded DNA
F_r	red fluorescence intensity
F_y	yellow fluorescence intensity
F_y/F_r	ratiometric measurement of yellow to red fluorescence intensity
G	guanine
GO	graphene oxide
h	hour
H1	hairpin 1
H2	hairpin 2
H3	hairpin 3
HCR	hybridisation chain reaction
Hg^{2+}	mercury ions

IFN	interferon
LOD	limit-of-detection
MB	magnetic bead
MFE	minimum free energy
min	minutes
miR	microRNA
MNPs	magnetic nanoparticles
mRNA	messenger RNA
N	nitrogen
$NaBH_4$	sodium borohydride
NCB	nanocluster beacon
NPC	nasopharyngeal cancer
P1	probe 1
P2	probe 2
PDGF-BB	platelet-derived growth factor BB
PNA	peptide nucleic acid
POCT	point-of-care testing
polyC	polycytosine
QD	quantum dot
RNA	ribonucleic acid
RSD	relative standard deviation
RT-qPCR	reverse transcription quantitative real-time polymerase chain reaction
s	seconds
SELEX	Systematic Evolution of Ligands by Exponential Enrichment
ssDNA	single stranded DNA
T	thymine
T_m	melting temperature
TEM	transmission electron microscopy
XPS	X-ray photoelectron spectroscopy

List of Figures

Figure 2.1 (A) DNA hairpin structure, with toehold, stem and loop. **(B)** Mechanism of HCR amplification between target, DNA hairpin 1 (H1) and 2 (H2), to form HCR product. 11

Figure 2.2 (A) DNA hairpin structure with two toeholds; primary (1^o) and secondary (2^o). **(B)** HCR product with hanging 'tails' after HCR amplification between target, H1 and H2. 15

Figure 2.3 (A) Direct detection. Initiator I hybridises directly and opens hairpin 1 (H1), which subsequently hybridises and opens hairpin 2 (H2) to form the complex I·H1·H2. This complex undergoes a series of hybridisation events between H1 and H2 to form nicked dsDNA. Adapted from [6]. Copyright (2004) The National Academy of Sciences. **(B)** Indirect label-free detection. An aptamer sequence for Hg^{2+} was integrated into a hairpin structure (H0), which also served as HCR initiator for DNA hairpins, H1 and H2. Adapted from [82], Copyright (2015), with permission from Elsevier. **(C)** Indirect label-based detection. The immunoassay utilised an antibody label for cytokine detection, with covalent-bonded HCR initiator for HCR amplification. Adapted from [85]. Copyright 2011 American Chemical Society.....20

Figure 2.4 Application of DNA-AgNCs. **(A)** Homo-polyC sequence for the detection of p53 gene mutation based on fluorescence quenching. Reprinted by permission from Springer Nature Customer Service Centre GmbH: Springer, Journal of Fluorescence, from [127], 2017. **(B)** Chemopalette sequence for the multiplexed analysis of target DNA based on fluorescence emission colour change. Republished with permission of John Wiley and Sons, from [130]; permission conveyed through Copyright Clearance Center, Inc. **(C)** DNA hairpin loop-bound AgNCs for the detection of Hg^{2+} based on switch-off mechanism upon Hg^{2+} interaction. Adapted from [131]. **(D)** NCBs reported a 500-fold fluorescence enhancement when a G-rich enhancer probe hybridises with a dark AgNCs nucleation (NC) probe. Reprinted with permission from [138]. Copyright 2010 American Chemical Society. 27

Figure 2.5 Reported HCR-AgNCs biosensors with differentially located AgNCs sites. **(A)** The detection of HIV DNA was performed via HCR-AgNCs with homo-polyC 2^o toeholds and GO. Reprinted from [13], Copyright 2017, with permission from Elsevier. **(B)** Fluorescence from AgNCs templating loops is quenched by HCR amplification in the presence of target miR-145. Reprinted by permission from Springer Nature: Springer, Journal of Fluorescence, [165], 2017. **(C)** The AgNCs templating sequence partially embedded in DNA hairpin stems, will open for AgNCs formation after HCR amplification in the presence of target miR-21. Adapted from [166]. **(D)** Four-hairpin HCR-AgNCs system to initiate proximity-dependent G-rich enhancement after HCR amplification in the presence of target mRNA. Republished with permission of Royal Society of Chemistry, from [169]; permission conveyed through Copyright Clearance Center, Inc.....33

Figure 3.1 (A) Agarose gel analysis of HCR products. **(B)** Emission spectra of AgNCs in the presence (solid) and absence (dashed) of miR-155, with images of real samples shown as inset. TEM images of **(C)** HCR-positive, and **(D)** HCR-negative samples. 57
Figure 3.2 Optimisation of experimental conditions. **(A)** HCR incubation temperature and duration. **(B)** Screenshot of prediction profiler in JMP used to find the optimised HCR incubation conditions. The prediction profiler utilises a desirability function, where the values from 0 to 1 indicates the scale of desirable response [237], i.e., F_y/F_r in this study. **(C)** Molar ratio of H1: Ag^+: $NaBH_4$. Normalised F_y/F_r represents the ratiometric measurement of HCR-positive to HCR-negative F_y/F_r. Data presented as mean ± SEM, and statistically analyzed relative to 1:14:14. *, $p<0.05$; ***, $p<0.001$; ****, $p<0.0001$. 59
Figure 3.3 (A) Sensitivity profile of the HCR-AgNCs biosensor with two detection ranges displayed (n = 4). First detection range between 10 nM and 1 µM. Second detection range (semi-log plot inset) between 100 fM and 10 nM **(B)** Selectivity test of the HCR-AgNCs biosensor against miR-155 (n = 4). Data presented as mean ± SEM. ****, $p<0.0001$; ns, non-significant. 61
Figure 3.4 Sensitivity profile of the HCR-AgNCs biosensor in diluted human serum sample (n = 4). First detection range between 10 nM and 1 µM. Second detection range (inset) between 100 fM and 10 nM. 63
Figure 4.1 (A) Agarose gel image of samples after HCR. **(B)** Excitation (dashed) and emission (solid) spectra of P2-AgNCs (black) and P1-P2-AgNCs (red). **(C)** Fluorescence profile of samples with and without DNA-214, with their real images shown as inset. Data presented as mean ± SEM. ****, $p<0.0001$. **(D)** TEM image of P1-P2-AgNI **(E)** XPS spectrum of P1-P2-AgNCs. 77
Figure 4.2 (A) Surface contour plot of fluorescence intensity as a function of P2-AgNCs molar ratio and P1-P2-AgNCs incubation period. **(B)** Screenshot of JMP prediction profiler used to find the optimised AgNCs preparation conditions. **(C)** Surface contour plot of fluorescence intensity as a function of HCR incubation temperature and duration. **(D)** Screenshot of JMP prediction profiler used to find the optimised HCR incubation conditions. The prediction profilers utilise a desirability function, where the values from 0 to 1 indicates the scale of desirable response [237]. 78
Figure 4.3 (A) Fluorescence emission spectra and sample images (inset) at different concentrations of DNA-214 (from bottom to top: 0 M, 100 fM, 1 pM, 10 pM, 100 pM, 1 nM, 10 nM, 100 nM, 200 nM, 400 nM, 600 nM, 800 nM, 1000 nM). **(B)** Calibration plot of fluorescence emission intensity at different concentrations of DNA-214 (n = 4). First detection range between 100 nM and 1 µM. Second detection range (inset) between 100 fM and 100 nM. 80
Figure 4.4 Selectivity test of HCR-AgNCs biosensor against DNA-214 and its different controls (n = 4). The real sample images are shown as inset. Data presented as mean ± SEM. ****, $p < 0.0001$; ns, non-significant. 82
Figure 5.1 Feasibility of MB-HCR-AgNCs biosensor. **(A)** Gel image to study the feasibility of HCR design. **(B)** Gel image to compare HCR performance with (Lanes 1 and 3) and without magnetic

separation (Lanes 2 and 4). **(C)** Fluorescence emission spectra of AgNCs with (solid) and without (dashed) miR-144-3p. **(D)** Comparison of relative intensity of AgNCs with (blue) and without (red) magnetic separation, in the presence and absence of miR-144-3p. Data presented as mean ± SEM and statistically analyzed relative to miR-144-3p groups. ****, p < 0.0001.**(E)** TEM and **(F)** XPS spectrum of HCR-AgNCs. 99

Figure 5.2 (A) Loading capacity of biotinylated-C1-MBs (n=3). Data presented as mean ± SEM and statistically analyzed relative to 1.0 nmol. ***, p<0.001; ****, p<0.0001. **(B)** Optimisation of miR-144-3p capture time with C1-MBs (n=3). **(C)** Optimisation of HCR incubation duration (h) and temperature (ºC) (n=5). **(D)** Capture efficiency of C1-MBs after beads regeneration (n=3). Data presented as mean ± SEM. ***, p<0.001; ****, p<0.0001. 100

Figure 5.3 (A) Sensitivity profile of MB-HCR-AgNCs, ranged between 100 and 1000 nM, and between 10 fM and 100 nM (inset) (n=5). First detection range between 100 nM and 1 µM. Second detection range (inset) between 10 fM and 100 nM. **(B)** Selectivity study of MB-HCR-AgNCs (n=5). Data presented as mean ± SEM. ****, p < 0.0001; ns, non-significant. 102

Figure 5.4 Performance of MB-HCR-AgNCs biosensor in different concentration of human serum samples (n=5). Data presented as mean ± SEM. ns, non-significant. 103

List of Schemes

Scheme 2.1 A schematic diagram showing the basic DNA-based biosensor assembly with DNA as the bioreceptor for different target analytes, coupled with a transducer to generate a measurable signal. 6

Scheme 2.2 Illustration of DNA-AgNCs synthesis. Ag^+ preferentially binds to C bases on DNA templating sequences. Reducing agents, such as $NaBH_4$, reduce these DNA-Ag^+ leading to the formation of DNA-AgNCs. 23

Scheme 2.3 Schematic diagram showing the basic HCR-AgNCs biosensor assembly. DNA hairpins serve as bioreceptor to recognise different target analytes (DNA, RNA, protein, ions, etc.), and for HCR signal amplification. AgNCs will be prepared thereafter for signal (i.e., fluorescence or electrochemical) transduction and measurement. 28

Scheme 3.1 Outline of ratiometric HCR-AgNCs biosensor for the detection of miR-155. 48

Scheme 3.2 HCR-AgNCs biosensor. Formation of AgNCs **(A)** without miR-155, and **(B)** with miR-155. 53

Scheme 4.1 Outline of HCR-AgNCs biosensor with externalised AgNCs probes for the detection of DNA-214. 68

Scheme 4.2 (A) Red fluorescence activation upon hybridisation of P1 and P2-AgNCs, via end-to-end cluster transfer. **(B)** HCR-AgNCs biosensor without DNA-214. **(C)** HCR-AgNCs biosensor with DNA-214. 73

Scheme 5.1 Outline of MB-HCR-AgNCs for the detection of miR-144-3p. 87

Scheme 5.2 Principle of MB-HCR-AgNCs biosensor, involving **(A)** magnetic separation, **(B)** HCR amplification and detection with AgNCs. 94

List of Tables

Table 2.1 Examples of serum miRs dysregulated in cancer. 8
Table 2.2 Guidelines to design metastable DNA hairpins for HCR systems. 16
Table 2.3 Reported HCR-AgNCs biosensors. 35
Table 3.1 Oligonucleotide sequences used in this work. Red letters indicate AgNCs templating sequence. Italicised letters indicate hairpin stem region. Bold letters indicate hairpin loop. Underlined letters indicate mismatch base(s). 49
Table 3.2 Comparison of the proposed HCR-AgNCs biosensor with other reported miR-155 biosensors. 62
Table 4.1 Oligonucleotide sequences used in this work. Red letters indicate the C-rich AgNCs templating sequence. Blue letters indicate the dark AgNCs templating sequence. Italicised letters indicate hairpin stem region. Bold letters indicate hairpin loop. Underlined letters indicate mismatch base(s). 69
Table 4.2 Comparison of the proposed HCR-AgNCs biosensor with other reported DNA biosensors 81
Table 4.3 Detection of DNA-214 in human serum samples using the proposed HCR-AgNCs biosensor (n=5). 83
Table 5.1 Oligonucleotide sequences used in this work. Red letters indicate AgNCs templating sequence. Italicised letters indicate hairpin stem region. Bold letters indicate hairpin loop. Underlined letters indicate mismatch base(s). 88
Table 5.2 Detection of miR-144-3p in human serum samples using MB-HCR-AgNCs (n=5). 104
Table 6.1 Comparison of the proposed HCR-AgNCs biosensors with reported HCR-AgNCs biosensors towards a nucleic acid target. 110

TABLE OF CONTENTS

ABSTRACT ..... **I**

ACKNOWLEDGEMENTS ..... **III**

LIST OF ABBREVIATIONS ..... **V**

LIST OF FIGURES ..... **VII**

LIST OF SCHEMES ..... **X**

LIST OF TABLES ..... **XI**

CHAPTER 1: INTRODUCTION **1**

1.1 Background **1**

1.2 Aim and objectives **2**

1.3 Significance of study **3**

1.4 Thesis structure **4**

CHAPTER 2: LITERATURE REVIEW **6**

2.1 DNA-based biosensors **6**

2.2 Significance of miRs **7**

2.2.1 MiRs as biomarkers 7

2.2.2 Detection of miRs 8

2.3 HCR amplification **10**

2.3.1 Principles of HCR amplification 10

2.3.2 Factors affecting HCR amplification 11

2.3.2.1 Effect of DNA sequence 12

2.3.2.2 Effect of buffer constituents 12

2.3.2.3 Effect of pH 12
2.3.2.4 Effect of temperature 13
2.3.2.5 Effect of concentration and mode of reaction 13
2.3.3 Designing a functional HCR system 13
2.3.4 Application of HCR in biosensing 17
2.3.4.1 Direct detection 17
2.3.4.2 Indirect label-free detection 18
2.3.4.3 Indirect label-based detection 19
2.3.5 Challenges and limitations of HCR systems 20

2.4 Fluorogenic DNA-AgNCs 22

2.4.1 Fluorescence-based biosensors 22
2.4.2 Principles of DNA-AgNCs as fluorescence transducers 22
2.4.3 Preparation of DNA-AgNCs 23
2.4.4 DNA-AgNCs in biosensing applications 24
2.4.4.1 Homo-polyC AgNCs templating sequences 24
2.4.4.2 Chemopalette AgNCs templating sequences 25
2.4.4.3 DNA-AgNCs templating hairpin loop sequences 25
2.4.4.4 Proximity-dependent AgNCs 25

2.5 HCR-AgNCs biosensors 28

2.5.1 Principles of HCR-AgNCs biosensors 28
2.5.2 Designing HCR-AgNCs biosensors 29
2.5.3 Factors affecting HCR-AgNCs performance 30
2.5.4 Application of HCR-AgNCs biosensors 31
2.5.5 Limitations of HCR-AgNCs biosensors 43

2.6 Future direction of HCR-AgNCs biosensors 44

CHAPTER 3: DEVELOPMENT OF A RATIOMETRIC FLUORESCENCE HCR-AGNCS BIOSENSOR FOR MIR DETECTION 46

3.1 Overview 46

3.2 Background 46

3.3 Methodology 48

3.3.1 Materials 48
3.3.2 Design of DNA oligonucleotides 49
3.3.3 MiR-155 detection in buffer 50
3.3.4 Gel electrophoresis 50
3.3.5 Fluorescence measurement 50
3.3.6 AgNCs characterisation 51
3.3.7 MiR-155 detection in human serum sample 51
3.3.8 Data analysis 51

3.4 Results and Discussion 52

3.4.1 Sensing strategy 52
3.4.2 Computational design of HCR-AgNCs biosensor 53
3.4.3 Feasibility of HCR-AgNCs biosensor 55
3.4.4 Condition optimisation of HCR-AgNCs biosensor 57
3.4.5 Analytical performance of HCR-AgNCs biosensor 59
3.4.5.1 Sensitivity test 59
3.4.5.2 Selectivity test 60
3.4.6 Application of HCR-AgNCs biosensor in human serum sample 63

3.5 Summary 64

CHAPTER 4: DEVELOPMENT OF A "SWITCH-ON" HCR-AGNCS BIOSENSOR BASED ON EXTERNALISED END-TO-END CLUSTER TRANSFER OF AGNCS FOR THE DETECTION OF DNA 65

4.1 Overview 65

4.2 Background 65

4.3 Methodology 68

4.3.1 Materials 68
4.3.2 Design of DNA oligonucleotides 69
4.3.3 Preparation of P2-AgNCs 69
4.3.4 DNA-214 detection in buffer 70

4.3.5 Gel electrophoresis 70
4.3.6 Fluorescence measurement 70
4.3.7 P1-P2-AgNCs characterisation 70
4.3.8 DNA-214 detection in human serum sample 71
4.3.9 Data analysis 71

4.4 Results and Discussion 71

4.4.1 Sensing strategy 71
4.4.2 Computational design of HCR-AgNCs biosensor 73
4.4.3 Feasibility of HCR-AgNCs design 76
4.4.4 Condition optimisation of HCR-AgNCs biosensor 77
4.4.5 Analytical performance of HCR-AgNCs biosensor 79
4.4.5.1 Sensitivity test 79
4.4.5.1 Selectivity test 82
4.4.6 Detection of DNA-214 in human serum sample 83

4.5 Summary 83

CHAPTER 5: DEVELOPMENT OF A MAGNETIC-ASSISTED HCR-AGNCS BIOSENSOR FOR THE DETECTION OF MIR-144-3P 85

5.1 Overview 85

5.2 Background 85

5.3 Methodology 88

5.3.1 Materials 88
5.3.2 Design of DNA oligonucleotides 89
5.3.3 Functionalisation of MBs with C1 89
5.3.4 Magnetic separation of miR-144-3p 89
5.3.5 Quantitative analysis of miR-144-3p 90
5.3.6 Gel electrophoresis 90
5.3.7 Fluorescence measurement 90
5.3.8 Characterisation of AgNCs 90
5.3.9 MBs regeneration 90

5.3.10 Detection of miR-144-3p in human serum sample 91
5.3.11 Data analysis 91

5.4 Results and Discussion 91

5.4.1 Sensing strategy 91
5.4.2 Computational design of MB-HCR-AgNCs biosensor 94
5.4.3 Feasibility of MB-HCR-AgNCs 97
5.4.4 Condition optimisation of MB-HCR-AgNCs biosensor 99
5.4.5 Analytical performance of MB-HCR-AgNCs biosensor 101
5.4.5.1 Sensitivity test 101
5.4.5.2 Selectivity test 101
5.4.6 Detection of miR-144-3p in human serum sample 102

5.5 Summary 105

CHAPTER 6: CONCLUSION AND FUTURE REMARKS 106

6.1 Overview 106

6.2 Summary 106

6.3 Perspectives and future remarks 111

6.4 Concluding remarks 116

REFERENCES 117

APPENDIX I: COMPUTATIONAL DATA FROM CHAPTER 3 154

APPENDIX II: COMPUTATIONAL DATA FROM CHAPTER 4 157

APPENDIX III: COMPUTATIONAL DATA FROM CHAPTER 5 161

APPENDIX IV: RESEARCH OUTCOMES 167

Chapter 1: Introduction

1.1 Background

The versatility of deoxyribonucleic acid (DNA) has been exploited for the development of biosensors, by utilising their specific sequences and base-pairing properties for human biomarker detection [1,2]. For instance, microRNAs (miRs) have been studied as potential diagnostic and prognostic biomarkers in various human conditions, and their detection could assist and complement current clinical diagnosis and therapeutic monitoring [3,4]. Current detection methods of miRs are restricted by specific conditions, such as expensive equipment, highly skilled personnel, and tedious procedures, which are usually only available at well-equipped medical laboratories and healthcare centres. An ideal miR biosensor can clinically screen miRs with good sensitivity and specificity, as well as robustness even in poorly resourced regions. DNA-based biosensors can be designed for miR detection, considering the specific base-pairing and similar material type, but would also have to take into account the challenges in miR detection namely their indigenous short length and low abundance in the human system [5].

As an alternative to conventional miR detection methods (*i.e.*, quantitative reverse transcription polymerase chain reaction (RT-qPCR), microarray, northern blotting and next generation sequencing), a different class of DNA-based biosensors is explored which utilises hybridisation chain reaction (HCR), as both bioreceptor for target recognition and signal amplifier [6], and silver nanoclusters (AgNCs) as fluorescence signal transducer [7]. HCR is an isothermal enzyme-free nucleic acid amplification strategy, whereby DNA hairpins self-assemble into long nicked DNA chains when a specific target is present. The mild reaction conditions highlight its ease of compatibility with diverse transducing platforms (*e.g.*, fluorescence, electrochemical, colorimetry, etc.), to develop sensitive and specific biosensors [8]. Meanwhile, AgNCs are label-free nanomaterials that induce a fluorescence response upon affinity binding on DNA sequences. This fluorogenic material is biocompatible in most biological systems and preserves the inherent characteristics of DNA [9,10]. By integrating AgNCs into a HCR system, hybrid HCR-AgNCs biosensors can synergistically capitalise on the specific biorecognition properties of DNA, good amplification efficiency of HCR and strong fluorescence properties of AgNCs [11–13].

Even with the remarkable potential, current HCR-AgNCs biosensors lack the coherence between studies and innovative approaches, thereby making it difficult to replicate and follow-up for progression in the field. The main challenge in developing a functional HCR-AgNCs biosensor lie in the designing phase of DNA hairpins. The reason behind this is because AgNCs templating sequences are often cytosine (C)- and guanine (G)-rich, and its addition into DNA hairpins can destabilise the kinetics and thermodynamics of the hairpin structure and subsequent HCR circuit. Furthermore, the selection and appropriate integration of AgNCs templating strand would have to elicit a significant change in the fluorescence properties that correspond to the structural changes from hairpin structure to long DNA chains. While the concept of HCR-AgNCs is easy to grasp, the development of a functional HCR-AgNCs biosensor faces critical challenges from *ab initio* design and feasibility testing to optimisation and sample analysis.

Thus, this study will explore the development of hybrid HCR-AgNCs platforms for sensing application and address their underlying technical challenges, which can be divided into three parts:

1. designed a HCR-AgNCs biosensor for ratiometric analysis (**Chapter 3**),
2. introduced HCR-AgNCs biosensor with AgNCs as externalised fluorogenic probes from HCR systems (**Chapter 4**), and
3. incorporated magnetic component into a ratiometric HCR-AgNCs biosensor (**Chapter 5**).

In summation, three different approaches towards HCR-AgNCs biosensors were designed and developed to detect target DNA and miRs.

1.2 Aim and objectives

The aim of this thesis is to design and develop new HCR-AgNCs biosensors for specific detection of short nucleic acid sequences (*i.e.*, DNA and miRs). Furthermore, this thesis also aims to increase the potential of DNA-based biosensors, with better sensitivity and applicability. These would be achieved *via* the following specific objectives:

- To design functional and stable HCR system that is specific towards nucleic acid target and to integrate AgNCs signal transduction into the developed HCR system.

- To investigate the performance of proposed HCR-AgNCs biosensors in buffer and complex samples.
- To explore alternative strategies that could enhance the diagnostic performance of HCR-AgNCs biosensors.

1.3 Significance of study

The importance of this research is related to the following scientific advances:

1. First, this research looks to contribute and make progress towards HCR-AgNCs biosensing research. This study features three novel mechanisms of HCR-AgNCs systems, that could open new routes future HCR-AgNCs designs. These include ratiometric analysis, end-to-end cluster transfer of externalised AgNCs, and magnetic-assisted HCR-AgNCs systems. Moreover, a unique design was incorporated for the DNA hairpin structures in all three studies, that could aid in the development of future HCR-AgNCs systems.
2. From the perspective of DNA-based biosensors, the HCR-AgNCs biosensors developed in this thesis open the possibility to enhance the sensitivity and adaptability for nucleic acid detection. The dual function of HCR to specifically recognise the target and amplify fluorescence, coupled with the efficient formation and functionality of AgNCs, presents an all-round quantitative biosensor with sensitive and specific performance even in complex matrices. This is an essential for actual clinical diagnostics as biomarker detection is performed with human samples (*i.e.,* saliva, urine, blood, serum, etc.)
3. The HCR-AgNCs biosensors reported in this study all employ a simple ‘mix-and-measure’ method in a small tube, with low-cost non-toxic materials (*i.e.,* short DNA, silver salt and weak reducing agent) and mild operational conditions. With further optimisation and inter-disciplinary work (*i.e.,* microfluidics, lab-on-chip devices, etc.), the proposed HCR-AgNCs biosensors have the potential to be developed for point-of-care testing (POCT). This can significantly improve patient care with reliable and rapid results outside of a laboratory, which may not be readily available at poorly resourced regions.

1.4 Thesis structure

This thesis is divided into six chapters, starting with introduction and literature review, followed by three experimental studies on HCR-AgNCs. To demonstrate the versatility of the hybrid sensors for biosensing, each of these studies employs different design strategy and focuses on different nucleic acid targets (*i.e.*, miR-155, DNA, and miR-144-3p). The thesis is then concluded with a summary and future outlook.

Chapter 1 introduces the background of HCR-AgNCs biosensors, the aims and objectives of the thesis, and the significance of the research work conducted towards the field of HCR-AgNCs and DNA biosensors.

Chapter 2 presents a comprehensive literature review focusing on the principles and applications of HCR-AgNCs biosensing. It starts with a brief discussion on recent developments of nucleic acid-based biosensors and the challenges in biomarker detection. The concepts of HCR amplification and AgNCs fluorescence are then introduced, followed by a deep-dive into the framework of hybrid HCR-AgNCs biosensors.

Chapter 3 reports the development of a fluorogenic HCR-AgNCs biosensor for the analysis of miR-155, a potential breast cancer miR biomarker. The design features a novel approach towards HCR-AgNCs ratiometric fluorescence analysis, whereby a portion of the AgNCs templating sequence-emitter pair at the toehold actively participates in HCR itself. This initiates a proximal change on the AgNCs templating sequence-emitter pair, thus enabling a highly sensitive and selective ratiometric analysis. The feasibility and practicality of the biosensor are tested in buffered solution and then in human serum sample.

Chapter 4 accounts the development of a fluorogenic HCR-AgNCs biosensor, that externalises AgNCs as separate units from the HCR amplification system. This approach eases the designing stage for functional and stable DNA hairpins, with predictable HCR performance. Concurrently, this also ensures the specific formation of the desired AgNCs species, free from other interfering molecules (*i.e.*, nucleic acids, proteins, and metal ions) present in a reaction mixture. Moreover, the AgNCs transducing unit emphasises on an underdeveloped strategy termed ‘end-to-end cluster transfer’, whereby dark AgNCs are end-to-end transferred to a homo-polyC AgNCs templating sequence to activate a strong fluorescence response. The model target used for this study is a short DNA sequence (DNA-214) modelled from miR-214, a potential miR biomarker that has reported dysregulated

expression in various types of cancers, such as melanoma, breast, gastric and ovarian cancers. The compartmentalised HCR-AgNCs biosensor displayed high sensitivity and selectivity, with the capability for naked-eye detection of DNA-214.

Chapter 5 introduces a novel concept of HCR-AgNCs coupled with a magnetic component for the detection of miR-144-3p, a potential nasopharyngeal cancer (NPC) miR biomarker. The detection strategy utilises DNA-functionalised magnetic beads (MB) to magnetically separate miR-144-3p from a complex sample, and bidirectional strand displacement reaction to collect miR-144-3p for HCR-AgNCs analysis. This is followed by a ratiometric analysis with a fluorogenic HCR-AgNCs biosensor. The ratiometric HCR-AgNCs system is a conceptual follow-up from the study in **Chapter 3**, whereby a section of the AgNCs templating sequence actively participates in HCR amplification. The combined MB-HCR-AgNCs strategy displayed remarkable performance when tested in raw human serum samples, with high sensitivity and selectivity.

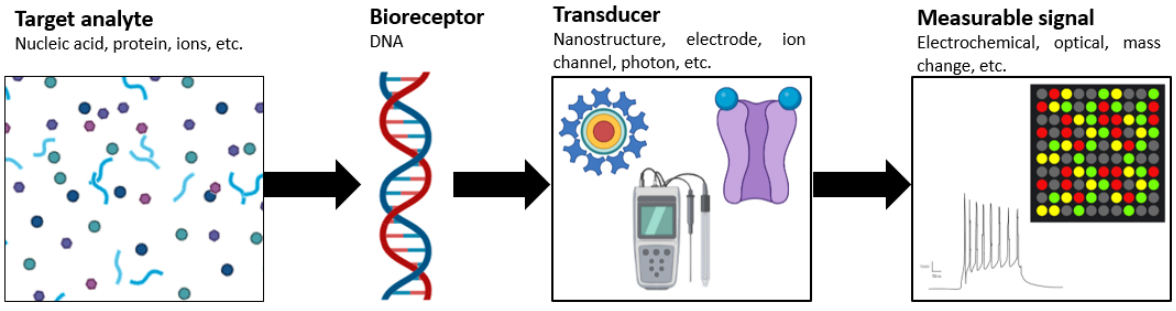
Chapter 6 concludes the research work conducted, highlighting the unique aspects of each study, as well as the challenges and implications for future research of HCR-AgNCs biosensors. This thesis closes with the bibliography and appendices.

Chapter 2: Literature review

2.1 DNA-based biosensors

Biosensors are tools that detect and analyse target analytes, from the presence of the target and its concentration. They are mainly composed of two components: bioreceptor and transducer. A bioreceptor recognises and interacts with the target analyte. A variety of molecules have been used as bioreceptors, such as antibodies, DNA, and proteins. Following that, a transducer converts the captured stimulus into a measurable signal, such as fluorescence, electrochemical and colorimetric response [14,15].

DNA-based biosensors have shown great potential in biomedical detection. These biosensors feature synthetic DNA probes for biorecognition, with a selection of transducing units for signal measurement **(Scheme 2.1)** [15]. DNA is a biomacromolecule, known to be highly biocompatible in most biological systems, with good chemical and thermal stability. The biophysical properties of DNA, namely Watson-Crick base-pairing and the distinct interaction between DNA aptamers and non-nucleotide targets, have led to the detection of a wide range of targets, including nucleic acids (*i.e.*, DNA and RNA), proteins, metal ions and small biological molecules, with high sensitivity and specificity [16,17]. Furthermore, the DNA sequence is highly versatile that it can be designed and tailored for specific analyte detection [2]. With the advancement of DNA nanotechnology, DNA-based biosensors can integrate complex 3D nanostructures and other functional units for signal amplification [18].



Scheme 2.1 A schematic diagram showing the basic DNA-based biosensor assembly with DNA as the bioreceptor for different target analytes, coupled with a transducer to generate a measurable signal.

With recent research efforts driven towards point-of-care and point-of-need detection of biomarkers, DNA-based biosensors are expected to generate rapid results with good accuracy, precision, sensitivity and selectivity, over a large detection range [19]. A specific class of DNA-based biosensor, termed DNA hybridisation-based biosensor, would be the primary focus of this thesis. This detection technique is based on DNA hybridisation amplification to improve the overall signal-to-noise ratio [18,20]. The DNA hybridisation-based biosensors proposed in this thesis have been fabricated with miRs or their DNA analogues, as model targets.

2.2 Significance of miRs

2.2.1 MiRs as biomarkers

MiRs are short non-coding RNAs (18-24 nucleotides in length) that are involved in the post-transcriptional regulation of gene expression in various signalling pathways and complex cellular processes, such as cell differentiation, apoptosis, proliferation and metabolism [21–23]. MiRs suppress the translation of mRNA through association with RNA-induced silencing complex [24].

Given their regulatory roles in gene expression and cell communication, miR signatures are touted as potential biomarkers with diagnostic, prognostic, and/or predictive values and have been abundantly studied in various types of cancer (Table 2.1). Recent literature and reports have indicated the advancement of miR-based non-invasive clinical assays in tissue and bodily fluids by exploiting the differential expression of miRs in the onset and progression of cancer, as opposed to conventional approaches of diagnostic biopsies and surgery. In particular, miRs in the blood has garnered relative attention for miR analysis, which is inclusive of serum and plasma [25–28].

Despite the intense and prolific research efforts to motivate preclinical and clinical applications, miR-based applications are difficult to fully translate into clinical practice due to standing technical challenges that will be discussed in detail in the following section [28–31].

Table 2.1 Examples of serum miRs dysregulated in cancer.

Type of cancer	Serum miRs affected	Reference
Brain	miR-4763, miR-1915, miR-3679	[32]
Breast	miR-1246, miR-1307, miR-4634, miR-6861, miR-6875	[33]
Lung	miR-1268b, miR-6075	[34]
Liver	miR-320b, miR-663a, miR-4448, miR-4651, miR-4749, miR-6724, miR-6877, miR-6885	[35]
Ovary	miR-320a, miR-665, miR-3184, miR-6717, miR-4459, miR-6076, miR-3195, miR-1275, miR-3185, miR-4640	[36]
Prostate	miR-17, miR-1185	[37]

2.2.2 Detection of miRs

Several conventional miR detection techniques have been established to detect miRs from patient samples (particularly from blood plasma and serum), such as RT-qPCR, microarray, northern blotting and next generation sequencing [24,38–40]. Perhaps RT-qPCR is the most reliable option, as it offers a balance between the cost, small sample size and high precision over a large detection range [41,42]. Briefly, the miR sequence is extracted from a sample, and converted into a complementary DNA sequence *via* reverse transcription. This is followed by qPCR using miR-specific and universal qPCR primer sets, with a fluorescence readout (*e.g.,* TaqMan probe cleavage, SYBR Green double-stranded DNA (dsDNA) intercalation) [24].

Each technique has its own strengths and is selected based on their availability and detection criteria. However, these techniques are also challenged by their application, such that the accuracy and reliability of the results are dependent on the quality of the miRs extracted. Intensive sample preparation and extraction are crucial for a good yield of high integrity miRs, because miR degradation can introduce analytical errors in the detection process [43,44]. Besides that, these methods require sophisticated equipment, professionally trained personnel, relatively long processing times, and complex methodology [24]. As the research on miRs advances, more miR biomarkers have been identified, which expands and diversifies the miR profiles that could compromise and complicate the detection process [24]. Additionally, the diagnostic application of circulating miRNA signatures is also challenged

by their specificity for specific cancer types or their broad involvement in other physiological (e.g., pregnancy) and pathological conditions (e.g., chronic inflammation, COVID-19 comorbidities, etc.), and their diagnostic performance as compared to other more established clinical biomarkers.

Modern miR biosensors have been developed to focus on strategies that combine or complement existing clinical indicators rather than attempting to replace them. For example, the combination of miR signatures and serum levels of prostate-specific antigen (PSA) can enhance diagnostic power and performance [45]. In view of this, uniplex and small-scale multiplex detection of specific subsets of miRs with high sensitivity and simpler methodology have been comprehensively investigated. These biosensors typically capitalise on highly selective bioreceptors and highly sensitive transducers to overcome some of the limitations mentioned above [18]. That said, to construct a miR biosensor, the intrinsic properties of miRs must also be taken into account; short length, short half-life, highly similar miRs (one-base difference) in the same miR family, varying expression levels from different sample (blood, saliva, urine, etc.), and low abundance of miRs (attomole quantities) [24]. In this regard, independent biosensor studies on miRs for clinical application often reported inconsistent miR expression data and results, which could be due to the different detection mechanism, normalization and analytical tools used, sample preparation, source and quality of starting RNA material, patient characteristics (e.g., sex, age, ethnicity, stage, treatment history), sample size, study design (e.g., single cohort, training and validation set), and statistical tools used for analysis [45]. Hence, a better understanding of these variables with further studies and more robust protocols can ease the translation of miRs into clinical assays for cancer detection.

In this thesis, fluorogenic AgNCs transducers were integrated into DNA hybridisation amplified HCR systems, with the use of specifically designed DNA hairpins. Of note, three different miRs or their DNA analogues (*i.e.,* miR-155, miR-214, and miR-144) were selected as model targets for the fabrication of HCR-AgNCs biosensors to be tested in human serum samples. Given the relatively low concentration and dynamic changes of miRs in the human blood/serum, the sensitive and selective detection of miR expression with the proposed HCR-AgNCs biosensors in this thesis could serve as companion diagnostic tests to complement current detection techniques and to provide clinical information based on the significant changes in miR expression in the human body/sample. In its entirety, HCR-AgNCs

biosensors and its variations could offer an alternative approach to advance miR research in cancer biology.

2.3 HCR amplification

2.3.1 Principles of HCR amplification

HCR is an amplification strategy that employs a set of DNA hairpins at isothermal condition, without the need of enzymes [6,8,46–48]. DNA hairpins **(Figure 2.1 (A))** are single-stranded DNA (ssDNA) strands that fold into the shape of a hairpin, consisting of three sections: short sticky-ended toehold, long duplex stem and loop [49]. The toehold regulates the kinetics of target recognition, DNA hairpin opening and subsequent hybridisation, with regards to both its length and sequence [50–52]. Meanwhile, the stem is responsible for maintaining the thermodynamic stability of DNA hairpins, by kinetically trapping the potential energy stored in the loop region. To make HCR amplification possible, the DNA hairpins are designed to be partially complementary to one another. Thus, when one hairpin is opened, it can facilitate the continuous cross-hybridisation with other DNA hairpins. As a matter of fact, the different DNA hairpins should be able to coexist metastably in a HCR system, to avoid non-specific hybridisation events, high background signals, and false positive results in the absence of a target. Henceforth, this undesired event of non-specific hybridisation is defined as system 'leakage' [51,52].

HCR amplification operates on the basis of conventional DNA hybridisation, initiated by a target sequence that serves as a key to unlock the kinetic trap in DNA hairpins **(Figure 2.1 (B))**. The first step, called 'nucleation', involves the complementarily base-pairing between the target sequence and the toehold region of the first hairpin (H1). This process is rate-limiting as it relies on the random diffusion of target and DNA hairpins in a solution, for contact formation. Thereafter, 'zippering' occurs, whereby the target simultaneously hybridises with the DNA hairpin and opens it up, along the stem towards the loop section. At this point, zippering process becomes rate-limiting due to the separation of intrastrand base-pairs (bp) of DNA hairpins, and the formation of interstrand bp between DNA hairpins [53].The now exposed DNA hairpin sequence will open the other DNA hairpins in a similar pattern. Over time, this cascade of hybridisation events will proceed until thermodynamic equilibrium is reached. As a result, long nicked double-stranded dsDNAs will be formed. As

is evident from the mechanism, HCR amplification is an automated process that operates without the need of external components (*e.g.*, enzymes) and tedious reaction conditions (*e.g.*, thermal cycling) [54–56].

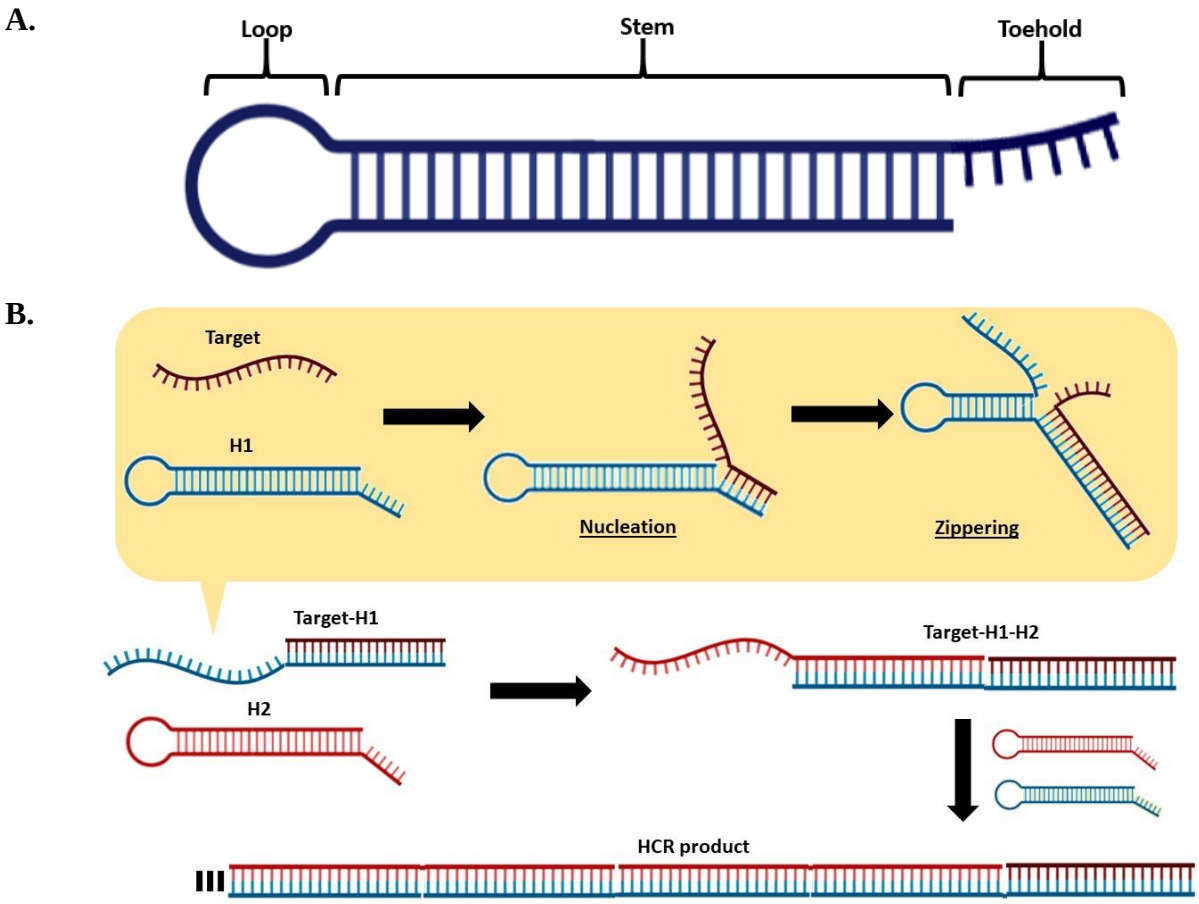


Figure 2.1 (A) DNA hairpin structure, with toehold, stem and loop. **(B)** Mechanism of HCR amplification between target, DNA hairpin 1 (H1) and 2 (H2), to form HCR product.

2.3.2 Factors affecting HCR amplification

The performance of HCR is dependent on DNA hybridisation, which is composed of thermodynamic and kinetic aspects. Having said that, DNA hybridisation can be regulated through various factors, such as DNA sequence, buffer constituents, pH, temperature and more. Fundamentally, the impact of these factors are evaluated through the association (binding) and dissociation (separation) constant in the hybridisation process [57].

2.3.2.1 Effect of DNA sequence

In a DNA strand, adenine (A)-thymine (T) bp form two hydrogen bonds, whereas C-G bp form three hydrogen bonds. This means that DNA strands with more C-G bp hybridise with better stability (association > dissociation). Besides that, the length of DNA affects the hybridisation process, such that longer DNA strands hybridise with better stability over shorter DNA strands. On top of that, mismatch bases can stymie the process of DNA hybridisation, and the degree of inhibition is determined by the location of the mismatch. In fact, the steric inhibitory effects on DNA hybridisation become more prominent when the mismatch is located towards the middle than the end segments of the DNA [58].

2.3.2.2 Effect of buffer constituents

The microenvironment of DNA strands plays a significant role in the hybridisation process. DNA itself is negatively charged due to the phosphate group in the DNA backbone. This builds up electrostatic forces that repel other DNA strands and inhibit DNA hybridisation. As a solution to balance the charges and improve hybridisation, salts containing cations are normally introduced. These cations target sites with high electron density, and 'shield' the negative charges. As a result, the repulsion forces between DNA strands are reduced to promote DNA hybridisation at a lower energy level. Monovalent (*e.g.,* sodium (Na^+)) and divalent (*e.g.,* magnesium (Mg^{2+})) salts are commonly used in hybridisation buffers for this purpose. Divalent cations have a more prominent effect over monovalent cations, owing to their stronger electrostatic and hydrogen bonding with the bases and phosphate backbone. Despite the direct correlation between salt concentration and the association constant, the concentration must be optimised, especially when DNA hairpins are optimized. A high salt solution strongly stabilises the hairpin structure, thereby making it significantly more difficult to open for hybridisation [59].

2.3.2.3 Effect of pH

Optimal DNA hybridisation normally occurs near physiological pH, between 5 and 9. The charge of the nucleobases within this range is relatively neutral and hydrophobic, which

facilitates better interaction and stability between DNA strands. DNA molecules are deprotonated and protonated at higher and lower pH, respectively. This makes the DNA molecules more hydrophilic and soluble, which hinders the DNA hybridisation process and destabilises hybridised DNA duplexes. At extreme pH conditions, DNA molecules are prone to damage by depurination and deamination [60].

2.3.2.4 Effect of temperature

Temperature should be optimised within a narrow range as well. An optimum temperature must provide the DNA molecules with sufficient energy to facilitate diffusion and hybridisation *via* nucleation and zippering. At low temperature, DNA hybridisation is dependent on the rate of diffusion, making the initial nucleation stage the rate-determining step. As the temperature increases, the additional thermal energy provides a positive activation energy, which enables the DNA strands to overcome the energy barrier posed by electrostatic forces. However, the increasing temperature could adversely result in dissociation, especially with short DNA duplexes. When the temperature exceeds the optimum range, DNA hybridisation has a negative activation energy, and the destabilisation of hybridised DNA duplexes becomes more prominent [61].

2.3.2.5 Effect of concentration and mode of reaction

To an extent, the concentration of each DNA species also affects the hybridisation process, such that the DNA concentration is proportional to the efficiency of DNA hybridisation [61]. Besides that, studies have shown that the kinetics of DNA hybridisation is 20- to 40-fold faster in solution-based than surfaced-based DNA hybridisation [59].

2.3.3 Designing a functional HCR system

Taking the aforementioned factors that affect HCR performance into consideration, a functional HCR system can be systematically designed. Besides that, additional guidelines have been reported to effectively construct DNA hairpins, and are summarised in **Table 2.2**

below [49,62–65]. These guidelines aim to balance the metastability of DNA hairpins with their hybridisation efficiency during HCR.

The metastability of DNA hairpins can be controlled by regulating their size and sequence. In fact, the metastability of DNA hairpins shares an inverse correlation with the efficiency of DNA hairpin opening. For example, a shorter stem length and a larger loop size will promote the opening of a DNA hairpin, at the expense of its metastability. Green *et al.* added that DNA hairpins can be opened from either an external toehold or the hairpin loop, and reported that toeholds facilitate faster DNA hairpin opening than hairpin loops. Moreover, DNA hairpins with larger loops can interact with each other to form undesired duplex structures, called 'kissed-complex' [49].

The DNA sequence defines the base-pairing between complementary strands, and base-stacking between adjacent bases. Ang *et al.* investigated the effects of different DNA bases on the metastability of DNA hairpins, and found that both C and G bases should be more concentrated in the stem than the toehold to confer relative metastability. Likewise, Ang and co-workers also reported good DNA hairpin metastability from a long stem and short toehold design [62].

As previously mentioned, unstable DNA hairpins can result in HCR system leakage and false-positive results, which are detrimental especially in biosensing applications. To develop a leak-proof HCR design, Li *et al.* studied the thermodynamic properties of DNA hairpin structures, with regards to their free energies and behaviour. In this study, the free energy (ΔG) of DNA bases was comprehensively calculated, with C-G and A-T bp possessing -1.5 and -0.8 kcal mol^{-1}, respectively. It was concluded that -16 kcal mol^{-1} is the minimum free energy (MFE) required to prevent HCR leakage [63]. The ends of DNA hairpin stems are prone to frequent transient localised opening events, normally confined to the two terminal bp. This occurrence, otherwise known as 'fraying', is due to reduced structural constraints from base-stacking at the end of the helical stem structure [66,67]. Moreover, this structural behaviour might be the cause HCR leakage in certain situations. To minimise this effect, Li *et al.* suggested to introduce mismatch bases in hairpin loops, minimising sequence symmetry, and ending the fraying regions with C-G bp, to create higher energy barriers [63].

Oftentimes, DNA hairpins can have a secondary (2^o) toehold, adjacent to the original primary (1^o) toehold **(Figure 2.2A)**. A recent study by Xing *et al.* briefly investigated the

effects that 2º toeholds have on the stability of DNA hairpin probes, and reported that 2º toeholds with more than 3 bases would risk destabilising the DNA hairpin structure, and cause HCR system leakage [64]. Meanwhile, Yu *et al.* studied the effect of hanging 'tails' on hybridised DNA structures. These hanging tails are defined as unbounded sequences that appear as appendages from HCR products **(Figure 2.2B)**. These tails typically originate from either long unreacted 1º toeholds or 2º toehold sequences. The negative charges and swaying motion of these tails can destabilise a hybridised DNA complex. In addition, the negative charges generate a repulsive effect that significantly slows down the nucleation rate between DNA strands. It is also speculated that this repulsive force is proportional to the length and number of tails in the hybridised structure [65].

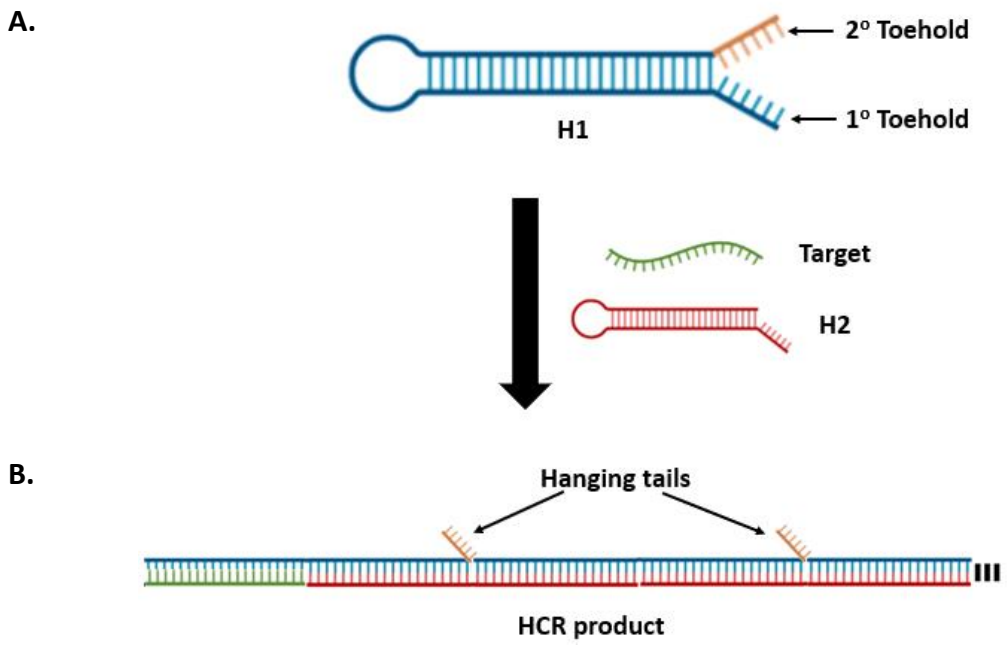


Figure 2.2 (A) DNA hairpin structure with two toeholds; primary (1º) and secondary (2º). **(B)** HCR product with hanging 'tails' after HCR amplification between target, H1 and H2.

Table 2.2 Guidelines to design metastable DNA hairpins for HCR systems.

DNA hairpin condition		Description	Reference
Base composition	-	C and G content at the toehold should be between 30 to 40%	[62]
	-	C-G bp must be more than 60% in the stem, if the stem length is the same as toehold length	[62]
Segment	-	DNA opening by external toehold is faster than loop-mediated opening.	[49]
	-	2^o toeholds can destabilise DNA hairpin structure, and suggested to be kept below 3 bases.	[64]
	-	Unbounded toehold sequences can produce "tails", which hinder subsequent DNA hybridisation/HCR.	[65]
	-	DNA hairpins have the tendency to fray at the ends of stem region, which might prematurely open DNA hairpins.	[63]
Size	-	Hairpin toehold must be less than 12 bases	[62]
	-	Stem length must be longer than toehold length	[62]
	-	Stem length must be longer than loop size	[49]
Folding energy	-	Threshold ΔG of stable DNA hairpins reported to be -16 $kcal.mol^{-1}$	[63]

Designing DNA hairpins can be complicated and cumbersome, given the restrictions mentioned above. This process would conventionally require screening thousands of sequences with heavy calculations to end up with just a handful of DNA probes. Some commonly used software are available to facilitate the hairpin design. Pierce and co-workers developed an online platform, called NUPACK (www.nupack.org), that specialises in the analysis and design of nucleic acid structures for systems containing one or more interacting strands [68]. This software predicts DNA hybridisation reactions based on the nearest neighbour model of base stacking. The thermodynamic calculation from the algorithm provides a relative prediction of partition function, MFE structures and melting temperatures of DNA constructs. The melting temperature can be defined as temperature at which 50% of dsDNA has dissociated into ssDNA, and is a measure for thermodynamic stability [69,70]. NUPACK is a particularly convenient tool to visualise all possible DNA secondary structures (hairpins, pseudoknots, etc.), and this is made possible from both positive and negative design paradigms embedded in the software. The former optimises the affinity for a desired outcome between a sequence and a target structure, whereas the latter optimises the

specificity of a sequence towards a target structure. NUPACK also presents the option of modifying the concentration of interacting strands, and reaction conditions of the DNA hybridisation process. However, the software is limited by the number of strands that it can analyse. It was reported that seven interacting strands (n = 7) were too much for the web-based software to super-compute, due to the high cost of analysis and computational complexity [71].

Although there are still gaps in the process of systematically designing a functional HCR system, these recent studies have proven to be insightful to improve the efficiency of future HCR designs and systems [49,62–65,68].

2.3.4 Application of HCR in biosensing

HCR has found widespread application in biosensing and can be categorised into three types of detection: direct detection, indirect label-free detection, and indirect label-based detection. These detection strategies implement different bioreceptors prior to HCR amplification. The direct detection strategy defines the interaction between the toehold sequence of HCR hairpins with nucleotide-based targets (*e.g.,* DNA and RNA). HCR amplification proceeds in a straightforward manner and exhibits a corresponding signal. On the contrary, indirect label-free strategy utilises an aptamer as the bioreceptor for a non-nucleotide target (*e.g.,* proteins, metal ions, etc.). An aptamer refers to a synthetic nucleic acid sequence capable of binding to a specific target, and its conformational folding will initiate HCR amplification and subsequent signal transduction. In contrast, the indirect label-based method uses non-nucleotide bioreceptors for analyte detection. In most HCR studies, antibodies would be commonly functionalised to detect the target molecules and initiate HCR amplification. The application of HCR with regards to these methods will be described in detail in the following subsections.

2.3.4.1 Direct detection

Direct detection is the most common application to detect nucleic acid targets (*e.g.,* DNA and RNA). The direct and simple hybridisation of the target sequence to the DNA hairpins is sufficient to initiate HCR, and that the HCR system can be easily designed by

translating the nucleic acid sequence onto the DNA hairpins. The mechanism behind this involves DNA hairpin opening typically from the toehold region of the DNA hairpins after complementary base-pairing with the target sequence. In one of the earlier studies, Pierce *et al.* developed the concept of HCR based on a 24-nt ssDNA sequence **(Figure 2.3A)** [6], and later detect mRNAs in living cells [47,72]. Other research groups have also implemented the direct approach for detection for miRs (*e.g.*, let-7a [73], miR-21 [74], miR-199a [75], etc.), and intracellular imaging [76–78].

2.3.4.2 Indirect label-free detection

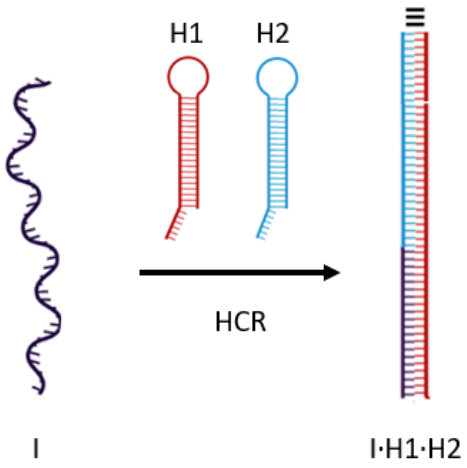
On the other hand, non-nucleotide targets (*e.g.*, metabolites, metal ions, proteins, etc.) would require an aptamer as both bioreceptor and initiator to the HCR system. For most non-nucleotide targets, their respective aptamers can be drawn from a library containing random sequences using a method called Systematic Evolution of Ligands by Exponential Enrichment (SELEX). The selected aptamer would then be used to recognise the analyte *via* intra-molecular interactions, before undergoing a conformational change to adopt a complex three-dimensional shape [79]. The folding action would then trigger the opening of DNA hairpins from the HCR system and initiate the entire cascade of hybridisation reaction. For example, Jianzhong *et al.* developed a fluorogenic biosensor with an aptamer-HCR initiator strand separated by a spacer, for platelet-derived growth factor BB (PDGF-BB) detection. When the aptamer-HCR initiator strand recognised PDGF-BB, it would undergo conformational change, initiate HCR, and produce a fluorescence readout from the resulting complex [80]. Similarly, Feng *et al.* optimised the aptamer sequence into a DNA hairpin structure for PDGF-BB detection *via* a graphene oxide (GO)-HCR biosensing system [81]. In contrast, Po *et al.* worked with a "turn-off" system where the aptamer sequences for anterior gradient protein 2 homolog (AGR2) also served as the HCR initiator. In other words, the addition of AGR2 would bind to these aptamer sequences and render them unavailable for HCR initiation [82]. The same concept was applied in an interferon (IFN)-γ biosensor, whereby the electrochemical signal observed was inversely proportional to the concentration of IFN-γ present [83]. This indirect label-free approach can also be tailored for metal ion detection. In a particular study by Wang *et al.*, the aptamer sequence for mercury ions (Hg^{2+}) was integrated into a hairpin structure **(Figure 2.3B)**, that would reconfigure to accommodate the Hg^{2+} ions. This conformational change would simultaneously initiate HCR amplification

for a gold nanoparticle-induced colorimetric readout, with a 30 nM limit-of-detection (LOD) in raw river water samples [84].

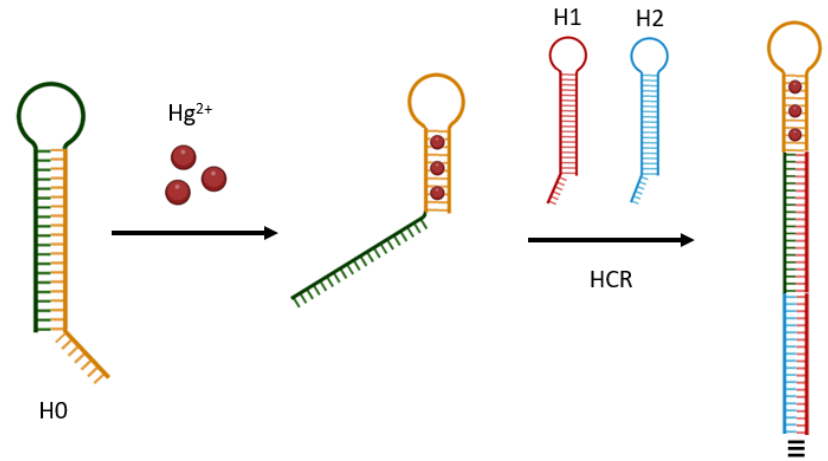
2.3.4.3 Indirect label-based detection

Apart from nucleic acid bioreceptors, non-nucleotide molecules have also been used in HCR biosensing applications. Antibodies are one of the most common options, because of their innate ability for analyte binding with high affinity and specificity. In most cases, when antibodies are coupled with HCR, the resultant immunosensors would a sandwich-type model. Christopher *et al.* utilised antibodies to tag chemokines and cytokines with fluorescent-labelled HCR amplification. The immune assay incorporated a covalently-bonded HCR initiator on to the antibody prior to the detection stage **(Figure 2.3C)** [85]. Comparably, Knopp *et al.* introduced HCR initiators onto gold nanoparticles to enhance the sensitivity of the sandwich-detection model, to detect human IgG [86]. Likewise, Yuan *et al.* devised a multiplexing platform with an antibody-bound HCR complex to detect four different antigens (AFP, CEA, CA125, and PSA) within a single electrochemical scan [87].

A.



B.



C.

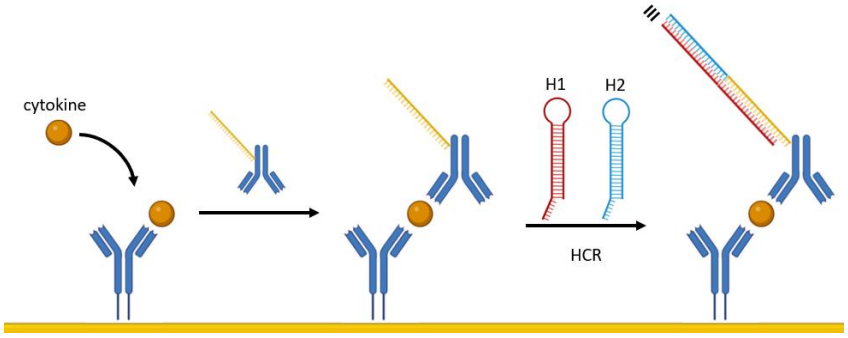


Figure 2.3 (A) Direct detection. Initiator I hybridises directly and opens hairpin 1 (H1), which subsequently hybridises and opens hairpin 2 (H2) to form the complex I·H1·H2. This complex undergoes a series of hybridisation events between H1 and H2 to form nicked dsDNA. Adapted from [6]. Copyright (2004) The National Academy of Sciences. **(B)** Indirect label-free detection. An aptamer sequence for Hg^{2+} was integrated into a hairpin structure (H0), which also served as HCR initiator for DNA hairpins, H1 and H2. Adapted from [82], Copyright (2015), with permission from Elsevier. **(C)** Indirect label-based detection. The immunoassay utilised an antibody label for cytokine detection, with covalent-bonded HCR initiator for HCR amplification. Adapted from [85]. Copyright 2011 American Chemical Society.

2.3.5 Challenges and limitations of HCR systems

Nevertheless, HCR systems are often challenged at both design and validation stages, which can limit their application.

Whilst the thermodynamic properties of HCR systems can be predicted with relative accuracy from the DNA sequence, the kinetics of HCR systems can be more inconsistent and tedious to evaluate. Most kinetic studies are carried out by trial-and-error optimisation experiments, where a pool of DNA oligonucleotides is manually screened across different

studies at different reaction conditions. Furthermore, these kinetic screening uses costly functionalised DNA oligonucleotides (*e.g.,* fluorophore and nanopore), which limits the practicality of screening specific sequences for HCR systems [88–90]. In other words, the entire design process is mainly experienced-based, considering the complicated kinetic studies and time-consuming thermodynamic analysis for feasible HCR systems. Thus, an ideal software that evaluates both kinetic and thermodynamic is in-demand to streamline the design of HCR systems.

HCR amplification operates at ambient conditions that must be pre-defined to balance between the stability of DNA hairpins and efficiency of HCR. This is particularly difficult to maintain, especially in biological samples that contain interfering molecules that can degrade the DNA hairpins and alter HCR performance [91]. Since HCR is a continuous process, it produces elongated dsDNA concatemers of different sizes and might lead to variability among different tests for the same target. If specific HCR products are required for further analysis, these can be isolated and extracted from gel electrophoresis. However, the process is both tedious and time-consuming, besides the fact that it would incur additional costs and risk of errors.

Since HCR focuses on linear amplification, this could limit the sensitivity and application of HCR biosensors. A suggestion to overcome this would be the implementation of branched HCR systems, that would exponentially amplify measurable signals [92]. Even so, branched HCR would require more complex DNA designs and more DNA hairpins in the system, that would complicate the entire HCR mechanics. Another common practice in HCR biosensors is the usage of different fluorophore combinations and/or fluorophore-quencher combination. Albeit their partial application, these fluorophores have their respective internal charges that can interact locally with each other and the DNA template. As a result, these differential interactions can offset the overall hybridisation kinetics [93,94].

Therefore, alternative approaches are highly regarded to improve the overall performance of HCR-based biosensors [95]. This thesis focuses on using AgNCs as fluorogenic signal reporters that can be easily integrated into HCR systems for biosensing purposes.

2.4 Fluorogenic DNA-AgNCs

2.4.1 Fluorescence-based biosensors

Fluorescence-based biosensors produce measurable signals based on changes in the fluorescence emission intensity and/or wavelength, from analyte detection. In addition, many fluorescence-based biosensors are solution-based, which rules out additional surface immobilisation and purification steps. This simple concept has led to selective and sensitive fluorescence-based biosensor development, with the versatility that allows multiplexing and point-of-need analysis. However, most fluorescence-based biosensors require chemical and structural modifications (*e.g.,* thiols, antibodies, and fluorophore attachments), which increase the cost, complexity, duration of analyte detection, and concurrently undermine the biorecognition of target analytes [96–98]. The progression of nanotechnology research has led to the fabrication of nano-fluorophores, and fluorogenic DNA-AgNCs are among the extensively applied, because of their cost-effectiveness, simplicity, and ease of integration into DNA networks (*e.g.,* HCR systems).

2.4.2 Principles of DNA-AgNCs as fluorescence transducers

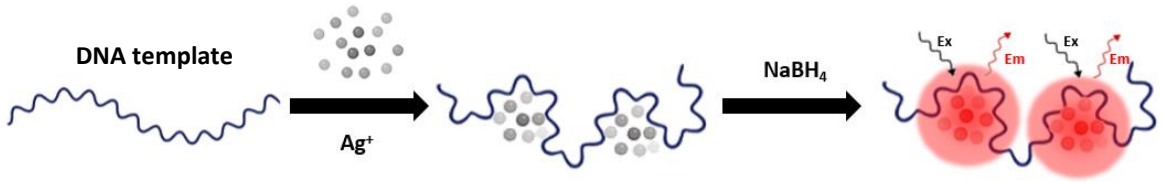
DNA-AgNCs are a class of nano-fluorophores that comprise ultrasmall silver atoms close to the Fermi wavelength of electrons [7]. In general, fluorogenic DNA-AgNCs have several advantages over other types of fluorescent dyes and materials, such as better solubility and photostability, as well as lower photobleaching and toxicity index [93,99,100].

The formation of DNA-AgNCs emphasises the affinity binding of silver ions (Ag^+) to nucleobases, especially C bases. On a molecular level, Ag^+ binds to the heterocyclic groups of purines and pyrimidines, with particular preference for nitrogen atom (N) 3 of C and T bases, and N7 of A and G bases [101,102]. Apart from being a template for AgNCs formation, DNA strand also stabilises the synthesised AgNCs to better regulate their morphology and size [101,103]. Over the years, extensive research around DNA-AgNCs, especially through the works of Gwinn *et al.*, have led to better understanding of their molecular and optical properties, such as the use of different DNA secondary structures [104,105], DNA sequences [106,107], and preparation methods [108]. Most importantly, DNA-AgNCs have tuneable

fluorescence emission from UV to near-infrared region, which can be regulated through the DNA sequence, AgNCs size, and buffer constituents [109,110].

2.4.3 Preparation of DNA-AgNCs

DNA-AgNCs can be controllably prepared in situ *via* a simple mixture of silver salt (*e.g.*, Ag^+), reducing agent (*e.g.*, $NaBH_4$) and a DNA template, in a buffered solution **(Scheme 2.2)**. This is followed by an incubation period for the nucleation and stabilisation of the nanoclusters [111].



Scheme 2.2 Illustration of DNA-AgNCs synthesis. Ag^+ preferentially binds to C bases on DNA templating sequences. Reducing agents, such as $NaBH_4$, reduce these DNA-Ag^+ leading to the formation of DNA-AgNCs.

Essentially, the amount Ag^+ and $NaBH_4$ with respect to the DNA concentration, can affect the fluorescence properties of DNA-AgNCs, where in most cases, the amount of silver salt is equivalent to that of the reducing agent. That said, neither one of these reactants (*i.e.*, Ag^+ and $NaBH_4$), when in excess, will affect the fluorescence analysis and thus need not be removed *via* additional purification steps [111–113]. Besides that, a buffer supplemented with monovalent and divalent salts, is required to facilitate AgNCs formation, by shielding the negative charges and stabilising the DNA structure [114], as described in **Section 2.3.2.2**.

The selection of a specific DNA template is a little more complicated. As aforementioned, the formation of DNA-AgNCs is sequence-specific, with high affinity towards C bases. Other than that, the fluorescence properties also rely on the structure of the DNA template. The most common type of DNA used is a linear ssDNA, known for its structural flexibility to accommodate Ag^+. The typical ssDNA template would contain between 12 and 30 bases, with the longer sequences producing AgNCs of better stability and

yield. In addition, longer strands are more prone to multi-base bonding, thereby forming AgNCs of greater sizes and fluorescence emission at longer wavelengths [115,116]. A majority of bright AgNCs species originate from consecutive C bases. The most basic sequence would be a homo-polyC sequence, comprising only C bases. The resultant fluorescence can be tuned between yellow and near-infrared region, by adjusting the number of C bases. A different type of sequence, termed 'chemopalette', blends the other bases (A, T and G) in between C-rich segments. As a result, different coloured bright species of AgNCs can be produced.

Another relevant structure that is known to host AgNCs is the DNA hairpin structure. AgNCs are highly susceptible to oxidation that can alter their fluorescence properties, and a closed hairpin structure can improve the stability of AgNCs. The hairpin loop can host AgNCs with a homo-polyC loop (6C, 12C, etc.). This configuration is known to produce red fluorescence emission similar to an average homo-polyC ssDNA. In fact, the fluorescence properties can be regulated by the C and G base composition within the stem sequence [117]. However, the resultant fluorescence intensity would significantly decrease when the DNA hairpin opens up [9]. In accordance with the variety of available DNA templates, DNA-AgNCs have been innovatively amalgamated into different biosensing platforms.

2.4.4 DNA-AgNCs in biosensing applications

DNA-AgNCs have found diverse applications in the field of biosensing, and their working principles generally revolve around (1) switch-on (intensity enhancement) [118], (2) switch-off (intensity quenching) [119], and (3) fluorescence pattern changes [120].

2.4.4.1 Homo-polyC AgNCs templating sequences

Homo-polyC AgNCs templating sequence can be easily integrated for biosensing purposes, due to it being a well-studied sequence and having a predictable fluorescence response [121–123]. Thus, homo-polyC AgNCs biosensors have been used to measure the oxidative activity in cancer cells [124], identify S1 nuclease activity [125], detect miR [121], and analyse antibiotic content [126]. For instance, Hosseini *et al.* reported a biosensor with 12C AgNCs templating sequence to discriminate p53 gene mutation, whereby single-base

mismatch sequences would decrease the intensity of the red AgNCs fluorescence emission **(Figure 2.4 (A))** [127]. Zhang *et al.* utilised a 12C sequence to develop a turn-on fluorescence assay that was used detect acetylcholinesterase activity and screen for acetylcholinesterase inhibitors [128].

2.4.4.2 Chemopalette AgNCs templating sequences

Chemopalette sequences feature a mixture of bases in between C-rich segments, and these subtle base substitutions can generate significant changes in the fluorescence species [129]. Zhang *et al.* applied two different chemopalette sequences with a dual-emissive green-orange fluorescence for the multiplex detection of H1N1 and H5N1 **(Figure 2.4 (B))**. Both chemopalette sequences comprise multiple consecutive C blocks separated by A and T bases [130].

2.4.4.3 DNA-AgNCs templating hairpin loop sequences

DNA hairpin loops with homo-polyC sequences have been reported to host AgNCs that produce intense red fluorescence emission, and that structural changes within the hairpin would change the fluorescence properties. For example, AgNCs hosted within a C13 loop resulted in a single peak bright-red emission, and the intensity was significantly quenched when Hg^{2+} interacted with the DNA hairpin **(Figure 2.4 (C))** [131]. In a different study, a 12C hairpin loop was used to detect miR-21 *via* dual-emissive response. The opening of the DNA hairpin would simultaneously quench the red fluorescence emission from the hairpin loop, and generate a green fluorescence emission from the opened structure [120]. Fluorescence quenching can also be induced *via* enzymatic activity on DNA hairpin loops, and this strategy was reported to successfully detect Hg^{2+} and DNA [132,133].

2.4.4.4 Proximity-dependent AgNCs

The most notable application of DNA-AgNCs comes in the form of proximity-dependent AgNCs. An example of this is nanocluster beacon (NCB) or in simpler terms, G-rich activation. This switch-on mechanism works with a non-fluorescent ‘dark’ AgNCs

templating sequence, that is optically activated when brought into close proximity with a G-rich 'enhancer' sequence. It is understood that both the physical interaction between N7 of G and Ag^+, as well as the electron transfer from G to AgNCs, led to the reassembly of Ag^+ on the combined enhancer-dark AgNCs templating sequence to form new clusters. As a result of the Ag^+ translocation and new AgNCs formation, the fluorescence from the templating sequence is activated and/or enhanced [134,135]. NCBs are initially developed to circumvent the issue of photobleaching, such that specific AgNCs fluorescence emission can be activated on-demand [135]. That said, the fluorescence activation of NCBs is regulated by numerous factors, namely the enhancer and dark AgNCs templating strands' sequence, length, and their relative position to each other. NCBs have been successfully integrated in AgNCs biosensors for sensitive and selective detection of various analytes (*e.g.*, cocaine, and adenosine triphosphate (ATP)) [136,137]. In one of the early studies on NCBs, Yeh *et al.* reported a 500-fold fluorescence enhancement ratio, when a G-rich enhancer sequence was brought close to a pre-prepared non-emissive AgNCs on a dark strand **(Figure 2.4 (D))** [138]. In contrast, a switch-off NCB assay was developed by Wen *et al.* to detect disease-related oligonucleotides, using C-rich and G-rich sequences as AgNCs template and enhancer, respectively [139]. Recently, another variation of proximity-dependent AgNCs led to the formation of 'chameleon' AgNCs or in simpler terms, colour-switching AgNCs fluorescence emission. Instead of using the conventional enhancer-dark strands, this adaptation features two fluorescence intensive AgNCs sequences (*i.e.*, AgNCs templating sequence and emitter-pair), whose fluorescence properties changes in a proximity-dependent manner between the two sequences [140–143]. For example, Xu *et al.* employed two 6C sequences that produce an orange/yellow fluorescence individually. In the presence of a target miR, these sequences were brought close together and the resultant fluorescence emission turned red [144]. This has significantly expanded the biosensing capabilities of DNA-AgNCs, in terms of ultrasensitive detection, intracellular imaging, ratiometric detection, in vivo studies and more [145–154]. A slightly different approach with regards to chameleon AgNCs is the splitting of a long AgNCs templating sequence into fragmented pairs. These fragmented pairs would not initiate any fluorescence response from partial AgNCs formation. Only when these split pairs are brought in close proximity to complete the AgNCs templating sequence, can the fluorescence emission can then be re-activated. This concept was successfully implemented in several works, such as the detection of miR and DNA in human serum samples [155].

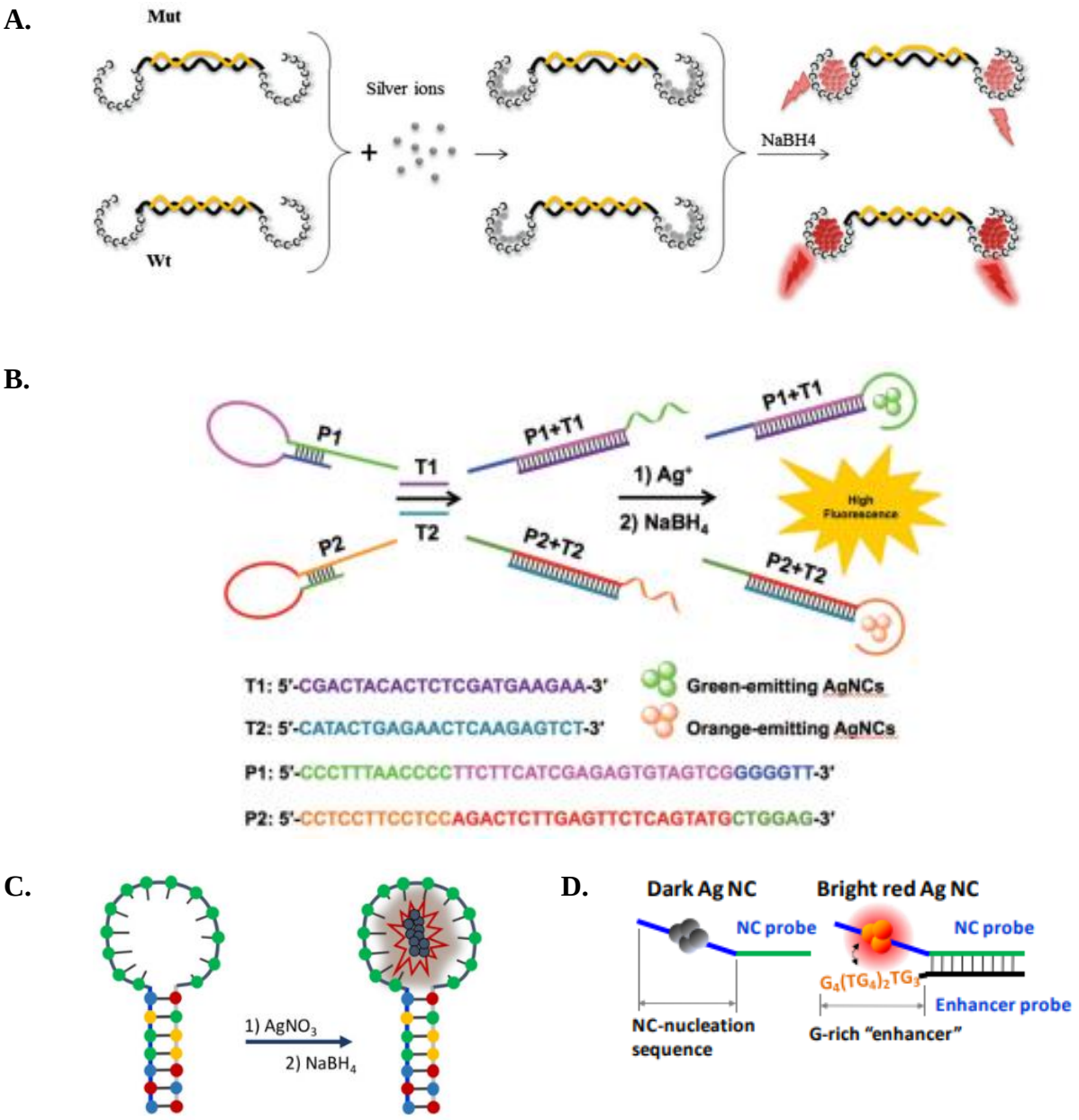


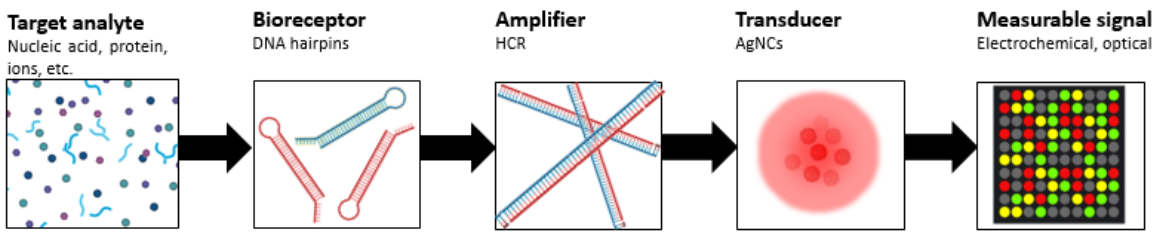
Figure 2.4 Application of DNA-AgNCs. **(A)** Homo-polyC sequence for the detection of p53 gene mutation based on fluorescence quenching. Reprinted by permission from Springer Nature Customer Service Centre GmbH: Springer, Journal of Fluorescence, from [127], 2017. **(B)** Chemopalette sequence for the multiplexed analysis of target DNA based on fluorescence emission colour change. Republished with permission of John Wiley and Sons, from [130]; permission conveyed through Copyright Clearance Center, Inc. **(C)** DNA hairpin loop-bound AgNCs for the detection of Hg^{2+} based on switch-off mechanism upon Hg^{2+} interaction. Adapted from [131]. **(D)** NCBs reported a 500-fold fluorescence enhancement when a G-rich enhancer probe hybridises with a dark AgNCs nucleation (NC) probe. Reprinted with permission from [138]. Copyright 2010 American Chemical Society.

The reported HCR-AgNCs biosensors in this thesis emphasise on the use of homo-polyC and chemopalette AgNCs templating sequences, and primarily focuses on the concept of proximity-dependent AgNCs (*i.e.*, chameleon and NCBs).

2.5 HCR-AgNCs biosensors

2.5.1 Principles of HCR-AgNCs biosensors

As introduced earlier, HCR-based biosensors hold remarkable potential in the field of diagnostics but have their own limitations, from the aspects of design, operating condition, and application. DNA-AgNCs can be integrated as signal transducers in HCR systems to overcome some of these limitations, and simultaneously enhance the diagnostic potential in a hybrid HCR-AgNCs biosensor **(Scheme 2.3)**. HCR-AgNCs biosensors measure the transduced AgNCs signal (fluorescence and/or electrochemical), as the DNA hairpins undergo structural changes during HCR amplification. Since both HCR and AgNCs share the same DNA material, AgNCs can be introduced into a HCR system with the simple addition of a AgNCs templating sequence into the DNA hairpin probes. The isothermal mild reaction conditions for HCR amplification provides an ideal stable and compatible environment for AgNCs preparation, considering the fact that AgNCs is highly sensitive to their microenvironment (*e.g.*, temperature, pH, ionic strength, etc.). In addition, AgNCs bind with high affinity towards specific AgNCs templating sequences, hence their formation will not affect HCR amplification efficiency [102,103]. Having said that, HCR-AgNCs biosensors can provide accurate, sensitive and reproducible measurement during analyte detection.



Scheme 2.3 Schematic diagram showing the basic HCR-AgNCs biosensor assembly. DNA hairpins serve as bioreceptor to recognise different target analytes (DNA, RNA, protein, ions, etc.), and for HCR signal amplification. AgNCs will be prepared thereafter for signal

(*i.e.*, fluorescence or electrochemical) transduction and measurement.

2.5.2 Designing HCR-AgNCs biosensors

HCR-AgNCs biosensors function with DNA hairpins, similar to conventional HCR systems introduced in **Section 2.3**, with the inclusion of a specific AgNCs templating sequence into the hairpin structure. These AgNCs templating sequences are normally laden with C and G bases, not to mention that the length of these sequences would range between 6 and 18 bases, as seen in **Section 2.4**. In other words, the design of HCR-AgNCs hairpins would defy most of the DNA hairpin metastability guidelines listed in **Table 2.2**.

In view of the lack of HCR-AgNCs hairpin design guidelines, several key factors have to be considered for a functional HCR-AgNCs system. A great deal of reported HCR-AgNCs hairpins contain AgNCs templating sequences either at the toehold or loop segment. For the former, the AgNCs templating sequence can be adopted as an extension of the 1^{o} toehold [156], or as an independent 2^{o} toehold [11]. As a result, the HCR products would contain tails for AgNCs formation. Based on the guidelines mentioned earlier, tails on dsDNA might impede the hybridisation efficiency of incoming DNA sequences [65]. Likewise, C-rich hairpin loops can accommodate AgNCs, as discussed earlier in **Section 2.4.4.3**. The resultant signal is normally quenched in fluorescence-based sensors [157], and enhanced in electrochemical sensors *via* HCR amplification [158].

Apart from that, the initiation of HCR amplification should be optimised, be it toehold- or loop-mediated hairpin openings. The former hairpin opening mechanism is favoured in most HCR-AgNCs biosensors [11,159], because of its more established and straightforward design, in addition to a quicker reaction time (by two magnitudes) as opposed the latter. However, the HCR-AgNCs biosensor by Jiang *et al.* featured loop-mediated opening mechanism, where the toehold segments were fully utilised for AgNCs templating sequences. This enabled a highly sensitive ratiometric response for miR-17-5p detection, at the expense of short HCR incubation period [160].

Certain HCR-AgNCs studies utilise more than two DNA hairpins for target detection, and these additional DNA molecules are normally termed assistive or capture probes. Capture probes link a target analyte to the main HCR system *via* an additional hybridisation stage

with partial or complete base-pairing. The additional probes confer better HCR amplification efficiency and stabilisation of the HCR product [75,158,159,161,162].

Overall, the design of HCR-AgNCs hairpins is more complicated than typical DNA hairpins, with the inclusion of AgNCs templating sequences. Moreover, there are insufficient HCR-AgNCs studies to properly develop systematic guidelines to integrate AgNCs templating sequences into DNA hairpins, let alone balance between hairpin metastability and HCR amplification efficiency.

2.5.3 Factors affecting HCR-AgNCs performance

Besides the DNA hairpin structure, the performance of HCR-AgNCs can be further regulated *via* reaction conditions. Reported HCR-AgNCs biosensors operate on selected isothermal conditions, within a temperature range between room temperature (20-25 ^{o}C) and 37 ^{o}C [156,163]. This narrow range provides the DNA hairpins with sufficient energy to overcome the energy barrier and initiate HCR amplification, without destabilising the dsDNA product. The DNA hairpins are incubated for a fixed period of time, ranging from 1 hour (h) to overnight incubation [164,165]. The duration of incubation is a subjective measure, as it relative to the hairpin design and mechanism of the respective HCR-AgNCs biosensors.

The microenvironment for HCR amplification is compatible for AgNCs formation. HCR-AgNCs biosensors reported the use of different buffer base (tris, phosphate, etc.), but relatively similar pH (neutral to slightly alkaline) and the common addition of Na^{+} and/or Mg^{2+} salts [75,165]. Nevertheless, the concentration of both the buffer base and metal salts were not fixed across the reported studies, which resulted in different fluorescence properties even for the same AgNCs templating sequence. This was shown in a single study by Orbach *et al.*, where high-salt (containing both Mg^{2+} and Na^{+}) buffer produced yellow fluorescence emission and low-salt (containing only Mg^{2+}) produced red fluorescence emission, from a common 6C DNA hairpin loop [164].

Most of the reported HCR-AgNCs studies utilise equimolar concentrations of DNA hairpins. There have been a few exceptions, where the amount of H2 would be higher than that of H1, without any justification to the concentration differences [157,165]. Another condition to optimise is the concentration of DNA hairpin containing the AgNCs templating

sequence with respect to the concentration of Ag^+ and $NaBH_4$ during AgNCs preparation. This is due to the fact that even when the same AgNCs templating sequences were used, the deviation in AgNCs preparation condition can generate significant differences in the fluorescence [11–13].

In most HCR-AgNCs studies, AgNCs were prepared post-HCR amplification for signal transduction [157,166]. The reason behind this approach is to prevent undesired Ag^+ binding towards consecutive C and G bases, apart from those in the AgNCs templating sequences. This action could block the bases required for DNA hybridisation and impede HCR amplification efficiency.

2.5.4 Application of HCR-AgNCs biosensors

In this section, several reported HCR-AgNCs biosensors will be reviewed, with respect to the location of AgNCs templating sequences and the innovative biosensing mechanisms.

Almost half of the reported HCR-AgNCs sensors consolidated AgNCs templating sequences at the DNA hairpin toehold region, either as extension of the 1^o and/or as adjacent 2^o toeholds. The selection of the AgNCs templating sequence would mostly be homo-polyC sequences. Zhang and co-workers integrated 12C AgNCs templating sequences onto the toeholds of both DNA hairpins for the detection of HIV DNA, with the assistance of GO **(Figure 2.5A)** [13]. Chemopalette sequences were used as terminal toehold AgNCs templating sequences as well. Jiang *et al.* constructed a HCR-AgNCs fluorescence logic gate by introducing a chemopalette sequence (-*CCC CCT AAT TCC CCC*-) at the toehold of one of the DNA hairpins, to detect telomerase miRs [156].

HCR-AgNCs biosensors with hairpin loops containing AgNCs templating sequences are also common in both electrochemical- and fluorescence-based biosensors [158]. Fluorogenic AgNCs templating loops focus on fluorescence quenching as the DNA hairpin loop sequence actively participate in HCR amplification. As a matter a fact, Qiu *et al.* did a study on the fluorescence properties of hairpin loops, and found that the resultant fluorescence intensity decreased with shorter hairpin stem length [157]. This finding could help optimise future designs of DNA hairpins with AgNCs templating loops. For instance,

Mansourian *et al.* utilised HCR-AgNCs templating loop to successfully detect plasma miR-145 in clinical samples, with minimal sample preparation **(Figure 2.5B)** [165].

Interestingly, AgNCs templating sequence can also be located at the stem region. Orbach *et al.* incorporated a 6C bulge at the stem of the DNA hairpin, which facilitated the detection of two different DNA targets [164]. The 6C bulge carries similar fluorescence properties as hairpin loops [167,168]. Meanwhile, Zhang *et al.* embedded part of a chemopalette sequence (-*CCC ACC CAC CC*-) within the DNA stem that can host near-IR emitting AgNCs when the DNA hairpin opens during HCR amplification for miR-21 detection **(Figure 2.5C)** [166]. However, the low number of stem-based HCR-AgNCs studies can be attributed to the challenge and complexity of maintaining good DNA hairpin metastability. Since hairpin stems are primarily responsible for stability, any variations (bulge, unbounded sequences, etc.) along the sequence can disrupt the ΔG from base-pairing and stacking, thereby destabilising the hairpin and dsDNA structure.

There have been two reported HCR-AgNCs biosensors that emphasised on proximity-dependent AgNCs designs. Liu *et al.* worked on a traditional NCB design with a dark AgNCs templating strand and a G-rich enhancer sequence. In this study, four DNA hairpins were used, whereby the AgNCs templating strand and enhancer sequence were located on two different DNA hairpins. HCR amplification would bring these sequences into close proximity and activate an intense red fluorescence, which was used to detect a mRNA target **(Figure 2.5D)** [169]. The ratiometric fluorescence HCR-AgNCs biosensor reported by Jiang *et al.* was constructed with two similar chemopalette sequence (-*CCC CCT TAA TCC CCC*-) as the terminal toeholds (1^o and 2^o) of one DNA hairpin species. When these AgNCs templating sequences are in close proximity, they collectively emit a red emission. When these are separated upon HCR amplification, the fluorescence emission changes to yellow, thus enabling ratiometric detection of miR-17-5p from the changes in fluorescence emissive species [160]. The concept of proximity-dependent AgNCs is an underexplored area due to the difficulty in designing stable DNA hairpins for HCR amplification. Along with a AgNCs templating sequence, an enhancer (G-rich, emitter-pair, etc.) sequence is required, and this is equally long and laden with C and G bases. Following that, it is also crucial to corroborate the mechanism of bringing the two separate strands together post-HCR amplification for signal activation.

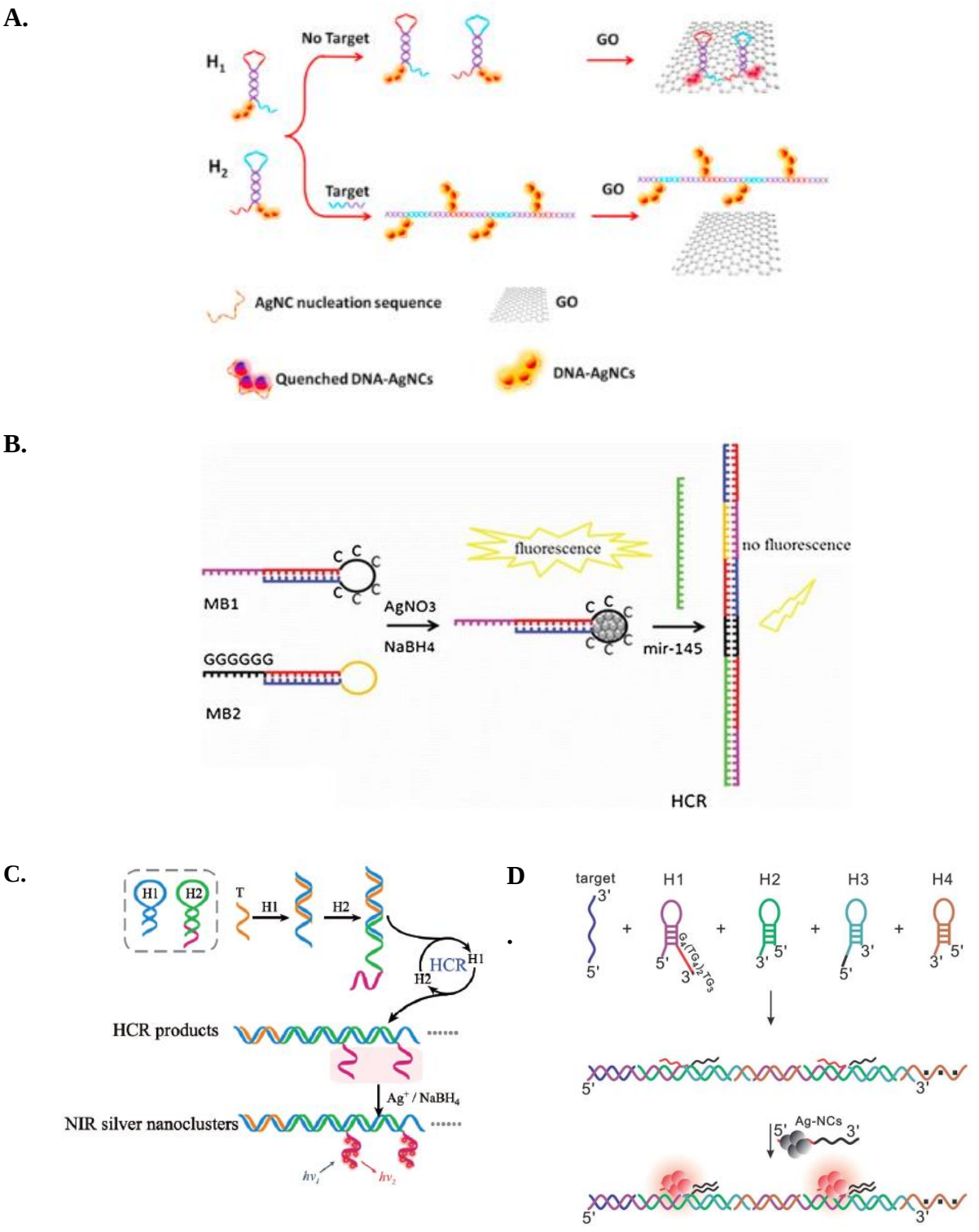


Figure 2.5 Reported HCR-AgNCs biosensors with differentially located AgNCs sites. **(A)** The detection of HIV DNA was performed *via* HCR-AgNCs with homo-polyC 2º toeholds and GO. Reprinted from [13], Copyright 2017, with permission from Elsevier. **(B)** Fluorescence from AgNCs templating loops is quenched by HCR amplification in the presence of target miR-145. Reprinted by permission from Springer Nature: Springer, Journal of Fluorescence, [165], 2017. **(C)** The AgNCs templating sequence partially embedded in DNA hairpin stems, will open for AgNCs formation after HCR amplification in the presence

of target miR-21. Adapted from [166]. **(D)** Four-hairpin HCR-AgNCs system to initiate proximity-dependent G-rich enhancement after HCR amplification in the presence of target mRNA. Republished with permission of Royal Society of Chemistry, from [169]; permission conveyed through Copyright Clearance Center, Inc.

Given the linear nature of HCR amplification, several HCR-AgNCs biosensors have been supplemented with additional components to improve their overall performance (*i.e.*, sensitivity and specificity). A familiar approach is the introduction of enzymatic activity into HCR-AgNCs designs, namely with DNA polymerase and nicking endonuclease. Enzymatic activity adds another amplification cycle in addition to HCR amplification. For instance, the HCR-AgNCs biosensor by Chen *et al.* featured a secondary autocatalytic strand displacement amplification for DNA target recycling, and achieved sub-femtomolar LOD [158]. This strategy has also been reported in other HCR-AgNCs studies with sub-femtomolar LOD for the detection of Dam MTase [161], mucin 1 [12], and miR-199a [75]. Nonetheless, the use of enzymes complicates the sensing platform by adding more components in an already sensitive HCR-AgNCs system, and additional cumbersome steps to remove the enzymes (*e.g.*, heat inactivation and washing).

External components, namely GO, have been capitalised in multiple HCR-AgNCs studies to minimise background fluorescence from unreacted hairpins [12,13,156]. GO has been known to be an effective nano-quencher for AgNCs fluorescence, due to long-range resonance energy transfer. DNA hairpins can reportedly adsorb onto GO at their toeholds and loops, *via* π–π stacking [75]. Upon recognising a target *via* hairpin toehold, the DNA hairpins can easily detach from GO due to the weak binding interaction, for HCR amplification and subsequent AgNCs formation. While this may be an appealing approach, the reaction condition has to be further regulated because high-salt conditions and certain components in biological samples may coagulate GO, thereby disrupting the performance of HCR-AgNCs biosensors [170,171].

Thus far, there have only been a total of 17 HCR-AgNCs studies conducted since 2013 [172]. These studies include both electrochemical- and fluorescence-based assays, and focus on the detection of different target analytes, and nucleic acids (DNA, RNA). **Table 2.3** summarises the reported HCR-AgNCs studies, detailing the DNA hairpin structures, AgNCs templating sequences, and reaction conditions for both HCR amplification and AgNCs formation.

Table 2.3 Reported HCR-AgNCs biosensors.

Type	Target	AgNCs templating sequence and location	AgNCs preparation	HCR condition	DNA hairpin structure	Reference
Electrochemical	P53 exon8 DNA	Hairpin loop: CCC CCC CCC CCC	0.5 μM H1/H2 10 μL 100 μM Ag^+ 2 μL 500 μM $NaBH_4$ Incubation condition: 1 h, room temperature	Buffer condition: 10 mM tris-HCl, 500 mM Na^+, 1 mM Mg^{2+} pH 7.4 Reaction condition: 2.5 h, room temperature	<u>H1 and H2</u> 8 base toehold 9 bp stem 12 base loop	[158]
Electrochemical	Dam MTase	ssDNA: CCC CCC CCC CCC	2 μM H1/H2 10 μL 200 μM Ag^+ 8 μL 500 μM $NaBH_4$ Incubation condition: 2 h	Buffer condition: 20 mM tris-HCl, 140 mM Na^+, 5 mM Mg^{2+} pH 7.4 Reaction condition: 70 minutes (min), 37 ^oC	Non-hairpin ssDNA	[161]
Fluorescence	Cell surface glycans	Hairpin toehold: CCC CCC CCC CCC	10 mM Ag^+ 2 mM $NaBH_4$ DNA: Ag^+: $NaBH_4$ 0.5: 10: 10 Incubation condition: 5 h, 4 ^oC	Buffer condition: 20 mM phosphate buffer, 1 mM Mg^{2+} pH 7.4 Reaction condition: 2 h, 25 ^oC	<u>H1</u> 5 base 1^o toehold 16 base 2^o toehold 16 bp stem 6 base loop <u>H2</u> 11 base 1^o toehold	[11]

					15 bp stem 6 base loop	
Fluorescence	miR-17-5p	Hairpin toehold: CCC CCT TAA TCC CCC	DNA: Ag^{+}: $NaBH_4$ 1: 10: 10 Incubation condition: 3 h, in dark	Buffer condition: 200 mM phosphate buffer pH 7.4 Reaction condition: 4 h, room temperature Side note: 3-hairpin system	<u>H1</u> 12 bp stem 29 base loop <u>H2</u> 28 base 1^{o} toehold 21 base 2^{o} toehold 12 bp stem 6 base loop <u>H3</u> 12 bp stem 12 base loop	[160]
Fluorescence	Mucin 1	Hairpin toehold: CCC CCC CCC CCC	1 μL 100 μM H1/H2 10 μL 60 μM Ag^{+} 10 μL 60 μM $NaBH_4$ Incubation condition: 1 h, in dark	Buffer condition: 20 mM tris-HNO_3, 50 mM K^{+}, 10 mM Mg^{2+}, 1 mM DTT pH 7.9 Reaction condition: 1 h, 37 ^{o}C	<u>H1 and H2</u> 12 base 1^{o} toehold 12 base 2^{o} toehold 15 bp stem 12 base loop	[12]
Fluorescence	miR-21	Hairpin stem: CCC ACC CAC CC	10 μL 10 μM H2 2.4 μL 0.5 mM Ag^{+}	Buffer condition: 10 mM HEPES, 200 mM	<u>H1</u> 8 base toehold	[166]

			2.4 μL 0.25 mM $NaBH_4$ Incubation condition: 4 h	Na^+ pH 7.2 Reaction condition: 2 h, room temperature	18 bp stem 10 base loop <u>H2</u> 6 base 1^o toehold 8 base 2^o toehold 24 bp stem 8 base loop	
Fluorescence	miR-145	Hairpin loop: CCC CCC	32.4 μL 100 μM DNA 32.4 μL 1 mM Ag^+ 32.4 μL 1 mM $NaBH_4$ Incubation condition: 1 h, room temperature	Buffer condition: 20 mM phosphate buffer, 1 mM Mg^{2+} pH 7 Reaction condition: 1 h, 37 ^oC Side note: Non-equimolar DNA hairpins used; 3 μM H1, 6 μM H2	<u>H1 and H2</u> 6 base toehold 17 bp stem 6 base loop	[165]
Electrochemical Electrochemi-luminescence	Thrombin	Hairpin loop: C-rich	1 μM H1/H2 8 μL 200 μM Ag^+ 5 μL 500 μM $NaBH_4$ Incubation condition: 2 h, room temperature, in	Buffer condition: 10 mM tris-HCl, 1 mM EDTA, 12.5 mM Mg^{2+} pH 7.4 Reaction condition:	Unspecified	[162]

			dark	2 h, 37 ^{o}C		
Fluorescence	HIV DNA	Hairpin toehold: CCC CCC CCC CCC	DNA: Ag^{+}: $NaBH_4$ 0.1: 0.6: 0.6 Incubation condition: 2 h, room temperature, in dark	Buffer condition: 10 mM phosphate buffer 100 mM Na^{+} 5 mM Mg^{2+} pH 7.5 Reaction condition: 4 h, room temperature	<u>H1</u> 15 base 1^{o} toehold 12 base 2^{o} toehold 16 bp stem 10 base loop <u>H2</u> 10 base 1^{o} toehold 12 base 2^{o} toehold 16 bp stem 15 base loop	[13]
Fluorescence	let-7	Hairpin loop: CCC CCC	DNA: Ag^{+}: $NaBH_4$ 1: 10: 10 Incubation condition: 5 h, room temperature	Buffer condition: 20 mM phosphate buffer, 1 mM Mg^{2+} pH 7 Reaction condition: 1 h, 37 ^{o}C Side note: Non-equimolar DNA hairpins used; 4 μM H1, 8 μM H2	<u>H1 and H2</u> 6 base toehold 16 bp stem 6 base loop	[157]

Electrochemical	Lysozyme	Hairpin toehold: CCC CCC CCC CCC	DNA: Ag^+: $NaBH_4$ 1: 6: 6 Incubation condition: 1 h, 4 ^oC, in dark	Buffer condition: 50 mM PBS pH 7.4 Reaction condition: 10 h, 35 ^oC	<u>H1</u> 6 base toehold 14 bp stem 4 base loop <u>H2</u> 12 base toehold 14 bp stem 4 base loop	[159]
Electrochemical	miR-199a	Hairpin loop: CCC CCC CCC CCC	0.5 μM DNA 10 μL 100 μM Ag^+ 2 μL 500 μM $NaBH_4$ Incubation condition: 2 h, room temperature, in dark	Buffer condition: 10 mM tris-HCl, 500 mM Na^+, 1 mM Mg^{2+} pH 7.4 Reaction condition: 2 h, room temperature	<u>H1</u> 8 base toehold 9 bp stem 12 base loop <u>H2</u> 11 base 1^o toehold 3 base 2^o toehold 6 bp stem 12 base loop	[75]
Fluorescence	mRNA	AgNCs templating sequence (external DNA template): CCC TTA ATC CCC Enhancer (hairpin toehold):	DNA: Ag^+: $NaBH_4$ 15: 90: 90 Incubation condition: 18 h, room temperature, in dark	Buffer condition: 50 mM phosphate buffer, 500 mM Na^+, 50 mM Mg^{2+} pH 6.8 Reaction condition:	<u>H1</u> 6 base 1^o toehold 24 base 2^o toehold 18 bp stem 6 base loop <u>H2 and H4</u>	[169]

		GGG TGG GGT GGG GTG GGG		4 h, 37 °C Side note: 4-hairpin system	6 base toehold 18 bp stem 6 base loop <u>H3</u> 34 base toehold 19 bp stem 4 base loop	
Fluorescence	DNA	Hairpin stem: CCC CCC	DNA: Ag^{+}: $NaBH_4$ 1: 3: 3 Incubation condition: 5 h	Buffer condition: **High-salt** 10 mM phosphate buffer, 200 mM Na^{+}, 1 mM Mg^{2+} pH 7.0 **Low-salt** 20 mM phosphate buffer, 1 mM Mg^{2+} pH 7.0 Reaction condition: Overnight incubation, room temperature	**High-salt** <u>H1</u> 9 base toehold 20 bp stem 7 base loop <u>H2</u> 9 base toehold 21 bp stem 6 base bulge 5 base loop **Low-salt** <u>H1</u> 8 base toehold 19 bp stem 8 base loop <u>H2</u>	[164]

					8 base toehold 21 bp stem 6 base bulge 4 base loop	
Electrochemical	Uranyl ion	Hairpin stem: Unspecified	0.5 μM DNA 5 μL 5 mM Ag^{+} 10 μL 12.5 mM $NaBH_4$ Incubation condition: 50 min, in dark	Buffer condition: Unspecified Reaction condition: 1.5 h, 35 ^{o}C	<u>H1 and H2</u> 6 base toehold 14 bp stem 6 base loop	[173]
Fluorescence	Telomerase miR	Hairpin toehold: CCC CCT AAT TCC CCC	DNA: Ag^{+}: $NaBH_4$ 1: 7: 7 Incubation condition: 3 h, 4 ^{o}C, in dark	Buffer condition: 20 mM tris-HCl, 1.5 mM Mg^{2+}, 63 mM K^{+}, 10 mM dNTPs, 0.05% Tween 20, 1 mM EGTA pH 8.3 Reaction condition: 2 h, 37 ^{o}C	<u>H1</u> 6 base toehold 8 bp stem 14 base loop <u>H2</u> 27 base toehold 8 bp stem 6 base loop	[156]
Electrochemical	miR-155	AgNCs templating sequence (hairpin toehold): CCT CCT TCC TCC Enhancer (hairpin	<u>Electrochemical deposition</u> 10 μL 1 mM Ag^{+} 1 h 0 to -1.35V 100 mV.s-1	Buffer condition: 20 mM tris, 1.0 mM Mg^{2+}, 1.0 mM Ca^{2+}, 140 mM Na^{+}, 5 mM K^{+} pH 7.4	<u>H1</u> 13 base toehold 13 bp stem 9 base loop <u>H2</u>	[163]

	toehold): TTT TTT TTT TTT TTT	Reaction condition: 2 h 20 min, room temperature Side note: 3 hairpin-system	18 base toehold 13 bp stem 6 base loop <u>H3</u> 6 base 1^o toehold 12 base 2^o toehold 14 bp stem 4 base loop

2.5.5 Limitations of HCR-AgNCs biosensors

The research advancement of HCR-AgNCs as a biosensor has been appealing thus far. However, HCR-AgNCs biosensors are still a relatively new detection strategy with their own limitations. Firstly, the reported HCR-AgNCs systems lack the systematic guidelines to effectively design DNA hairpin probes with AgNCs templating sequences (Table 2.3). The different approaches to design hairpin structures led to variations of hairpin size and corresponding signal output. Additionally, the reported HCR-AgNCs systems have different reaction conditions, such as the HCR incubation conditions (i.e., temperature and duration), AgNCs preparation (i.e., incubation condition and reactant concentrations), and the reaction buffers used. Besides that, there is a lack of correlation between the reported HCR-AgNCs biosensors. Even with the same AgNCs templating sequence (*i.e.*, 6C loop), different fluorescence emission properties have been reported, which highlights the insufficient knowledge on the molecular interactions of AgNCs in HCR systems [157,165].

Despite the simple preparation and mechanism of both HCR and AgNCs, the reported HCR-AgNCs biosensors require a relatively long incubation period (i.e., ranging from several hours to overnight incubation, some of which might not be comparable to current miR detection techniques such as RT-qPCR) and limiting conditions (i.e., 4^{o}C incubation for AgNCs preparation), which might not be practical for clinical applications and POCT (Table 2.3). In addition, most of the reported HCR-AgNCs biosensors have limited sensitivity, typically within the nM range [13]. These limitations could be due to the complex mechanism and hairpin probe designs of corresponding HCR-AgNCs systems.

These limitations make it challenging for HCR-AgNCs biosensors to fully realise their biosensing capabilities and applications, thereby deterring further research and development of HCR-AgNCs systems. This thesis addressed most of these limitations with simpler designs and enhancement features, all of which are covered in detail over the next section (Section 2.6) and chapters (Chapters 3, 4, and 5).

2.6 Future direction of HCR-AgNCs biosensors

The potential to expand the field of HCR-AgNCs biosensors is aplenty, and focus can be directed towards improving either the individual aspects of HCR and AgNCs respectively, or the entire HCR-AgNCs system.

HCR amplification has seen several modifications over the years. An interesting take is the concept of branched HCR amplification. This approach exponentially amplifies signals, by crosslinking DNA hairpin probes to form a network of DNA [76,92,174–179]. More than two DNA hairpins are used in this case, and their design would have two terminal toeholds for the branching to occur. This can be challenging to translate into branched HCR-AgNCs biosensors. Based on the current designs, AgNCs templating strands are mainly introduced at the terminal toehold or loop region, which will require significant thought process to integrate into branched HCR-AgNCs biosensors. It is possible to introduce AgNCs in the stem region whereby AgNCs can intercalate between the dsDNA strands [180–187], or having AgNCs as an external system. The former would require careful design of the DNA hairpin probes to ensure stability and feasibility of both HCR amplification and AgNCs fluorescence. The latter would be more straightforward and can be easily integrated into a stable branched HCR network. In **Chapter 4**, the possibility of integrating AgNCs as an external signal transducer into a linear HCR system will be explored in detail.

When it comes to fluorogenic AgNCs, the AgNCs templating sequence plays a crucial role. **Section 2.5.4** evaluated the different AgNCs templating sequences utilised in HCR-AgNCs biosensors, such as C-rich ssDNA, C-rich hairpin loops, and chemopalette sequences, as well as the concept of proximity-dependent AgNCs (*i.e.*, NCBs and chameleon AgNCs). Alternative AgNCs templating sequences that have yet to be tested in HCR-AgNCs biosensors include intercalation within dsDNA structure (gaps, abasic, mismatch sites, etc.) [181–187], or secondary structure scaffolds like g-quadruplex [188,189]. Despite the coinciding factor of introducing AgNCs in HCR dsDNA structures, the addition of specific sites would be difficult to design for DNA hairpins. A missing bp can disrupt the energy balance of DNA hairpins, not to mention the lack of studies implementing dsDNA-AgNCs. On the other hand, G-quadruplex could be integrated into HCR-AgNCs biosensors. From a collection of studies, G-quadruplex can be formed from G-rich sequences located as split pairs at the terminal toeholds of DNA sequences, or in a large loop [190–196]. The DNA hairpin design processed would be challenged as the former would introduce tremendous

steric effect from the hanging tails on HCR products, whereas the latter introduces numerous mismatch sequences in a relatively large loop sequence. Either way, these have to be factored into consideration to maintain the efficiency of HCR amplification, and DNA hairpin stability. In another perspective, principles like NCBs and chameleon AgNCs can be introduced in a different manner. This was shown in the HCR-AgNCs studies by Liu *et al.* with a 4-hairpin system, and Jiang *et al.* with loop-mediated DNA hairpin opening and the use of two AgNCs templating sequences [160,169]. In **Chapter 3**, the possibility of introducing chameleon AgNCs with the addition of a single short AgNCs templating sequence will be explored for the ratiometric fluorescence miR detection.

Finally, conventional HCR-AgNCs biosensors solely emphasise on linear amplification, which limits their performance (*i.e.*, sensitivity and specificity). Several modifications that reported overall performance enhancement were described in **Section 2.5.4**, such as the use of enzymatic activity and external elements (*e.g.*, GO) [13,158]. These add-ons resulted in HCR-AgNCs biosensors with better sensitivity, shorter reaction time, and lower background signal. Likewise, in **Chapter 5**, the possibility of integrating a magnetic component into HCR-AgNCs biosensors will be explored, and its application validated to exclude the tedious process of purifying and extracting analytes from a complex matrix.

Chapter 3: Development of a ratiometric fluorescence HCR-AgNCs biosensor for miR detection

3.1 Overview

This chapter explores the possibility of developing a HCR-AgNCs biosensor that functions with ratiometric fluorescence analysis, to detect miR-155. Ratiometric detection has known to produce better sensitivity and reliability based on its internal calibration from the changes between two signal intensities. However, this is rarely applied in modern biosensors, let alone HCR-AgNCs systems. In this work, stable ratiometric HCR-AgNCs biosensor is designed, by tailoring a specific AgNCs templating sequence with an adjacent C-rich sequence at the DNA hairpin toehold segment, for a proximity-dependent AgNCs fluorescence response. The working principle is based on the influence of microenvironment towards the hosted AgNCs, whereby unfolding the DNA hairpin upon HCR manipulates the distance between the AgNCs templating and C-rich sequence at the DNA hairpin toehold, thereby switching its fluorescence response accordingly. The results indicate the feasibility and stability of the proposed HCR-AgNCs biosensor, with a red-yellow dual-emissive fluorescence response. The dominant emission of AgNCs changes from red to yellow in the presence of miR-155, thereby enabling a ratiometric measurement of miR-155 with high sensitivity and selectivity. The LOD of the HCR-AgNCs biosensor is 1.13 fM in buffered solution, and a comparable LOD of 1.58 fM in human serum. At the end of the chapter, the findings are summarised to show the potential of translating the ratiometric HCR-AgNCs biosensor for clinical application.

3.2 Background

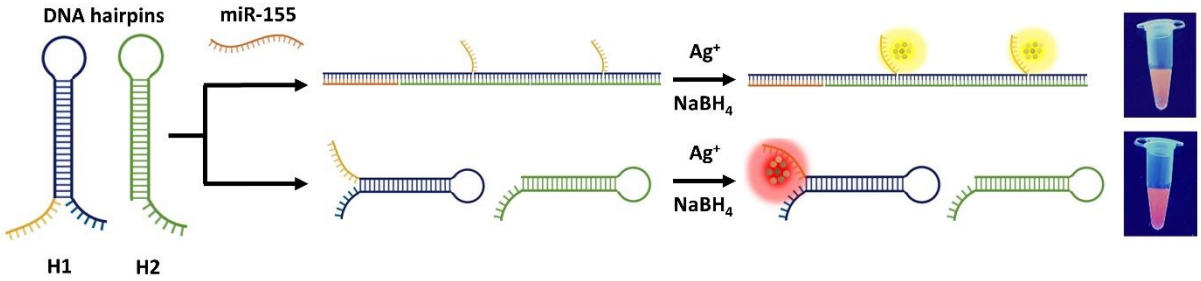
Fluorescence-based biosensors have gained relative traction for their high sensitivity, selectivity and simple operation [197–199], but a majority of these work through the changes of a single emission signal response. As a result, minor fluctuations in the system (*i.e.*, probe concentration, microenvironment) and systematic errors can cause significant variations in the signal response [200,201]. Ratiometric fluorescence detection can circumvent some of these problems. In principle, ratiometric sensors are designed with fluorescent probes that

undergo a stimuli-dependent emission wavelength shift upon excitation, whereby the fluorescence intensity is expected to decrease at one emission wavelength and concurrently increase at the other emission wavelength. Thus, by calculating the ratio of the intensity differences between the two emission wavelength regions, a highly accurate, precise, and sensitive analysis of a target can be achieved. In contrast to the mere intensity change of conventional fluorescence sensors, the signal enhancement ratio of ratiometric sensors relays an internal calibration of the fluorescent probes, thereby minimising any bias errors in the system and increasing the reliability of the measurements [132,144,202–205]. This concept has been adopted for various sensing, imaging and biomedical applications [206–210]. For instance, Luo *et al.* utilised two different fluorophores, Cy3 and Cy5, to detect mitochondrial ATP in living cells. ATP initiates fluorescence resonance energy transfer between Cy3 and Cy5, resulting in an emission wavelength shift from green to red fluorescence response, and this was used for ratiometric measurement [211]. Ratiometric sensing can be applied with DNA-AgNCs as well. Del Bonis-O'Donnell *et al.* identified two AgNCs templating sequences that emit green and red fluorescence respectively. When dopamine was added with these sequences, the green emission would sustain, whereas the red emission would be quenched. These changes enabled ratiometric detection of dopamine, with the potential for real-time monitoring in vivo [212]. With regards to HCR-AgNCs biosensors, Jiang *et al.* reported a HCR-AgNCs ratiometric biosensor, where the emission colour of AgNCs changed in the presence of target miR, even in a complex solution [160]. The dual-emissive species of AgNCs relies on the proximity of two identical AgNCs templating sequences at the DNA hairpin toehold, such that HCR amplification would separate the strands for a strong yellow emission. However, the reported design presented numerous discrepancies (*i.e.*, different hairpin structure and hairpin opening mechanism), which undermined its reliability and reproducibility.

In **Section 2.2.1**, miRs were introduced as diagnostic and prognostic biomarkers that have good stability in human blood and serum, and that their expression is dysregulated on the onset and progression of diseases [213–215]. The challenges faced current miR detectors (*i.e.*, tedious miRs extraction process, operational costs, and quality control) and the demand for alternative detection strategies, were highlighted in **Section 2.2.2** [216]. Herein, a ratiometric HCR-AgNCs biosensor is developed, with miR-155 as the model target. MiR-155 is a potential non-invasive biomarker of breast cancer and has reported significantly increased expression levels in breast cancer patients as compared to healthy individuals. The relative

serum miR-155 expression levels correlate to the progression of breast cancer (*i.e.*, tumour grade, stage, and size) in patients. MiR-155 has also shown a reduced expression post-surgery/chemotherapy, thereby highlighting its role to measure treatment response. Hence, the detection of circulating miR-155 expression is crucial to facilitate the diagnosis and prognosis assessment of early-stage breast cancer [217–220].

Scheme 3.1 outlines the functionality of the proposed HCR-AgNCs biosensor to detect miR-155, with two DNA hairpins (*i.e.*, H1 and H2). H1 was designed as the fluorescent probe with both AgNCs templating sequence and a C-rich sequence at its toehold segment. When miR-155 is introduced, HCR amplification is initiated between the two DNA hairpins (*i.e.*, H1 and H2) to yield a long nicked dsDNA product. Subsequent preparation of AgNCs will yield AgNCs on the extended tail from the HCR product, and this generates an intense yellow fluorescence signal. Without miR-155, AgNCs will be caged in the DNA hairpin toehold region and produce an intense red fluorescence signal. By measuring both the intensities of yellow fluorescence (F_y) and red fluorescence (F_r) at any given time, ratiometric measurements (F_y/F_r) of miR-155 can be determined.



Scheme 3.1 Outline of ratiometric HCR-AgNCs biosensor for the detection of miR-155.

3.3 Methodology

3.3.1 Materials

Silver nitrate ($AgNO_3$) and sodium borohydride ($NaBH_4$) were purchased from Nacalai Tesque (Kyoto, Japan). Tris ($(HOCH_2)_3CNH_2$) was purchased from Apical Scientific (Selangor, Malaysia). Acetic acid (CH_3COOH) was purchased from R&M Chemicals (Selangor, Malaysia). Magnesium nitrate ($Mg(NO_3)_2$) was purchased from Fisher Scientific (New Hampshire, USA). Other reagents were of analytical grade and used without further

purification. All solutions used throughout the experiments were prepared in ultrapure water (18 MΩ.cm).

All DNA and RNA samples were of desalted grade and purchased from Integrated DNA Technologies (IDT) (Iowa, USA). The sequences of miR-155 and non-target controls were adapted from www.mirbase.org. The sequences are listed in **Table 3.1**. All mismatch and non-target sequences used in this study were DNA analogues in place of their RNA counterparts, for cost-effectiveness, stability, and ease of handling. Prior to usage, the DNA oligonucleotides were dissolved in molecular grade water to obtain stock concentrations of 100 μM. MiR-155 was dissolved in DEPC-treated water to obtain stock concentration of 100 μM.

Table 3.1 Oligonucleotide sequences used in this work. Red letters indicate AgNCs templating sequence. Italicised letters indicate hairpin stem region. Bold letters indicate hairpin loop. Underlined letters indicate mismatch base(s).

DNA/RNA	Sequence (5' – 3')
H1	AAC CCC *TAT CAC GAT TAG CAT TAA G***GC TA***C TTA ATG CTA ATC GTG ATA* TTT ACC CAC CCA
H2	*TTA ATG CTA ATC GTG ATA* **GGG GTT** *TAT CAC GAT TAG CAT TAA* GTA GCC
miR-155	UUA AUG CUA AUC GUG AUA GGG GUU
mismatch 1	TTA ATG CTA ATC GTG ATA GGC GTT
mismatch 2	TTA ATG CTA ATC CTG ATA GGC GTT
mismatch 3	TTA ATG GTA ATC GTC ATA CGG GTT
miR-10b	TAC CCT GTA GAA CCG AAT TTG TG
miR-21	TAG CTT ATC AGA CTG ATG TTG A
miR-29b	TAG CAC CAT TTG AAA TCA GTG TT
miR-125b	TCC CTG AGA CCC TAA CTT GTG A
miR-145	GTC CAG TTT TCC CAG GAA TCC CT

3.3.2 Design of DNA oligonucleotides

Based on the sequence of miR-155, H1 and H2 were designed using NUPACK (http://www.nupack.org), OligoAnalyser Tool

(https://sg.idtdna.com/pages/tools/oligoanalyser), and Kinetics Calculator (http://nablab.rice.edu/nabtools/kinetics.html).

3.3.3 MiR-155 detection in buffer

DNA hairpins, H1 and H2, were heated at 95°C for 5 min and snap-cooled in an ice bath for 30 min before use, to ensure that the DNA probes fold into their most stable hairpin structure. HCR was initiated when the target miR-155 solution was introduced into an equimolar mixture of H1 and H2 probes (3 μM). The mixture was then topped up to 100 μL with the HCR buffer (20 mM tris-acetate, 2 mM $Mg(NO_3)_2$) and incubated for 2 h at 32 °C in a thermomixer.

Thereafter, AgNCs was prepared in the reaction mixture. Briefly, $AgNO_3$ was added into the reaction mixture, followed by vigorous shaking for 30 seconds (s). After 15 min, $NaBH_4$ was added with vigorous shaking for another 2 min. The molar ratio of H1, $AgNO_3$ and $NaBH_4$ was kept at 1:14:14 (μM). Subsequently, the resultant solution was incubated in the dark for 1.5 h before fluorescence measurement.

3.3.4 Gel electrophoresis

Agarose gel electrophoresis was conducted to verify the formation of HCR products. The gel was prepared from 2% agarose solution with 1X sodium borate buffer and pre-stained with SYBR Safe DNA gel stain. The gel was then run at 110 V for 50 min at room temperature. After completed, the gel was photographed and evaluated using Gel Doc System (Bio-Rad, USA).

3.3.5 Fluorescence measurement

Fluorescence measurements were performed using a Hitachi F-7000 Fluorescence Spectrophotometer (Hitachi, Japan). The excitation and emission slits of the spectrophotometer were set to 10 nm, and the PMT voltage was set to 950 V. The excitation wavelengths (λ_{EX}) used were 498 and 568 nm, for the respective peaks at emission

wavelengths (λ_{EM}) 561 and 616 nm. F_y/F_r were calculated from the emission intensities at 561 and 616 nm.

3.3.6 AgNCs characterisation

Transmission electron microscopy (TEM) was used to validate the formation of AgNCs. TEM images were taken using a FEI Tecnai G2 F20 Transmission Electron Microscope equipped with a Gatan Orius SC 1000 B camera.

3.3.7 MiR-155 detection in human serum sample

Whole blood samples were collected at Universiti Teknologi Mara (Selangor, Malaysia) and centrifuged for 13 min at 4000 xg to obtain human serum. The detection of miR-155 in human serum was performed based on standard addition method. Firstly, the human serum was diluted 100-fold with HCR buffer. The diluted human serum was then spiked with different concentrations of miR-155 (100 fM, 1, 10, 100 pM, 1, 10, 100, 200, 400, 600, 800, and 1000 nM). HCR was performed and AgNCs were prepared as aforementioned in **Section 3.3.3**. Finally, the fluorescence response was measurement as described in **Section 3.3.5**. In addition, four technical replicates were performed from one biological human serum sample.

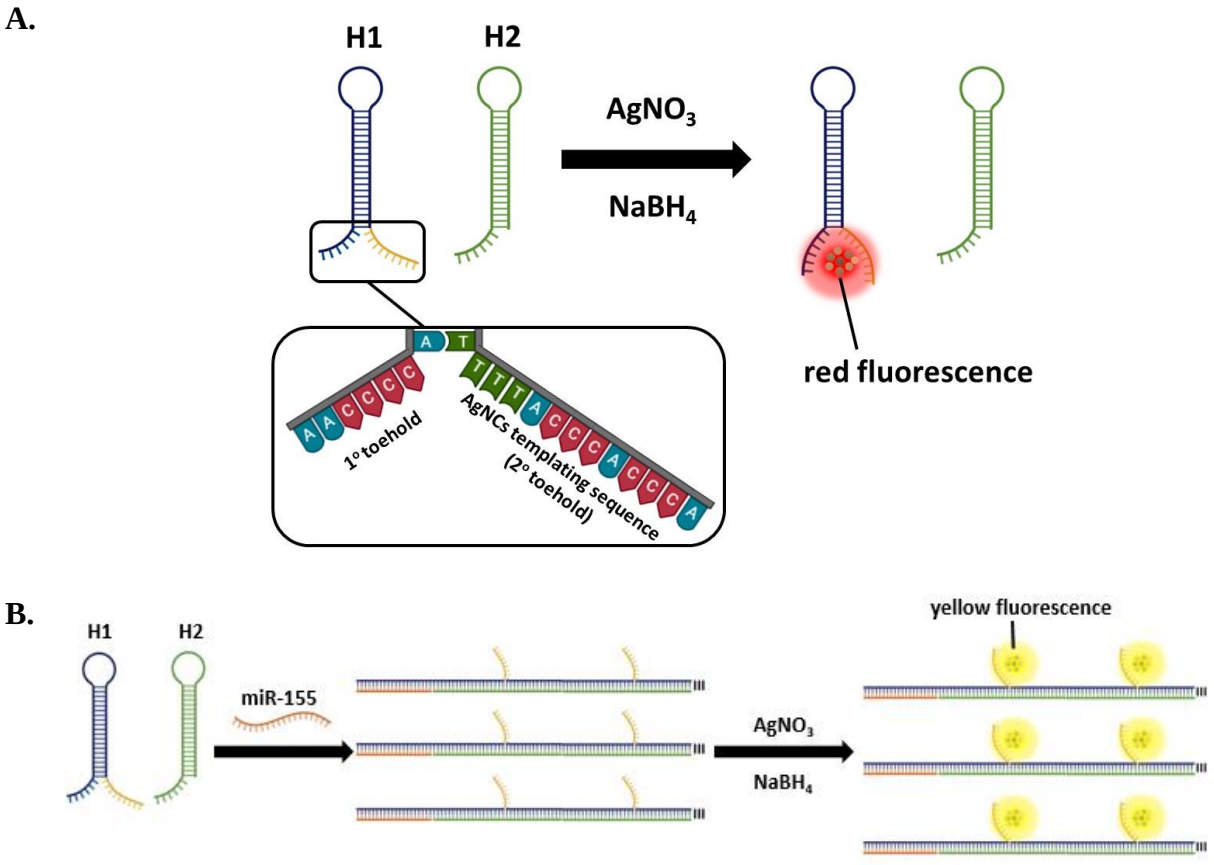
3.3.8 Data analysis

GraphPad Prism 7.4.6 was used to analyze the data, and the data were presented as mean ± standard error of the mean (SEM). Student's t-test was used to compare data between two groups. One-way ANOVA and the Tukey's test were used to compare data between more than two groups. Statistical significance was denoted by $p < 0.05$.

3.4 Results and Discussion

3.4.1 Sensing strategy

As illustrated in **Scheme 3.2**, the HCR-AgNCs biosensor comprised two DNA hairpin probes, (*i.e.,* H1 and H2) for HCR amplification. H1 was designed to have a AgNCs templating sequence (-*ACC CAC CCA*-) at the end of the hairpin structure as the 2^{o} toehold, adjacent to the 1^{o} toehold **(Scheme 3.2A)**. This particular sequence was previously reported to produce yellow and red emissive species, with the former as dominant [221]. Inspired by concept of proximity-dependent AgNCs (*i.e.,* NCBs and emitter-pairs), where their fluorescence properties were known to be influenced by adjacent sequences [140,145,222–225], it was deduced that the AgNCs hosted in H1 would change their fluorescence profile when the hairpin unfolds during HCR. Considering C-rich bases could result in AgNCs of greater size and with longer emission wavelength [226,227], the 3' end of miR-155 was selected as the initiating site for HCR amplification, for the four consecutive C bases. It was speculated that when the hairpin structure remained, AgNCs were in proximity with the C-rich 1^{o} toehold, hence favouring the formation of red emissive species. Upon HCR amplification, the H1 would open and the C-rich 1^{o} toehold would be used in the amplification process. This separated the C-rich sequence from the AgNCs templating sequence **(Scheme 3.2B)**, and influenced the yellow and red emission, subsequently enabling the detection of miR-155. This approach is novel for HCR-AgNCs biosensors, as the emitter-pair sequence actively participates in HCR amplification. In contrast to reported strategies, the proposed method featured a more direct and simpler mechanism. The design by Liu *et al.* utilised four DNA hairpin probes and a separate AgNCs templating strand, which resulted in a long HCR amplification process (*i.e.,* 4 h) [169]. On the other hand, the chameleon HCR-AgNCs by Jiang *et al.* utilised DNA hairpin probes with inconsistent secondary structures and reported loop-mediated DNA hairpin opening mechanism. Loop-mediated DNA hairpin opening was also reported as a slower approach than toehold-mediated opening [49], which led to a relatively long HCR amplification process (*i.e.,* 4 h) [160].



Scheme 3.2 HCR-AgNCs biosensor. Formation of AgNCs **(A)** without miR-155, and **(B)** with miR-155.

3.4.2 Computational design of HCR-AgNCs biosensor

In this HCR-AgNCs design, HCR amplification was simplified down to the use of only two DNA hairpin probes. By taking into consideration the guidelines discussed earlier in **Section 2.3.3** [49,62–65], several changes were made to the traditional DNA hairpin probe. In this case, the combined length of the DNA hairpin stem and toehold was equivalent to the length of miR-155 (24-mer). The toehold length for both hairpin probes were fixed at 6-mer, which was common in HCR studies [8]. Meanwhile, the stem of H1 leading towards the loop had an additional C-G bp, which reduced the loop size by two nucleotides for better DNA hairpin metastability and ensuring a leak-proof design. The final structure (excluding AgNCs templating sequence) of H1 and H2 adopted the toehold: stem: loop base length ratio of 6: 19: 4 and 6: 18: 6, respectively.

For an effective ratiometric analysis, there needed to be a change in fluorescence response brought about by HCR amplification. That said, to facilitate a change in the

fluorescence properties, a AgNCs templating sequence (-*ACC CAC CCA*-) was integrated on H1 as the 2^{o} toehold. This particular sequence was one of the shortest chemopalette sequence and had been reported to emit both red and yellow fluorescence, with the latter being more dominant [9,221]. A short T-rich spacer was used to connect the AgNCs templating sequence to the DNA hairpin structure, to minimise the steric effect of the AgNCs templating sequence during DNA hairpin opening for HCR amplification. Furthermore, the HCR initiation site was optimised to start from the 3' end of miR-155, as the first six bases would complementarily translate into a short C-rich sequence (5'-*AAC CCC*-3') for the 1^{o} toehold. In its DNA hairpin structure, the close proximity between the AgNCs templating sequence and C-rich 1^{o} toehold was expected to emit red fluorescence, as greater number of C bases would lead to fluorescence emission of a longer wavelength [131,228–230]. As H1 opened in the presence of miR-155 for HCR, the C-rich 1^{o} toehold actively participated in the HCR amplification process, thus leaving only the AgNCs templating sequence available for AgNCs synthesis and subsequent yellow fluorescence emission.

The DNA sequences were initially run in NUPACK, to determine the best possible sequence for the loop and toehold of H1 and H2, respectively. This was performed through a script input as shown in **Figure S1 (Appendix I)**. From here, a list of sequences was generated, and these sequences were screened with NABLAB for the best kinetic conditions. Henceforth, the best sequence was selected based on a balance between thermodynamic and kinetic aspects determined from computational screening. The final sequence of H1 and H2 were as listed in **Table 3.1**.

These thermodynamic properties of these sequences were validated with OligoAnalyser Tool, which was modelled after the UNAfold software (http://www.unafold.org) to study oligonucleotide folding. This enabled the identification of the T_m and ΔG of each DNA hairpin. In **Table S1 (Appendix I)**, the ΔG of H1 and H2 were estimated to be -18.38 kcal.mol^{-1} and -15.57 kcal.mol^{-1}, respectively. According to the energy level guidelines mentioned earlier, the MFE threshold for metastable DNA hairpins was reported to be approximately -16 kcal.mol^{-1} [63]. The ΔG of H2 was slightly below the threshold, which was a concern, as it might initiate non-specific HCR without miR-155. On the other hand, the MFE DNA hairpin structures (*i.e.*, H1 and H2) folded according to the planned HCR-AgNCs design, which prevented any dubious interactions in the HCR mechanism. For example, the DNA hairpin structure reported by Jiang *et al.* was different

than the MFE structure after sequence analysis with OligoAnalyser, and this indicated that the DNA hairpins could have been opened from the toehold instead of the reported loop segment [160].

As a pre-requisite to running the actual experiments, the interactions among the oligonucleotides (*i.e.,* miR-155, H1 and H2) were analysed with NUPACK to confirm the feasibility of the design and identify possible system leakage during HCR amplification. The settings for prediction were set at 2 μM H1 and H2, and 1 μM miR-155, with the temperature fixed at 37 ^{o}C. From **Figure S2A (Appendix I)**, HCR amplification was shown to be feasible, and this was evidenced by both depletion of DNA hairpins (*i.e.,* 0.32 μM H1 and 0.33 μM H2) and the formation of DNA concatemers between miR-155, H1 and H2 (*e.g.,* miRNA155-H1-H1-H2-H2, miRNA155-H1-H2, and miRNA155-H1-H1-H2). In **Figure S2B (Appendix I)**, the HCR product based on a total of five strands (*i.e.,* miR155-H1-H1-H2-H2) was presented. The ΔG of the HCR complex was estimated to be -122.03 kcal.mol^{-1}. The HCR product in **Figure S2B (Appendix I)** confirmed the complementary base-pairing between miR-155, H1 and H2, as well as the hanging tail (12-mer) corresponding to the AgNCs templating sequence on H1. The equilibrium probability of base-pairing throughout the structure remained mostly at 1.0, except for the A and T bases at the terminal ends of the DNA strands. As DNA duplexes are prone to fraying (mentioned in **Section 2.3.3**), terminal bases were susceptible to transient openings and this was more prominent with terminal A-T bp, as they were reported to have weaker hydrogen bonds than C-G bp [231]. The metastability of the DNA hairpins were preliminarily confirmed as shown in **Figure S2C (Appendix I)**, whereby no indication of hybridisation between H1 and H2 at the absence of miR-155 was reported in the prediction by NUPACK.

3.4.3 Feasibility of HCR-AgNCs biosensor

To verify the feasibility of the proposed HCR-AgNCs biosensor, HCR amplification was first analysed. To do this, gel electrophoresis was performed to validate the amplification efficiency of HCR, and the stability of the DNA hairpins for a leak-proof HCR design. In **Figure 3.1A**, as shown in Lane 3, in the absence of target miR-155, only two bands corresponding to H1 and H2 (Lanes 1 and 2) were observed. This implied that H1 and H2 were metastable, and no circuit leakage occurred. HCR was specifically triggered when miR-

155 was introduced, as evidenced by multiple bands of HCR products in Lane 4. On the contrary, the tailings observed in the lanes were most likely due to the high concentration of DNA samples loaded into each well.

Next, the fluorescence of AgNCs was measured in the absence and presence of miR-155. As shown in **Figure 3.1B**, the HCR-AgNCs exhibited two fluorescence peaks at λ_{EM} 561 and 616 nm respectively. This is in accordance with the dual-emissive character of the AgNCs hosted at the templating sequence of H1, as aforementioned [221]. Interestingly, the red emission at 616 nm was slightly more dominant in the absence of miR-155 (*i.e.*, HCR-negative); whereas the yellow emission at 561 nm was significantly enhanced in the presence of miR-155 (*i.e.*, HCR-positive). Without miR-155, the hairpin structure of H1 remained conserved, whereby the C-rich 1^o toehold came in close proximity to the AgNCs and resulted in predominance of red emission. When HCR was triggered by miR-155, the AgNCs templating sequence was separated from the C-rich 1^o toehold, leading to an enhancement of yellow fluorescence. By measuring the fluorescence intensities at both 561 and 616 nm, and calculating the F_y/F_r, the concentration of miR-155 can be determined.

The TEM images **(Figure 3.1C** and **D)** illustrated the successful formation of DNA-AgNCs with uniform size. Notably, AgNCs formed in HCR-positive samples **(Figure 3.1C)** were regularly shaped with an average diameter of approximately 4 nm, which was comparable to several DNA-AgNCs species [232,233]. On the other hand, the AgNCs caged in the HCR-negative sample **(Figure 3.1D)** were irregularly shaped with diameter that was twice the size of HCR-positive samples, at approximately 8 nm. The observation indirectly coincided with an earlier report, whereby different sizes of AgNCs were observed by manipulating distances of two individual nucleation sequences [160]. Additionally, it had been deduced that nanoclusters of smaller sizes tend to give emission at lower wavelength [226,234], which in this case, AgNCs of HCR-positive samples were smaller in size and showed higher proportion of yellow emission.

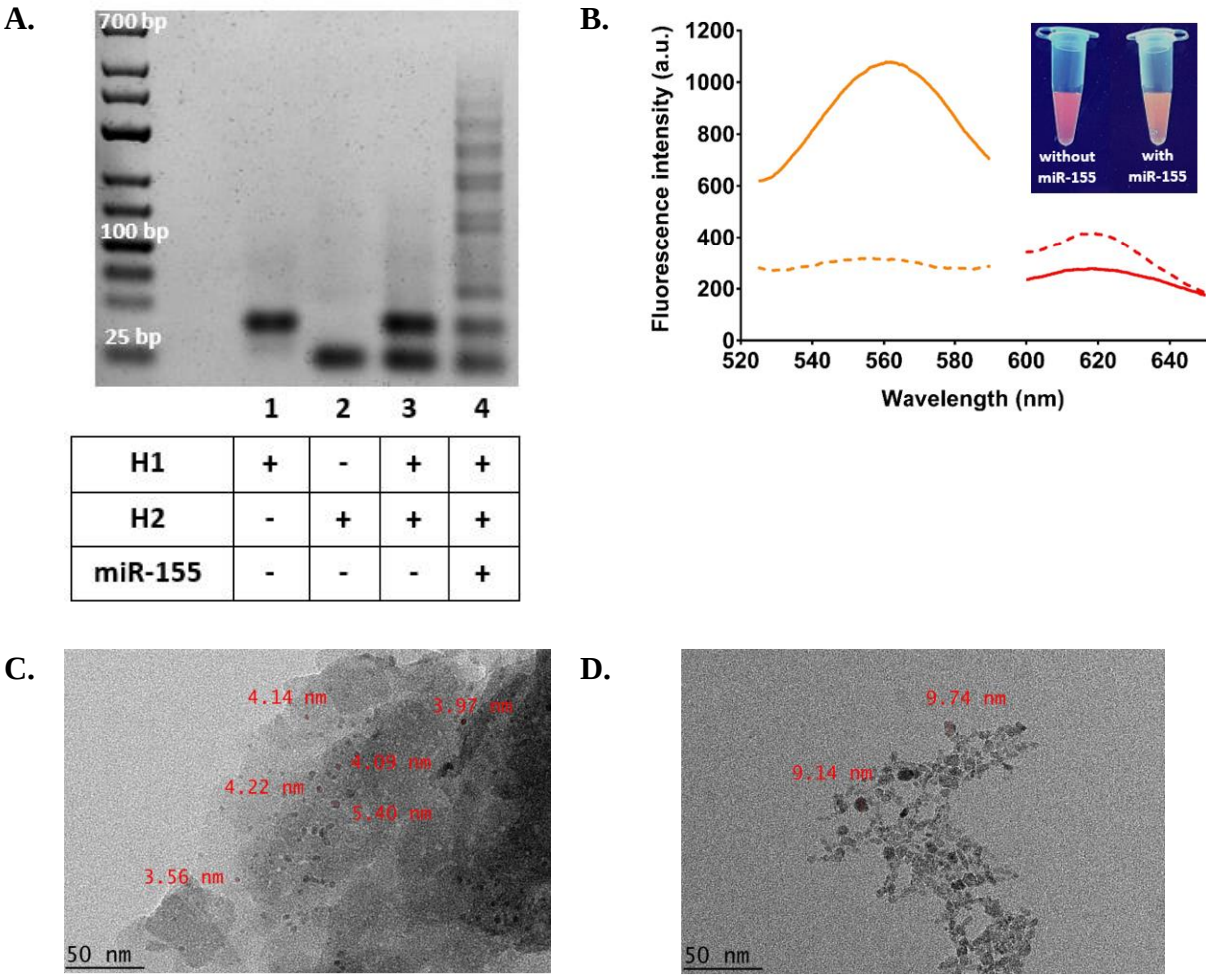


Figure 3.1 (A) Agarose gel analysis of HCR products. **(B)** Emission spectra of AgNCs in the presence (solid) and absence (dashed) of miR-155, with images of real samples shown as inset. TEM images of **(C)** HCR-positive, and **(D)** HCR-negative samples.

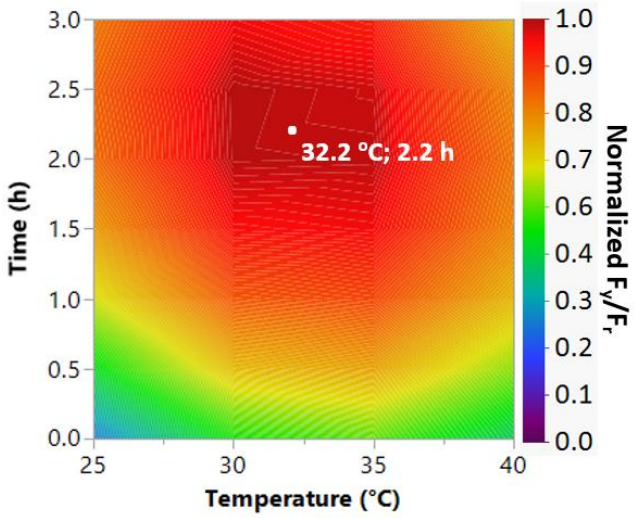
3.4.4 Condition optimisation of HCR-AgNCs biosensor

To ensure the highest performance of the HCR-AgNCs biosensor for the detection of miR-155, several parameters were systematically tested, including HCR incubation condition and concentrations of Ag^+ and $NaBH_4$ for AgNCs preparation. First, the duration and temperature of HCR incubation were investigated simultaneously in a full factorial experimental design. The performance of the biosensor was screened from 25 to 45 °C at a 5 °C interval, over a period of 2.5 h at a 0.5 h interval. The F_y/F_r values obtained from each data point were normalised to that of HCR-negative samples under the same condition and employed as input parameters for JMP (https://www.jmp.com/en_us/home.html), a Design of Experiments (DoE) software. A response surface model was then built to illustrate the changes in fluorescence response across the tested parameters and the possible interactions

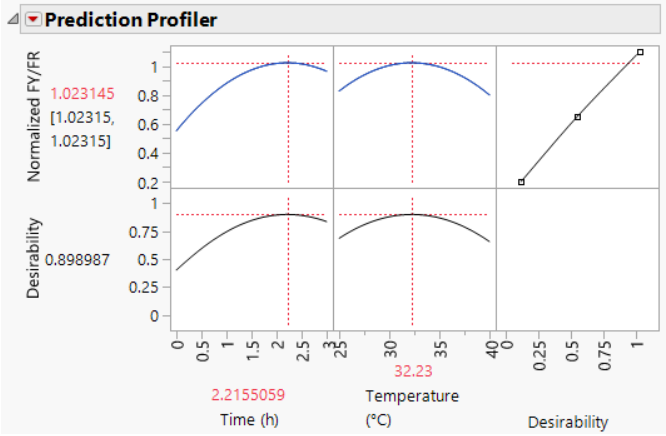
among the parameters [235,236]. To determine the optimum reaction conditions, a prediction profiler based on the maximum desirability factor was utilised [237]. Based on the surface plot **(Figure 3.2A)** and prediction profiler **(Figure 3.2B)**, the most probable parameters to obtain the maximum F_y/F_r were 2.2-h incubation period and 32.2 °C incubation temperature. This condition was henceforth used for the subsequent experiments. Given the large amount of data input in the full factorial design and the relatively small interval between datapoints, the predicted conditions were considered reliable. Hence, no further experiments were conducted.

The combination of the AgNCs templating sequence and emitter-pair was new and untested, thus needing optimisation. The preparation of AgNCs was optimised by varying the molar ratio of H1: Ag^+: $NaBH_4$, from 1: 6: 6 to 1: 30: 30, with consecutive increments of Ag^+ and $NaBH_4$ by 4 parts and normalising the F_y/F_r values obtained from each data point to that of HCR-negative samples under the same condition. **Figure 3.2C** showed that 1: 14: 14 of H1: Ag^+: $NaBH_4$ exhibited the highest F_y/F_r value and hence, was used for subsequent experiments.

A.



B.



C.

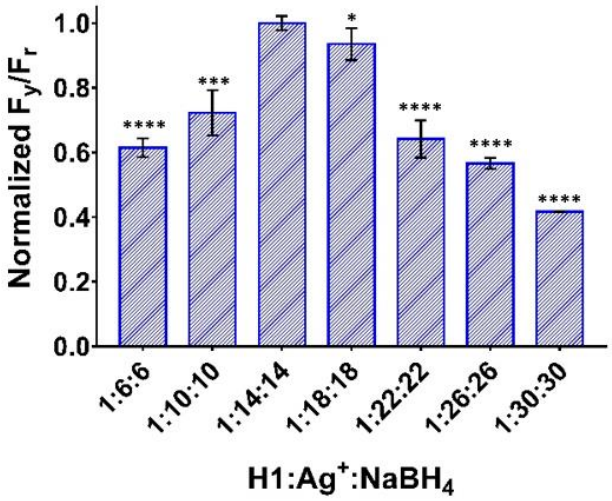


Figure 3.2 Optimisation of experimental conditions. **(A)** HCR incubation temperature and duration. **(B)** Screenshot of prediction profiler in JMP used to find the optimised HCR incubation conditions. The prediction profiler utilises a desirability function, where the values from 0 to 1 indicates the scale of desirable response [237], *i.e.*, F_y/F_r in this study. **(C)** Molar ratio of H1: Ag^+: $NaBH_4$. Normalised F_y/F_r represents the ratiometric measurement of HCR-positive to HCR-negative F_y/F_r. Data presented as mean ± SEM, and statistically analyzed relative to 1:14:14. *, $p<0.05$; ***, $p<0.001$; ****, $p<0.0001$.

3.4.5 Analytical performance of HCR-AgNCs biosensor

3.4.5.1 Sensitivity test

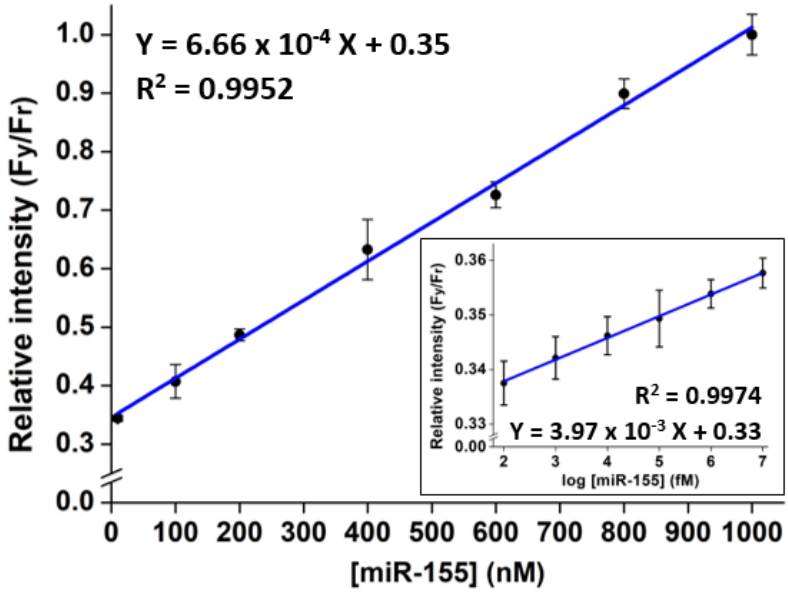
Based on the optimised experimental conditions, different concentrations of miR-155 were used to evaluate the performance of the proposed HCR-AgNCs biosensor for quantitative analysis. As shown in **Figure 3.3A**, the F_y/F_r increased proportionally to the concentration of target miR-155 in a detection range from 100 fM to 1 μM. The correlation of

F_y/F_r to the concentration of miR-155, was attributed to the fraction of reacted DNA hairpins to unreacted DNA hairpins, such that higher concentration of miR-155 would utilise more DNA hairpin probes for HCR amplification. Two detection range identified. The first detection range (10 nM–1 μM) is shown in **Figure 3.3A**. The second detection range (100 fM–10 nM) is shown in the inset of **Figure 3.3A** as a semi-log-plot for better visualization of the fluorescence profile. The LOD was calculated to be 1.13 fM according to the formula $LOD = k\ \sigma_B/b$, where k represents the expansion factor, σ_B as the standard deviation and b as the slope of the line [238]. In comparison to recently reported methods for the detection of miR-155 **(Table 3.2)**, the proposed ratiometric HCR-AgNCs biosensor displayed excellent analytical performance, with higher sensitivity and wider detection range than most fluorescence-based biosensors, and comparable to some electrochemical-based biosensors. This could be ascribed to the high amplification efficiency of HCR and the ratiometric fluorescence derived from the dual-emissive AgNCs.

3.4.5.2 Selectivity test

The selectivity behaviour of the HCR-AgNCs biosensor towards miR-155 was also investigated. Different controls including blank sample (*i.e.,* without miR-155), sequences with mismatched bases (*i.e.,* mismatch *n,* where *n* indicates the number of mismatches in the sequence), and DNA analogues of other miRs (i. e. miR-10b, miR-21, miR-29, miR-125b and miR-145), as well as a mixture of miR-155 with all non-target controls (i. e. mixture) were tested. The concentration used for miR-155 and controls (*i.e.,* mismatch and non-target sequences) used in the selectivity test was fixed at 1 μM. Note that the other miRs were chosen based on their dysregulated expression found in breast cancer [239–243]. As shown in **Figure 3.3B**, the relative intensities of samples containing miR-155 were significantly higher than the other controls, proving that the HCR-AgNCs biosensor had excellent selectivity towards miR-155. No significant difference was observed in the relative intensity between miR-155 and the mixture samples, indicating the presence of other controls did not affect the performance of the HCR-AgNCs assay. An in-depth observation identified the relative intensities of mismatches 1, 2 and 3 were almost comparable to that of blank sample, implying the assay could discriminate down to a single base difference. The ability for HCR to discriminate mismatch bases was due to the fact that mismatch can disrupt process of DNA hairpin opening, as well as decreasing the T_m of associated dsDNA structures [244].

A.



B.

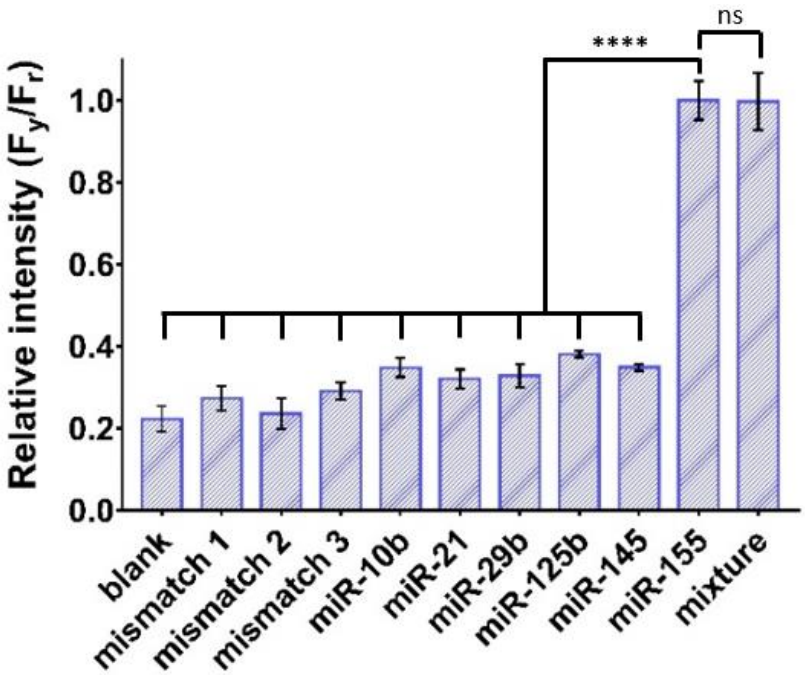


Figure 3.3 (A) Sensitivity profile of the HCR-AgNCs biosensor with two detection ranges displayed (n = 4). First detection range between 10 nM and 1 µM. Second detection range (semi-log plot inset) between 100 fM and 10 nM **(B)** Selectivity test of the HCR-AgNCs biosensor against miR-155 (n = 4). Data presented as mean ± SEM. ****, p<0.0001; ns, non-significant.

Table 3.2 Comparison of the proposed HCR-AgNCs biosensor with other reported miR-155 biosensors.

Detection system	Materials	LOD	Detection range	Reference
Electrochemical	Amino-functionalised graphene	12.50 pM	30 pM – 1 nM	[245]
Fluorescence	Quantum dots (QDs)	14.00 pM	20 – 100 pM	[246]
Fluorescence	Multi-walled carbon nanotube/gold nanocomposites	33.40 fM	100 fM – 1.0 nM	[247]
Colorimetric/Electrochemical	Streptavidin MBs/alkaline phosphatase	29.00 pM	81 pM – 1.2 nM	[248]
Fluorescence	DNA-copper nanoclusters (CuNCs)	2.20 pM	5 pM – 10 nM	[249]
Fluorescence	DNA-CuNCs	11.00 pM	50 pM – 10 nM	[250]
Fluorescence	Polystyrene beads/DNAzyme	30.00 pM	10 pM – 1 nM	[251]
Fluorescence	GO/enzymatic amplification	4.50 pM	5 pM – 5 nM	[252]
Fluorescence	Double-hairpin molecular beacon	0.18 nM	1.02 – 144 nM	[253]
Colorimetric	DNA walker/gold nanoparticles	16.70 fM	50 fM – 10 pM	[254]
Fluorescence	AgNCs/cadmium telluride QDs	1.20 pM	5 pM – 50 nM	[255]
Fluorescence	Tetrahedral DNA nanostructure	100 fM	100 fM – 10 nM	[256]
Electrochemical	gold nanoparticles/graphene QDs/GO	0.33 fM	1 fM – 1000 pM	[257]
Electrochemical	GO/gold nanorod	0.6 fM	2 fM – 8 pM	[258]
Fluorescence	HCR-AgNCs	1.13 fM	100 fM – 1 μM	This work

3.4.6 Application of HCR-AgNCs biosensor in human serum sample

To verify the applicability of the proposed HCR-AgNCs biosensor in complex samples, the biosensor was tested in diluted human serum samples spiked with different concentrations of miR-155. Similar to that of buffered samples (**Figure 3.3A**), two detection ranges were obtained **(Figure 3.4)**. However, there was a slight deviation in the fluorescence profile as compared to the buffered samples (**Figure 3.3A**), which was likely attributed to interfering agents such as proteins and other biomolecules, that could be found in the serum [259]. In spite of the difference, the relative standard deviation (RSD) (n=4) of the first detection range (10 – 1000 nM) were all below 10%, whereas the RSD of the second detection range (100 fM – 10 nM) were all below 4%, which indicated high reliability and reproducibility of this detection method for real sample analysis. The calculated LOD was very comparable to that with buffered samples, *i.e.*, 1.58 fM. Note that concentration of miRs ranges from fM to nM concentrations (i.e., taken into account the variations across individuals and the different studies) [260,261], and that the concentrations of miR-155in primary and metastatic breast cancer were once reported in a study to be approximately 2 pM and 6 pM, respectively [245]. This finding suggested that the proposed HCR-AgNCs biosensor has great potential for application in complex biological samples.

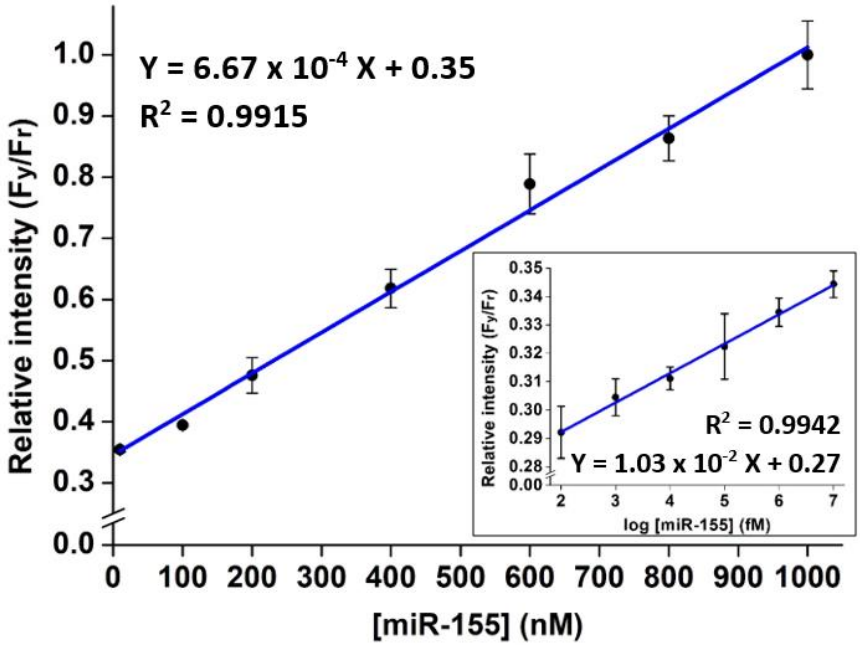


Figure 3.4 Sensitivity profile of the HCR-AgNCs biosensor in diluted human serum sample (n = 4). First detection range between 10 nM and 1 µM. Second detection range (inset) between 100 fM and 10 nM.

3.5 Summary

In summary, a HCR-AgNCs biosensor was successfully developed for the detection of miR-155. It was also proven that the principle of ratiometric analysis with the addition of a single AgNCs templating sequence emitted a strong red-yellow fluorescence response. In the presence of miR-155, the HCR-AgNCs biosensor would produce a significant enhancement of the yellow fluorescence emission and a concurrent quenching of the red fluorescence emission, both of which are proportional to the concentration of miR-155. The ratiometric response calculated from both fluorescence emission, exhibited a proportional relationship with the concentration of miR-155 ranging from 100 fM to 1 μM, and the LOD was 1.13 fM. Moreover, the HCR-AgNCs biosensor showed high selectivity, with the capability of sharply discriminating between target miR-155, single-base mismatch sequence, and non-complementary sequences. The ratiometric HCR-AgNCs biosensor reported a decent response in serum sample, which proved its reliability and reproducibility. Hence, with further optimisation (*e.g.,* detection with clinical samples), the proposed ratiometric HCR-AgNCs could be used in the early detection of breast cancer, by direct detection of the miR-155, with minimal sample preparation procedures. This study had several limitations that could be further explored in future research, which will be covered in detail in Chapter 6. For example, the gel data from Figure 3.1A could be improved with the use lower concentrations of samples to prevent tailing. Additionally, the tailings could be further analyzed to identify possible non-specific interactions between samples (e.g., dimerization of similar DNA hairpins), despite the minimal to no risk of occurrence based on the comprehensive preliminary computational design. On the contrary, the thick/main bands on the gel could be further analyzed for their intensity to evaluate the specific concentration of DNA hairpins used. Subsequently, this could be used to supplement and support the fluorescence profile of the HCR-AgNCs biosensor. Apart from that, the performance of the biosensor could be further validated in future studies at higher concentrations and lower dilution of complex samples (e.g., human serum diluted by 10- or 20-folds), given that only 100-fold dilution was tested in this study, which might further reduce the concentration of the already low-abundant miRs in real samples.

Chapter 4: Development of a "switch-on" HCR-AgNCs biosensor based on externalised end-to-end cluster transfer of AgNCs for the detection of DNA

4.1 Overview

In this chapter, the possibility of developing a HCR-AgNCs biosensor with externalised AgNCs fluorogenic probes from the HCR amplification system is explored. The rationale behind this lies in simplifying the design process of a stable leak-proof HCR system, without the need of integrating long C-rich AgNCs templating sequences onto DNA hairpins. By externalising AgNCs signal transduction, an end-to-end cluster-transfer approach is utilised to activate a fluorescence response that corresponds to HCR amplification. Preliminary work of this study focuses on designing the DNA hairpins and probes for both HCR amplification and AgNCs fluorescence activation. This is followed by a series of experiments to prove the feasibility of the proposed HCR-AgNCs biosensor. Results indicated a strong red fluorescence emission that is detectable with the naked eye down to 1 pM. Moreover, the quantitative analysis from the proposed HCR-AgNCs biosensor reported great sensitivity and selectivity towards a DNA target. The biosensor also performed well in human serum samples, with a good recovery and reproducibility. Overall, the cluster-transfer approach provides a good alternative to construct HCR-AgNCs assay with a lower risk of circuit leakage and produce AgNCs in a controllable manner. At the end of this chapter, the key findings are summarised and potential of translating the proposed HCR-AgNCs biosensor for real-world application is highlighted.

4.2 Background

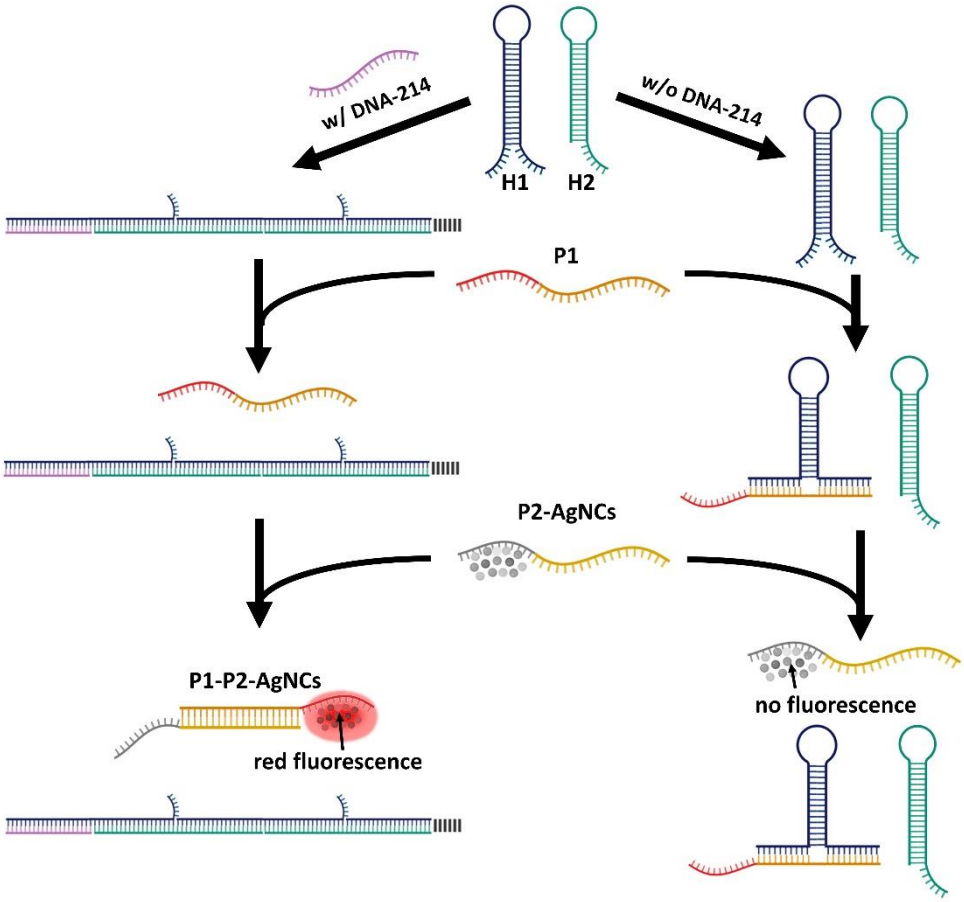
In **Section 2.4.4.4**, the mechanism and application of proximity-dependent NCBs were covered in detail. Briefly, non-fluorescent 'dark' AgNCs species can be optically activated with an enhancer sequence that is in close proximity. G-rich strands are the most common enhancer sequences used for NCBs [138,139,262,263]. Interestingly, AgNCs fluorescence can also be activated *via* 'cluster transfer'. This approach was initially introduced as means of transferring AgNCs from polymer to DNA sequences [109,264,265].

The cluster transfer approach was then adapted for application between DNA sequences (*i.e.,* dark and bright AgNCs species) [225]. A study by Teng *et al.* reported the cluster transfer of AgNCs from a dark AgNCs templating sequence to a C-rich sequence for an intense red fluorescence activation [149]. The deduced mechanism was that the C-rich sequence captured AgNCs from the dark AgNCs templating sequence presumably due to the higher specific affinity of Ag^+ towards C-rich sequences. Furthermore, it was demonstrated by Teng *et al.*, that the different positions of both dark AgNCs templating and C-rich sequence (*i.e.,* on the same or opposite sides of DNA duplexes) could result in different degree of enhancement [149]. Nonetheless, these studies undoubtedly reveal the high sensitivity of AgNCs towards subtle changes in their environment, endowing them the versatility to integrate with amplification methods for biosensing purposes [266,267]. With regards to HCR-AgNCs biosensors, the concept of NCBs is under-utilised within the field. The only reported NCB-based HCR-AgNCs biosensor was by Liu *et al.* with their four-hairpin 'switch-on' system. The design featured a dark AgNCs templating sequence and a G-rich enhancer sequence on the hairpin toehold, for red fluorescence activation in the presence of a mRNA target [169].

Most HCR-AgNCs biosensors have the AgNCs templating sequence tailored into the DNA hairpin structure, to yield significant fluorescence change during HCR amplification. This approach, while feasible, poses several key challenges for HCR-AgNCs biosensors. Firstly, most AgNCs templating sequences are long C-rich sequences, and these can destabilise DNA hairpin structures, according to the HCR design guidelines highlighted in **Section 2.3.3** [49,62–65]. On top of that, the purification and production of long oligonucleotides are costly, which limits the practical application of HCR-AgNCs in the long run. Next, the preparation of AgNCs is dependent on a specific ratio of reactants (*i.e.,* Ag^+ and $NaBH_4$) to a AgNCs templating sequence. When AgNCs are prepared post-HCR amplification, the cluster can nucleate within different molecules (*i.e.,* HCR product, C- and G-rich RNA and DNA probes, proteins, and metal ions) [7,232,268–273], resulting in multiple AgNCs species. As a result of the inconsistent preparation of a specific AgNCs species, the reliability and accuracy of the biosensor could be compromised. That said, the approach of externalising AgNCs from the HCR system, can simplify the design of stable and leak-proof HCR system based on the established guidelines [49,62–65], and ensure that AgNCs form specifically and consistently on a desired AgNCs templating sequence. Among the reported HCR-AgNCs studies, only the HCR-AgNCs design by Liu *et al.* utilised an external AgNCs templating sequence probe [169].

Herein, the proposed HCR-AgNCs biosensor is designed with a DNA target, DNA-214. The selected DNA-214 is modelled as the DNA analogue of miR-214, which is a potential miR biomarker in different types of diseases, such as cancer, viral infections and autoimmune diseases. With regards to cancer, miR-214 has been reported to exhibit both tumorigenic and tumour-suppressive behaviour in different types of cancer. For example, miR-214 is significantly downregulated in gastric, pancreatic, melanoma and ovarian cancer, and significantly upregulated in CNS lymphoma and cervical cancer. In addition, the aberrant expression of miR-214 is correlated to cancer progression in patients, depending on the type of cancer. These findings suggest that miR-214 can be established as a potential diagnostic and prognostic biomarker for cancer detection [274–276].

The design of the HCR-AgNCs biosensor is as illustrated in **Scheme 4.1**. The first part of the biosensor is HCR amplification with two DNA hairpins (*i.e.*, H1 and H2), both of which strictly follow the established guidelines for HCR system design mentioned in Section **2.3.3**. HCR is only feasible when DNA-214 is introduced into the biosensor. The next part concerns the AgNCs fluorogenic probes. In this work, two DNA probes (*i.e.*, P1 and P2) are designed to induce proximity-dependent fluorescence activation. P1 contains a C-rich AgNCs templating sequence (indicated as red strand) that is known to host bright red-emissive AgNCs [149]; whereas P2 hosts dark AgNCs species prepared using a reported AgNCs templating sequence (indicated as grey strand) [262]. Prior to HCR amplification, AgNCs will be prepared in a controlled environment on P2, for a non-fluorescent AgNCs species. The hybridisation of P1 and P2 will activate a distinct red fluorescence, *via* end-to-end cluster transfer from P2 to the C-rich AgNCs templating sequence on P1. In the study by Teng *et al.*, end-to-end cluster transfer was reported to emit significantly stronger fluorescence enhancement as compared to side-to-side NCBs [149]. To ensure a distinct change in the fluorescence response during HCR amplification, the hybridisation sequence between P1 and P2 is modelled to be similar to a portion of H1. Hence, in the absence of DNA-214, P1 hybridises with H1, and the dark AgNCs remain encapsulated in P2. On the other hand, DNA-214 triggers HCR amplification, thus allowing P1 to hybridise with P2-AgNCs for red fluorescence activation. As seen in **Scheme 4.1**, both P1-P2-AgNCs and the HCR product remain as separated entities, and the resultant fluorescence intensity is expected to correspond with the concentration of DNA-214. Overall, this homogenous HCR-AgNCs biosensor minimises the complexity of the designing process, with an effective fluorescence detection of DNA-214.



Scheme 4.1 Outline of HCR-AgNCs biosensor with externalised AgNCs probes for the detection of DNA-214.

4.3 Methodology

4.3.1 Materials

The materials used in this study were similar to the study in **Chapter 3**, and the details were as described in **Section 3.3.1**.

All DNA samples were of standard desalted grade and obtained from IDT (Iowa, USA). The sequences of DNA-214 and non-target controls were adapted from www.mirbase.org, and listed in **Table 4.1**. Prior to usage, the oligonucleotides were dissolved in molecular grade water to produce stock concentrations of 100 µM.

Table 4.1 Oligonucleotide sequences used in this work. Red letters indicate the C-rich AgNCs templating sequence. Blue letters indicate the dark AgNCs templating sequence. Italicised letters indicate hairpin stem region. Bold letters indicate hairpin loop. Underlined letters indicate mismatch base(s).

DNA	Sequence (5' – 3')
H1	ACT GCC *TGT CTG TGC CTG CTG TG* **CAT T** *CAC AGC AGG CAC AGA CA* CAC CTC
H2	*ACA GCA GGC ACA GAC A* **GGC AGT** *TGT CTG TGC CTG CTG T* GAA TGC
P1	CCC CCC CCC CCC GAG GTG TGT CTG CAG ACA GGC AGT
P2	CCC CTA ATT CCC ACT GCC TGT CTG CAG ACA CAC CTC
DNA-214	ACA GCA GGC ACA GAC AGG CAG T
DNA-141	TAA CAC TGT CTG GTA AAG ATG G
DNA-199a	CCC AGT GTT CAG ACT ACC TGT TC
DNA-205	TCC TTC ATT CCA CCG GAG TCT G
DNA-200a	TAA CAC TGT CTG GTA ACG ATG T
mismatch 1	ACA GCA GGC ACA GAC A<u>C</u>G CAG T
mismatch 2	ACA GCA GG<u>G</u> ACA GAC A<u>C</u>G CAG T
mismatch 3	ACA G<u>G</u>A GG<u>G</u> ACA GAC A<u>C</u>G CAG T

4.3.2 Design of DNA oligonucleotides

DNA hairpin and probes (*i.e.*, H1, H2, P1 and P2) were designed according to the sequence of DNA-214 using NUPACK, OligoAnalyser tool and Kinetics Calculator.

4.3.3 Preparation of P2-AgNCs

AgNCs was first prepared on P2. Briefly, $AgNO_3$ was mixed with P2, then reduced with $NaBH_4$. The molar ratio of P2: $AgNO_3$: $NaBH_4$ used was 1: 15.4: 15.4 (μM). The solution was incubated in dark for 3 h prior to DNA-214 detection.

4.3.4 DNA-214 detection in buffer

To ensure the most stable hairpin structures were formed, H1 and H2 were first heated at 90 ^{o}C for 2 min and snap-cooled in ice bath for 30 min before usage. HCR was initiated by mixing both H1 (2 μM) and H2 (2 μM) with DNA-214. The solution was topped up to 100 μL with HCR buffer (20 mM tris-acetate, 2 mM $Mg(NO_3)_2$, pH 8.0) and incubated at 32 ^{o}C for 1.4 h in a thermomixer. Next, P1 (2 μM) was added into the solution and further incubated for 55 min, followed by P2-AgNCs for another 55 min. The resultant solution was collected for fluorescence measurement.

4.3.5 Gel electrophoresis

Agarose gel electrophoresis was conducted similarly as described in **Section 3.3.4**.

4.3.6 Fluorescence measurement

Fluorescence images were obtained with a UV transilluminator (Extra Gene Inc., Taiwan). Fluorescence measurements were performed using a Hitachi F-7000 Fluorescence Spectrophotometer (Hitachi, Japan) with similar settings, as described in **Section 3.3.5**. In this study, the λ_{EX} was set at 562 nm for a corresponding λ_{EM} of 611 nm.

4.3.7 P1-P2-AgNCs characterisation

To validate the AgNCs transfer from P2 to P1, P1-P2-AgNCs were characterised with TEM and X-ray photoelectron spectroscopy (XPS). TEM images were taken using a FEI Tecnai G2 F20 Transmission Electron Microscope (FEI Company, United States of America) equipped with a Gatan Orius SC 1000 B camera (Gatan Inc., United States of America). For XPS analysis, the as-synthesised P1-P2 AgNCs was ethanol precipitated before drying, for better stability in aerobic and high temperature environment in XPS characterisation [277]. XPS spectra were recorded using an XPS Quanterra II (ULVAC-PHI, Inc., Japan).

4.3.8 DNA-214 detection in human serum sample

Human serum samples obtained from Universiti Teknologi Mara (Selangor, Malaysia) were prepared similarly as described in **Section 3.3.7**. In this study, the 100-fold diluted human serum was spiked with different concentrations of DNA-214 (500 nM, 50 nM, 500 pM and 5 pM). In addition, five technical replicates were performed from one biological human serum sample. These spiked samples were detected as described in **Section 4.3.4**, with their fluorescence measured as described in **Section 4.3.6**.

4.3.9 Data analysis

GraphPad Prism 7.4.6 was used to analyze the data, and the data were presented as mean ± SEM. Student's t-test was used to compare data between two groups. One-way ANOVA and the Tukey's test were used to compare data between more than two groups. Statistical significance was denoted by $p < 0.05$.

4.4 Results and Discussion

4.4.1 Sensing strategy

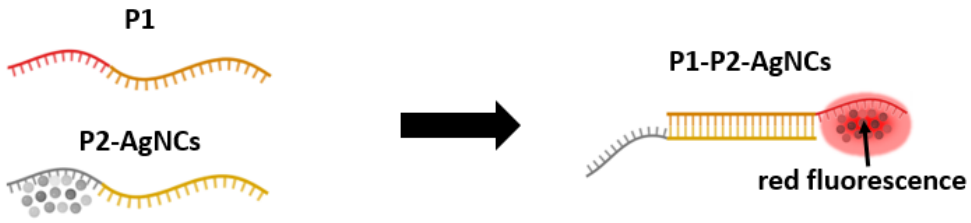
For the selection of AgNCs as an external fluorescence signal transducer, a variation of NCBs was incorporated [149], that involved an end-to-end cluster transfer of AgNCs from a dark to a homo-polyC AgNCs templating sequence when brought into close proximity. **Scheme 4.2A** showed two ssDNA probes (*i.e.,* P1 and P2). P1 had a homo-polyC *(-CCC CCC CCC CCC-*) AgNCs templating sequence (indicated as red strand), whereas P2 has a dark AgNCs (*-CCC CTA ATT CCC-*) templating sequence (indicated as grey strand). Both P1 and P2 featured a complementary hybridisation segment (indicated as orange and yellow strands, respectively). After preparing AgNCs on P2 in a controlled environment, the caged AgNCs could be shuttled to the homo-polyC AgNCs templating sequence of P1, when both probes were hybridised. This was expected to activate a red fluorescence emission, common for homo-polyC AgNCs templating sequence [121–123].

When AgNCs was introduced as an external fluorescence signal transducer, it was also anticipated to evoke a change in the fluorescence properties upon HCR amplification. To

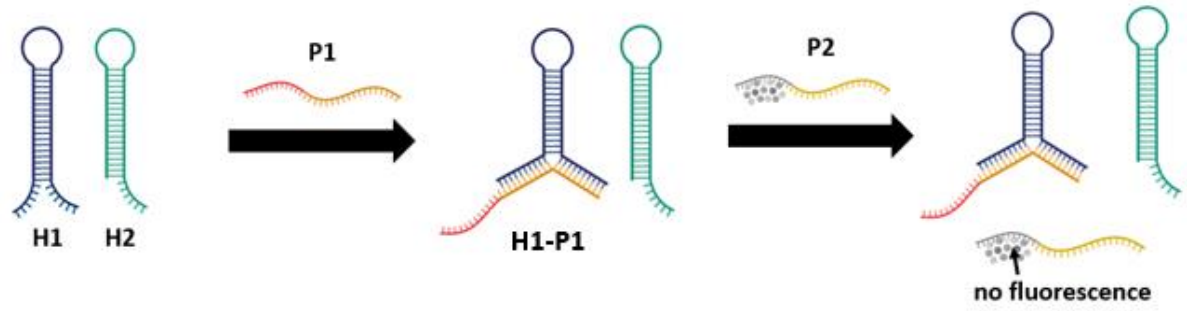
do this, a portion of H1 was designed to hybridise with P1. Moreover, a 2^{o} toehold was added onto H1 to facilitate a complete hybridisation of H1 and P1. This interaction between H1 and P1 was only possible when HCR amplification did not occur (*i.e.*, in the absence of DNA-214). In **Scheme 4.2B**, P1 would partially open and bind to the toehold segments of H1, thereby forming a H1-P1 duplex structure. Subsequently, P2-AgNCs would remain a non-fluorescent species, as the AgNCs caged within the templating sequence of P2 would not be transferred to C-rich AgNCs templating sequence on P1.

On the other hand, when DNA-214 was introduced into the pool of H1 and H2, HCR was expected occur and this process would utilise both H1 and H2 (**Scheme 4.2C**). Henceforth, P1 would be able to hybridise with P2-AgNCs upon addition, to form the P1-P2 complex, as shown in **Scheme 4.2A**. This hybridisation would facilitate the end-to-end cluster transfer of AgNCs, thereby activating the red fluorescence emission. The intensity of the fluorescence signal would be proportional to the concentration of DNA-214. Interestingly, P1 could also serve as a HCR terminator, as the hybridisation between P1 and H1 rendered the toehold of H1 inaccessible for hairpin opening and subsequent hybridisation with H2.

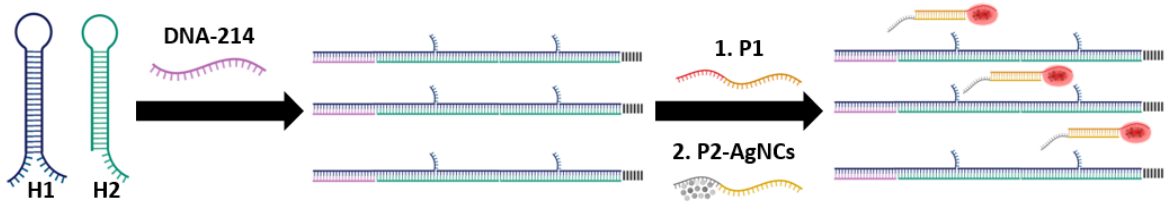
A.



B.



C.



Scheme 4.2 (A) Red fluorescence activation upon hybridisation of P1 and P2-AgNCs, *via* end-to-end cluster transfer. **(B)** HCR-AgNCs biosensor without DNA-214. **(C)** HCR-AgNCs biosensor with DNA-214.

As previously mentioned, the only other HCR-AgNCs biosensor with an external AgNCs probe was by Liu *et al.* However, their work featured more DNA hairpins, with long C- and G-rich toeholds. As a result, the reported HCR structure featured long two-tail extensions on one side of the complex [169]. As highlighted in **Section 2.3.3**, two-tail appendages from DNA structures present unnecessary steric hindrance which might reduce the rate and efficiency of DNA hybridisation [65]. This could have led to the longer HCR incubation period (*i.e.*, 4 h) in the study by Liu *et al.* [169]. In contrast, the proposed HCR design in this work would only contain a shorter one-tail extension at one side of the HCR product.

4.4.2 Computational design of HCR-AgNCs biosensor

To translate the design for practical applications, the sequence of DNA probes was optimised to ensure a leak-proof HCR circuit, and efficient hybridisation between the respective probes. The computational optimisation process was performed in two parts.

First, a feasible and stable HCR circuit was designed. The HCR portion of the biosensor comprised a simple two-hairpin system. Taking into consideration the guidelines discussed earlier in **Section 2.3.3** [49,62–65] and the results of the ratiometric HCR-AgNCs biosensor reported in **Chapter 3**, the structures of H1 and H2 were carefully optimised. Similarly, the combined length of the toehold and stem of both H1 and H2, was dependent on the length of DNA-214 (22-mer). The toehold lengths were fixed at 6-mer, which was common in most HCR studies and shown to be feasible with the HCR-AgNCs biosensor reported in **Chapter 3**. In addition, the loop size was truncated for an additional C-G bp in the stem of H1, to confer better DNA hairpin metastability. For H1, a 2^{o} toehold was added to facilitate its hybridisation with P1. This toehold was set to six bases, which was suggested by Ang *et al.* that the maximum recommended toehold length was 12 bases [62]. Overall, the final hairpin structure of H1 and H2 adopted the toehold: stem: loop length ratio of 12: 17: 4 and 6: 16: 6, respectively.

The DNA design was run in NUPACK, to determine the best loop and toehold sequence for H1 and H2. This was performed with a NUPACK script input as shown in **Figure S1 (Appendix II)**. From here, a list of sequences was generated and these were screened with NABLAB for the best kinetic conditions [278]. Henceforth, the best sequence was selected based on a balance between thermodynamic and kinetic aspects determined from computational screening. The final sequence of H1 and H2 were as listed in **Table 4.1**.

These thermodynamic properties of these sequences were validated with OligoAnalyser Tool, to study oligonucleotide folding through T_m and ΔG. From **Table S1 (Appendix 2)**, the ΔG was estimated to be -21.02 and -19.12 kcal.mol^{-1} for H1 and H2, respectively. Based on the guidelines discussed earlier [63], both H1 and H2 met the minimum energy threshold (*i.e.*, -16 kcal.mol^{-1}) for metastable DNA hairpins.

Whilst both H1 and H2 were confirmed to be thermodynamically stable, NUPACK analysis was performed to gauge the feasibility and functionality of the design and identify the possibility for HCR circuit leakage. The parameters for the prediction were set at 2 μM H1 and H2, 1 μM DNA-214, with the temperature of the reaction fixed at 37 ^{o}C. From **Figure S2A (Appendix II)**, HCR amplification was shown to be feasible, and this was evidenced by both depletion of DNA hairpins (*i.e.*, 0.37 μM H1 and 0.62 μM H2) and the formation of DNA concatemers between DNA-214, H1 and H2 (*e.g.*, DNA214-H1-H1-H2-H2, DNA214-H1-H2, and DNA214-H1-H1-H2). **Figure S2B (Appendix II)** illustrated the

structure of the HCR product based on a total of five strands (*i.e.,* DNA214-H1-H1-H2-H2). The ΔG of the HCR complex was estimated to be -130.31 kcal.mol^{-1}. The HCR product in **Figure S2B (Appendix II)** also confirmed the complementary base-pairing between DNA-214, H1 and H2, as well as the short (6-mer) hanging tail that corresponds to the 2^{o} toehold of H1. The equilibrium probability of base-pairing throughout the structure remained mostly at 1.0, except for the A-T bp at the terminal ends of the DNA strands. This was addressed earlier in **Section 3.4.2** because of fraying and the weak hydrogen bonds of A-T bp [76]. Based on the thermodynamic calculation and prediction by NUPACK, the absence of DNA-214 did not initiate any interactions between H1 and H2 (**Figure S2C (Appendix II)**), thus indicating a stable and leak-proof HCR system.

The second part of the HCR-AgNCs biosensor concerned the application of the end-to-end AgNCs transfer between two DNA probes. As mentioned earlier, both DNA probes (*i.e.,* P1 and P2) shared a complementary hybridisation segment. Whilst the length of this complementary hybridisation segment was previously reported to be 13 bp [149], the hybridisation efficiency between P1 and H1 had to be considered. From preliminary screening of the interaction between P1 and H1, the 12-mer toehold of H1 was not sufficient to maintain a stable duplex structure (H1-P1) with P1. With this in mind, the number of hybridisation bp between P1 and H1 was increased. The increase in hybridisation bases meant that part of the stem of H1 would open and hybridise with P1. By increasing the number of hybridisation bp by 4-mer (*i.e.,* 16, 20, 24 and 28), the stability of the H1-P1 duplex could be determined with the aid of NUPACK. The findings shown in **Figure S3A (Appendix II)** displayed an increase in stability of the H1-P1 duplex, which was proportional to the number of interactive bases. This was also reflected in the estimated ΔG value of the duplex structure. For example, the ΔG values of H1-P1 at 12 and 24 bp were estimated to be -32.89 and -41.09 kcal.mol^{-1}, respectively. Moreover, the equilibrium H1-P1 duplex concentration of 12 and 24 bp were 1.3 and 98%, respectively. Based on these evaluations, 24 bases were selected as the length of the hybridisation segment between H1 and P1. **Figure S3B (Appendix II)** illustrated the MFE H1-P1 duplex structure with the estimated ΔG of -41.09 kcal.mol^{-1}, with complementary base-pairing throughout the sequence. This sequence was then translated to the complementary hybridisation segment between P1 and P2. **Figure S3C (Appendix II)** illustrated the MFE P1-P2 duplex structure with an estimated ΔG of -35.58 kcal.mol^{-1}.

4.4.3 Feasibility of HCR-AgNCs design

To experimentally verify the feasibility of the HCR-AgNCs design, the HCR performance was first investigated. As depicted in **Figure 4.1A**, in the presence of DNA-214 (**lane 4**), a series of high molecular weight bands were detected, indicating that DNA-214 specifically initiated HCR and formed elongated products. In contrast, without DNA-214 (**lane 3**), the sample did not show any signs of hybridisation, indicating that the two hairpin probes can coexist stably in solution. This finding was consistent with the NUPACK analysis shown earlier in **Figure S2 (Appendix II)**.

Next, the fluorescence properties of P2-AgNCs and P1-P2-AgNCs, which represent dark and bright AgNCs respectively, were studied. P2-AgNCs displayed a weak fluorescence emission at 611 nm; whereas P1-P2-AgNCs showed a significantly enhanced fluorescence emission in the same region (**Figure 4.1B**). The λ_{EM} was in accordance with the reported value for AgNCs caged in C-rich sequence (*i.e.*,610 nm) [149]. This confirmed the successful end-to-end transfer of the dark AgNCs species from P2 to P1 upon hybridisation, despite the distance between them (*i.e.,* 24 bp) being almost twice the reported distance (*i.e.,* 13 bp). After proven the successful end-to-end cluster transfer, P1 and P2-AgNCs were sequentially introduced to the HCR system. Without DNA-214, the conformation of hairpins remained intact, thereby enabling the toehold region of H1 to hybridise with P1. As such, the dark AgNCs could not be transferred to P1 and remained in P2, as evidenced from the low fluorescence intensity of the sample without DNA-214 (**Figure 4.1C**). Comparatively, in the presence of DNA-214, H1 probes were used for HCR amplification, leading to formation of P1-P2-AgNCs duplexes. The close proximity, as well as higher binding affinity of AgNCs to C-rich region of P1, facilitated the end-to-end cluster transfer from P2 to P1, and activated the red emission of the AgNCs. Notably, the fluorescence was so intense that it was even observable with naked eyes under a UV transilluminator (**Figure 4.1C**).

P1-P2-AgNCs were further characterised using TEM and XPS. The TEM image in **Figure 4.1D** shows that the as-synthesised AgNCs have an average diameter of ~3 nm, which was comparable to other C-rich DNA AgNCs species [266]. The XPS spectrum shows two peaks at 367.9 and 373.9 eV (**Figure 4.1E**), which correspond to $3d_{5/2}$ and $3d_{3/2}$ transition bands of Ag(0), respectively. This indicated successful formation of AgNCs [279].

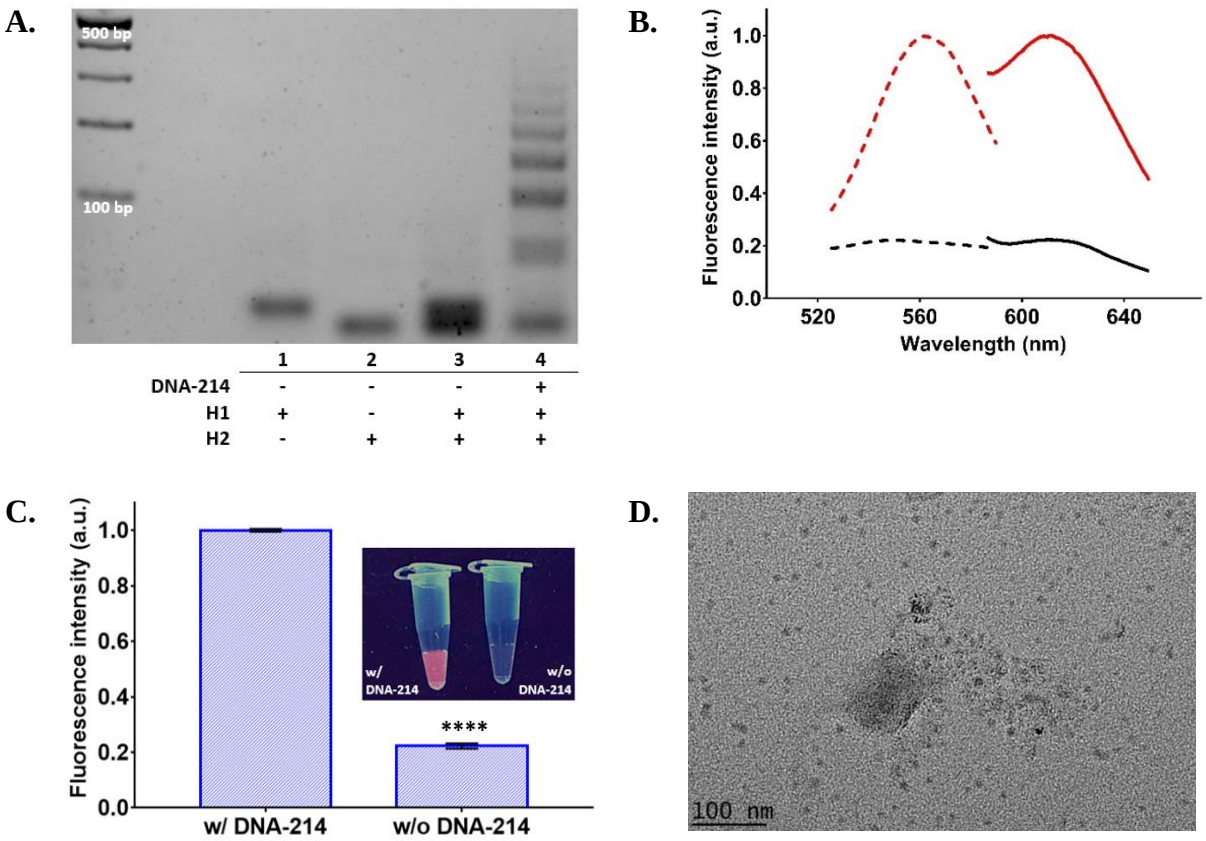


Figure 4.1 (A) Agarose gel image of samples after HCR. **(B)** Excitation (dashed) and emission (solid) spectra of P2-AgNCs (black) and P1-P2-AgNCs (red). **(C)** Fluorescence profile of samples with and without DNA-214, with their real images shown as inset. Data presented as mean ± SEM. ****, $p<0.0001$. **(D)** TEM image of P1-P2-AgNI **(E)** XPS spectrum of P1-P2-AgNCs.

4.4.4 Condition optimisation of HCR-AgNCs biosensor

Since the biosensor performance was dependent on both HCR amplification and AgNCs transfer from P2 to P1, their respective reaction conditions were further optimised to enhance the biosensor sensitivity. The optimisation was performed using JMP, whereby fluorescence intensities of the samples measured under each experimental condition were used as inputs for the software. A response surface model was then built to illustrate the changes in fluorescence intensity across the tested parameters [235,236]. To determine the

optimum reaction conditions, a prediction profiler based on the maximum desirability factor was employed [237].

The correlation between molar ratio of P2: Ag^+: $NaBH_4$ and the incubation time of P1 and P2-AgNCs, was first investigated in a full factorial design. The former was to determine the best molar ratio to produce the dark AgNCs; whereas the latter was to ensure sufficient time for an efficient end-to-end cluster transfer of dark AgNCs from P2 to P1. Based on the surface plot (**Figure 4.2A**) and prediction profiler (**Figure 4.2B**), a molar ratio of 1: 15.4: 15.4 with an incubation period of 55 min were chosen. Next, the correlation between HCR incubation temperature and HCR duration, was also studied in a full factorial design. The experiments were conducted from 25 to 40 ^oC with a 5 ^oC interval, across a 2 h period with a 0.5 h interval. The plot (**Figure 4.2C**) and prediction profiler (**Figure 4.2D**) showed that 32 ^oC for 1.4 h incubation produced the maximum fluorescence intensity. These optimised conditions were then used throughout the experiments.

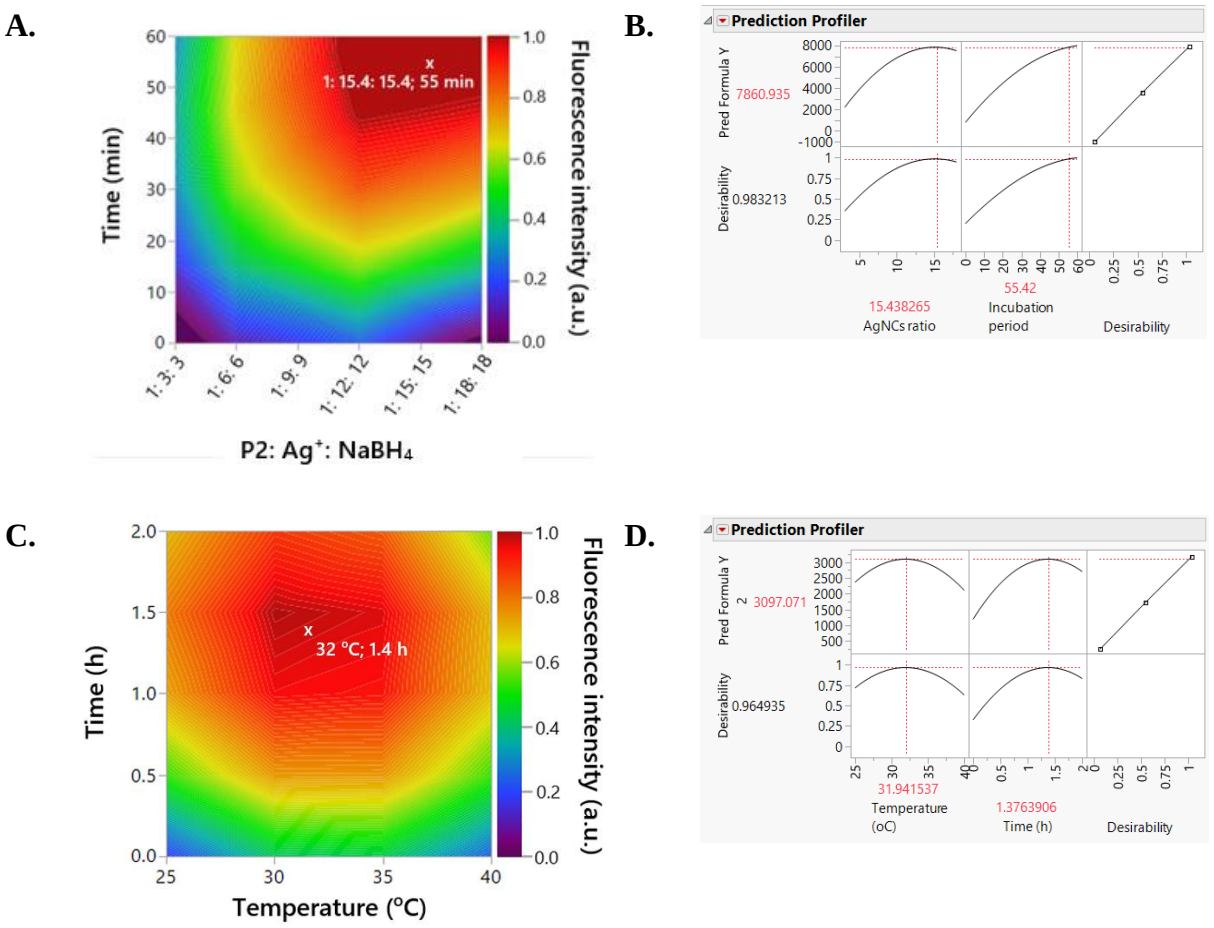


Figure 4.2 (A) Surface contour plot of fluorescence intensity as a function of P2-AgNCs molar ratio and P1-P2-AgNCs incubation period. **(B)** Screenshot of JMP prediction profiler used to find the optimised AgNCs preparation conditions. **(C)** Surface contour plot of

fluorescence intensity as a function of HCR incubation temperature and duration. **(D)** Screenshot of JMP prediction profiler used to find the optimised HCR incubation conditions. The prediction profilers utilise a desirability function, where the values from 0 to 1 indicates the scale of desirable response [237].

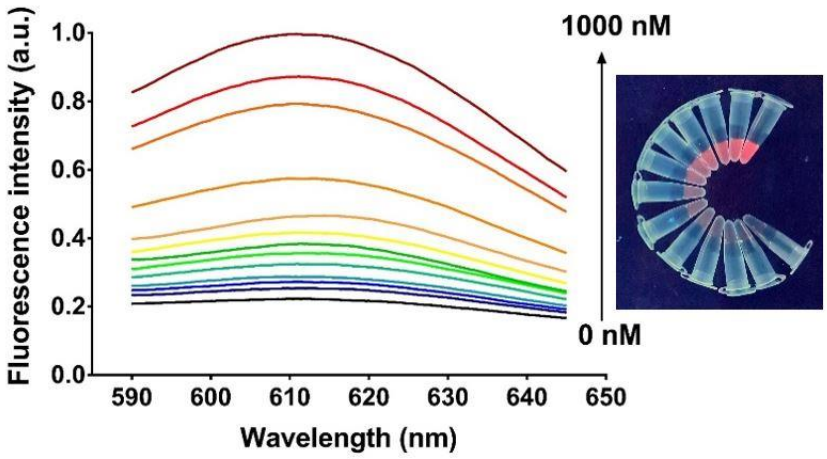
4.4.5 Analytical performance of HCR-AgNCs biosensor

4.4.5.1 Sensitivity test

Under the optimised conditions, the performance of the proposed HCR-AgNCs biosensor towards DNA-214 detection was investigated. As shown in **Figure 4.3A**, the fluorescence intensity at 611 nm gradually increased with increasing concentrations of DNA-214. Notably, the colour change was also observable to the naked eye, with the minimum concentration detected at ~1 pM. In contrast to the known HCR-AgNCs biosensors, only a handful of studies actually reported visible fluorescence emission (*i.e.,* intracellular imaging) [11,160,164]. The lack of qualitative fluorescent HCR-AgNCs studies could be due to the selection of AgNCs templating sequence, preparation method, and the presence of interfering molecules.

Figure 4.3B represented the detection ranges of the biosensor. Note that the RSD of the first detection range (100 – 1000 nM) were below 8%, whereas those of second detection range (100 fM – 100 nM) were below 3%. This implied the high precision and reproducibility of the HCR-AgNCs biosensor. The LOD was calculated to be 3.35 fM based on LOD = k σ_B/b, where k represents the expansion factor, σ_B as the standard deviation and b as the slope of the line [238].

A.



B.

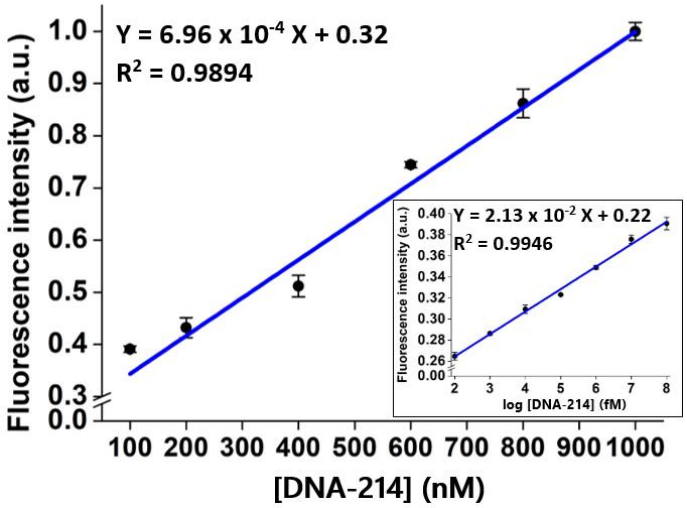


Figure 4.3 (A) Fluorescence emission spectra and sample images (inset) at different concentrations of DNA-214 (from bottom to top: 0 M, 100 fM, 1 pM, 10 pM, 100 pM, 1 nM, 10 nM, 100 nM, 200 nM, 400 nM, 600 nM, 800 nM, 1000 nM). **(B)** Calibration plot of fluorescence emission intensity at different concentrations of DNA-214 (n = 4). First detection range between 100 nM and 1 µM. Second detection range (inset) between 100 fM and 100 nM.

The performance of the proposed HCR-AgNCs biosensor was compared with other recently reported methods used for DNA detection, including colorimetric, electrochemical and fluorescence strategies (**Table 4.2**). The wide detection range and low LOD can be ascribed to the simplicity of the HCR design, as well as versatility of the transferable AgNCs approach.

Table 4.2 Comparison of the proposed HCR-AgNCs biosensor with other reported DNA biosensors

Method	**Material**	**LOD**	**Detection range**	**Reference**
Electrochemical	Cobalt oxide porous nanocubes	0.38 pM	1 pM – 1 μM	[280]
Electrochemical	Peptide nucleic acid	57 fM	0.1 – 100 pM	[281]
Colorimetric	PCR/gold nanoparticles	4.3 fM	16 fM – 1.6 nM	[282]
Fluorescence	Plasmonic metasurface/peptide nucleic acid	50 fM	50 fM – 5 pM	[283]
Electrochemiluminescence	gold nanotriangle/gold nanoparticles/carbon dots	514 aM	50 fM – 100 nM	[284]
Fluorescence	Catalytic hairpin assembly/DNAzyme	0.5 pM	0.5 – 10 pM	[285]
Chemiluminescence	Exonuclease-assisted HCR	5.7 fM	10 fM – 100 pM	[286]
Electrochemical	Carbon nanotube	2 fM	1 pM – 1 μM	[287]
Fluorescence	HCR-AgNCs	3.35 fM	100 fM – 1 μM	This work

4.4.5.2 Selectivity test

The selectivity of the HCR-AgNCs biosensor was further against different controls, including blank (*i.e.*, without DNA-214), sequences with mismatched bases (*i.e.*, mismatch n, where n indicates the number of mismatches in the sequence), and non-target sequences (*i.e.*, DNA analogues of miR-141 (DNA-141), miR-199a (DNA-199a), miR-205 (DNA-205) and miR-200a (DNA-200a)), as well as mixture (*i.e.*, DNA-214 mixed with the aforementioned non-target controls) were studied in this test. The concentration used for DNA-214 and controls (*i.e.*, mismatch and non-target sequences) used in the selectivity test was fixed at 1 μM. **Figure 4.4** showed that the fluorescence intensities of samples containing DNA-214 (*i.e.*, DNA-214 and mixture) were about 5-fold higher than those without DNA-214. Moreover, the fluorescence intensities of the negative controls (*i.e.*, mismatches and non-targets) showed non-significant difference as compared to that of blank solution. This finding showed that the HCR-AgNCs biosensor was highly selective and capable of discriminating down to single-base mismatch even in a mixture sample with target DNA-214.

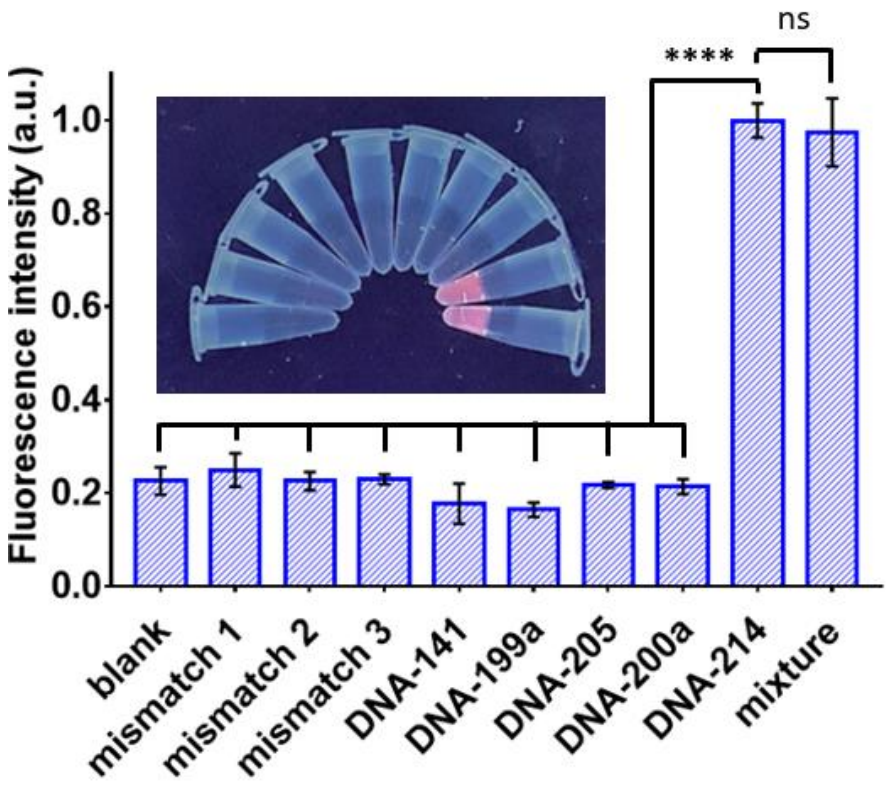


Figure 4.4 Selectivity test of HCR-AgNCs biosensor against DNA-214 and its different controls (n = 4). The real sample images are shown as inset. Data presented as mean ± SEM. ****, $p < 0.0001$; ns, non-significant.

4.4.6 Detection of DNA-214 in human serum sample

To evaluate the performance of the HCR-AgNCs biosensor in a real biological sample solution, spike-and-recovery experiments were conducted by spiking different concentrations of DNA-214 into diluted human serum samples, similar to other reported studies [288,289]. Based on the detection range obtained in **Figure 4.3B**, the concentrations of DNA-214 to be tested in diluted human serum samples were selected to be 5 pM, 500 pM, 50 nM and 500 nM. Five independent biosensor responses to the spiked samples of DNA-214 were measured to calculate their respective concentrations from the calibration plot in **Figure 4.3B**. Then the average recovery (%) was calculated with the following **Equation (1)**:

$$\text{Recovery (\%)} = \frac{\text{Concentration of DNA-214 detected}}{\text{Concentration of DNA-214 added}} \, x \, 100 \qquad \textbf{(1)}$$

As shown in **Table 4.3**, the recoveries of DNA-214 ranged from 92 to 102% with RSD less than 10%. These findings highlighted that the biosensor was relatively accurate and stable in complex samples.

Table 4.3 Detection of DNA-214 in human serum samples using the proposed HCR-AgNCs biosensor (n=5).

Sample	Added	Detected	Recovery (%)	RSD (%)
1	500 nM	510 nM	102	9.87
2	50 nM	50 nM	100	4.75
3	500 pM	480 pM	96	6.16
4	5 pM	4.6 pM	92	1.46

4.5 Summary

In summary, a new approach to build a HCR-AgNCs biosensor was adopted with AgNCs as externalised fluorogenic. This method facilitated the design of a stable HCR system without additional constraints posed by long C-rich AgNCs templating sequences and

detect DNA-214 with high precision. In addition, AgNCs could be prepared separately in a controlled environment, free from interfering molecules. Another key feature of the proposed HCR-AgNCs biosensor was the end-to-end cluster-transfer approach to activate AgNCs fluorescence. As previously mentioned, this approach lacked follow-up studies and adaptations since its introduction [147]. However, the results reported in this chapter showed a significant fluorescence enhancement in conjunction to HCR amplification. The proposed HCR-AgNCs biosensor produced a strong red fluorescence that was proportional to the concentration of DNA-214, with fluorescence changes that were visible to the naked eye, down to 1 pM. The HCR-AgNCs biosensor exhibited good sensitivity with LOD of 3.35 fM, good selectivity to discriminate single-base mismatch and non-target sequences, as well as the satisfactory accuracy and reproducibility in human serum samples. However, further experiments are required to validate its overall performance, especially in human serum. For example, more sample concentrations within the detection range (i.e., 100 fM – 1 μM) should be evaluated (e.g., at every magnitude from 100 fM – 1 μM). Similar to the work in Chapter 3, specific limitations in the study included incomplete gel data evaluation and the insufficient use of biological replicates to test applicability of the HCR-AgNCs biosensor, which could be considered for future work in the field. Given the simplicity and versatility of the working principle, the proposed HCR-AgNCs biosensor is highly adoptable and can be easily translated to detect other types of analytes by simply replacing the target sequence with a specific DNA aptamer sequence.

Chapter 5: Development of a magnetic-assisted HCR-AgNCs biosensor for the detection of miR-144-3p

5.1 Overview

In this chapter, the process of integrating a magnetic module into a ratiometric HCR-AgNCs biosensor for the detection of miR-144-3p is described. The rationale behind this is to isolate the target miR directly from its source and analyse it, instead of the conventional processing and dilution of an already low miR abundance. With this in mind, magnetic separation is suggested and designed to be compatible to the operation and performance of HCR-AgNCs, through the use of assistive DNA probes for an isothermal bidirectional strand displacement strategy. In addition, this study also serves as a follow-up study of the ratiometric HCR-AgNCs biosensor introduced in **Chapter 3**. In this work, a split AgNCs chemopalette templating sequence is utilised for a red-yellow dual-emissive fluorescence response. Preliminary work focuses on DNA probe design with computational analysis, for a feasible magnetic separation process, as well as a stable and efficient HCR-AgNCs ratiometric analysis. Results from this study validate the feasibility of the MB-HCR-AgNCs biosensor, with great sensitivity and selectivity towards miR-144-3p. Towards the end of the study, the effectiveness and reliability of the MB-HCR-AgNCs biosensor are tested in raw human serum sample, with a satisfactory recovery percentage. At the end of this chapter, the key findings of this MB-HCR-AgNCs biosensor study are summarised, that highlight its potential to translate conventional HCR-AgNCs biosensors from the laboratory to real world application.

5.2 Background

As implied in **Section 2.2.2**, most of the currently available miR detection strategies require high quality extraction, preparation, and purification, aside from the technical skills and equipment that are necessary for accurate and precise analysis. For that reason, more cost, labor and time are added into the process of miR detection [24,43,44]. To reiterate from **Section 2.5**, HCR-AgNCs biosensors operate on a simple DNA hybridisation mechanism and have reported practical applications in complex samples (*i.e.*, human serum), with remarkable accuracy and reproducibility. However, the practical applications of these HCR-AgNCs

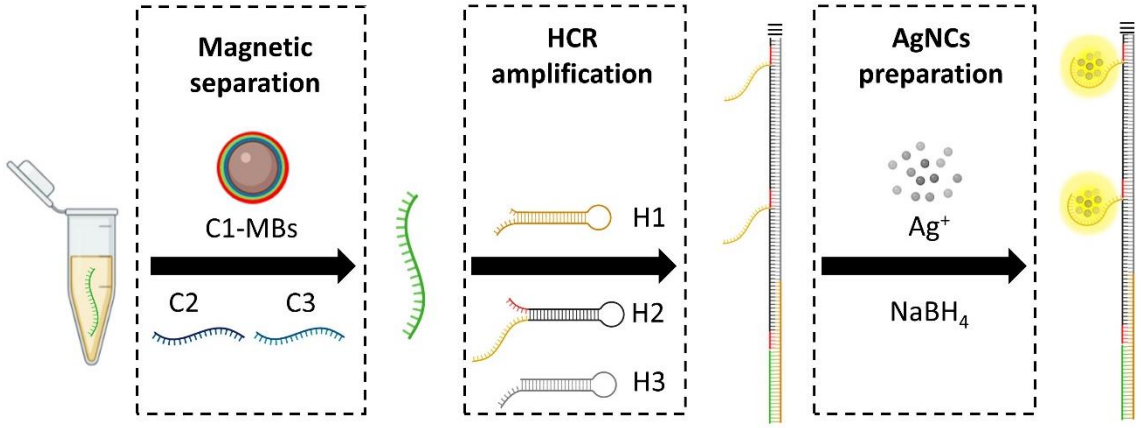
biosensors would still require a dilution (10- to 100-folds) of the complex sample solution, due to the interfering molecules in the solution that can affect specific AgNCs formation after HCR amplification. This was evidenced in **Section 3.4.6**, where even with 100-fold dilution, there was a relative difference in the calibration plots when compared to buffered condition in **Section 3.4.5.1**. In fact, the dilution of complex samples can further reduce the concentration of the already low-abundant miRs [12,75,161,165]. That being the case, the accuracy and reliability of HCR-AgNCs biosensors may be compromised, especially when extremely low levels of miRs are concerned.

To curb with this issue, it is suggested that miRs need to be separated from their complex matrices. Some of the separation techniques, such as mass-based centrifugation and size-based filtration, are unable to discriminate the target sequence from non-targets of relatively similar sizes. Moreover, these methods are only strictly operational in the lab and unsuitable for on-site applications. On the contrary, MBs are one of the most commonly used tools in biosensing for purification, detection and quantification of biomolecules from complex matrices, with better versatility, accuracy and sensitivity [290–292]. These beads are normally functionalised with a biological recognition element, such as nucleic acids and antibodies. As compared to centrifugation and filtration, magnetic separation features good specificity, better recovery of biological targets, and avoids undesired sample dilution due to the lesser buffer used. As demonstrated by Yao *et al.* on a HCR assay for detection of pesticides, introducing magnetic separation has significantly reduced the background interference with LOD for chlorpyrifos as 2 $ng.mL^{-1}$ [293]. Similarly, a recent study reported by Zhang and co-workers have shown that magnetic separation could eliminate inner filter effect of their fluorogenic biosensor, resulting in a wider detection range and a lower LOD, as compared to that without magnetic separation [294]. To the best of found knowledge, studies have been done on magnetic-based HCR sensors [86,293,295–300], but not all three MBs, HCR and AgNCs in a single assay.

In the process of developing the MB-HCR-AgNCs biosensor, miR-144-3p is selected as a model target, which is a potential biomarker for NPC. NPC is a type of head and neck cancer, which is highly prevalent in Southeast Asia and North Africa. Current NPC detection (*i.e.,* nasopharyngoscopy, biopsy and imaging tests) are rather invasive, costly, and require both highly skilled professionals and well-equipped medical facilities. Thus, alternative strategies, like miR cancer biomarker detection, are sought to facilitate NPC detection. MiR-144-3p has been identified to be consistently upregulated in NPC tissues, with an oncogenic

and pro-angiogenic role in NPC tumorigenesis. MiR-144 directly targets the tumour suppressor PTEN that regulates cell proliferation, invasion, and metastasis in NPC samples. In contrast, the downregulation of miR-144 led to cell cycle arrest of NPC cells [301–306]. This implies that the detection of miR-144-3p can assist with the assessment of NPC.

Herein, a MB-HCR-AgNCs ratiometric biosensor is developed as illustrated in **Scheme 5.1**. The entire detection procedure operates at mild isothermal conditions, with the use of only DNA hairpins and probes (*i.e.*, C1, C2, C3, H1, H2 and H3). MiR-144-3p is first magnetically isolated by C1-MBs from a complex solution, and then displaced by two short assistive probes, C2 and C3, for subsequent HCR amplification. HCR amplification is performed by a set of three DNA hairpins (*i.e.*, H1, H2, and H3). Finally, AgNCs will be prepared, and their fluorescence emission measured for ratiometric analysis. The ratiometric fluorescence approach in this biosensor bears some resemblance to that introduced in **Chapter 3**, with another proximity-dependent AgNCs strategy. In this study, a split AgNCs chemopalette templating sequence is hosted on H2 for a red-yellow fluorescence response. Split AgNCs templating sequences were previously introduced in **Section 2.4.4.4**, whereby the fragmented pairs would not initiate any fluorescence response from partial AgNCs formation. Only when these split pairs are brought in close proximity, the AgNCs templating sequence can be completed for the fluorescence emission can then be re-activated. By combining the three components into a single MB-HCR-AgNCs assay, direct and simple detection of low-abundant miR in complex samples could be achieved.



Scheme 5.1 Outline of MB-HCR-AgNCs for the detection of miR-144-3p.

5.3 Methodology

5.3.1 Materials

Most of the materials used in this study were similar to the study in **Chapter 3**, and the details were as described in **Section 3.3.1**. In addition, Streptavidin MBs were purchased from New England Biolabs (Massachusetts, USA). EDTA ($[CH_2N(CH_2CO_2H)_2]_2$), sodium acetate (CH_3COONa), sodium chloride (NaCl), sodium hydroxide (NaOH) and sodium nitrate ($NaNO_3$) were obtained from Nacalai Tesque (Kyoto, Japan). Hydrochloric acid (HCl) and boric acid (H_3BO_3) were obtained from Fisher Scientific (New Hampshire, USA).

DNA and miR samples were of standard desalted grade and obtained from IDT (Iowa, USA). The sequences of miR-144 and non-target controls were adapted from www.mirbase.org. The sequences are listed in **Table 5.1**. All mismatch and non-target sequences used were DNA analogues in place of their RNA counterparts, for cost-effectiveness, stability and ease of handling. Prior to usage, the oligonucleotides were dissolved in molecular grade water to produce stock concentrations of 100 μM. MiR-144-3p was dissolved in DEPC-treated water to obtain stock concentration of 100 μM.

Table 5.1 Oligonucleotide sequences used in this work. Red letters indicate AgNCs templating sequence. Italicised letters indicate hairpin stem region. Bold letters indicate hairpin loop. Underlined letters indicate mismatch base(s).

DNA/RNA	Sequence (5' – 3')
C1	Biotin – TTA TTA TTA TCT CTC GAG TAC ATC ATC TAT ACT GTA TCA TGA
C2	ATG ATG TAC TCG AGA G
C3	TCA TGA TAC AGT ATA G
H1	CC*A TAG ATG ATG TAC T***AG CGG TG***A GTA CAT CAT CTA T*AC TGT A
H2	CAC CGC T*AG TAC ATC ATC TAT GGC* **ATC G***GC CAT AGA TGA TGT ACT* TTT TGC CTT TTG GGG ACG GAT A
H3	*CCA TAG ATG ATG TAC T***AG CGG TG***A GTA CAT CAT CTA TGG* CCG ATG
miR-144-3p	UAC AGU AUA GAU GAU GUA CU
mismatch 1	TAC AGT ATA CAT GAT GTA CT

mismatch 2	TAC AGT TTA CAT GAT GTA CT
mismatch 3	TAC AGT TTA CAT GAT GAA CT
miR-9-5p	TCT TTG GTT ATC TAG CTG TAT GA
miR-21-5p	TAG CTT ATC AGA CTG ATG TTG A
miR-144-5p	GGA TAT CAT ATA CTG TAA G

5.3.2 Design of DNA oligonucleotides

DNA hairpins and probes (*i.e.*, C1, C2, C3, H1, H2 and H3) were designed according to the sequence of miR-144-3p using NUPACK, OligoAnalyser tool, and Kinetics Calculator.

5.3.3 Functionalisation of MBs with C1

Briefly, the MBs were first washed three times with binding buffer (20 mM tris-HCl, 0.5 M NaCl, 1 mM EDTA, pH 7.5). Biotinylated C1 (5 μM) was then added to the MBs and incubated for 30 min at 30 ^{o}C with mild shaking. The C1-MBs were then collected and washed three times, to remove the excess unbound C1. Finally, the C1-MBs were dispersed in HCR buffer (10 mM tris-acetate, 1 mM $Mg(NO_3)_2$, 100 mM $NaNO_3$, pH 8) and stored at 4 ^{o}C prior to usage.

5.3.4 Magnetic separation of miR-144-3p

Sample solution containing miR-144-3p was mixed with C1-MBs and incubated for 4 min with mild shaking. The captured miR-144-3p was magnetically separated, washed three times and re-suspended in HCR buffer. Next, excess C2 and C3 (1 μM each) were added to the mixture and incubated for 40 min with mild shaking to displace miR-144-3p. The MBs were then magnetically separated, and the supernatant containing miR-144-3p was collected for further analysis.

5.3.5 Quantitative analysis of miR-144-3p

The DNA hairpins (H1, H2 and H3) were heated at 95 ^{o}C for 5 min and snap-cooled in an ice bath for 30 min before use. HCR was initiated when supernatant containing miR-144-3p was mixed with H1, H2 and H3 (1: 2: 2; μM) and incubated for 2 h at 35 ^{o}C. Thereafter, AgNCs were prepared based on a H2: $AgNO_3$: $NaBH_4$ molar ratio of 1: 12: 6 (μM) [148,150,307,308]. Briefly, $AgNO_3$ solution was added into the hybridisation solution, followed by vigorous shaking for 30 s. After 15 min, $NaBH_4$ was added with vigorous shaking for another 2 min. The reaction mixture was left in the dark for 1 h before fluorescence measurement.

5.3.6 Gel electrophoresis

Agarose gel electrophoresis was conducted similarly as described in **Section 3.3.4**.

5.3.7 Fluorescence measurement

Fluorescence measurements were performed using a Hitachi F-7000 Fluorescence Spectrophotometer with similar settings, as described in **Section 3.3.5**. In this study, the λ_{EX} used were 502 and 596 nm, for the respective peaks at λ_{EM} of 564 and 650 nm. F_y/F_r were calculated from the fluorescence intensities at λ_{EM} of 564 and 650 nm.

5.3.8 Characterisation of AgNCs

The formation of AgNCs was characterised with TEM and XPS, similar to that described in **Section 4.3.7**.

5.3.9 MBs regeneration

To regenerate and reuse MBs, the MBs were suspended in 50 μL HCR buffer after magnetic separation of miR-144-3p. The MBs solution was heated at 95 ^{o}C for 90 s to

remove C2 and C3 probes from C1-MBs. The supernatant was discarded and the MBs were re-dispersed in 50 μL HCR buffer. The MBs solution was then stored at 4 ^{o}C prior to usage.

5.3.10 Detection of miR-144-3p in human serum sample

Human serum samples obtained from Universiti Teknologi Mara (Selangor, Malaysia) were prepared similarly as described in **Section 3.3.7**. In this study, a range of concentrations of miR-144-3p (500 fM, 50 pM, 5 nM and 50 nM) were spiked in different concentrations human serum samples (100% and 10%) and analysed immediately with the MB-HCR-AgNCs biosensor. 10% human serum samples were diluted using HCR buffer. In addition, five technical replicates were performed from one biological human serum sample. These spiked samples were detected as described in **Section 5.3.5**, with their fluorescence measured as described in **Section 5.3.7**.

5.3.11 Data analysis

GraphPad Prism 7.4.6 was used to analyze the data, and the data were presented as mean ± SEM. Student's t-test was used to compare data between two groups. One-way ANOVA and the Tukey's test were used to compare data between more than two groups. Statistical significance was denoted by $p < 0.05$.

5.4 Results and Discussion

5.4.1 Sensing strategy

The MB-HCR-AgNCs biosensor consisted of three main steps as detailed below:

a) Magnetic separation

The process of magnetic separation was as shown in **Scheme 5.2A**, which involved three DNA probes (*i.e.*, C1, C2 and C3). C1 probes were complementary to miR-144-3p on MBs to isolate miR-144-3p from sample solution. After magnetic separation and washing step, excess C2 and C3 were added to induce bidirectional strand displacement of miR-144-3p, hence forming C1-C2-C3-MBs. Different ways to elute the captured miR-144-3p from MBs were studied, and it was found that conventional elution methods of nucleic acids, such

as heating, changing ionic strength or pH [309], were inappropriate in this case. This is because high temperature could degrade the miR [310,311], whereas changing ionic strength or pH may disrupt the performance of HCR and AgNCs in subsequent steps [312]. Additionally, unidirectional displacement would involve probes with the same sequence as target miR and cause false-positive results. As such, a bidirectional strand displacement strategy was chosen. The DNA probes (i.e., C2 and C3) were designed in a way that they would induce the bidirectional strand displacement of miR-144-3p, but these probes would not initiate HCR amplification with the DNA hairpins (i.e., H1, H2, and H3) when in excess. This could be ascribed to the short length of the probes (i.e., having half the length of the H1 stem region) and the terminal sequence (i.e., non-complementary sequence to the H1 toehold) that are only complementary to C1. These characteristics would render C2 and C3 unreactive towards H1 and subsequent HCR amplification.

b) HCR amplification

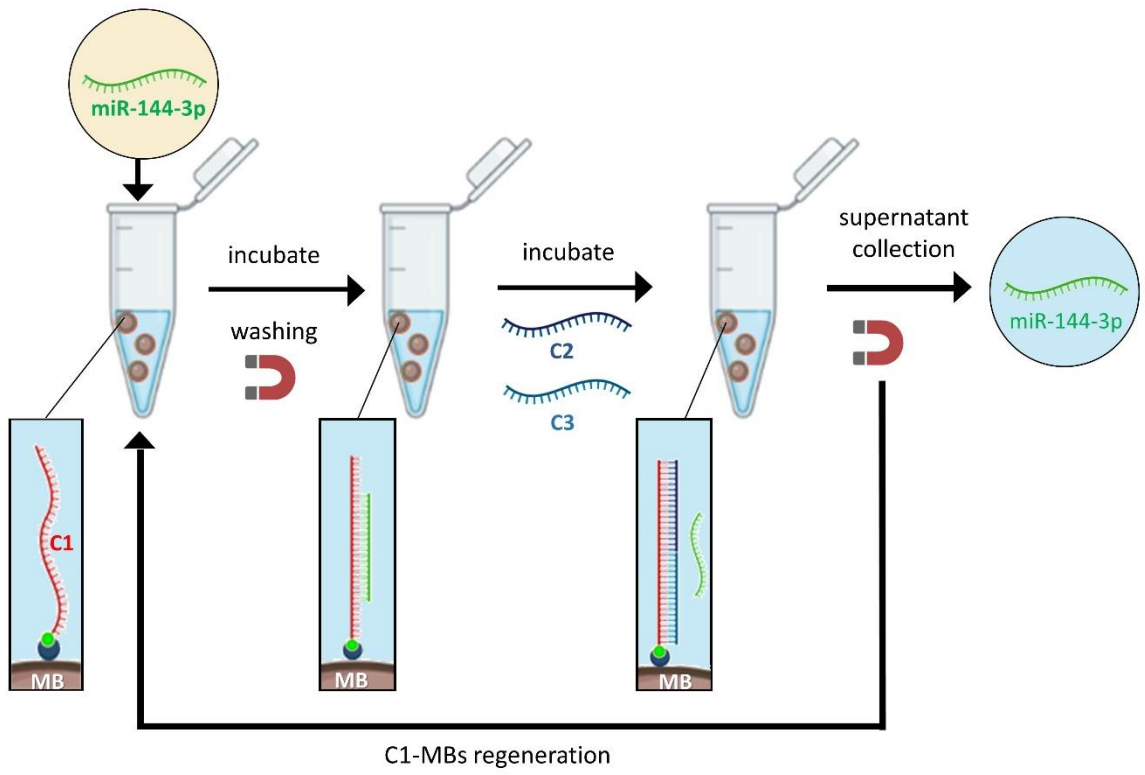
The eluted miR-144-3p in supernatant was then amplified by HCR using a pool of three DNA hairpins (*i.e.*, H1, H2 and H3) **(Scheme 5.2B)**. Due to the relatively short length of miR-144-3p (20-mer), H1 was introduced as a preliminary capture probe, to better stabilise and improve efficiency of the subsequent HCR amplification process. H1 would also determine the specificity for the HCR-AgNCs biosensor towards miR-144-3p. In **Chapter 3**, it was shown that the effective design of the proposed ratiometric HCR-AgNCs yielded great sensitivity and selectivity. In this case, the toehold region of H2 contained split AgNCs templating sequences (*i.e., -CAC CGC T-* and *-TTT TGC CTT TTG GGG ACG GAT A-*), which were reported to generate dark and yellow/green-emissive species, respectively. Interestingly, when the two sequences were brought into close proximity, red emissive species was obtained instead [148,150,307,308]. Leveraging on the template transformation of AgNCs, locating these AgNCs templating sequences at the toehold region of H2 would enable a ratiometric analysis of miR-144-3p as described below.

c) Detection using AgNCs

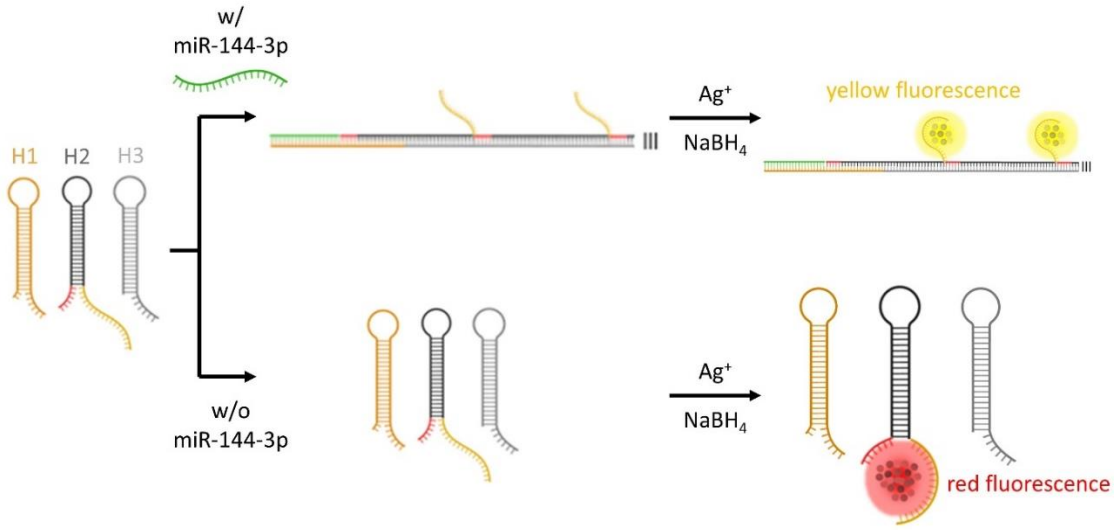
After steps (a) and (b), AgNCs were prepared to generate emission signal (**Scheme 5.2B**). Without miR-144-3p, only unreacted C2 and C3 were collected from the supernatant.

As such, H2 retained its hairpin conformation with the two toehold regions physically close to each other. Preparing AgNCs from this sample solution would hence result in red emission. However, in the presence of miR-144-3p, that had been magnetically isolated in the supernatant, HCR would be initiated among the DNA hairpins to form HCR products. During this process, part of the split AgNCs templating sequence (-*CAC CGC T*-) would be actively used in the hybridisation reaction and form dsDNA concatemers, thus leaving another part of the split AgNCs templating sequence (-*TTT TGC CTT TTG GGG ACG GAT A*-) hanging as tails from the HCR product to host yellow emissive clusters. Hence, measuring the F_y and F_r would enable a ratiometric analysis of miR-144-3p.

A.



B.



Scheme 5.2 Principle of MB-HCR-AgNCs biosensor, involving **(A)** magnetic separation, **(B)** HCR amplification and detection with AgNCs.

5.4.2 Computational design of MB-HCR-AgNCs biosensor

With the outline in mind, the DNA hairpins and probes were designed for the MB-HCR-AgNCs biosensor. For the process of magnetic separation, three DNA probes (*i.e.*, C1, C2, and C3) were designed. C1 would be biotinylated at the 5'-end terminals for binding to the streptavidin-coated MBs. A spacer, comprising only A and T bases, was introduced between the biotin and capture region of C1 to prevent molecular crowding and mediate a better capture process. As implied earlier, C1 was responsible for capturing miR-144-3p and thus would be complementary to the sequence of miR-144-3p. To facilitate the bidirectional strategy, C1 would contain additional 6 bases at both ends of the complementary sequence. NUPACK was used to check the hybridisation efficiency between C1 and miR-144-3p. **Figure S1A (Appendix III)** showed complete hybridisation between C1 and miR-144-3p when equimolar concentration (1 μM) of both were analysed. **Figure S1B (Appendix III)** illustrated the duplex structure of C1-miR-144-3p, which showed that the hybridisation between C1 and miR-144-3p is complete with binding probability of 1.0 throughout the entire duplex. The ΔG of the duplex structure was estimated to be -23.15 kcal.mol^{-1}.

Following that, C2 and C3 were designed to each contain half the sequence of miR-144-3p and the six additional bases at the terminal segments of C1. NUPACK was used to

check the efficiency of the bidirectional strand displacement strategy, with equimolar (1 μM) C1 and miR-144-3p, along with excess (2 μM) C2 and C3. **Figure S2A (Appendix III)** indicated the complete hybridisation of C1, C2 and C3. MiR-144-3p was noted to be unreacted, thus indicating the high possibility of displacement. The MFE complex structure in **Figure S2B (Appendix III)** showed the probability binding of C1, C2 and C3, with most bp having an equilibrium probability close to 1.0. The estimated ΔG of the duplex structure was -38.05 kcal.mol^{-1}.

The design of DNA hairpins (*i.e.*, H1, H2 and H3) presented a challenge due to the short length of miR-144 (20-mer). As aforementioned, H1 was expected to serve as a capture probe for miR-144-3p, and a stabiliser for H2 and H3 hybridisation. H1 was designed to have a 2-mer 2^{o} toehold to increase the stem length of H2 and H3 by two bp, which strengthens their structural stability. This was in compliance with the guideline that suggested 2^{o} toehold length to be less than 3 bases [64]. H2 comprised the split AgNCs chemopalette templating sequence at the toehold segment. The loop was truncated to four bases and the stem lengthened by one bp, similar to earlier designs in **Chapters 3** and **4**. Overall, the final hairpin structure (inclusive of AgNCs templating sequence) of H1, H2 and H3 adopted the toehold: stem: loop length ratio of 8: 14: 7, 29: 17: 4 and 6: 16: 7, respectively.

The DNA design was run in NUPACK, to determine the best loop and toehold sequence for H1, H2 and H3. This was performed with a similar script input as shown in **Figure S3 (Appendix III)**. From here, a list of sequences was generated and these were screened with NABLAB for the best kinetic conditions [278]. Henceforth, the best sequence was selected based on a balance between thermodynamic and kinetic aspects determined from computational screening. The final sequence of H1, H2 and H3 were as listed in **Table 5.1**.

The thermodynamic properties of these sequences were validated with OligoAnalyser Tool, to study oligonucleotide folding through T_m and ΔG. From **Table S2 (Appendix III)**, the ΔG was estimated to be -10.69, -18.71 and -13.49 kcal.mol^{-1} for H1, H2 and H3, respectively. Based on the guidelines discussed earlier [63], only H2 met the minimum energy threshold (*i.e.,* -16 kcal.mol^{-1}) for metastable DNA hairpins, even with the long C- and G-rich AgNCs templating sequence at the toehold segment. The weak ΔG of H1 and H3 could possibly be associated with the slightly larger loop size (*i.e.,* 7 bases), and the base composition of the DNA hairpin (*i.e.,* more A-T than C-G bp in the hairpin stem). This

finding indicated a substantial concern, as H1 and H3 might cause leakage in the HCR circuit. As a side note, this finding also highlighted the notion that loop size should be prioritised over both the base composition and length of toehold when designing metastable DNA hairpin probes.

Similar to earlier works (**Chapter 3** and **4**), the DNA interactions between the DNA hairpin probes (*i.e.,* H1, H2 and H3) were checked with and without miR-144-3p, through NUPACK analysis. The settings for the analysis were set to equimolar concentration (2 μM) DNA hairpin probes (*i.e.,* H1, H2, and H3), and 1 μM miR-144-3p, with the temperature fixed at 37 ^{o}C. From **Figure S4A (Appendix III)**, HCR amplification was shown to be feasible, and this was evidenced by both depletion of DNA hairpins (*i.e.,* 0.99 μM H1, 0.42 μM H2, and 0.99 μM H3) and the formation of DNA concatemers between miR-144-3p, H1 and H2 (*e.g.,* miR144-H2-H2-H3-H1, and miR144-H2-H3-H1). **Figure S4B (Appendix III)** illustrated the structure of the HCR complex (ΔG = -114.04 kcal.mol^{-1}), based on the equilibrium probability base-pairing. As predicted from the design, the HCR product had one tail, which corresponded to part of the split AgNCs templating sequence (-*TTT TGC CTT TTG GGG ACG GAT A*-). The base-pairing between the DNA probes and miR-144-3p displayed equilibrium probability of 1.0 throughout the entire complex. Since H1 and H3 had estimated ΔG less than the threshold value of -16 kcal.mol^{-1}, the DNA hairpins were checked for any possible non-specific interaction without miR-144-3p. Based on NUPACK analysis, **Figure S4C (Appendix III)** indicated that there were no interactions between H1, H2 and H3, from a thermodynamic standpoint, thus indicating metastable DNA hairpins and a leak-proof HCR system.

As shown in **Scheme 5.2**, C2 and C3 were added in excess and would be collected in the supernatant along with the displaced miR-144-3p for subsequent HCR-AgNCs analysis. With a stable HCR system between the DNA hairpins and miR-144-3p, the possibility of C2 and C3 initiating HCR amplification was determined with NUPACK analysis. Briefly, the interactions between C2, C3, H1, H2 and H3 were tested. The DNA probes were set at equimolar concentration of 1 μM, and the temperature fixed at 37 ^{o}C. **Figure S5A (Appendix III)** displayed the possible interactions between the DNA species. There was no indication of non-specific HCR amplification without miR-144-3p, evidenced by the lack of long DNA concatemer formation between all DNA probes, and the relatively unchanged concentration (*i.e.,* 0.99 to 1 μM) of all DNA probes (except C2-C2 for their negligible duplex formation).

The only cross-species interaction was the formation of C3-H1 (ΔG = -26.08 kcal.mol^{-1}) duplex, but the hybridisation event did not completely open H1 as seen in **Figure S5B (Appendix III)**.

5.4.3 Feasibility of MB-HCR-AgNCs

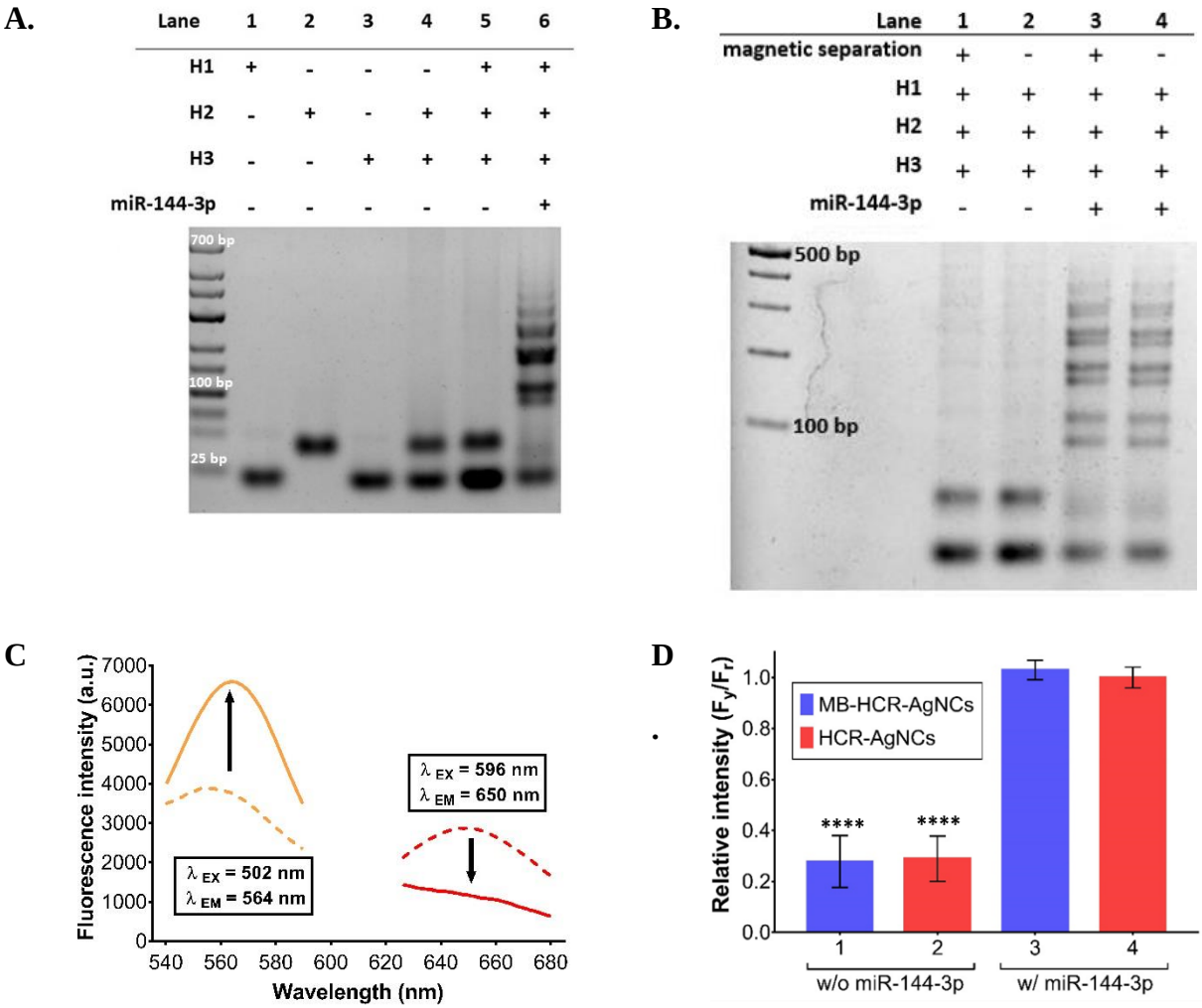
The feasibility of HCR design was first evaluated using gel electrophoresis, as shown in **Figure 5.1A**. As displayed by a series of high molecular weight bands in Lane 6, HCR elongated products only formed in the presence of miR-144-3p and all three DNA hairpins. Without miR-144-3p, only bands that correspond to the unreacted DNA hairpins were observed (Lanes 1-5). This implied that all the three partially complementary DNA hairpins could metastably co-exist with each other.

After confirming the successful HCR design, the bidirectional displacement strategy to elute miR-144-3p was tested for its feasibility. At the same time, the supernatant containing excess C2 and C3 was checked for possible effect on HCR performance. The supernatant samples collected after magnetic separation were incubated with the DNA hairpins and subjected to gel electrophoresis, with results shown in **Figure 5.1B**. Notably, the supernatant sample containing miR-144-3p showed bands of elongated products (Lane 3), similar as sample prepared by directly adding miR-144-3p to the HCR hairpins (Lane 4). This confirmed that miR-144-3p was successfully isolated using MBs, and initiated HCR. It was also note-worthy that both supernatant samples with or without miR-144-3p (Lanes 3 and 1) showed similar band patterns as those prepared directly without magnetic separation steps (Lanes 4 and 2). This indicated that excess C2 and C3 in the supernatant samples did not affect the HCR performance.

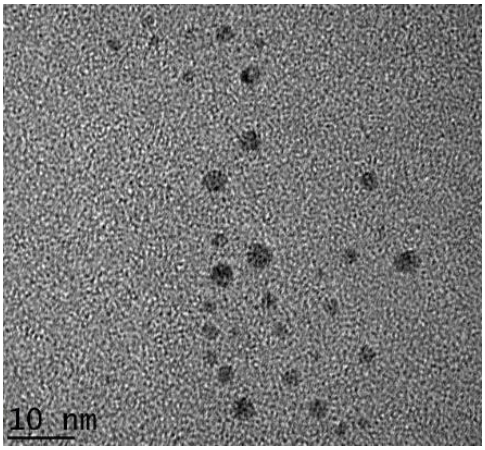
Next, the AgNCs were studied to check whether their fluorescence emission signal would correspond to the amount of miR-144-3p. AgNCs were prepared by directly adding target miR with HCR hairpins as per above, without involving magnetic separation. As displayed in **Figure 5.1C**, sample containing miR-144-3p showed increased yellow emission (λ_{EM} = 564 nm) and decreased red emission (λ_{EM} = 650 nm), as compared to that without target miR. Such changes enabled a ratiometric measurement (F_y/F_r) to quantify miR-144-3p. Similarly, AgNCs were prepared using supernatant samples collected from magnetic

separation. Again, the AgNCs prepared from supernatant samples yielded similar results as those without magnetic separation step (**Figure 5.1D**). Thus, it could be concluded that the proposed MB-HCR-AgNCs was feasible, and that the addition of MBs did not compromise the performance of HCR-AgNCs.

The AgNCs were further characterised using TEM and XPS. Based on the TEM image, AgNCs were spherical in shape with an approximate diameter of 3.34 nm (**Figure 5.1E**). XPS spectrum (**Figure 5.1F**) displayed two peaks at 368.08 and 374.12 eV, which corresponded to Ag $3d_{5/2}$ and $3d_{3/2}$ transition bands, respectively [279]. These results demonstrated that AgNCs had been successfully prepared.



E



F.

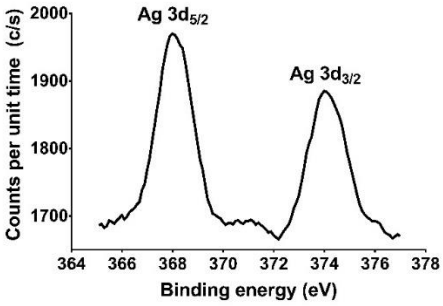


Figure 5.1 Feasibility of MB-HCR-AgNCs biosensor. **(A)** Gel image to study the feasibility of HCR design. **(B)** Gel image to compare HCR performance with (Lanes 1 and 3) and without magnetic separation (Lanes 2 and 4). **(C)** Fluorescence emission spectra of AgNCs with (solid) and without (dashed) miR-144-3p. **(D)** Comparison of relative intensity of AgNCs with (blue) and without (red) magnetic separation, in the presence and absence of miR-144-3p. Data presented as mean ± SEM and statistically analyzed relative to miR-144-3p groups. ****, $p < 0.0001$.**(E)** TEM and **(F)** XPS spectrum of HCR-AgNCs.

5.4.4 Condition optimisation of MB-HCR-AgNCs biosensor

The reaction conditions of MB-HCR-AgNCs biosensor were optimised to enhance its performance. Firstly, the loading capacity of C1 probes on MBs was studied by preparing C1-MBs using different amount of biotinylated C1. The amount of C1 probes conjugated on MB should neither be too little nor too pack. Having small amount of C1 would result in inefficient capture reaction. However, if the capture probes were too closely packed on the magnetic peaks, it may lead to crowding effect, where the DNA probes could not participate in hybridisation reaction due to excessive steric hindrance and electrostatic interactions [313]. The C1-MBs were then used for magnetic separation, HCR and AgNCs formation as described earlier. Their performance was analysed by comparing the F_y/F_r of AgNCs in the presence and absence of target miR. For easy comparison, the F_y/F_r values obtained were normalised to that of sample without target miR. The findings showed that using 1 nmol C1 probes yielded the best result (**Figure 5.2A**), with the final concentration of C1-MBs calculated as 833 pmol.mg^{-1}.

Next, to determine the time needed for miR-144-3p to be captured by C1-MBs, excess target miR was incubated with C1-MBs and measured the leftover miR in supernatant over time. The best binding time was found to be 4 min, considering there was no significant increase in miR recovery as time increased further (**Figure 5.2B**).

For HCR conditions, the fluorescence intensity was measured for samples prepared at different HCR incubation temperatures (25 °C to 40 °C; with a 5 °C interval) and incubation periods (over a 2.5-h period; with a 0.5-h interval) (**Figure 5.2C**). The results showed that samples at 35 °C exhibited the highest relative fluorescence intensity. In terms of HCR duration, there was no significant difference between those prepared at 2 h and at 2.5 h. As such, HCR incubation at 35 °C for 2 h was used in subsequent experiments.

C1-MBs could be regenerated by removing C2 and C3 from C1-C2-C3-MBs complexes *via* heating, which breaks hydrogen bonds between C1 and C2/C3. To ensure the heating step did not dissociate streptavidin-biotin bonds [314,315], the capture efficiency of C1-MBs was calculated instantly after each recovery process (**Equation (2)**). It was shown that the capture efficiency decreased to 90% only after three repeated cycles (**Figure 5.2D**).

$$Capture\ efficiency\ (\%) = \frac{Captured\ miR-144}{Total\ miR-144} * 100\% \qquad \textbf{(2)}$$

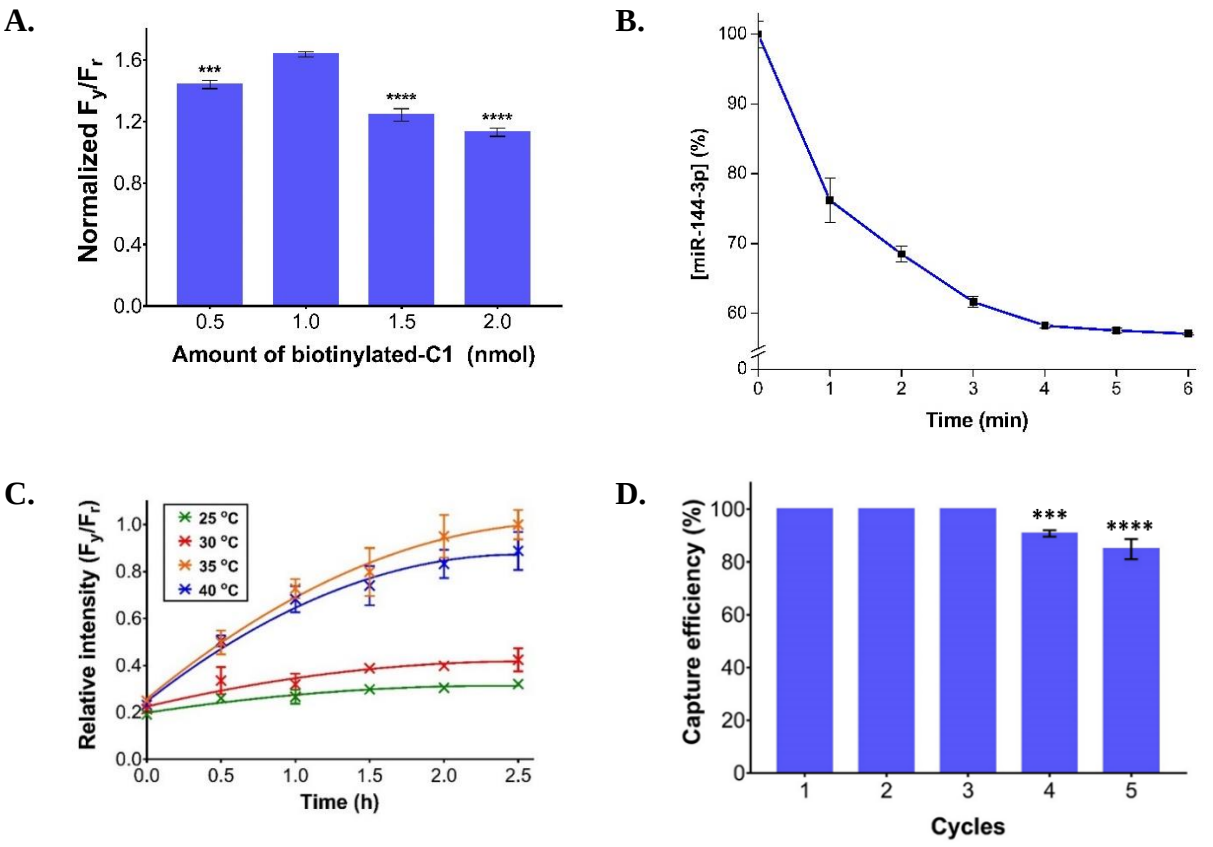


Figure 5.2 (A) Loading capacity of biotinylated-C1-MBs (n=3). Data presented as mean ± SEM and statistically analyzed relative to 1.0 nmol. ***, p<0.001; ****, p<0.0001. **(B)**

Optimisation of miR-144-3p capture time with C1-MBs (n=3). **(C)** Optimisation of HCR incubation duration (h) and temperature (°C) (n=5). **(D)** Capture efficiency of C1-MBs after beads regeneration (n=3). Data presented as mean ± SEM. ***, p<0.001; ****, p<0.0001.

5.4.5 Analytical performance of MB-HCR-AgNCs biosensor

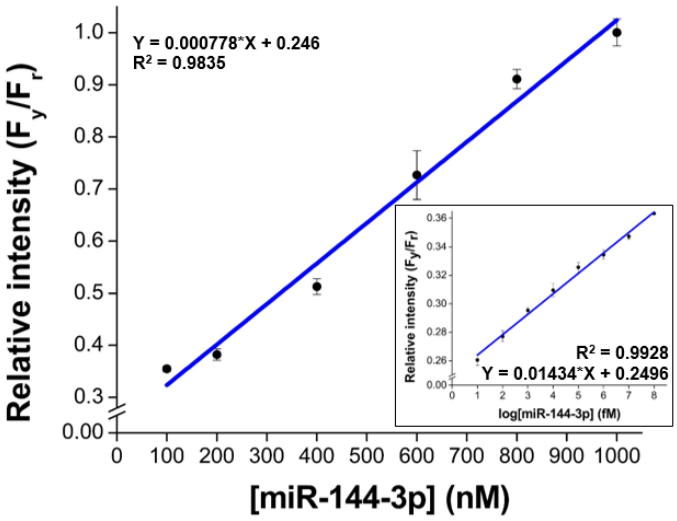
5.4.5.1 Sensitivity test

After validating the feasibility of the MB-HCR-AgNCs biosensor, its sensitivity towards miR-144-3p was studied. **Figure 5.3A** represented the detection ranges of the biosensor from 100 to 1000 nM and from 10 fM to 100 nM (inset), respectively. The RSD from five replicates of the former and latter range were below 8 and 4%, respectively, indicating high reproducibility and reliability of the biosensor. The LOD was calculated to be 4.88 fM, based on LOD = k σB/b, where k represents the expansion factor, σB as the standard deviation, and b as the slope of the line.

5.4.5.2 Selectivity test

The selectivity of the MB-HCR-AgNCs biosensor was then tested with a panel of controls, including blank, mismatch sequences (*i.e.,* mismatch *n*, where *n* indicates the number of mismatches in the sequence) and non-target sequences (*i.e.,* miR-9, miR-21 and miR-144-5p) (**Figure 5.3B**). Results had proven the high selectivity of the MB-HCR-AgNCs biosensor, where it showed significantly low F_y/F_r for the control samples, even at ten-fold higher working concentration (*i.e.,* 10 μM) than the target miR-144-3p (*i.e.,* 1 μM).

A.



B.

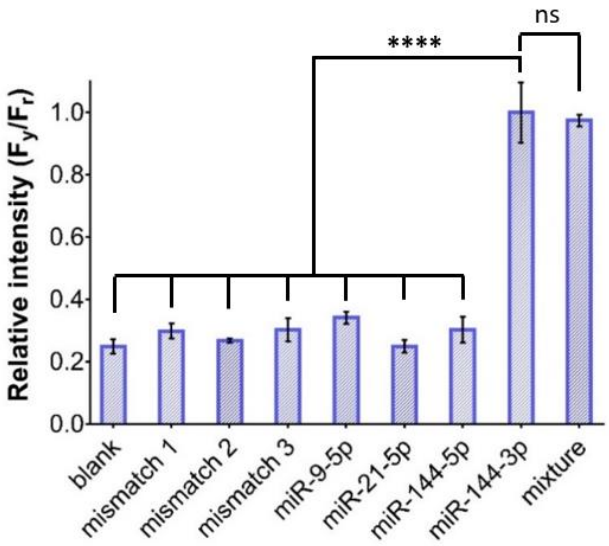


Figure 5.3 (A) Sensitivity profile of MB-HCR-AgNCs, ranged between 100 and 1000 nM, and between 10 fM and 100 nM (inset) (n=5). First detection range between 100 nM and 1 µM. Second detection range (inset) between 10 fM and 100 nM. **(B)** Selectivity study of MB-HCR-AgNCs (n=5). Data presented as mean ± SEM. ****, $p < 0.0001$; ns, non-significant.

5.4.6 Detection of miR-144-3p in human serum sample

The performance of the proposed MB-HCR-AgNCs biosensor in human serum samples was evaluated with the spike-and-recovery method, whereby 500 fM, 50 pM, 5 nM and 50 nM of miR-144-3p were added into different concentration of human serum samples (100, 10 and 0%). Interestingly, the sensitivity performance showed no significant difference among all samples (**Figure 5.4**). The recovery range for all concentrations, calculated with **Equation (1)**, were within 10%, with RSD (n=5) range less than 4% (**Table 5.2**). The robust and consistent performance of the biosensor even in 100% serum sample can be attributed to

the good magnetic separation efficiency of miR-144-3p. Overall, the findings suggested that the MB-HCR-AgNCs biosensor is highly potential for direct miR detection in biological samples.

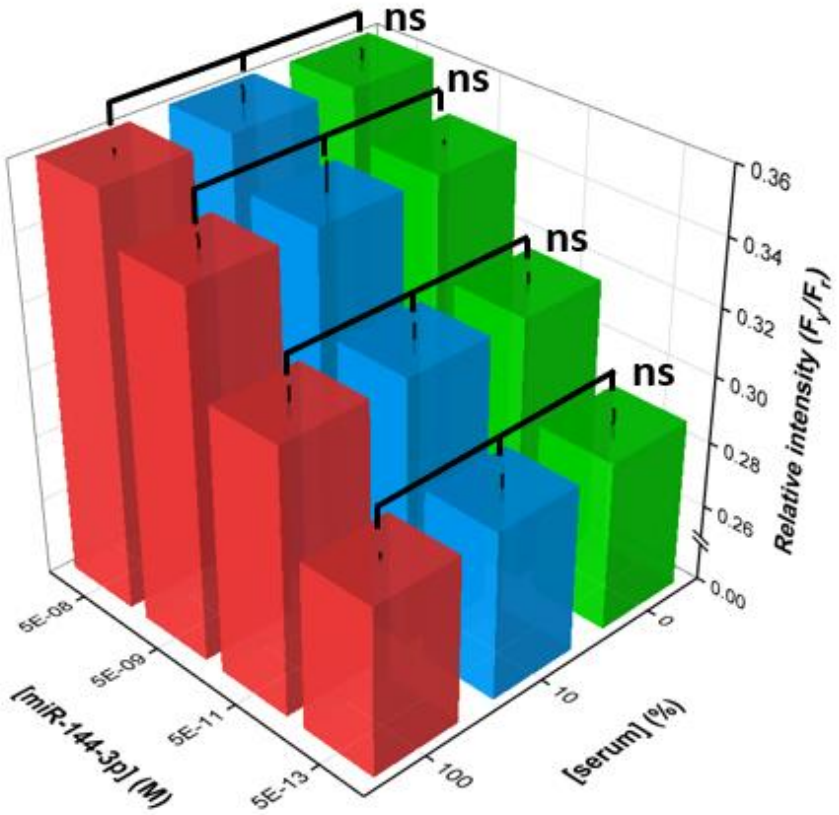


Figure 5.4 Performance of MB-HCR-AgNCs biosensor in different concentration of human serum samples (n=5). Data presented as mean ± SEM. ns, non-significant.

Table 5.2 Detection of miR-144-3p in human serum samples using MB-HCR-AgNCs (n=5).

Sample	miR-144-3p (M)	Found (M)			Recovery (%)	RSD (%)
		[serum] (%)				
		100%	10%	0%		
1	5.0×10^{-8}	4.8×10^{-8}	5.3×10^{-8}	5.0×10^{-8}	95.0 – 106.7	1.0 – 3.0
2	5.0×10^{-9}	4.7×10^{-9}	5.1×10^{-9}	5.0×10^{-9}	94.9 – 101.6	0.3 – 3.4
3	5.0×10^{-11}	5.2×10^{-11}	5.0×10^{-11}	5.0×10^{-11}	99.3 – 104.7	1.4 – 2.8
4	5.0×10^{-13}	4.5×10^{-13}	4.7×10^{-13}	5.0×10^{-13}	90.0 – 93.6	0.7 – 2.4

5.5 Summary

Overall, this chapter presented a MB-HCR-AgNCs biosensor to magnetically isolate and detect miR-144-3p through fluorescence analysis. The study started with designing and optimising the magnetic module, inclusive of C1 functionalisation and bidirectional strand displacement strategy with C2 and C3 assistive probes. The results showed successful immobilisation of the magnetic platform into the HCR-AgNCs biosensor, with remarkable separation of miR-144-3p and regeneration of C1-MBs for multiple usage. The ratiometric approach for HCR-AgNCs, previously introduced in **Chapter 3**, was tested here in this work with an entirely different set of AgNCs templating sequence, and displayed a similar red-yellow fluorescence response. As a result, the biosensor exhibited a relatively low LOD of 4.88 fM and high selectivity towards miR-144-3p, with capabilities of sharply discriminating between target miR-144-3p, mismatch and non-target sequences. Lastly, it was demonstrated that the MB-HCR-AgNCs biosensor also exhibited remarkable performance in raw human serum samples, with reproducible and reliable detection. Similar to the work in the earlier Chapters, specific limitations in the study included insufficient gel data analysis and the insufficient use of biological replicates to test applicability of the MB-HCR-AgNCs biosensor.

Chapter 6: Conclusion and future remarks

6.1 Overview

This thesis has described original research work towards the design and development of HCR-AgNCs biosensors. In addition, this thesis has demonstrated the simplification of HCR-AgNCs biosensors in terms of preparation and analysis, as well as their diagnostic efficiency in complex samples. In this chapter, the findings with regards to each HCR-AgNCs design are summarised, followed by the perspectives for future research within the field of HCR-AgNCs biosensors and biodiagnostics.

6.2 Summary

At the beginning of the thesis, multiple objectives were put together with the aim of improving the performance of nucleic acid biosensors, by the principles of HCR-AgNCs. The overall work presented in this thesis consisted of developing and testing different fluorogenic DNA-based biosensors for the detection of nucleic acid targets (*i.e.,* DNA and miRs). In each of the proposed biosensor, DNA hairpin probes were successfully designed with dual functionality, *i.e.,* for self-assembly during HCR amplification and to host AgNCs for fluorescence signal transduction.

The first project (**Chapter 3**) focused on developing a ratiometric HCR-AgNCs biosensor for the detection of miR-155. The proposed ratiometric approach incorporated a AgNCs templating sequence as the 2^{o} toehold, adjacent to an actively HCR-participating C-rich 1^{o} toehold sequence. This design could induce a change in the fluorescence properties (*i.e.,* red and yellow fluorescence emission) during HCR amplification. Since this strategy had not been explored in HCR-AgNCs studies, it was a challenge to design the DNA hairpins that can sustain both metastability and hybridisation efficiency. The feasibility of the ratiometric HCR-AgNCs biosensor was proven and its DNA nanostructure characterised. The fluorescence enhancement could also be correlated with the concentration of miR-155. At optimised conditions, the biosensor reported LOD at 1.13 fM and was able to sharply discriminate between miR-155, single-base mismatch and non-target sequences. The HCR-AgNCs biosensor also exhibited good performance in human serum sample. In contrast to the

other reported ratiometric HCR-AgNCs biosensor [160,169], the approach with proximity-dependent AgNCs featured a simpler and direct mechanism, with faster detection time and well-designed DNA hairpin probes.

In the next project (**Chapter 4**), the possibility of externalising AgNCs signal transduction from the HCR system was investigated, for target DNA detection. This was rationalised to simplify the designing stage of DNA hairpins, improve both DNA metastability and HCR predictability, as well as to reduce the production cost of DNA oligonucleotides. Aside from that, it was also anticipated that the formation of specific AgNCs in an externalised well-regulated environment, free from interfering molecules (*i.e.*, non-specific nucleic acid sequences, metals, proteins, etc.), ensured reproducibility for each analysis with consistent fluorescence properties. However, this approach was challenged by the notion that the AgNCs signal transduction should reflect the changes brought about by HCR amplification. Therefore, another proximity-dependent AgNCs concept was employed, termed end-to-end cluster transfer. This approach reported the transfer of non-fluorescent AgNCs from a dark AgNCs templating sequence to a homo-polyC AgNCs templating sequence located at opposite ends of a hybridised DNA probe for fluorescence activation [109,149]. Through this strategy, a HCR-AgNCs biosensor was designed to yield fluorescence activation in the presence of the target DNA. Through the reported results, the effectiveness of the proposed design and working principle of the proposed compartmentalised HCR-AgNCs biosensor were validated. The biosensor exhibited high sensitivity (*i.e.*, LOD of 3.35 fM) and selectivity towards the target DNA. Furthermore, the direct correlation between fluorescence intensity and target DNA concentration, could be observed with the naked eye down to 1 pM. In contrast to the externalised AgNCs probe in the HCR-AgNCs biosensor by Liu *et al.* [169], this approach worked with only two short DNA hairpins and an overall shorter detection time.

In the final project (**Chapter 5**), a magnetic component was introduced into a ratiometric HCR-AgNCs biosensor to facilitate the isolation of miR-144-3p from raw human serum sample. In **Section 2.2.2**, the importance of precise extraction of miRs for high quality and yield during miR detection was highlighted, and this was normally achieved through tedious procedures with additional cost, time, and labour. This study aimed to simplify the extraction process with regards to the time and labour work. Aside from that, this project also served as a follow-up study to the proposed ratiometric approach previously introduced in

Chapter 3. This time, another proximity-dependent mechanism was employed with a split AgNCs templating sequence, for a red-yellow ratiometric fluorescence response. For magnetic assistance, the concept of bidirectional strand displacement was utilised to isolate miR-144-3p. From the findings, the efficiency of the magnetic separation of miR-144-3p, and the feasibility of the proposed ratiometric HCR-AgNCs biosensor were validated. At optimised conditions, the proposed MB-HCR-AgNCs biosensor exhibited high sensitivity (*i.e.*, LOD at 4.88 fM) and selectivity towards miR-144-3p. At the end of the study, the MB-HCR-AgNCs biosensor displayed good detection of miR-144-3p in raw human serum sample.

From a collective understanding of this thesis, several key findings were implicated with regards to designing HCR-AgNCs biosensors. In all three studies, a DNA hairpin species was designed with a C-G bp to replace two bases of the DNA hairpin loop. This minor modification simultaneously increased the stem length and decreased the loop size, as means to improve the metastability of DNA hairpins by creating a high energy barrier, previously discussed in **Section 2.3.3**. The location of the C-G bp was also in accordance with the suggestion by Li *et al.* to close the fraying regions with a C-G bp [63], that was also discussed in **Section 2.3.3**. This design feature had led to the stable HCR systems presented in this work. Besides that, the underlying concept for all three HCR-AgNCs biosensors capitalised on proximity-dependent AgNCs to reflect the DNA structural changes brought about by HCR amplification. The design and implementation of proximity-dependent AgNCs have been challenging, but the findings reported in this thesis validated their feasibility and working principle.

Another common aspect from all three HCR-AgNCs biosensors is the reported analytical performance (*i.e.,* sensitivity and selectivity). **Table 6.1** compares the three proposed HCR-AgNCs biosensors to other reported HCR-AgNCs biosensors with a nucleic acid-based target (*i.e.,* DNA, miR, and mRNA). While it is understandable that the underlying mechanism for all the studies may differ, the three proposed HCR-AgNCs biosensors generally outperform the other fluorescence-based HCR-AgNCs biosensors, with regards to the LOD and detection range. However, the works from this thesis fall short when compared to the electrochemical-based HCR-AgNCs. Electrochemical-based HCR-AgNCs normally feature enzymatic components to further enhance their biosensing performance, but at the same time introduce additional steps, such as washing and deactivating the enzymes

[75,158]. All three proposed designs in this thesis have relatively similar fM-level LOD, and detection range from fM to nM levels. This covers the typical concentration range (*i.e.*, fM to nM) of miRs in the body [316,317]. On the other hand, the slight deviations seen across the designs could be attributed to the different detection mechanisms, as well as the choice of AgNCs templating sequence. To reiterate, **Chapters 3** and **5** reported ratiometric HCR-AgNCs fluorescence analysis, where the former utilised a combination of AgNCs templating sequence and a C-rich emitter-pair, while the latter utilised a split AgNCs templating sequence. Meanwhile, **Chapter 4** reported a compartmentalised HCR-AgNCs biosensor, with externalised AgNCs fluorogenic probes comprising a combination of a dark and a C-rich AgNCs templating sequence.

Despite the conceptual success of the three HCR-AgNCs biosensors proposed in this thesis, the performance and application of these concepts can be further improved with additional optimisation and validation experiments. These will be discussed in detail in the following section (**Section 6.3**).

Table 6.1 Comparison of the proposed HCR-AgNCs biosensors with reported HCR-AgNCs biosensors towards a nucleic acid target.

Method	Target	Material	LOD	Detection range	Reference
Fluorescence	miR-17-5p	HCR-AgNCs	2.8 pM	1 pM – 1 nM	[160]
Fluorescence	miR-21	HCR-AgNCs	19.9 pM	0.25 nM – 8 nM	[166]
Fluorescence	miR-145	HCR-AgNCs	16 pM	0.1 nM – 1.6 nM	[165]
Fluorescence	HIV DNA	GO/HCR-AgNCs	1.18 nM	10 nM – 0.2 μM	[13]
Fluorescence	let-7	HCR-AgNCs	0.78 nM	1.56 nM – 0.4 μM	[157]
Fluorescence	mRNA	HCR-AgNCs	7 pM	10 pM – 0.1 μM	[169]
Fluorescence	miR-21	GO/HCR-AgNCs	2.8 pM	5 pM – 1 nM	[156]
Electrochemical	DNA	Autocatalytic strand displacement amplification/HCR-AgNCs	0.16 fM	0.2 fM – 1 pM	[158]
Electrochemical	miR-155	T-rich nucleic acid-enhanced HCR-AgNCs	0.39 fM	0.5 fM – 1 nM	[163]
Electrochemical	miR-199a	Target-assisted polymerisation nicking reaction/HCR-AgNCs	0.64 fM	1 fM – 0.1 nM	[75]
Fluorescence	miR-155	HCR-AgNCs	1.13 fM	100 fM – 1 μM	**Chapter 3**
Fluorescence	DNA	HCR-AgNCs	3.35 fM	100 fM – 1 μM	**Chapter 4**
Fluorescence	miR-144-3p	MB-HCR-AgNCs	4.88 fM	10 fM – 1 μM	**Chapter 5**

6.3 Perspectives and future remarks

DNA-based biosensors rely on the structural and mechanistic properties of DNA for a highly selective binding interaction with a particular target. In this thesis, several HCR-AgNCs biosensors were designed by integrating AgNCs into HCR amplified circuits. In **Section 2.5**, the advantages of HCR-AgNCs biosensors were highlighted, from its simplicity in operation with a mix-and-measure method in a one-pot system, to the automatic and mild operational conditions. On the contrary, there are also challenges that limit their potential and application, namely the design of stable DNA hairpins with a functional AgNCs templating sequence (as described in **Section 2.5.5**). Throughout this thesis, these limitations were investigated through the development of three HCR-AgNCs biosensors with their respective mechanisms and design features, followed by the reported findings that validate their biosensing performance (summarised in **Section 6.2**). Nonetheless, these proposed HCR-AgNCs biosensors can be further improved with future research and applied fundamentally in future HCR-AgNCs systems. Herein, the key areas of improvement for each of the proposed HCR-AgNCs biosensor are evaluated.

In **Chapter 3**, the HCR-AgNCs biosensor design utilised a C-rich emitter-pair 1^{o} toehold sequence that actively participated in HCR amplification, to induce a change in the fluorescence properties and subsequent ratiometric response. This strategy was never reported before in prior HCR-AgNCs studies, and the findings in **Chapter 3** proved the feasibility and practicality of its working principle. However, more work can be performed to validate the mechanism, such as testing with a different target, and a different combination of emitter-pair/AgNCs templating sequences.

In **Chapter 4**, the proposed HCR-AgNCs biosensor featured multiple innovative approaches. Firstly, P1 comprised a hybridisation region and a AgNCs templating sequence, and it was primarily responsible for the fluorescence activation *via* end-to-end cluster transfer. However, the hybridisation of P1 with H1 could also be seen as HCR termination. This can be explored further in future studies, as a dual-functional DNA probe (*i.e.,* signal transduction and HCR terminator) can provide precise regulation of an otherwise automated HCR process. That being the case, specific sizes of HCR products can be optimised and isolated for downstream analysis. Next, it was proven in **Chapter 4** that the end-to-end cluster-transfer concept initiated a significant fluorescence activation and was applicable for the HCR-AgNCs biosensor to detect the target DNA. The end-to-end cluster-transfer concept

is generally an underexplored AgNCs strategy, let alone in HCR systems. However, the reported findings in **Chapter 4** offer an alternative method to introduce AgNCs instead of the conventional side-by-side (*i.e.*, emitter-pair/AgNCs templating sequence, G-rich enhancer/AgNCs templating sequence, etc.) proximity-dependent approach. For instance, end-to-end cluster-transfer can be implemented in HCR products with AgNCs templating tails at both sides of the concatemer, instead of crowding everything on one side and slowing down the DNA hybridisation process. Likewise, as aforementioned in Section 4.5, the applicability of the HCR-AgNCs system in human serum could be further optimised and validated by including more sample concentrations within the detection range (i.e., 100 fM – 1 μM) for human serum testing (e.g., at every magnitude from 100 fM – 1 μM). Lastly, the proposed HCR-AgNCs biosensor exhibited qualitative fluorescence response with respect to the concentration of the target DNA. Qualitative analysis with HCR-AgNCs systems is rarely studied, and future work in this direction can result in more direct analysis as compared to quantitative measurement, with the potential for point-of-care application.

In **Chapter 5**, the novel design of MB-HCR-AgNCs reported feasibility and practicality for the detection of miR-144-3p. In addition to reported results, there are several aspects in this work that can be further explored in the future. Firstly, this work utilised commercial MBs, which arrived in a small volume and a high cost. While this was shown to work with the MB-HCR-AgNCs biosensor, it might not be a viable and sustainable option for long-term application. Hence, in-house MBs can be easily prepared with better regulation of their properties (e.g., size, coating substance, and core material), and thus, could be a potentially better option, in terms of cost per unit volume [318]. Besides that, the present study worked with MBs with 1 μm diameter. Smaller MBs, ideally within the nm range, provides a larger surface area to volume ratio, which could enhance the binding capacity, subsequent capture efficiency of miR-144-3p, and dispersion. As part of the work, magnetic nanoparticles (MNPs) were briefly explored as an option, with some assistance to comprehend the preparation, characterisation, and functionalisation of MNPs. However, this option was not integrated into the final design due to the lack of resources and time. Next, the proposed MBs recovery method in this work was performed with thermal dissociation of DNA probes (*i.e.*, C1, C2 and C3). An alternative MBs recovery method should be explored, preferably with mild reaction conditions which would ensure that the entire operation of MB-HCR-AgNCs is consistent [315]. This would make it even more practical when applied at areas with low-resource settings. Even so, the condition should specifically target the

hydrogen bonds of DNA (*i.e.*, between C1, C2 and C3), without affecting the streptavidin-biotin bond of C1-MBs. Also, the design of H2 featured the two base loop replacement with a C-G bp (similar to the H1 of the HCR-AgNCs designs in **Chapters 3** and **4**), and a relatively bulky C- and G-rich toehold segment (29-mer). In terms of DNA hairpin metastability, the reported findings highlighted the notion that loop size should be prioritised over both the toehold base composition and length when designing metastable DNA hairpin probes. This warrants further research not only to verify the claim but also to develop a systematic guideline towards designing metastable DNA hairpins for HCR-AgNCs systems. Lastly, this work also validated the ratiometric approach with a HCR-active 1^{o} AgNCs templating toehold (*i.e.*, part of a split AgNCs templating sequence in this work), that was introduced in **Chapter 3**. This opens new possibilities that can indeed broaden the field of HCR-AgNCs biosensing. In addition to that, it is also important to note that the detection range tested for all three designs in this thesis may not represent the full working range of each these HCR-AgNCs biosensors and require further experiments to fully realise their biosensing capabilities. Besides that, the mechanism of each design should be further validated with different miRs. This would involve a simple change in target sequence to yield relatively similar fluorescence properties, given that most conditions remain the same (i.e., nucleation sequence). But changing the target sequence might affect the thermodynamics and kinetics of the DNA hairpin probes. Hence, a quick and simple re-optimization of the temperature and duration of HCR incubation should finetune the reaction conditions for the HCR-AgNCs biosensor.

For the optimisation and characterisation of HCR-AgNCs biosensors, the DNA nanostructures from all the proposed designs could be further verified with other techniques. Atomic force microscopy (AFM) can provide a visual comparison of the DNA nanostructures (DNA hairpins vs HCR chains). AFM is more often utilised in branched HCR designs where their exponential amplification produces a more prominent DNA network, as opposed to one-dimensional HCR amplification [174]. Moreover, AFM can also analyse the formation of AgNCs on DNA molecules [169]. From the reported HCR-AgNCs studies and this thesis, more effort should also be directed towards the molecular interaction of AgNCs towards DNA concatemers, such as the binding of Ag(I) to different DNA hairpin segments, or the preparation of AgNCs in a complex DNA network [319]. There were no detailed experiments performed to investigate the specific effect of AgNCs sequence on HCR kinetics, and the results from the different studies in the thesis cannot be compared directly. A quick

observation between the two ratiometric designs (Chapters 3 and 5) did not yield that much of a difference. For example, it was reported that HCR incubation was optimally performed for 2.2 hours in Chapter 3 and 2 hours in Chapter 5, but this might have been ascribed to the different components involved (e.g., size of DNA hairpins and DNA sequence). Hence, the effect of different AgNCs templating sequence, particularly length and sequence, should be investigated on the kinetics of HCR in future studies. Another component to explore would be the effect of AgNCs templated appended to the DNA hairpins (i.e., at the toehold or loop sequence), and investigate the possibility and extent of steric hindrance on HCR kinetics.

In order to apply HCR-AgNCs for actual clinical diagnostics, target analyte detection should be extended beyond simple complex matrices (human serum, blood plasma, etc.) and more into in vitro and in vivo settings. This is crucial because it gauges the stability and applicability of HCR-AgNCs in the relevant fields of diagnostics. For example, the studies in this thesis used human serum samples as the choice of complex matrix, but this is insufficient especially for miR targets. Although serum miRs in bodily fluids present remarkable stability (*i.e.,* from encapsulation in exosomes, microvesicles and/or protein complex), there are miRs that are site-specific and concentrate near the cells and tissues. Hence, testing the HCR-AgNCs biosensors in cell lysates and actual patient samples would solidify the potential of the HCR-AgNCs biosensors proposed in this thesis. Another area of improvement would be the comparison of HCR-AgNCs biosensors with current methods of detection. A direct comparison of HCR-AgNCs biosensors with qPCR and/or RT-qPCR for nucleic acid targets (*i.e.,* DNA and miRs), can enable critical performance analysis, including the overall cost, runtime, and operational difficulty. Such comparison was only performed once by Liu *et al.* [169], and they reported relatively similar analytical performance between their HCR-AgNCs biosensors and RT-qPCR, to detect a target mRNA. Another area of interest is the possibility of preparing AgNCs on DNA hairpin probes prior to HCR amplification. Most of the current HCR-AgNCs biosensors function with AgNCs formation post-HCR amplification. This concept may be challenging to design and execute, but it offers more practical applications with real-time detection by monitoring the signal changes during HCR amplification, and an overall shorter operation time.

To fully realise the potential of HCR-AgNCs biosensors for clinical application, future research in HCR-AgNCs biosensors should be directed towards multiplex detection and POCT. Multiplex detection enables the detection of multiple targets in a single reaction.

This can be challenging for HCR-AgNCs biosensors as it requires not only additional DNA hairpins, but also different AgNCs templating sequences to elicit different AgNCs species. Meanwhile, POCT typically means detection with a device in the presence of the patient and without the need to send a sample to a laboratory. Hitherto most of the reported studies developing HCR-AgNCs biosensors are conceptual and remain in the laboratory testing phase. To fully realise their potential in POCT, inter-disciplinary research should be initiated to integrate HCR-AgNCs into a versatile platform (*e.g.*, lab-on-chip devices and smartphone attachments) [320–324]. Another area of improvement would be the long operational time of HCR-AgNCs biosensors. As it stands, HCR-AgNCs biosensors feature a relatively long operational time (*i.e.,* at least 1 hour) to accommodate both HCR amplification and preparation of AgNCs, as shown in **Table 2.3**. Several propositions could significantly improve the operational time of HCR-AgNCs biosensors. The bulk preparation of stable AgNCs (*i.e.*, on DNA hairpins or externalised AgNCs probes) prior to HCR amplification can prevent time-consuming AgNCs preparation after each run of HCR in conventional HCR-AgNCs biosensors. Apart from that, the interaction between DNA hairpins and target during HCR could be improved by bringing them closer to one another if the reaction volume was significantly reduced. Another approach to reduce the overall biosensing time would be to utilise different variations of HCR, such as a branched design and/or target recycling for exponential signal amplification (previously introduced in **Section 2.3.5**).

In its entirety, this thesis has contributed towards addressing and understanding the challenges of developing HCR-AgNCs biosensors. A solid foundation has been established from the aspects of material preparation, designing of DNA probes, biosensor characterisation, operational condition optimisation, and analytical performance. By way of comparison, the diagnostic potential achieved with the proposed HCR-AgNCs biosensors in this thesis (from Chapters 3, 4, and 5) has shown to be quite competitive with other recently published works thus far (as listed in **Tables 3.2, 4.2** and **6.1**). In this regard, HCR-AgNCs and MB-HCR-AgNCs offer a unique detection strategy for miRs as a supplementary tool to complement the diagnosis and understanding of cancer biology, taking into account the specificity of DNA probes, strong and sensitive AgNCs fluorescence, and the practicality of the designs (e.g., the successful implementation of MBs for miR extraction in complex serum). Additionally, with global efforts striving towards point-of-care diagnostics, there will undoubtedly be greater opportunities to integrate HCR-AgNCs into clinical diagnostics, within the field of miRs and other biomolecules.

6.4 Concluding remarks

Overall, this thesis has presented original works that contribute to both disciplines of analytical chemistry and biotechnology, with particular emphasis on DNA-based biosensors and DNA nanotechnology. The presented results provide a framework for further research based on biosensor development, HCR amplification, DNA-AgNCs, and hybrid HCR-AgNCs biosensors. From *ab initio* design to proof-of-concept and complex matrix application, this thesis has provided the fundamentals to drive future research in the fields of DNA-based biosensing.

References

[1] L. Shen, P. Wang, Y. Ke, DNA Nanotechnology-Based Biosensors and Therapeutics, Adv. Healthcare Mater. 10 (2021) 2002205. https://doi.org/10.1002/ADHM.202002205.

[2] Q. Wang, J. Wang, Y. Huang, Y. Du, Y. Zhang, Y. Cui, D. Ming Kong, Development of the DNA-based biosensors for high performance in detection of molecular biomarkers: More rapid, sensitive, and universal, Biosens. Bioelectron. 197 (2022) 113739. https://doi.org/10.1016/J.BIOS.2021.113739.

[3] C.E. Condrat, D.C. Thompson, M.G. Barbu, O.L. Bugnar, A. Boboc, D. Cretoiu, N. Suciu, S.M. Cretoiu, S.C. Voinea, miRNAs as Biomarkers in Disease: Latest Findings Regarding Their Role in Diagnosis and Prognosis, Cells. 9 (2020) 276. https://doi.org/10.3390/CELLS9020276.

[4] J. Wang, J. Chen, S. Sen, MicroRNA as Biomarkers and Diagnostics, J. Cell. Physiol. 231 (2016) 25–30. https://doi.org/10.1002/JCP.25056.

[5] M. Lai, G. Slaughter, Label-Free MicroRNA Optical Biosensors, Nanomaterials. 9 (2019) 1573. https://doi.org/10.3390/NANO9111573.

[6] R.M. Dirks, N.A. Pierce, Triggered amplification by hybridisation chain reaction, Proc. Natl. Acad. Sci. U.S.A. 101 (2004) 15275–15278. https://doi.org/10.1073/pnas.0407024101.

[7] A. Latorre, R. Lorca, Á. Somoza, Fluorescent DNA stabilised silver nanoclusters as biosensors, J. Chem. 2013 (2013) 631421. https://doi.org/10.1155/2013/631421.

[8] S. Bi, S. Yue, S. Zhang, Hybridisation chain reaction: a versatile molecular tool for biosensing, bioimaging, and biomedicine, Chem. Soc. Rev. 46 (2017) 4281–4298. https://doi.org/10.1039/C7CS00055C.

[9] S.Y. New, S.T. Lee, X.D. Su, DNA-templated silver nanoclusters: structural correlation and fluorescence modulation, Nanoscale. 8 (2016) 17729–17746. https://doi.org/10.1039/C6NR05872H.

[10] Y. Guo, X. Pan, W. Zhang, Z. Hu, K.W. Wong, Z. He, H.W. Li, Label-free probes using DNA-templated silver nanoclusters as versatile reporters, Biosens. Bioelectron.

150 (2020) 111926. https://doi.org/10.1016/J.BIOS.2019.111926.

[11] J. Wu, N. Li, Y. Yao, D. Tang, D. Yang, J. Ong'achwa Machuki, J. Li, Y. Yu, F. Gao, DNA-Stabilised Silver Nanoclusters for Label-Free Fluorescence Imaging of Cell Surface Glycans and Fluorescence Guided Photothermal Therapy, Anal. Chem. 90 (2018) 14368–14375. https://doi.org/10.1021/acs.analchem.8b03837.

[12] H. Wu, J. Wu, Y. Liu, H. Wang, P. Zou, Silver nanoclusters-based fluorescent biosensing strategy for determination of mucin 1: Combination of exonuclease I-assisted target recycling and graphene oxide-assisted hybridisation chain reaction, Anal. Chim. Acta. 1129 (2020) 40–48. https://doi.org/10.1016/J.ACA.2020.06.040.

[13] S. Zhang, K. Wang, K. Bin Li, W. Shi, W.P. Jia, X. Chen, T. Sun, D.M. Han, A DNA-stabilised silver nanoclusters/graphene oxide-based platform for the sensitive detection of DNA through hybridisation chain reaction, Biosens. Bioelectron. 91 (2017) 374–379. https://doi.org/10.1016/j.bios.2016.12.060.

[14] F.R.R. Teles, L.P. Fonseca, Trends in DNA biosensors, Talanta. 77 (2008) 606–623. https://doi.org/10.1016/J.TALANTA.2008.07.024.

[15] S. Patel, R. Nanda, S. Sahoo, E. Mohapatra, Biosensors in health care: The milestones achieved in their development towards lab-on-chip-analysis, Biochem. Res. Int. 2016 (2016) 3130469. https://doi.org/10.1155/2016/3130469.

[16] K. V, DNA Biosensors-A Review, J. Bioeng. Biomed. Sci. 7 (2017) 222. https://doi.org/10.4172/2155-9538.1000222.

[17] K.M. Abu-Salah, M.M. Zourob, F. Mouffouk, S.A. Alrokayan, M.A. Alaamery, A.A. Ansari, DNA-Based Nanobiosensors as an Emerging Platform for Detection of Disease, Sensors. 15 (2015) 14539–14568. https://doi.org/10.3390/S150614539.

[18] Y. Hua, J. Ma, D. Li, R. Wang, DNA-Based Biosensors for the Biochemical Analysis: A Review, Biosens. 12 (2022) 183. https://doi.org/10.3390/BIOS12030183.

[19] A.C. Carpenter, I.T. Paulsen, T.C. Williams, Blueprints for Biosensors: Design, Limitations, and Applications, Genes. 9 (2018) 375. https://doi.org/10.3390/GENES9080375.

[20] Y. Hu, Y. Wang, J. Yan, N. Wen, H. Xiong, S. Cai, Q. He, D. Peng, Z. Liu, Y. Liu, Dynamic DNA Assemblies in Biomedical Applications, Adv. Sci. 7 (2020) 2000557.

https://doi.org/10.1002/advs.202000557.

[21] J.A. Vidigal, A. Ventura, The biological functions of miRNAs: lessons from in vivo studies, Trends Cell Biol. 25 (2015) 137-147. https://doi.org/10.1016/J.TCB.2014.11.004.

[22] H.W. Hwang, J.T. Mendell, MicroRNAs in cell proliferation, cell death, and tumorigenesis, Br. J. Cancer. 94 (2006) 776–780. https://doi.org/10.1038/SJ.BJC.6603023.

[23] S. Chandra, D. Vimal, D. Sharma, V. Rai, S.C. Gupta, D.K. Chowdhuri, Role of miRNAs in development and disease: Lessons learnt from small organisms, Life Sci. 185 (2017) 8–14. https://doi.org/10.1016/J.LFS.2017.07.017.

[24] E.A. Hunt, D. Broyles, T. Head, S.K. Deo, MicroRNA Detection: Current Technology and Research Strategies, Annu. Rev. Anal. Chem. 8 (2015) 217–237. https://doi.org/10.1146/ANNUREV-ANCHEM-071114-040343.

[25] X. Li, M. Ye, W. Zhang, D. Tan, N. Jaffrezic-Renault, X. Yang, Z. Guo, Liquid biopsy of circulating tumor DNA and biosensor applications, Biosens. Bioelectron. 126 (2019) 596–607. https://doi.org/10.1016/J.BIOS.2018.11.037.

[26] J. Matsuzaki, T. Ochiya, Circulating microRNAs: Next-generation Cancer Detection, Keio J. Med. 69 (2020) 88–96. https://doi.org/10.2302/KJM.2019-0011-OA.

[27] A. Turchinovich, L. Weiz, A. Langheinz, B. Burwinkel, Characterisation of extracellular circulating microRNA, Nucleic Acids Res. 39 (2011) 7223–7233. https://doi.org/10.1093/NAR/GKR254.

[28] L.F. Sempere, A.S. Azmi, A. Moore, microRNA-based diagnostic and therapeutic applications in cancer medicine, Wiley Interdiscip Rev RNA. 12 (2021) e1662. https://doi.org/10.1002/WRNA.1662.

[29] S. Sethi, S. Ali, S. Sethi, F.H. Sarkar, MicroRNAs in personalized cancer therapy, Clin. Genet. 86 (2014) 68–73. https://doi.org/10.1111/CGE.12362.

[30] Y. Peng, C.M. Croce, The role of MicroRNAs in human cancer, Signal Transduct. Target. Ther. 1 (2016) 15004. https://doi.org/10.1038/SIGTRANS.2015.4.

[31] G.A. Calin, C.M. Croce, MicroRNA signatures in human cancers, Nat. Rev. Cancer. 6

(2006) 857–866. https://doi.org/10.1038/NRC1997.

[32] M. Ohno, J. Matsuzaki, J. Kawauchi, Y. Aoki, J. Miura, S. Takizawa, K. Kato, H. Sakamoto, Y. Matsushita, M. Takahashi, Y. Miyakita, K. Ichimura, Y. Narita, T. Ochiya, Assessment of the Diagnostic Utility of Serum MicroRNA Classification in Patients With Diffuse Glioma, JAMA Netw. Open. 2 (2019) e1916953. https://doi.org/10.1001/JAMANETWORKOPEN.2019.16953.

[33] A. Shimomura, S. Shiino, J. Kawauchi, S. Takizawa, H. Sakamoto, J. Matsuzaki, M. Ono, F. Takeshita, S. Niida, C. Shimizu, Y. Fujiwara, T. Kinoshita, K. Tamura, T. Ochiya, Novel combination of serum microRNA for detecting breast cancer in the early stage, Cancer Sci. 107 (2016) 326–334. https://doi.org/10.1111/CAS.12880.

[34] K. Asakura, T. Kadota, J. Matsuzaki, Y. Yoshida, Y. Yamamoto, K. Nakagawa, S. Takizawa, Y. Aoki, E. Nakamura, J. Miura, H. Sakamoto, K. Kato, S. ichi Watanabe, T. Ochiya, A miRNA-based diagnostic model predicts resectable lung cancer in humans with high accuracy, Commun. Biol. 3 (2020) 134. https://doi.org/10.1038/s42003-020-0863-y.

[35] Y. Yamamoto, S. Kondo, J. Matsuzaki, M. Esaki, T. Okusaka, K. Shimada, Y. Murakami, M. Enomoto, A. Tamori, K. Kato, Y. Aoki, S. Takizawa, H. Sakamoto, S. Niida, F. Takeshita, T. Ochiya, Highly Sensitive Circulating MicroRNA Panel for Accurate Detection of Hepatocellular Carcinoma in Patients With Liver Disease, Hepatol. Commun. 4 (2019) 284–297. https://doi.org/10.1002/HEP4.1451.

[36] A. Yokoi, J. Matsuzaki, Y. Yamamoto, Y. Yoneoka, K. Takahashi, H. Shimizu, T. Uehara, M. Ishikawa, S. ichi Ikeda, T. Sonoda, J. Kawauchi, S. Takizawa, Y. Aoki, S. Niida, H. Sakamoto, K. Kato, T. Kato, T. Ochiya, Integrated extracellular microRNA profiling for ovarian cancer screening, Nat. Commun. 2018 91. 9 (2018) 4319. https://doi.org/10.1038/s41467-018-06434-4.

[37] F. Urabe, J. Matsuzaki, Y. Yamamoto, T. Kimura, T. Hara, M. Ichikawa, S. Takizawa, Y. Aoki, S. Niida, H. Sakamoto, K. Kato, S. Egawa, H. Fujimoto, T. Ochiya, Large-scale Circulating microRNA Profiling for the Liquid Biopsy of Prostate Cancer, Clin. Cancer Res. 25 (2019) 3016–3025. https://doi.org/10.1158/1078-0432.CCR-18-2849.

[38] R.M. Graybill, R.C. Bailey, Emerging Biosensing Approaches for microRNA Analysis, Anal. Chem. 88 (2015) 431–450.

https://doi.org/10.1021/ACS.ANALCHEM.5B04679.

[39] V.P. Dave, T.A. Ngo, A.K. Pernestig, D. Tilevik, K. Kant, T. Nguyen, A. Wolff, D.D. Bang, MicroRNA amplification and detection technologies: opportunities and challenges for point of care diagnostics, Lab. Investig. 99 (2018) 452–469. https://doi.org/10.1038/s41374-018-0143-3.

[40] T. Ouyang, Z. Liu, Z. Han, Q. Ge, MicroRNA Detection Specificity: Recent Advances and Future Perspective, Anal. Chem. 91 (2019) 3179-3186. https://doi.org/10.1021/acs.analchem.8b05909.

[41] R.S. Goswami, L. Waldron, J. Machado, N.K. Cervigne, W. Xu, P.P. Reis, D.J. Bailey, I. Jurisica, M.R. Crump, S. Kamel-Reid, Optimisation and analysis of a quantitative real-time PCR-based technique to determine microRNA expression in formalin-fixed paraffin-embedded samples, BMC Biotechnol. 10 (2010) 47. https://doi.org/10.1186/1472-6750-10-47.

[42] C. Chen, D.A. Ridzon, A.J. Broomer, Z. Zhou, D.H. Lee, J.T. Nguyen, M. Barbisin, N.L. Xu, V.R. Mahuvakar, M.R. Andersen, K.Q. Lao, K.J. Livak, K.J. Guegler, Real-time quantification of microRNAs by stem-loop RT-PCR, Nucleic Acids Res. 33 (2005) e179. https://doi.org/10.1093/nar/gni178.

[43] C. Becker, A. Hammerle-Fickinger, I. Riedmaier, M.W. Pfaffl, mRNA and microRNA quality control for RT-qPCR analysis, Methods. 50 (2010) 237–243. https://doi.org/10.1016/J.YMETH.2010.01.010.

[44] P. Chugh, D.P. Dittmer, Potential pitfalls in microRNA profiling, Wiley Interdiscip. Rev. RNA. 3 (2012) 601–616. https://doi.org/10.1002/wrna.1120.

[45] M. Cui, H. Wang, X. Yao, D. Zhang, Y. Xie, R. Cui, X. Zhang, Circulating MicroRNAs in Cancer: Potential and Challenge, Front Genet. 10 (2019) 626. https://doi.org/10.3389/FGENE.2019.00626.

[46] P. Yin, H.M.T. Choi, C.R. Calvert, N.A. Pierce, Programming biomolecular self-assembly pathways, Nature. 451 (2008) 318-322. https://doi.org/10.1038/nature06451.

[47] H.M.T. Choi, J.Y. Chang, L.A. Trinh, J.E. Padilla, S.E. Fraser, N.A. Pierce, Programmable in situ amplification for multiplexed imaging of mRNA expression, Nat. Biotechnol. 28 (2010) 1208-1212. https://doi.org/10.1038/nbt.1692.

[48] E.E. Augspurger, M. Rana, M. V. Yigit, Chemical and Biological Sensing Using Hybridisation Chain Reaction, ACS Sens. 3 (2018) 878–902. https://doi.org/10.1021/ACSSENSORS.8B00208.

[49] S.J. Green, D. Lubrich, A.J. Turberfield, DNA hairpins: fuel for autonomous DNA devices, Biophys. J. 91 (2006) 2966–2975. https://doi.org/10.1529/biophysj.106.084681.

[50] N. Srinivas, T.E. Ouldridge, P. Šulc, J.M. Schaeffer, B. Yurke, A.A. Louis, J.P.K. Doye, E. Winfree, On the biophysics and kinetics of toehold-mediated DNA strand displacement, Nucleic Acids Res. 41 (2013) 10641–10658. https://doi.org/10.1093/NAR/GKT801.

[51] Y. Zhao, F. Chen, Q. Li, L. Wang, C. Fan, Isothermal Amplification of Nucleic Acids, Chem. Rev. 115 (2015) 12491–12545. https://doi.org/10.1021/acs.chemrev.5b00428.

[52] H. Deng, Z. Gao, Bioanalytical applications of isothermal nucleic acid amplification techniques, Anal. Chim. Acta. 853 (2015) 30–45. https://doi.org/10.1016/J.ACA.2014.09.037.

[53] G. Niranjani, R. Murugan, Theory on the Mechanism of DNA Renaturation: Stochastic Nucleation and Zipping, PLoS One. 11 (2016) e0153172. https://doi.org/10.1371/JOURNAL.PONE.0153172.

[54] Y. Yin, X.S. Zhao, Kinetics and Dynamics of DNA Hybridisation, Acc. Chem. Res. 44 (2011) 1172–1181. https://doi.org/10.1021/AR200068J.

[55] F. Wang, B. Willner, I. Willner, DNA nanotechnology with one-dimensional self-assembled nanostructures, Curr. Opin. Biotechnol. 24 (2013) 562–574. https://doi.org/10.1016/J.COPBIO.2013.02.005.

[56] D. Yang, Y. Tang, P. Miao, Hybridisation chain reaction directed DNA superstructures assembly for biosensing applications, TrAC - Trends Anal. Chem. 94 (2017) 1–13. https://doi.org/10.1016/J.TRAC.2017.06.011.

[57] K.L. Wong, J. Liu, Factors and methods to modulate DNA hybridisation kinetics, Biotechnol. J. 16 (2021) 2000338. https://doi.org/10.1002/BIOT.202000338.

[58] D. de Bruin, N. Bossert, A. Aartsma-Rus, D. Bouwmeester, Measuring DNA hybridisation using fluorescent DNA-stabilised silver clusters to investigate mismatch

effects on therapeutic oligonucleotides, J. Nanobiotechnology. 16 (2018) 37. https://doi.org/10.1186/S12951-018-0361-2.

[59] Y. Gao, L.K. Wolf, R.M. Georgiadis, Secondary structure effects on DNA hybridisation kinetics: a solution versus surface comparison, Nucleic Acids Res. 34 (2006) 3370–3377. https://doi.org/10.1093/NAR/GKL422.

[60] J. Zhang, H.P. Lang, G. Yoshikawa, C. Gerber, Optimisation of DNA hybridisation efficiency by pH-driven nanomechanical bending, Langmuir. 28 (2012) 6494–6501. https://doi.org/10.1021/LA205066H.

[61] C.B. Markegard, C.P. Gallivan, D.D. Cheng, H.D. Nguyen, Effects of Concentration and Temperature on DNA Hybridisation by Two Closely Related Sequences *via* Large-Scale Coarse-Grained Simulations, J. Phys. Chem. B. 120 (2016) 7795–7806. https://doi.org/10.1021/ACS.JPCB.6B03937.

[62] Y.S. Ang, L.Y.L. Yung, Rational design of hybridisation chain reaction monomers for robust signal amplification, Chem. Commun. 52 (2016) 4219-4222. https://doi.org/10.1039/c5cc08907g.

[63] S. Li, P. Li, M. Ge, H. Wang, Y. Cheng, G. Li, Q. Huang, H. He, C. Cao, D. Lin, L. Yang, Elucidation of leak-resistance DNA hybridisation chain reaction with universality and extensibility, Nucleic Acids Res. 48 (2020) 2220-2231. https://doi.org/10.1093/nar/gkaa016.

[64] Y. Xing, X. Li, T. Yuan, W. Cheng, D. Li, T. Yu, X. Ding, S. Ding, Engineering high-performance hairpin stacking circuits for logic gate operation and highly sensitive biosensing assay of microRNA, Analyst. 142 (2017) 4834–4842. https://doi.org/10.1039/C7AN01624G.

[65] C. Yu, Y. Wang, R. Wu, Z. Zhu, B. Li, Study on the Functionalisation and Signaling Efficiency of the Hybridisation Chain Reaction Using Traditional and Single Molecular Characterisations, ACS Appl. Bio Mater. 4 (2021) 3649–3657. https://doi.org/10.1021/ACSABM.1C00136.

[66] D. Andreatta, S. Sen, J.L. Pérez Lustres, S.A. Kovalenko, N.P. Ernsting, C.J. Murphy, R.S. Coleman, M.A. Berg, Ultrafast Dynamics in DNA: “Fraying” at the End of the Helix, J. Am. Chem. Soc. 128 (2006) 6885-6892. https://doi.org/10.1021/JA0582105.

[67] M. Zgarbová, M. Otyepka, J. Šponer, F. Lankaš, P. Jurečka, Base pair fraying in molecular dynamics simulations of DNA and RNA, J. Chem. Theory Comput. 10 (2014) 3177–3189. https://doi.org/10.1021/CT500120V.

[68] J.N. Zadeh, C.D. Steenberg, J.S. Bois, B.R. Wolfe, M.B. Pierce, A.R. Khan, R.M. Dirks, N.A. Pierce, NUPACK: Analysis and design of nucleic acid systems, J. Comput. Chem. 32 (2011) 170–173. https://doi.org/10.1002/jcc.21596.

[69] L.Y. Chuang, Y.H. Cheng, C.H. Yang, Specific primer design for the polymerase chain reaction, Biotechnol. Lett. 35 (2013) 1541–1549. https://doi.org/10.1007/S10529-013-1249-8.

[70] R. Owczarzy, B.G. Moreira, Y. You, M.A. Behlke, J.A. Wälder, Predicting stability of DNA duplexes in solutions containing magnesium and monovalent cations, Biochemistry. 47 (2008) 5336–5353. https://doi.org/10.1021/BI702363U.

[71] W. Zhu, Y. Han, H. Wu, Y. Liu, X. Nan, Q. Zhou, Predicting the results of molecular specific hybridisation using boosted tree algorithm, Concurr. Comput. Pract. Exp. 32 (2020) e4982. https://doi.org/10.1002/CPE.4982.

[72] H.M.T. Choi, C.R. Calvert, N. Husain, D. Huss, J.C. Barsi, B.E. Deverman, R.C. Hunter, M. Kato, S.M. Lee, A.C.T. Abelin, A.Z. Rosenthal, O.S. Akbari, Y. Li, B.A. Hay, P.W. Sternberg, P.H. Patterson, E.H. Davidson, S.K. Mazmanian, D.A. Prober, M. Van De Rijn, J.R. Leadbetter, D.K. Newman, C. Readhead, M.E. Bronner, B. Wold, R. Lansford, T. Sauka-Spengler, S.E. Fraser, N.A. Pierce, Mapping a multiplexed zoo of mRNA expression, Development. 143 (2016) 3632-3637. https://doi.org/10.1242/dev.140137.

[73] T. Hou, W. Li, X. Liu, F. Li, Label-Free and Enzyme-Free Homogeneous Electrochemical Biosensing Strategy Based on Hybridisation Chain Reaction: A Facile, Sensitive, and Highly Specific MicroRNA Assay, Anal. Chem. 87 (2015) 11368-11374. https://doi.org/10.1021/acs.analchem.5b02790.

[74] L. Li, J. Feng, H. Liu, Q. Li, L. Tong, B. Tang, Two-color imaging of microRNA with enzyme-free signal amplification *via* hybridisation chain reactions in living cells, Chem. Sci. 7 (2016) 1940-1945. https://doi.org/10.1039/c5sc03909f.

[75] C. Yang, K. Shi, B. Dou, Y. Xiang, Y. Chai, R. Yuan, In situ DNA-templated

synthesis of silver nanoclusters for ultrasensitive and label-free electrochemical detection of MicroRNA, ACS Appl. Mater. Interfaces. 7 (2015) 1188-1193. https://doi.org/10.1021/am506933r.

[76] J. Wei, X. Gong, Q. Wang, M. Pan, X. Liu, J. Liu, F. Xia, F. Wang, Construction of an autonomously concatenated hybridisation chain reaction for signal amplification and intracellular imaging, Chem. Sci. 9 (2017) 52-61. https://doi.org/10.1039/c7sc03939e.

[77] H. Wang, C. Li, X. Liu, X. Zhou, F. Wang, Construction of an enzyme-free concatenated DNA circuit for signal amplification and intracellular imaging, Chem. Sci. 9 (2018) 5842-5849. https://doi.org/10.1039/C8SC01981A.

[78] Z. Wu, G.Q. Liu, X.L. Yang, J.H. Jiang, Electrostatic nucleic acid nanoassembly enables hybridisation chain reaction in living cells for ultrasensitive mRNA Imaging, J. Am. Chem. Soc. 137 (2015) 6829-6836. https://doi.org/10.1021/jacs.5b01778.

[79] H. Bakhtiari, A. Palizban, H. Khanahmad, M. Mofid, Aptamer-based approaches for in vitro molecular detection of cancer, Res. Pharm. Sci. 15 (2020) 107-122. https://doi.org/10.4103/1735-5362.283811.

[80] W. Song, K. Zhu, Z. Cao, C. Lau, J. Lu, Hybridisation chain reaction-based aptameric system for the highly selective and sensitive detection of protein, Analyst. 137 (2012) 1396-1401. https://doi.org/10.1039/c2an16232f.

[81] X. Wang, A. Jiang, T. Hou, H. Li, F. Li, Enzyme-free and label-free fluorescence aptasensing strategy for highly sensitive detection of protein based on target-triggered hybridisation chain reaction amplification, Biosens. Bioelectron. 70 (2015) 324-329. https://doi.org/10.1016/j.bios.2015.03.053.

[82] Z. Li, X. Miao, Z. Cheng, P. Wang, Hybridisation chain reaction coupled with the fluorescence quenching of gold nanoparticles for sensitive cancer protein detection, Sens. Actuators B Chem. 243 (2017) 731-737. https://doi.org/10.1016/j.snb.2016.12.047.

[83] J. Zhao, C. Chen, L. Zhang, J. Jiang, R. Yu, An electrochemical aptasensor based on hybridisation chain reaction with enzyme-signal amplification for interferon-gamma detection, Biosens. Bioelectron. 36 (2012) 129-134. https://doi.org/10.1016/j.bios.2012.04.013.

[84] Q. Wang, X. Yang, X. Yang, P. Liu, K. Wang, J. Huang, J. Liu, C. Song, J. Wang, Colorimetric detection of mercury ion based on unmodified gold nanoparticles and target-triggered hybridisation chain reaction amplification, Spectrochim. Acta A. 136 (2015) 283–287. https://doi.org/10.1016/J.SAA.2014.08.129.

[85] J. Choi, K. Routenberg Love, Y. Gong, T.M. Gierahn, J.C. Love, Immuno-Hybridisation Chain Reaction for Enhancing Detection of Individual Cytokine-Secreting Human Peripheral Mononuclear Cells, Anal. Chem. 83 (2011) 6890–6895. https://doi.org/10.1021/ac2013916.

[86] B. Zhang, B. Liu, D. Tang, R. Niessner, G. Chen, D. Knopp, DNA-Based Hybridisation Chain Reaction for Amplified Bioelectronic Signal and Ultrasensitive Detection of Proteins, Anal. Chem. 84 (2012) 5392–5399. https://doi.org/10.1021/ac3009065.

[87] Q. Zhu, Y. Chai, Y. Zhuo, R. Yuan, Ultrasensitive simultaneous detection of four biomarkers based on hybridisation chain reaction and biotin-streptavidin signal amplification strategy, Biosens. Bioelectron. 68 (2015) 42-48. https://doi.org/10.1016/j.bios.2014.12.023.

[88] S. Howorka, L. Movileanu, O. Braha, H. Bayley, Kinetics of duplex formation for individual DNA strands within a single protein nanopore, Proc. Natl. Acad. Sci. U.S.A. 98 (2001) 12996–13001. https://doi.org/10.1073/PNAS.231434698.

[89] E.M. Peterson, J.M. Harris, Identification of Individual Immobilized DNA Molecules by Their Hybridisation Kinetics Using Single-Molecule Fluorescence Imaging, Anal. Chem. 90 (2018) 5007–5014. https://doi.org/10.1021/ACS.ANALCHEM.7B04512.

[90] M. Xiao, W. Lai, F. Wang, L. Li, C. Fan, H. Pei, Programming Drug Delivery Kinetics for Active Burst Release with DNA Toehold Switches, J. Am. Chem. Soc. 141 (2019) 20354–20364. https://doi.org/10.1021/JACS.9B10765.

[91] H. Wang, H. Wang, I. Willner, F. Wang, High-performance biosensing based on autonomous enzyme-free DNA circuits, Top. Curr. Chem. 378 (2020) 20. https://doi.org/10.1007/S41061-020-0284-X.

[92] G. Xu, M. Lai, R. Wilson, A. Glidle, J. Reboud, J.M. Cooper, Branched hybridisation chain reaction—using highly dimensional DNA nanostructures for label-free, reagent-

less, multiplexed molecular diagnostics, Microsyst. Nanoeng. 5 (2019) 37. https://doi.org/10.1038/S41378-019-0076-Z.

[93] R.L. Stoermer, C.D. Keating, Distance-dependent emission from dye-labeled oligonucleotides on striped Au/Ag nanowires: Effect of secondary structure and hybridisation efficiency, J. Am. Chem. Soc. 128 (2006) 13243–13254. https://doi.org/10.1021/JA0637200.

[94] C. Lin, J.K. Nangreave, Z. Li, Y. Liu, H. Yan, Signal amplification on a DNA-tile-based biosensor with enhanced sensitivity, Nanomedicine (Lond). 3 (2008) 521–528. https://doi.org/10.2217/17435889.3.4.521.

[95] J. Ikbal, G.S. Lim, Z. Gao, The hybridisation chain reaction in the development of ultrasensitive nucleic acid assays, TrAC - Trends Anal. Chem. 64 (2015) 86–99. https://doi.org/10.1016/J.TRAC.2014.08.014.

[96] S. Shi, X. Wang, W. Sun, X. Wang, T. Yao, L. Ji, Label-free fluorescent DNA biosensors based on metallointercalators and nanomaterials, Methods. 64 (2013) 305–314. https://doi.org/10.1016/J.YMETH.2013.07.004.

[97] G. Tikhomirov, S. Hoogland, P.E. Lee, A. Fischer, E.H. Sargent, S.O. Kelley, DNA-based programming of quantum dot valency, self-assembly and luminescence, Nat. Nanotechnol. 6 (2011) 485-490. https://doi.org/10.1038/nnano.2011.100.

[98] H.T. Maune, S.P. Han, R.D. Barish, M. Bockrath, W.A.G. Iii, P.W.K. Rothemund, E. Winfree, Self-assembly of carbon nanotubes into two-dimensional geometries using DNA origami templates, Nat. Nanotechnol. 5 (2010) 61-66. https://doi.org/10.1038/nnano.2009.311.

[99] I. Chakraborty, T. Pradeep, Atomically Precise Clusters of Noble Metals: Emerging Link between Atoms and Nanoparticles, Chem. Rev. 117 (2017) 8208–8271. https://doi.org/10.1021/ACS.CHEMREV.6B00769.

[100] R. Jin, C. Zeng, M. Zhou, Y. Chen, Atomically Precise Colloidal Metal Nanoclusters and Nanoparticles: Fundamentals and Opportunities, Chem. Rev. 116 (2016) 10346–10413. https://doi.org/10.1021/ACS.CHEMREV.5B00703.

[101] B. Wang, M. Zhao, M. Mehdi, G. Wang, P. Gao, K.Q. Zhang, Biomolecule-assisted synthesis and functionality of metal nanoclusters for biological sensing: a review,

Mater. Chem. Front. 3 (2019) 1722–1735. https://doi.org/10.1039/C9QM00165D.

[102] A. Gonzàlez-Rosell, C. Cerretani, P. Mastracco, T. Vosch, S.M. Copp, Structure and luminescence of DNA-templated silver clusters, Nanoscale Adv. 3 (2021) 1230–1260. https://doi.org/10.1039/D0NA01005G.

[103] T. Qing, B. Feng, P. Zhang, K. Zhang, X. He, K. Wang, Beyond native deoxyribonucleic acid, templating fluorescent nanomaterials for bioanalytical applications: A review, Anal. Chim. Acta. 1105 (2020) 11–27. https://doi.org/10.1016/J.ACA.2020.01.023.

[104] *E.G.*,Gwinn, P. O'Neill, A.J. Guerrero, D. Bouwmeester, D.K. Fygenson, Sequence-Dependent Fluorescence of DNA-Hosted Silver Nanoclusters, Adv. Mater. 20 (2008) 279–283. https://doi.org/10.1002/adma.200702380.

[105] D. Schultz, S.M. Copp, N. Markešević, K. Gardner, S.S.R. Oemrawsingh, D. Bouwmeester, E. Gwinn, Dual-color nanoscale assemblies of structurally stable, few-atom silver clusters, as reported by fluorescence resonance energy transfer, ACS Nano. 7 (2013) 9798–9807. https://doi.org/10.1021/NN4033097.

[106] D. Schultz, E. Gwinn, Stabilisation of fluorescent silver clusters by RNA homopolymers and their DNA analogs: C,G versus A,T(U) dichotomy, Chem. Commun. 47 (2011) 4715-4717. https://doi.org/10.1039/c0cc05061j.

[107] S.M. Copp, S.M. Swasey, A. Gorovits, P. Bogdanov, *E.G.*,Gwinn, General Approach for Machine Learning-Aided Design of DNA-Stabilised Silver Clusters, Chem. Mater. 32 (2020) 430–437. https://doi.org/10.1021/ACS.CHEMMATER.9B04040.

[108] D. Schultz, *E.G.*,Gwinn, Silver atom and strand numbers in fluorescent and dark Ag:DNAs, Chem. Commun. 48 (2012) 5748–5750. https://doi.org/10.1039/C2CC17675K.

[109] J. Yu, S. Choi, R.M. Dickson, Shuttle-Based Fluorogenic Silver-Cluster Biolabels, Angew. Chemie Int. Ed. 48 (2009) 318–320. https://doi.org/10.1002/ANIE.200804137.

[110] W.Y. Mu, R. Yang, A. Robertson, Q.Y. Chen, A near-infrared BSA coated DNA-AgNCs for cellular imaging, Colloids Surf. B. Biointerfaces. 162 (2018) 427–431. https://doi.org/10.1016/J.COLSURFB.2017.12.023.

[111] Y. Chen, M.L. Phipps, J.H. Werner, S. Chakraborty, J.S. Martinez, DNA Templated Metal Nanoclusters: From Emergent Properties to Unique Applications, Acc. Chem. Res. 51 (2018) 2756–2763. https://doi.org/10.1021/ACS.ACCOUNTS.8B00366.

[112] P. Shah, S.K. Cho, P.W. Thulstrup, Y.-J. Bhang, J.C. Ahn, S.W. Choi, A. Rørvig-Lund, S.W. Yang, Effect of salts, solvents and buffer on miRNA detection using DNA silver nanocluster (DNA/AgNCs) probes, Nanotechnology. 25 (2014) 045101. https://doi.org/10.1088/0957-4484/25/4/045101.

[113] K. Ma, Q. Cui, Y. Shao, F. Wu, S. Xu, G. Liu, Emission modulation of dna-templated fluorescent silver nanoclusters by divalent magnesium ion, J. Nanosci. Nanotechnol. 12 (2012) 861–869. https://doi.org/10.1166/JNN.2012.5665.

[114] P. Shah, S.W. Choi, R. Nagda, R. Geczy, S.K. Cho, Y.J. Bhang, T.H. Kim, T.Y. Song, P.H. Lee, J.H. Kang, P.W. Thulstrup, M.J. Bjerrum, I.L. Jung, S.W. Yang, The structural shift of a DNA template between a hairpin and a dimer tunes the emission color of DNA-templated AgNCs, Nanoscale. 10 (2018) 20717–20722. https://doi.org/10.1039/C8NR06186F.

[115] M. Yang, X. Chen, Y. Su, H. Liu, H. Zhang, X. Li, W. Xu, The Fluorescent Palette of DNA-Templated Silver Nanoclusters for Biological Applications, Front. Chem. 8 (2020) 601621. https://doi.org/10.3389/FCHEM.2020.601621.

[116] M. Chandler, O. Shevchenko, J.L. Vivero-Escoto, C.D. Striplin, K.A. Afonin, DNA-Templated Synthesis of Fluorescent Silver Nanoclusters, J. Chem. Educ. 97 (2020) 1992–1996. https://doi.org/10.1021/ACS.JCHEMED.0C00158.

[117] Y. Guo, F. Shen, Y. Cheng, H. Yu, Y. Xie, W. Yao, R. Pei, H. Qian, H.W. Li, DNA-Hairpin-Templated Silver Nanoclusters: A Study on Stem Sequence, J. Phys. Chem. B. 124 (2020) 1592–1601. https://doi.org/10.1021/ACS.JPCB.9B09741.

[118] Z. Lu, P. Wang, W. Xiong, B. Qi, R. Shi, D. Xiang, K. Zhai, Simultaneous detection of mercury (II), lead (II) and silver (I) based on fluorescently labelled aptamer probes and graphene oxide, Environ. Technol. 42 (2020) 3065–3072. https://doi.org/10.1080/09593330.2020.1721565.

[119] B. Adhikari, A. Banerjee, Facile synthesis of water-soluble fluorescent silver nanoclusters and Hg^{II} sensing, Chem. Mater. 22 (2010) 4364–4371.

https://doi.org/10.1021/CM1001253.

[120] L.E. Yourston, A. V. Krasnoslobodtse, Micro RNA Sensing with Green Emitting Silver Nanoclusters, Mol. 25 (2020) 3026. https://doi.org/10.3390/MOLECULES25133026.

[121] M. Hosseini, A. Akbari, M.R. Ganjali, M. Dadmehr, A.H. Rezayan, A Novel Label-Free microRNA-155 Detection on the Basis of Fluorescent Silver Nanoclusters, J. Fluoresc. 25 (2015) 925–929. https://doi.org/10.1007/S10895-015-1574-5.

[122] M.R. Carro Temboury, V. Paolucci, E.N. Hooley, L. Latterini, T. Vosch, Probing DNA-stabilised fluorescent silver nanocluster spectral heterogeneity by time-correlated single photon counting, Analyst. 141 (2015) 123–130. https://doi.org/10.1039/C5AN02011E.

[123] R. Cheng, J. Xu, X. Zhang, Z. Shi, Q. Zhang, Y. Jin, A selective and label-free strategy for rapid screening of telomere-binding Ligands *via* fluorescence regulation of DNA/silver nanocluster, Sci. Rep. 7 (2017) 42629. https://doi.org/10.1038/srep42629.

[124] J. Lan, B. Feng, X. Wu, L. Yang, J. Liu, G. Shi, F. Wang, Aptamer-Modified Silver Nanoclusters for Fluorescence Detection of Intracellular 8-Hydroxydeoxyguanosine, ACS Appl. Nano Mater. 3 (2020) 1332–1338. https://doi.org/10.1021/ACSANM.9B02179.

[125] L. Wang, K. Ma, Y. Zhang, Label-free fluorometric detection of S1 nuclease activity by using polycytosine oligonucleotide-templated silver nanoclusters, Anal. Biochem. 468 (2015) 34–38. https://doi.org/10.1016/J.AB.2014.09.011.

[126] M. Hosseini, F. Mehrabi, M.R. Ganjali, P. Norouzi, A fluorescent aptasensor for sensitive analysis oxytetracycline based on silver nanoclusters, Luminescence. 31 (2016) 1339–1343. https://doi.org/10.1002/BIO.3112.

[127] M. Hosseini, S. Mohammadi, Y.S. Borghei, M.R. Ganjali, Detection of p53 Gene Mutation (Single-Base Mismatch) Using a Fluorescent Silver Nanoclusters, J. Fluoresc. 27 (2017) 1443–1448. https://doi.org/10.1007/S10895-017-2083-5.

[128] Y. Zhang, Y. Cai, Z. Qi, L. Lu, Y. Qian, DNA-Templated Silver Nanoclusters for Fluorescence Turn-on Assay of Acetylcholinesterase Activity, Anal. Chem. 85 (2013) 8455–8461. https://doi.org/10.1021/ac401966d.

[129] G. Liu, D.Q. Feng, X. Mu, W. Zheng, T. Chen, L. Qi, D. Li, DNA-functionalised silver nanoclusters as a chemopalette: tunable fluorescence for turn-on detection of cysteine, J. Mater. Chem. B. 1 (2013) 2128–2131. https://doi.org/10.1039/C3TB20208A.

[130] Y. Zhang, C. Zhu, L. Zhang, C. Tan, J. Yang, B. Chen, L. Wang, H. Zhang, DNA-Templated Silver Nanoclusters for Multiplexed Fluorescent DNA Detection, Small. 11 (2015) 1385–1389. https://doi.org/10.1002/SMLL.201402044.

[131] L. Yourston, P. Dhoqina, N. Marshall, R. Mahmud, E. Kuether, A.V. Krasnoslobodtsev, Hg^{2+} Detection with Rational Design of DNA-Templated Fluorescent Silver Nanoclusters, Process. 9 (2021) 1699. https://doi.org/10.3390/PR9101699.

[132] F. Shen, H. Qian, Y. Cheng, Y. Xie, H. Yu, W. Yao, R. Pei, Y. Guo, H.W. Li, Three-way junction-promoted recycling amplification for sensitive DNA detection using highly bright DNA-silver nanocluster as label-free output, Talanta. 206 (2020) 120216. https://doi.org/10.1016/J.TALANTA.2019.120216.

[133] M. Xu, Z. Gao, Q. Wei, G. Chen, D. Tang, Label-free hairpin DNA-scaffolded silver nanoclusters for fluorescent detection of Hg^{2+} using exonuclease III-assisted target recycling amplification, Biosens. Bioelectron. 79 (2016) 411–415. https://doi.org/10.1016/J.BIOS.2015.12.081.

[134] M.A. Kapitonova, Z. V. Reveguk, A.I. Kononov, Revealing a possible sensor mechanism of DNA - Based silver nanoclusters, J. Phys. Conf. Ser. 1695 (2020) 012058. https://doi.org/10.1088/1742-6596/1695/1/012058.

[135] S. Walczak, K. Morishita, M. Ahmed, J. Liu, Towards understanding of poly-guanine activated fluorescent silver nanoclusters, Nanotechnology. 25 (2014) 155501. https://doi.org/10.1088/0957-4484/25/15/155501.

[136] T. Suo, M. Sohail, Y. Ma, B. Li, Y. Chen, X. Zhang, X. Zhou, A versatile turn-on fluorometric biosensing profile based on split aptamers-involved assembly of nanocluster beacon sandwich, Sens. Actuators B Chem. 324 (2020) 128586. https://doi.org/10.1016/J.SNB.2020.128586.

[137] X. Li, H. Zhang, Y. Zhao, L. Lian, X. Wang, W. Gao, B. Zhu, D. Lou, Design and

Synthesis of Ag Nanocluster Molecular Beacon for Adenosine Triphosphate Detection, J. Anal. Methods Chem. 2019 (2019) 2786156. https://doi.org/10.1155/2019/2786156.

[138] H.-C. Yeh, J. Sharma, J.J. Han, J.S. Martinez, J.H. Werner, A DNA−Silver Nanocluster Probe That Fluoresces upon Hybridisation, Nano Lett. 10 (2010) 3106–3110. https://doi.org/10.1021/nl101773c.

[139] Q.L. Wen, J. Peng, A.Y. Liu, J. Wang, Y.L. Hu, J. Ling, Q.E. Cao, DNA bioassays based on the fluorescence 'turn off' of silver nanocluster beacon, Luminescence. 35 (2020) 702–708. https://doi.org/10.1002/BIO.3775.

[140] J.L. Ma, B.C. Yin, B.C. Ye, DNA template-regulated intergrowth of a fluorescent silver nanocluster emitter pair, RSC Adv. 5 (2015) 98467–98471. https://doi.org/10.1039/C5RA21159J.

[141] W. Zhou, J. Zhu, Y. Teng, B. Du, X. Han, S. Dong, Novel dual fluorescence temperature-sensitive chameleon DNA-templated silver nanocluster pair for intracellular thermometry, Nano Res. 11 (2018) 2012–2023. https://doi.org/10.1007/s12274-017-1817-7.

[142] J.L. Ma, B.C. Yin, B.C. Ye, A versatile proximity-dependent probe based on light-up DNA-scaffolded silver nanoclusters, Analyst. 141 (2016) 1301–1306. https://doi.org/10.1039/C5AN02446C.

[143] Y. Jiang, P. Miao, DNA Dumbbell and Chameleon Silver Nanoclusters for miRNA Logic Operations, Research. 2020 (2020) 1091605. https://doi.org/10.34133/2020/1091605.

[144] S. Xu, L. Jiang, J. Wang, Y. Gao, X. Luo, Ratiometric Multicolor Analysis of Intracellular MicroRNA Using a Chain Hybrid Substitution-Triggered Self-Assembly of Silver Nanocluster-Based Label-Free Sensing Platform, ACS Appl. Mater. Interfaces. 12 (2020) 373–379. https://doi.org/10.1021/ACSAMI.9B19709.

[145] H.-C. Yeh, J. Sharma, I.-M. Shih, D.M. Vu, J.S. Martinez, J.H. Werner, A fluorescence light-up Ag nanocluster probe that discriminates single-nucleotide variants by emission color, J. Am. Chem. Soc. 134 (2012) 11550–11558. https://doi.org/10.1021/ja3024737.

[146] S. Juul, J.M. Obliosca, C. Liu, Y.L. Liu, Y.A. Chen, D.M. Imphean, B.R. Knudsen,

Y.P. Ho, K.W. Leong, H.C. Yeh, NanoCluster Beacons as reporter probes in rolling circle enhanced enzyme activity detection, Nanoscale. 7 (2015) 8332–8337. https://doi.org/10.1039/C5NR01705J.

[147] M. Alipour, S. Jalili, H. Shirzad, E. Ansari Dezfouli, M.H. Fouani, A.A. Sadeghan, H. Bardania, S. Hosseinkhani, Development of dual-emission cluster of Ag atoms for genetically modified organisms detection, Microchim. Acta. 187 (2020) 628. https://doi.org/10.1007/S00604-020-04591-2.

[148] L. Ge, X. Sun, Q. Hong, F. Li, Ratiometric NanoCluster Beacon: A Label-Free and Sensitive Fluorescent DNA Detection Platform, ACS Appl. Mater. Interfaces. 9 (2017) 13102–13110. https://doi.org/10.1021/ACSAMI.7B03198.

[149] Y. Teng, X. Jia, S. Zhang, J. Zhu, E. Wang, A nanocluster beacon based on the template transformation of DNA-templated silver nanoclusters, Chem. Commun. 52 (2016) 1721–1724. https://doi.org/10.1039/C5CC09138A.

[150] L. Ge, X. Sun, Q. Hong, F. Li, Ratiometric Catalyzed-Assembly of NanoCluster Beacons: A Nonenzymatic Approach for Amplified DNA Detection, ACS Appl. Mater. Interfaces. 9 (2017) 32089–32096. https://doi.org/10.1021/acsami.7b09034.

[151] J. Liu, F. Sun, Y. Wang, W. Yang, H. Xiao, Y. Zhang, R. Lu, H. Zhu, Y. Zhuang, Z. Pan, Z. Wang, Z. Du, Y. Lu, Suppression of microRNA-16 protects against acute myocardial infarction by reversing beta2-adrenergic receptor down-regulation in rats, Oncotarget. 8 (2017) 20122–20132. https://doi.org/10.18632/oncotarget.15391.

[152] L. Hong, F. Zhou, G. Wang, X. Zhang, Synthesis and sensing integration: A novel enzymatic reaction modulated Nanoclusters Beacon (NCB) “Illumination” strategy for label-free biosensing and logic gate operation, Biosens. Bioelectron. 86 (2016) 588–594. https://doi.org/10.1016/J.BIOS.2016.07.011.

[153] M. Peng, N. Na, J. Ouyang, A Fluorescence Light-Up Silver Nanocluster Beacon Modulated by Metal Ions and Its Application in Telomerase-Activity Detection, Chem. Eur. J. 25 (2019) 3598–3605. https://doi.org/10.1002/CHEM.201805308.

[154] Z. Liu, Y. Wang, J. Li, Y. Yuan, X. Wu, W. Liu, Y. Liu, A label-free fluorescent enhancement nanosensor for ultrasensitive and highly selective detection of miRNA-378 through signal synergy amplification, Anal. Chim. Acta. 1087 (2019) 86–92.

https://doi.org/10.1016/J.ACA.2019.08.052.

[155] Z. Jia, K. Tu, Q. Xu, W. Gao, C. Liu, B. Fang, M. Zhang, A novel disease-associated nucleic acid sensing platform based on split DNA-scaffolded sliver nanocluster, Anal. Chim. Acta. 1175 (2021) 338734. https://doi.org/10.1016/J.ACA.2021.338734.

[156] Y. Jiang, Z. Guo, M. Wang, J. Cui, P. Miao, Construction of fluorescence logic gates responding to telomerase and miRNA based on DNA-templated silver nanoclusters and the hybridisation chain reaction, Nanoscale. 14 (2022) 612–616. https://doi.org/10.1039/D1NR05622K.

[157] X. Qiu, P. Wang, Z. Cao, Hybridisation chain reaction modulated DNA-hosted silver nanoclusters for fluorescent identification of single nucleotide polymorphisms in the let-7 miRNA family, Biosens. Bioelectron. 60 (2014) 351–357. https://doi.org/10.1016/j.bios.2014.04.040.

[158] Z. Chen, Y. Liu, C. Xin, J. Zhao, S. Liu, A cascade autocatalytic strand displacement amplification and hybridisation chain reaction event for label-free and ultrasensitive electrochemical nucleic acid biosensing, Biosens. Bioelectron. 113 (2018) 1–8. https://doi.org/10.1016/j.bios.2018.04.046.

[159] L. Chen, L. Sha, Y. Qiu, G. Wang, H. Jiang, X. Zhang, An amplified electrochemical aptasensor based on hybridisation chain reactions and catalysis of silver nanoclusters, Nanoscale. 7 (2015) 3300–3308. https://doi.org/10.1039/C4NR06664B.

[160] Y. Jiang, X. Ma, X. Shao, M. Wang, Y. Jiang, P. Miao, Chameleon silver nanoclusters for ratiometric sensing of miRNA, Sens. Actuators B Chem. 297 (2019) 126788. https://doi.org/10.1016/j.snb.2019.126788.

[161] X. Peng, J. Zhu, W. Wen, T. Bao, X. Zhang, H. He, S. Wang, Silver nanoclusters-assisted triple-amplified biosensor for ultrasensitive methyltransferase activity detection based on AuNPs/ERGO hybrids and hybridisation chain reaction, Biosens. Bioelectron. 118 (2018) 174–180. https://doi.org/10.1016/j.bios.2018.07.048.

[162] G. Jie, L. Tan, Y. Zhao, X. Wang, A novel silver nanocluster in situ synthesised as versatile probe for electrochemiluminescence and electrochemical detection of thrombin by multiple signal amplification strategy, Biosens. Bioelectron. 94 (2017) 243–249. https://doi.org/10.1016/j.bios.2017.03.015.

[163] Y. Zhao, C. Lu, X.-E. Zhao, W. Kong, S. Zhu, F. Qu, A T-rich nucleic acid-enhanced electrochemical platform based on electroactive silver nanoclusters for miRNA detection, Biosens. Bioelectron. 208 (2022) 114215. https://doi.org/10.1016/J.BIOS.2022.114215.

[164] R. Orbach, W. Guo, F. Wang, O. Lioubashevski, I. Willner, Self-Assembly of Luminescent Ag Nanocluster-Functionalised Nanowires, Langmuir. 29 (2013) 13066–13071. https://doi.org/10.1021/la402888b.

[165] N. Mansourian, M. Rahaie, M. Hosseini, A Nanobiosensor Based on Fluorescent DNA-Hosted Silver Nanocluster and HCR Amplification for Detection of MicroRNA Involved in Progression of Multiple Sclerosis, J. Fluoresc. 27 (2017) 1679–1685. https://doi.org/10.1007/s10895-017-2105-3.

[166] L. Zhang, M. Pan, Z. Q. Zou, L. Fan, X. Q. Liu, Hybridisation Chain Reaction-Mediated Luminescent Silver Nanocluster System for Amplified Detection of miRNA-21. Chin. J. Anal. Chem. 48 (2020) 1193–1201. https://doi.org/10.19756/j.issn.0253-3820.201144.

[167] W. Guo, J. Yuan, E. Wang, Strand exchange reaction modulated fluorescence "off-on" switching of hybridised DNA duplex stabilised silver nanoclusters, Chem. Commun. 47 (2011) 10930–10932. https://doi.org/10.1039/C1CC11921D.

[168] W. Guo, J. Yuan, Q. Dong, E. Wang, Highly Sequence-Dependent Formation of Fluorescent Silver Nanoclusters in Hybridised DNA Duplexes for Single Nucleotide Mutation Identification, J. Am. Chem. Soc. 132 (2010) 932–934. https://doi.org/10.1021/ja907075s.

[169] L. Liu, Q. Li, L.-J. Tang, R.-Q. Yu, J.-H. Jiang, Silver nanocluster-lightened hybridisation chain reaction, RSC Adv. 6 (2016) 57502–57506. https://doi.org/10.1039/c6ra09337j.

[170] L. Duan, R. Hao, Z. Xu, X. He, A.S. Adeleye, Y. Li, Removal of graphene oxide nanomaterials from aqueous media *via* coagulation: Effects of water chemistry and natural organic matter, Chemosphere. 168 (2017) 1051–1057. https://doi.org/10.1016/J.CHEMOSPHERE.2016.10.104.

[171] V. Palmieri, G. Perini, M. De Spirito, M. Papi, Graphene oxide touches blood:: In vivo

interactions of bio-coronated 2D materials, Nanoscale Horiz. 4 (2019) 464–471. https://doi.org/10.1039/C8NH00318A.

[172] Clarivate, ISI Web of Science. (2021). www.webofscience.com (accessed 11.06.22)

[173] L. Chen, J. Liu, C. Cao, S. Tang, C. Lv, X. Xiao, S. Yang, L. Liu, L. Sun, B. Zhu, L. Li, Dual-signal amplification electrochemical sensing for the sensitive detection of uranyl ion based on gold nanoparticles and hybridisation chain reaction-assisted synthesis of silver nanoclusters, Anal. Chim. Acta. 1184 (2021) 338986. https://doi.org/10.1016/J.ACA.2021.338986.

[174] Z. Zeng, R. Zhou, R. Sun, X. Zhang, Z. Cheng, C. Chen, Q. Zhu, Nonlinear hybridisation chain reaction-based functional DNA nanostructure assembly for biosensing, bioimaging applications, Biosens. Bioelectron. 173 (2021) 112814. https://doi.org/10.1016/J.BIOS.2020.112814.

[175] F. Xuan, I.-M. Hsing, Triggering Hairpin-Free Chain-Branching Growth of Fluorescent DNA Dendrimers for Nonlinear Hybridisation Chain Reaction, J. Am. Chem. Soc. 136 (2014) 9810–9813. https://doi.org/10.1021/ja502904s.

[176] Y. Chu, A.P. Deng, W. Wang, J.J. Zhu, Concatenated Catalytic Hairpin Assembly/Hyperbranched Hybridisation Chain Reaction Based Enzyme-Free Signal Amplification for the Sensitive Photoelectrochemical Detection of Human Telomerase RNA, Anal. Chem. 91 (2019) 3619–3627. https://doi.org/10.1021/ACS.ANALCHEM.8B05610.

[177] J. Wang, M. Pan, J. Wei, X. Liu, F. Wang, A C-HCR assembly of branched DNA nanostructures for amplified uracil-DNA glycosylase assays, Chem. Commun. 53 (2017) 12878–12881. https://doi.org/10.1039/C7CC07057H.

[178] D. Ren, C. Sun, Z. Huang, Z. Luo, C. Zhou, Y. Li, A novel FRET biosensor based on four-way branch migration HCR for Vibrio parahaemolyticus detection, Sens. Actuators B Chem. 296 (2019) 126577. https://doi.org/10.1016/J.SNB.2019.05.054.

[179] S. Bi, M. Chen, X. Jia, Y. Dong, Z. Wang, Hyperbranched Hybridisation Chain Reaction for Triggered Signal Amplification and Concatenated Logic Circuits, Angew. Chemie Int. Ed. 54 (2015) 8144–8148. https://doi.org/10.1002/anie.201501457.

[180] W. Li, L. Liu, Y. Fu, Y. Sun, J. Zhang, R. Zhang, Effects of polymorphic DNA on the

fluorescent properties of silver nanoclusters, Photochem. Photobiol. Sci. 12 (2013) 1864–1872. https://doi.org/10.1039/C3PP50026H.

[181] K. Ma, Y. Shao, Q. Cui, F. Wu, S. Xu, G. Liu, Base-Stacking-Determined Fluorescence Emission of DNA Abasic Site-Templated Silver Nanoclusters, Langmuir. 28 (2012) 15313–15322. https://doi.org/10.1021/la301957m.

[182] Q. Cui, K. Ma, Y. Shao, S. Xu, F. Wu, G. Liu, N. Teramae, H. Bao, Gap site-specific rapid formation of fluorescent silver nanoclusters for label-free DNA nucleobase recognition, Anal. Chim. Acta. 724 (2012) 86–91. https://doi.org/10.1016/j.aca.2012.02.044.

[183] J. Peng, Y. Shao, L. Liu, L. Zhang, H. Liu, Y. Wang, Ag nanoclusters as probes for turn-on fluorescence recognition of TpG dinucleotide with a high selectivity, Anal. Chim. Acta. 850 (2014) 78–84. https://doi.org/10.1016/J.ACA.2014.08.032.

[184] K. Ma, Q. Cui, G. Liu, F. Wu, S. Xu, Y. Shao, DNA abasic site-directed formation of fluorescent silver nanoclusters for selectivenucleobase recognition, Nanotechnology. 22 (2011) 305502. https://doi.org/10.1088/0957-4484/22/30/305502.

[185] Z. Huang, F. Pu, D. Hu, C. Wang, J. Ren, X. Qu, Site-Specific DNA-Programmed Growth of Fluorescent and Functional Silver Nanoclusters, Chem. Eur. J. 17 (2011) 3774–3780. https://doi.org/10.1002/chem.201001795.

[186] J. Peng, Y. Shao, L. Liu, L. Zhang, W. Fu, H. Liu, Role of anion polarizability in fluorescence sensitization of DNA-templated silver nanoclusters, Nanotechnology. 25 (2014) 235501. https://doi.org/10.1088/0957-4484/25/23/235501.

[187] J. Peng, Y. Shao, L. Liu, L. Zhang, H. Liu, Specific recognition of DNA bulge sites by in situ grown fluorescent Ag nanoclusters with high selectivity, Dalton Trans. 43 (2013) 1534–1541. https://doi.org/10.1039/C3DT52042K.

[188] T. Li, L. Zhang, J. Ai, S. Dong, E. Wang, Ion-Tuned DNA/Ag Fluorescent Nanoclusters As Versatile Logic Device, ACS Nano. 5 (2011) 6334–6338. https://doi.org/10.1021/NN201407H.

[189] J. Ai, W. Guo, B. Li, T. Li, D. Li, E. Wang, DNA G-quadruplex-templated formation of the fluorescent silver nanocluster and its application to bioimaging, Talanta. 88 (2012) 450–455. https://doi.org/10.1016/J.TALANTA.2011.10.057.

[190] J. Dong, X. Cui, Y. Deng, Z. Tang, Amplified detection of nucleic acid by G-quadruplex based hybridisation chain reaction, Biosens. Bioelectron. 38 (2012) 258–263. https://doi.org/10.1016/J.BIOS.2012.05.042.

[191] Y. Bai, H. Zhang, L. Zhao, Y. Wang, X. Chen, H. Zhai, M. Tian, R. Zhao, T. Wang, H. Xu, F. Feng, A novel aptasensor based on HCR and G-quadruplex DNAzyme for fluorescence detection of Carcinoembryonic Antigen, Talanta. 221 (2021) 121451. https://doi.org/10.1016/J.TALANTA.2020.121451.

[192] C. Yin, Q. Zhao, A. Yue, W. Du, D. Liu, J. Zhao, Y. Zhang, M. Wang, Colorimetric Detection of Class A Soybean Saponins by G-Quadruplex-Based Hybridisation Chain Reaction, J. Anal. Methods Chem. 2020 (2020) 8813239. https://doi.org/10.1155/2020/8813239.

[193] E. Hosseinzadeh, H. Ravan, A. Mohammadi, H. Pourghadamyari, Colorimetric detection of miRNA-21 by DNAzyme-coupled branched DNA constructs, Talanta. 216 (2020) 120913. https://doi.org/10.1016/J.TALANTA.2020.120913.

[194] B.T. Roembke, S. Nakayama, H.O. Sintim, Nucleic acid detection using G-quadruplex amplification methodologies, Methods. 64 (2013) 185–198. https://doi.org/10.1016/J.YMETH.2013.10.003.

[195] Y. Zhang, L. Wang, Y. Dong, A Label-free and Universal Platform for the Construction of Various Logic Circuits Based on Graphene Oxide and G-Quadruplex Structure, Anal. Sci. 35 (2019) 181–187. https://doi.org/10.2116/ANALSCI.18P349.

[196] Y. Han, F. Zhang, H. Gong, C. Cai, Multifunctional G-quadruplex-based fluorescence probe coupled with DNA-templated AgNCs for simultaneous detection of multiple DNAs and MicroRNAs, Anal. Chim. Acta. 1053 (2019) 105–113. https://doi.org/10.1016/J.ACA.2018.11.062.

[197] J. Sun, X. Sun, Recent advances in the construction of DNA nanostructure with signal amplification and ratiometric response for miRNA sensing and imaging, TrAC - Trends Anal. Chem. 127 (2020) 115900. https://doi.org/10.1016/J.TRAC.2020.115900.

[198] Y. Sun, L. Shi, L. Mi, R. Guo, T. Li, Recent progress of SERS optical nanosensors for miRNA analysis, J. Mater. Chem. B. 8 (2020) 5178–5183.

https://doi.org/10.1039/D0TB00280A.

[199] M. Cardoso Dos Santos, N. Hildebrandt, Recent developments in lanthanide-to-quantum dot FRET using time-gated fluorescence detection and photon upconversion, TrAC - Trends Anal. Chem. 84 (2016) 60–71. https://doi.org/10.1016/J.TRAC.2016.03.005.

[200] Y. Zhou, Q. Zou, J. Qiu, L. Wang, L. Zhu, Rational Design of a Green-Light-Mediated Unimolecular Platform for Fast Switchable Acidic Sensing, J. Phys. Chem. Lett. 9 (2018) 550–556. https://doi.org/10.1021/ACS.JPCLETT.7B03233.

[201] W. Sun, S. Guo, C. Hu, J. Fan, X. Peng, Recent Development of Chemosensors Based on Cyanine Platforms, Chem. Rev. 116 (2016) 7768–7817. https://doi.org/10.1021/ACS.CHEMREV.6B00001.

[202] M.H. Lee, J.S. Kim, J.L. Sessler, Small molecule-based ratiometric fluorescence probes for cations, anions, and biomolecules, Chem. Soc. Rev. 44 (2015) 4185–4191. https://doi.org/10.1039/C4CS00280F.

[203] B. Li, Y. Liu, Y. Liu, T. Tian, B. Yang, X. Huang, J. Liu, B. Liu, Construction of Dual-Color Probes with Target-Triggered Signal Amplification for in Situ Single-Molecule Imaging of MicroRNA, ACS Nano. 14 (2020) 8116-8125. https://doi.org/10.1021/acsnano.0c01061.

[204] T. Shu, J. Wang, X. Lin, Z. Zhou, F. Liang, L. Su, X. Zhang, Dual-emissive gold nanoclusters for label-free and separation-free ratiometric fluorescence sensing of 4-nitrophenol based on the inner filter effect, J. Mater. Chem. C. 6 (2018) 5033-5038. https://doi.org/10.1039/c8tc00448j.

[205] Y. Wang, N. Wu, F. Guo, R. Gao, T. Yang, J. Wang, g-C3N4 nanosheet-based ratiometric fluorescent probes for the amplification and imaging of miRNA in living cells, J. Mater. Chem. B. 7 (2019) 7566–7573. https://doi.org/10.1039/C9TB02021G.

[206] M.K. Kuimova, S.W. Botchway, A.W. Parker, M. Balaz, H.A. Collins, H.L. Anderson, K. Suhling, P.R. Ogilby, Imaging intracellular viscosity of a single cell during photoinduced cell death, Nat. Chem. 1 (2009) 69–73. https://doi.org/10.1038/nchem.120.

[207] X. Peng, Z. Yang, J. Wang, J. Fan, Y. He, F. Song, B. Wang, S. Sun, J. Qu, J. Qi, M.

Yan, Fluorescence ratiometry and fluorescence lifetime imaging: Using a single molecular sensor for dual mode imaging of cellular viscosity, J. Am. Chem. Soc. 133 (2011) 6626–6635. https://doi.org/10.1021/JA1104014.

[208] X. Li, G. Baryshnikov, C. Deng, X. Bao, B. Wu, Y. Zhou, H. Ågren, L. Zhu, A three-dimensional ratiometric sensing strategy on unimolecular fluorescence–thermally activated delayed fluorescence dual emission, Nat. Commun. 10 (2019) 731. https://doi.org/10.1038/s41467-019-08684-2.

[209] H.Q. Yin, J.C. Yang, X.B. Yin, Ratiometric Fluorescence Sensing and Real-Time Detection of Water in Organic Solvents with One-Pot Synthesis of Ru@MIL-101(Al)-NH2, Anal. Chem. 89 (2017) 13434–13440. https://doi.org/10.1021/ACS.ANALCHEM.7B03723.

[210] J.H. Wang, Y.M. Liu, J. Bin Chao, H. Wang, Y. Wang, S.M. Shuang, A simple but efficient fluorescent sensor for ratiometric sensing of Cd2+ and bio-imaging studies, Sens. Actuators B Chem. 303 (2020) 127216. https://doi.org/10.1016/J.SNB.2019.127216.

[211] L. Luo, M. Wang, Y. Zhou, D. Xiang, Q. Wang, J. Huang, J. Liu, X. Yang, K. Wang, Ratiometric Fluorescent DNA Nanostructure for Mitochondrial ATP Imaging in Living Cells Based on Hybridisation Chain Reaction, Anal. Chem. 93 (2021) 6715–6722. https://doi.org/10.1021/ACS.ANALCHEM.1C00176.

[212] J.T. Del Bonis-O'Donnell, A. Thakrar, J.W. Hirschberg, D. Vong, B.N. Queenan, D.K. Fygenson, S. Pennathur, DNA-Stabilised Silver Nanoclusters as Specific, Ratiometric Fluorescent Dopamine Sensors, ACS Chem. Neurosci. 9 (2018) 849–857. https://doi.org/10.1021/ACSCHEMNEURO.7B00444.

[213] A. Turchinovich, W.C. Cho, The origin, function and diagnostic potential of extracellular microRNA in human body fluids, Front. Genet. 5 (2014) 30. https://doi.org/10.3389/FGENE.2014.00030.

[214] J.C. Brase, D. Wuttig, R. Kuner, H. Sültmann, Serum microRNAs as non-invasive biomarkers for cancer, Mol. Cancer. 9 (2010) 306. https://doi.org/10.1186/1476-4598-9-306.

[215] N. Kosaka, H. Iguchi, T. Ochiya, Circulating microRNA in body fluid: A new

potential biomarker for cancer diagnosis and prognosis, Cancer Sci. 101 (2010) 2087–2092. https://doi.org/10.1111/J.1349-7006.2010.01650.X.

[216] D. Gustafson, K. Tyryshkin, N. Renwick, microRNA-guided diagnostics in clinical samples, Best Pract. Res. Clin. Endocrinol. Metab. 30 (2016) 563–575. https://doi.org/10.1016/J.BEEM.2016.07.002.

[217] S.Y. Zhao, Q. Wu, F. Gao, C.B. Zhang, X.W. Yang, Serum microRNA-155 as a potential biomarker for breast cancer screening, Chinese Sci. Bull. 57 (2012) 3466–3468. https://doi.org/10.1007/S11434-012-5362-1.

[218] J. Guo, W. Jiang, X. Xu, X. Zheng, Serum microRNA-155 in early diagnosis and prognosis of breast cancer, Int. J. Clin. Exp. Med. 9 (2016) 10289-10296. ISSN:1940-5901/IJCEM0022470.

[219] Z. Su-ying, W. Qian, G. Fen, Z. Chun-bing, Y. Xue-wen, Increased Expression of MicroRNA-155 in the Serum of Women with Early-Stage Breast Cancer, Lab. Med. 43 (2012) 177–180. https://doi.org/10.1309/LMD71DRHD9SJPWBR.

[220] F. Hosseini Mojahed, A.H. Aalami, V. Pouresmaeil, A. Amirabadi, M. Qasemi Rad, A. Sahebkar, Clinical Evaluation of the Diagnostic Role of MicroRNA-155 in Breast Cancer, Int. J. Genomics. 2020 (2020) 9514831. https://doi.org/10.1155/2020/9514831.

[221] S.T. Lee, D. Beaumont, X. Di Su, K. Muthoosamy, S.Y. New, Formulation of DNA chimera templates: Effects on emission behavior of silver nanoclusters and sensing, Anal. Chim. Acta. 1010 (2018) 62–68. https://doi.org/10.1016/j.aca.2018.01.012.

[222] J. Li, X. Zhong, H. Zhang, X.C. Le, J.J. Zhu, Binding-induced fluorescence turn-on assay using aptamer-functionalised silver nanocluster DNA probes, Anal. Chem. 84 (2012) 5170–5174. https://doi.org/10.1021/ac3006268.

[223] M. Zhang, S.-M. Guo, Y.-R. Li, P. Zuo, B.-C. Ye, A label-free fluorescent molecular beacon based on DNA-templated silver nanoclusters for detection of adenosine and adenosine deaminase, Chem. Commun. 48 (2012) 5488-5490. https://doi.org/10.1039/c2cc31626a.

[224] L. Zhang, J. Zhu, Z. Zhou, S. Guo, J. Li, S. Dong, E. Wang, A new approach to light up DNA/Ag nanocluster-based beacons for bioanalysis, Chem. Sci. 4 (2013) 4004–

4010. https://doi.org/10.1039/C3SC51303C.

[225] J. Park, J. Lee, C. Ban, W.J. Kim, An approach toward SNP detection by modulating the fluorescence of DNA-templated silver nanoclusters, Biosens. Bioelectron. 43 (2013) 419–424. https://doi.org/10.1016/J.BIOS.2012.12.042.

[226] G.-Y. Lan, W.-Y. Chen, H.-T. Chang, Control of synthesis and optical properties of DNA templated silver nanoclusters by varying DNA length and sequence, RSC Adv. 1 (2011) 802–807. https://doi.org/10.1039/C1RA00181G.

[227] A. Mao, C. Wei, Cytosine-rich ssDNA-templated fluorescent silver and copper/silver nanoclusters: optical properties and sensitive detection for mercury(II), Microchim. Acta. 186 (2019) 541. https://doi.org/10.1007/S00604-019-3658-4.

[228] J. Ma, H. Niu, S. Gu, The spatial organization of trace silver atoms on a DNA template, RSC Adv. 11 (2021) 1153–1163. https://doi.org/10.1039/D0RA08066G.

[229] J.Y.C. Lim, Y. Yu, G. Jin, K. Li, Y. Lu, J. Xie, Y.N. Tan, Establishing empirical design rules of nucleic acid templates for the synthesis of silver nanoclusters with tunable photoluminescence and functionalities towards targeted bioimaging applications, Nanoscale Adv. 2 (2020) 3921–3932. https://doi.org/10.1039/D0NA00381F.

[230] L.E. Yourston, A.Y. Lushnikov, O.A. Shevchenko, K.A. Afonin, A. V. Krasnoslobodtsev, First Step Towards Larger DNA-Based Assemblies of Fluorescent Silver Nanoclusters: Template Design and Detailed Characterisation of Optical Properties, Nanomater. 9 (2019) 613. https://doi.org/10.3390/NANO9040613.

[231] I. Ferreira, T.D. Amarante, G. Weber, DNA terminal base pairs have weaker hydrogen bonds especially for AT under low salt concentration, J. Chem. Phys. 143 (2015) 175101. https://doi.org/10.1063/1.4934783.

[232] P. Filipczuk, A. Świtalska, J. Kosman, G. Nowaczyk, A. Dembska, Fluorescent AgNCs formed on bifunctional DNA template for potassium ion detection, Chemosensors. 9 (2021) 349. https://doi.org/10.3390/CHEMOSENSORS9120349.

[233] S. Fu, X. Yang, L. Pang, S. Cheng, D. Song, X. Qin, C. Man, Y. Jiang, A Novel Fluorescence Aptasensor Based on Magnetic Beads/Gold Nanoparticles/DNA-Stabilised Silver Nanoclusters for Detection of Salmonella Typhimurium, Foods. 11

(2022) 595. https://doi.org/10.3390/FOODS11040595.

[234] M. Kozlowski, Polymeric Nanomaterials for Nanotherapeutics. Ed. C. Vasile, Elsevier, 1st Edition. 2018. Series Volume Editors: Cornelia Vasile, eBook ISBN: 9780128139332; Paperback ISBN: 9780128139325: Elsevier, Published Date: 2nd November 2018; 558 pages. In Micro and Nano Technologies Series, Polym. 11 (2019) 1452. https://doi.org/10.3390/POLYM11091452.

[235] Y. Huaccallo-Aguilar, S. Álvarez-Torrellas, M. Larriba, V.I. Águeda, J.A. Delgado, G. Ovejero, J. García, Optimisation Parameters, Kinetics, and Mechanism of Naproxen Removal by Catalytic Wet Peroxide Oxidation with a Hybrid Iron-Based Magnetic Catalyst, Catal. 9 (2019) 287. https://doi.org/10.3390/CATAL9030287.

[236] S. Arumugam, G. Sriram, T. Rajmohan, K. Sivakumar, Optimisation of transesterification process parameters of castor oil ethanolysis using response surface methodology-based genetic algorithm, Energy Sources A: Recovery Util. Environ. Eff. 38 (2016) 300–308. https://doi.org/10.1080/15567036.2013.809390.

[237] B. Jones, The prediction profiler at 30, Qual. Eng. 33 (2021) 417–424. https://doi.org/10.1080/08982112.2021.1874015.

[238] D.E. Brunetti B, About Estimating the Limit of Detection by the Signal to Noise Approach, Pharm. Anal. Acta. 6 (2015) 1000355. https://doi.org/10.4172/2153-2435.1000355.

[239] W. Chen, F. Cai, B. Zhang, Z. Barekati, X.Y. Zhong, The level of circulating miRNA-10b and miRNA-373 in detecting lymph node metastasis of breast cancer: potential biomarkers, Tumor Biol. 34 (2012) 455–462. https://doi.org/10.1007/S13277-012-0570-5.

[240] Y. Luo, X. Wang, W. Niu, H. Wang, Q. Wen, S. Fan, R. Zhao, Z. Li, W. Xiong, S. Peng, Z. Zeng, X. Li, G. Li, M. Tan, M. Zhou, Elevated microRNA-125b levels predict a worse prognosis in HER2-positive breast cancer patients, Oncol. Lett. 13 (2017) 867–874. https://doi.org/10.3892/OL.2016.5482.

[241] Z. Wu, X. Huang, X. Huang, Q. Zou, Y. Guo, The inhibitory role of Mir-29 in growth of breast cancer cells, J. Exp. Clin. Cancer Res. 2013 321. 32 (2013) 98. https://doi.org/10.1186/1756-9966-32-98.

[242] Y. Quan, X. Huang, X. Quan, Expression of miRNA-206 and miRNA-145 in breast cancer and correlation with prognosis, Oncol. Lett. 16 (2018) 6638–6642. https://doi.org/10.3892/OL.2018.9440.

[243] P. Yadav, M. Mirza, K. Nandi, S.K. Jain, R.C.M. Kaza, N. Khurana, P.C. Ray, A. Saxena, Serum microRNA-21 expression as a prognostic and therapeutic biomarker for breast cancer patients, Tumor Biol. 37 (2016) 15275–15282. https://doi.org/10.1007/S13277-016-5361-Y.

[244] P.A.E. Piunno, J. Watterson, C.C. Wust, U.J. Krull, Considerations for the quantitative transduction of hybridisation of immobilized DNA, Anal. Chim. Acta. 400 (1999) 73–89. https://doi.org/10.1016/S0003-2670(99)00609-1.

[245] A. Salimi, B. Kavosi, A. Navaee, Amine-functionalised graphene as an effective electrochemical platform toward easily miRNA hybridisation detection, Meas. J. Int. Meas. Confed. 143 (2019) 191-198. https://doi.org/10.1016/j.measurement.2019.05.008.

[246] Y.S. Borghei, M. Hosseini, M.R. Ganjali, A label-free luminescent light switching system for miRNA detection based on two color quantum dots, J. Photochem. Photobiol. A Chem. 391 (2020) 112351. https://doi.org/10.1016/j.jphotochem.2019.112351.

[247] H. Ma, N. Xue, Z. Li, K. Xing, X. Miao, Ultrasensitive detection of miRNA-155 using multi-walled carbon nanotube-gold nanocomposites as a novel fluorescence quenching platform, Sens. Actuators B Chem. 266 (2018) 221-227. https://doi.org/10.1016/j.snb.2018.03.071.

[248] H. Mohammadi, A. Amine, Spectrophotometric and Electrochemical Determination of MicroRNA-155 Using Sandwich Hybridisation Magnetic Beads, Anal. Lett. 51 (2018) 411-423. https://doi.org/10.1080/00032719.2017.1302460.

[249] Y.S. Borghei, M. Hosseini, M.R. Ganjali, S. Hosseinkhani, Label-free fluorescent detection of microRNA-155 based on synthesis of hairpin DNA-templated copper nanoclusters by etching (top-down approach), Sens. Actuators B Chem. 248 (2017) 133-139. https://doi.org/10.1016/j.snb.2017.03.148.

[250] Y.S. Borghei, M. Hosseini, M.R. Ganjali, Fluorescence based turn-on strategy for

determination of microRNA-155 using DNA-templated copper nanoclusters, Microchim. Acta. 184 (2017) 2671-2677. https://doi.org/10.1007/s00604-017-2272-6.

[251] N. Wang, L. Song, T. Deng, J. Li, Microsphere-based suspension array for simultaneous recognition and quantification of multiple cancer-associated miRNA *via* DNAzyme-Mediated signal amplification, Anal. Chim. Acta. 1140 (2020) 69-77. https://doi.org/10.1016/j.aca.2020.10.003.

[252] Y. Zheng, J. Chen, Y. Li, Y. Xu, L. Chen, W. Chen, A. Liu, X. Lin, S. Weng, Dual-probe fluorescent biosensor based on T7 exonuclease-assisted target recycling amplification for simultaneous sensitive detection of microRNA-21 and microRNA-155, Anal. Bioanal. Chem. 413 (2021) 1605-1614. https://doi.org/10.1007/s00216-020-03121-6.

[253] K. Shahsavar, E. Shokri, M. Hosseini, A fluorescence-readout method for miRNA-155 detection with double-hairpin molecular beacon based on quadruplex DNA structure, Microchem. J. 158 (2020) 105277. https://doi.org/10.1016/j.microc.2020.105277.

[254] L. Wang, Z.J. Liu, H.X. Cao, G.X. Liang, Ultrasensitive colorimetric miRNA detection based on magnetic 3D DNA walker and unmodified AuNPs, Sens. Actuators B Chem. 337 (2021) 129813. https://doi.org/10.1016/j.snb.2021.129813.

[255] Y.S. Borghei, M. Hosseini, M.R. Ganjali, Fluorometric determination of microRNA *via* FRET between silver nanoclusters and CdTe quantum dots, Microchim. Acta. 184 (2017) 4713-4721. https://doi.org/10.1007/s00604-017-2512-9.

[256] X. Hui, C. Yang, D. Li, X. He, H. Huang, H. Zhou, M. Chen, C. Lee, X. Mu, Infrared Plasmonic Biosensor with Tetrahedral DNA Nanostructure as Carriers for Label-Free and Ultrasensitive Detection of miR-155, Adv. Sci. 8 (2021) 2100583. https://doi.org/10.1002/ADVS.202100583.

[257] C. Pothipor, J. Jakmunee, S. Bamrungsap, K. Ounnunkad, An electrochemical biosensor for simultaneous detection of breast cancer clinically related microRNAs based on a gold nanoparticles/graphene quantum dots/graphene oxide film, Analyst. 146 (2021) 4000–4009. https://doi.org/10.1039/D1AN00436K.

[258] M. Azimzadeh, M. Rahaie, N. Nasirizadeh, K. Ashtari, H. Naderi-Manesh, An electrochemical nanobiosensor for plasma miRNA-155, based on graphene oxide and

gold nanorod, for early detection of breast cancer, Biosens. Bioelectron. 77 (2016) 99–106. https://doi.org/10.1016/J.BIOS.2015.09.020.

[259] M. Leeman, J. Choi, S. Hansson, M.U. Storm, L. Nilsson, Proteins and antibodies in serum, plasma, and whole blood—size characterisation using asymmetrical flow field-flow fractionation (AF4), Anal. Bioanal. Chem. 410 (2018) 4867-4873. https://doi.org/10.1007/S00216-018-1127-2.

[260] Y. Sun, M. Wang, G. Lin, S. Sun, X. Li, J. Qi, J. Li, Serum MicroRNA-155 as a Potential Biomarker to Track Disease in Breast Cancer, PLoS One. 7 (2012). https://doi.org/10.1371/JOURNAL.PONE.0047003.

[261] C. Foye, I.K. Yan, W. David, N. Shukla, Y. Habboush, L. Chase, K. Ryland, V. Kesari, T. Patel, Comparison of miRNA quantitation by Nanostring in serum and plasma samples, PLoS One. 12 (2017). https://doi.org/10.1371/JOURNAL.PONE.0189165.

[262] J.M. Obliosca, M.C. Babin, C. Liu, Y.L. Liu, Y.A. Chen, R.A. Batson, M. Ganguly, J.T. Petty, H.C. Yeh, A complementary palette of NanoCluster Beacons, ACS Nano. 8 (2014) 10150–10160. https://doi.org/10.1021/NN505338E.

[253] H.C. Yeh, J. Sharma, J.J. Han, J.S. Martinez, J.H. Werner, A Beacon of Light: A new molecular probe for homogeneous detection of nucleic acid targets, IEEE Nanotechnol. Mag. 5 (2011) 28–33. https://doi.org/10.1109/MNANO.2011.940951.

[264] Z. Huang, Y. Tao, F. Pu, J. Ren, X. Qu, Versatile Logic Devices Based on Programmable DNA-Regulated Silver-Nanocluster Signal Transducers, Chem. Eur. J. 18 (2012) 6663–6669. https://doi.org/10.1002/CHEM.201103859.

[265] Z. Liu, W. Chen, Y. Han, J. Ouyang, M. Chen, S. Hu, L. Deng, Y.N. Liu, A label-free sensitive method for membrane protein detection based on aptamer and AgNCs transfer, Talanta. 175 (2017) 470–476. https://doi.org/10.1016/J.TALANTA.2017.07.071.

[266] P.J. Asiello, A.J. Baeumner, Miniaturized isothermal nucleic acid amplification, a review, Lab Chip. 11 (2011) 1420–1430. https://doi.org/10.1039/C0LC00666A.

[267] L. Yan, J. Zhou, Y. Zheng, A.S. Gamson, B.T. Roembke, S. Nakayama, H.O. Sintim, Isothermal amplified detection of DNA and RNA, Mol. BioSyst. 10 (2014) 970–1003.

https://doi.org/10.1039/C3MB70304E.

[268] N. Zhang, Y. Si, Z. Sun, L. Chen, R. Li, Y. Qiao, H. Wang, Rapid, selective, and ultrasensitive fluorimetric analysis of mercury and copper levels in blood using bimetallic gold-silver nanoclusters with “silver effect”-enhanced red fluorescence, Anal. Chem. 86 (2014) 11714–11721. https://doi.org/10.1021/AC503102G.

[269] L. Feng, Z. Huang, J. Ren, X. Qu, Toward site-specific, homogeneous and highly stable fluorescent silver nanoclusters fabrication on triplex DNA scaffolds, Nucleic Acids Res. 40 (2012) e122. https://doi.org/10.1093/NAR/GKS387.

[270] J. Sharma, H.-C. Yeh, H. Yoo, J.H. Werner, J.S. Martinez, A complementary palette of fluorescent silver nanoclusters, Chem. Commun. 46 (2010) 3280-3282. https://doi.org/10.1039/b927268b.

[271] X. Lin, F. Xiao, X. Li, F. Li, C. Liu, X. Xiao, N. Hu, S. Yang, A cytosine-rich hairpin DNA loaded with silver nanoclusters as a fluorescent probe for uranium(IV) and mercury(II) ions, Mikrochim. Acta. 186 (2019) 519. https://doi.org/10.1007/S00604-019-3625-0.

[272] L. Shang, R.M. Dörlich, V. Trouillet, M. Bruns, G.U. Nienhaus, Ultrasmall fluorescent silver nanoclusters: Protein adsorption and its effects on cellular responses, Nano Res. 5 (2012) 531–542. https://doi.org/10.1007/S12274-012-0238-X.

[273] L. Yourston, L. Rolband, C. West, A. Lushnikov, K.A. Afonin, A. V. Krasnoslobodtsev, Tuning properties of silver nanoclusters with RNA nanoring assemblies, Nanoscale. 12 (2020) 16189–16200. https://doi.org/10.1039/D0NR03589K.

[274] E. Penna, F. Orso, D. Taverna, miR-214 as a key hub that controls cancer networks: small player, multiple functions, J. Invest. Dermatol. 135 (2015) 960–969. https://doi.org/10.1038/JID.2014.479.

[275] T. Sharma, R. Hamilton, C.C. Mandal, miR-214: a potential biomarker and therapeutic for different cancers, Future Oncol. 11 (2015) 349–363. https://doi.org/10.2217/FON.14.193.

[276] Q. Wang, Y. Liu, Y. Wu, J. Wen, C. Man, Immune function of miR-214 and its application prospects as molecular marker, PeerJ. 9 (2021) e10924.

https://doi.org/10.7717/PEERJ.10924.

[277] Y.X. Lin, C.W. Chang, Preparation and characterisation of solid DNA silver nanoclusters with superior aerobic and thermal stability, RSC Adv. 9 (2019) 26061–26066. https://doi.org/10.1039/C9RA04533C.

[278] J.X. Zhang, J.Z. Fang, W. Duan, L.R. Wu, A.W. Zhang, N. Dalchau, B. Yordanov, R. Petersen, A. Phillips, D.Y. Zhang, Predicting DNA hybridisation kinetics from sequence, Nat. Chem. 10 (2017) 91–98. https://doi.org/10.1038/nchem.2877.

[279] I.L. Volkov, A. Smirnova, A.A. Makarova, Z.V. Reveguk, R.R. Ramazanov, D.Y. Usachov, V.K. Adamchuk, A.I. Kononov, DNA with Ionic, Atomic, and Clustered Silver: An XPS Study, J. Phys. Chem. B. 121 (2017) 2400–2406. https://doi.org/10.1021/ACS.JPCB.6B11218.

[280] P. Kannan, P. Subramanian, T. Maiyalagan, Z. Jiang, Cobalt Oxide Porous Nanocubes-Based Electrochemical Immunobiosensing of Hepatitis B Virus DNA in Blood Serum and Urine Samples, Anal. Chem. 91 (2019) 5824–5833. https://doi.org/10.1021/ACS.ANALCHEM.9B00153.

[281] P. Jolly, J. Rainbow, A. Regoutz, P. Estrela, D. Moschou, A PNA-based Lab-on-PCB diagnostic platform for rapid and high sensitivity DNA quantification, Biosens. Bioelectron. 123 (2019) 244–250. https://doi.org/10.1016/J.BIOS.2018.09.006.

[282] L. Zou, R. Shen, L. Ling, G. Li, Sensitive DNA detection by polymerase chain reaction with gold nanoparticles, Anal. Chim. Acta. 1038 (2018) 105–111. https://doi.org/10.1016/J.ACA.2018.07.006.

[283] V. Di Meo, M. Moccia, G. Sanità, A. Crescitelli, A. Lamberti, V. Galdi, I. Rendina, E. Esposito, Advanced DNA Detection *via* Multispectral Plasmonic Metasurfaces, Front. Bioeng. Biotechnol. 9 (2021) 666121. https://doi.org/10.3389/FBIOE.2021.666121.

[284] L. Gutiérrez-Gálvez, R. del Caño, I. Menéndez-Luque, D. García-Nieto, M. Rodríguez-Peña, M. Luna, T. Pineda, F. Pariente, T. García-Mendiola, E. Lorenzo, Electrochemiluminescent nanostructured DNA biosensor for SARS-CoV-2 detection, Talanta. 240 (2022) 123203. https://doi.org/10.1016/J.TALANTA.2021.123203.

[285] I. Iwe, Z. Li, An isothermal, non-enzymatic, and dual-amplified fluorescent sensor for highly sensitive DNA detection, Rev. Anal. Chem. 40 (2021) 312–322.

https://doi.org/10.1515/REVAC-2021-0140.

[286] H. Qi, S. Yue, S. Bi, W. Song, C. Ding, A versatile homogeneous chemiluminescence biosensing platform based on exonuclease-assisted hybridisation chain reaction, Sens. Actuators B Chem. 273 (2018) 1525–1531. https://doi.org/10.1016/J.SNB.2018.07.060.

[287] S. Ma, Y. Zhang, Q. Ren, X. Wang, J. Zhu, F. Yin, Z. Li, M. Zhang, Tetrahedral DNA nanostructure based biosensor for high-performance detection of circulating tumor DNA using all-carbon nanotube transistor, Biosens. Bioelectron. 197 (2022) 113785. https://doi.org/10.1016/J.BIOS.2021.113785.

[288] B. Arévalo, V. Serafín, M. Sánchez-Paniagua, A. Montero-Calle, R. Barderas, B. López-Ruíz, S. Campuzano, P. Yáñez-Sedeño, J.M. Pingarrón, Fast and sensitive diagnosis of autoimmune disorders through amperometric biosensing of serum anti-dsDNA autoantibodies, Biosens. Bioelectron. 160 (2020) 112233. https://doi.org/10.1016/J.BIOS.2020.112233.

[289] Y. Meng, F. Chen, M. Jiang, Q. Guo, Y. Wang, J. Wang, D.W. Zhang, A Homogeneous Label-Free Electrochemical microRNA Biosensor Coupling With G-Triplex/Methylene Blue Complex and λ-Exonuclease-Assisted Recycling Amplification, Front. Chem. 9 (2021) 753253. https://doi.org/10.3389/FCHEM.2021.753253.

[290] B. Zhou, H. Yang, Y. Deng, M. Liu, B. Liu, N. He, Z. Li, Ultrasensitive quantitation of MicroRNAs *via* magnetic beads-based chemiluminesent assay, Sci. China Chem. 59 (2016) 1051–1058. https://doi.org/10.1007/S11426-015-0504-0.

[291] E. Paleček, M. Fojta, Magnetic beads as versatile tools for electrochemical DNA and protein biosensing, Talanta. 74 (2007) 276–290. https://doi.org/10.1016/J.TALANTA.2007.08.020.

[292] L. Wang, J. Lin, Recent advances on magnetic nanobead based biosensors: From separation to detection, TrAC - Trends Anal. Chem. 128 (2020) 115915. https://doi.org/10.1016/J.TRAC.2020.115915.

[293] Y. Yao, Y. Liu, H. Zhang, X. Wang, A highly sensitive and low-background fluorescence assay for pesticides residues based on hybridisation chain reaction

amplification assisted by magnetic separation, Methods Appl. Fluoresc. 7 (2019) 035006. https://doi.org/10.1088/2050-6120/AB1E7A.

[294] Y. Sun, C. Wang, L. Tang, Y. Zhang, G.J. Zhang, Magnetic-enhanced fluorescence sensing of tumor miRNA by combination of MNPs@PDA with duplex specific nuclease, RSC Adv. 11 (2021) 2968–2975. https://doi.org/10.1039/D0RA09237A.

[295] M. Oishi, Enzyme-free and isothermal detection of microRNA based on click-chemical ligation-assisted hybridisation coupled with hybridisation chain reaction signal amplification, Anal. Bioanal. Chem. 407 (2015) 4165–4172. https://doi.org/10.1007/S00216-015-8629-Y.

[296] Y. Wang, X. Zhao, M. Zhang, X. Sun, J. Bai, Y. Peng, S. Li, D. Han, S. Ren, J. Wang, T. Han, Y. Gao, B. Ning, Z. Gao, A fluorescent amplification strategy for high-sensitive detection of 17 β-estradiol based on EXPAR and HCR, Anal. Chim. Acta. 1116 (2020) 1–8. https://doi.org/10.1016/J.ACA.2020.04.010.

[297] G. Yang, S. Yu, Y. Liu, J. Huang, Q. Li, Z.P. Aguilar, H. Xu, A fluorescence-positioned hybridisation chain reaction system for sensitive detection of Salmonella in milk, Anal. Methods. 12 (2020) 1958–1965. https://doi.org/10.1039/D0AY00184H.

[298] Y. Chen, L. Chen, Y. Ou, Z. Wang, F. Fu, L. Guo, DNAzyme-based biosensor for Cu2+ ion by combining hybridisation chain reaction with fluorescence resonance energy transfer technique, Talanta. 155 (2016) 245–249. https://doi.org/10.1016/J.TALANTA.2016.04.057.

[299] S. Yu, Y. Tang, M. Yan, Z.P. Aguilar, W. Lai, H. Xu, A fluorescent cascade amplification method for sensitive detection of Salmonella based on magnetic Fe3O4 nanoparticles and hybridisation chain reaction, Sens. Actuators B Chem. 279 (2019) 31–37. https://doi.org/10.1016/J.SNB.2018.09.091.

[300] S. Niu, Y. Jiang, S. Zhang, Fluorescence detection for DNA using hybridisation chain reaction with enzyme-amplification, Chem. Commun. 46 (2010) 3089–3091. https://doi.org/10.1039/C000166J.

[301] X. Zeng, J. Xiang, M. Wu, W. Xiong, H. Tang, M. Deng, X. Li, Q. Liao, B. Su, Z. Luo, Y. Zhou, M. Zhou, Z. Zeng, X. Li, S. Shen, C. Shuai, G. Li, J. Fang, S. Peng, Circulating miR-17, miR-20a, miR-29c, and miR-223 Combined as Non-Invasive

Biomarkers in Nasopharyngeal Carcinoma, PLoS One. 7 (2012) e46367. https://doi.org/10.1371/JOURNAL.PONE.0046367.

[302] O. Kooshkaki, Z. Rezaei, M. Rahmati, P. Vahedi, A. Derakhshani, O. Brunetti, A. Baghbanzadeh, B. Mansoori, N. Silvestris, B. Baradaran, MiR-144: A New Possible Therapeutic Target and Diagnostic/Prognostic Tool in Cancers, Int. J. Mol. Sci. 21 (2020) 2578. https://doi.org/10.3390/IJMS21072578.

[303] X. Tian, Y. Liu, Z. Wang, S. Wu, miR-144 delivered by nasopharyngeal carcinoma-derived EVs stimulates angiogenesis through the FBXW7/HIF-1α/VEGF-A axis, Mol. Ther. Nucleic Acids. 24 (2021) 1000–1011. https://doi.org/10.1016/J.OMTN.2021.03.016.

[304] H. Zhang, X. Zou, L. Wu, S. Zhang, T. Wang, P. Liu, W. Zhu, J. Zhu, Identification of a 7-microRNA signature in plasma as promising biomarker for nasopharyngeal carcinoma detection, Cancer Med. 9 (2020) 1230-1241. https://doi.org/10.1002/cam4.2676.

[305] L.-Y. Zhang, V.H.F. Lee, A.M.G. Wong, D.L.-W. Kwong, Y.-H. Zhu, S.-S. Dong, K.-L. Kong, J. Chen, S.-W. Tsao, X.-Y. Guan, L. Fu, MicroRNA-144 promotes cell proliferation, migration and invasion in nasopharyngeal carcinoma through repression of PTEN, Carcinogenesis. 34 (2013) 454–463. https://doi.org/10.1093/carcin/bgs346.

[306] C.W. Wu, S.G. Wang, M.L. Lin, S.S. Chen, Downregulation of miR-144 by triptolide enhanced p85α−PTEN complex formation S phase arrest of human nasopharyngeal carcinoma cells, Eur. J. Pharmacol. 855 (2019) 137-148. https://doi.org/10.1016/j.ejphar.2019.04.052.

[307] J. Wang, Z. Zhang, X. Gao, X. Lin, Y. Liu, S. Wang, A single fluorophore ratiometric nanosensor based on dual-emission DNA-templated silver nanoclusters for ultrasensitive and selective Pb2+ detection, Sens. Actuators B Chem. 282 (2019) 712–718. https://doi.org/10.1016/j.snb.2018.11.121.

[308] L. Liu, S. Zhu, J. Sun, M. Xia, X. Zhao, G. Xu, Ratiometric fluorescence detection of bleomycin based on proximity-dependent fluorescence conversion of DNA-templated silver nanoclusters, Chinese Chem. Lett. 32 (2021) 906–909. https://doi.org/10.1016/J.CCLET.2020.07.015.

[309] S. Berensmeier, Magnetic particles for the separation and purification of nucleic acids, Appl. Microbiol. Biotechnol. 73 (2006) 495-504. https://doi.org/10.1007/S00253-006-0675-0.

[310] A.-L. Fabre, M. Colotte, A. Luis, S. Tuffet, J. Bonnet, An efficient method for long-term room temperature storage of RNA, Eur. J. Hum. Genet. 22 (2014) 379–385. https://doi.org/10.1038/ejhg.2013.145.

[311] K.A. Lemire, Y.Y. Rodriguez, M.T. McIntosh, Alkaline hydrolysis to remove potentially infectious viral RNA contaminants from DNA, Virol. J. 13 (2016) 88. https://doi.org/10.1186/S12985-016-0552-0.

[312] C.R. Park, S.J. Park, W.G. Lee, B.H. Hwang, Biosensors Using Hybridisation Chain Reaction - Design and Signal Amplification Strategies of Hybridisation Chain Reaction, Biotechnol. Bioprocess Eng. 23 (2018) 355–370. https://doi.org/10.1007/S12257-018-0182-Z.

[313] S.B. Nimse, K. Song, M.D. Sonawane, D.R. Sayyed, T. Kim, Immobilisation Techniques for Microarray: Challenges and Applications, Sensors. 14 (2014) 22208–22229. https://doi.org/10.3390/S141222208.

[314] A. Holmberg, A. Blomstergren, O. Nord, M. Lukacs, J. Lundeberg, M. Uhlén, The biotin-streptavidin interaction can be reversibly broken using water at elevated temperatures, Electrophoresis. 26 (2005) 501–510. https://doi.org/10.1002/ELPS.200410070.

[315] J.S. Cheah, S. Yamada, A Simple Elution Strategy for Biotinylated Proteins Bound to Streptavidin Conjugated Beads using Excess Biotin and Heat, Biochem. Biophys. Res. Commun. 493 (2017) 1522-1527. https://doi.org/10.1016/J.BBRC.2017.09.168.

[316] K.E.A. Max, K. Bertram, K.M. Akat, K.A. Bogardus, J. Li, P. Morozov, I.Z. Ben-Dov, X. Li, Z.R. Weiss, A. Azizian, A. Sopeyin, T.G. Diacovo, C. Adamidi, Z. Williams, T. Tuschl, Human plasma and serum extracellular small RNA reference profiles and their clinical utility, Proc. Natl. Acad. Sci. U. S. A. 115 (2018) E5334–E5343. https://doi.org/10.1073/PNAS.1714397115.

[317] H. Geekiyanage, S. Rayatpisheh, J.A. Wohlschlegel, R. Brown, V. Ambros, Extracellular microRNAs in human circulation are associated with miRISC complexes

that are accessible to anti-AGO2 antibody and can bind target mimic oligonucleotides, Proc. Natl. Acad. Sci. U. S. A. 117 (2020) 24213–24223. https://doi.org/10.1073/PNAS.2008323117.

[318] J. Kudr, Y. Haddad, L. Richtera, Z. Heger, M. Cernak, V. Adam, O. Zitka, Magnetic Nanoparticles: From Design and Synthesis to Real World Applications, Nanomaterials. 7 (2017) 243. https://doi.org/10.3390/NANO7090243.

[319] A. de la Hoz, A. Navarro, A. Aviñó, R. Eritja, R. Gargallo, Studies on the interactions of Ag(I) with DNA and their implication on the DNA-templated synthesis of silver nanoclusters and on the interaction with complementary DNA and RNA sequences, RSC Adv. 11 (2021) 9029–9042. https://doi.org/10.1039/D1RA00194A.

[320] J. Liu, Z. Geng, Z. Fan, J. Liu, H. Chen, Point-of-care testing based on smartphone: The current state-of-the-art (2017-2018), Biosens. Bioelectron. 132 (2019) 17–37. https://doi.org/10.1016/J.BIOS.2019.01.068.

[321] W. Jung, J. Han, J.W. Choi, C.H. Ahn, Point-of-care testing (POCT) diagnostic systems using microfluidic lab-on-a-chip technologies, Microelectron. Eng. 132 (2015) 46–57. https://doi.org/10.1016/J.MEE.2014.09.024.

[322] T. Nguyen, S.Z. Andreasen, A. Wolff, D.D. Bang, From Lab on a Chip to Point of Care Devices: The Role of Open Source Microcontrollers, Micromachines. 9 (2018) 403. https://doi.org/10.3390/MI9080403.

[323] Q. Song, X. Sun, Z. Dai, Y. Gao, X. Gong, B. Zhou, J. Wu, W. Wen, Point-of-care testing detection methods for COVID-19, Lab Chip. 21 (2021) 1634–1660. https://doi.org/10.1039/D0LC01156H.

[324] L. Guo, S. Chen, Y.L. Yu, J.H. Wang, A Smartphone Optical Device for Point-of-Care Testing of Glucose and Cholesterol Using Ag NPs/UiO-66-NH2-Based Ratiometric Fluorescent Probe, Anal. Chem. 93 (2021) 16240–16247. https://doi.org/10.1021/ACS.ANALCHEM.1C04126.

Appendix I: Computational data from Chapter 3

```
#
# design a HCR system
# design material, temperature (C), trials, magnesium [M], sodium [M], dangles
#
material = dna
temperature = 37.0
trials = 10
magnesium = 0.02
sodium = 0.05
dangles = none

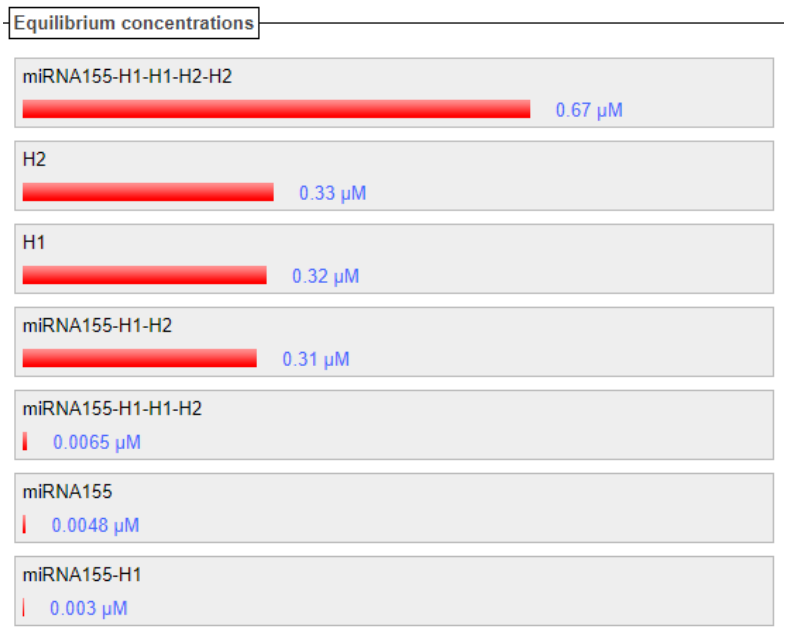
#
# target structures
#
structure H1 = U6 D19 U4 U12
structure H2 = D18 U6 U6
structure miRNA155 = U24

#
# sequence domains
#
domain a = TTAATGCTAATCGTGATA
domain b = GGGGTT
domain c = C
domain d = N4
domain e = TTTACCCACCCA

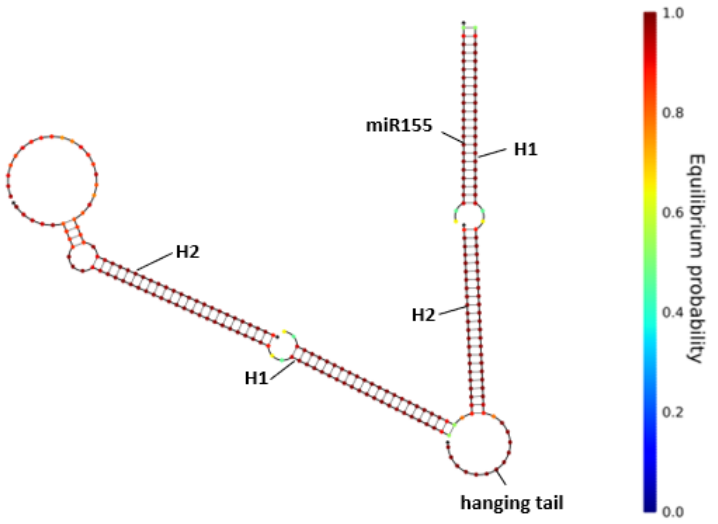
#
# thread sequence domains onto target structures
#
H1.seq = b* a* c d c* a e
H2.seq = a b a* c d* c*
miRNA155.seq = a b
```

Figure S1 NUPACK script for the design of DNA hairpins (*i.e.,* H1 and H2) based on target miR-155 sequence.

A.



B.



C.

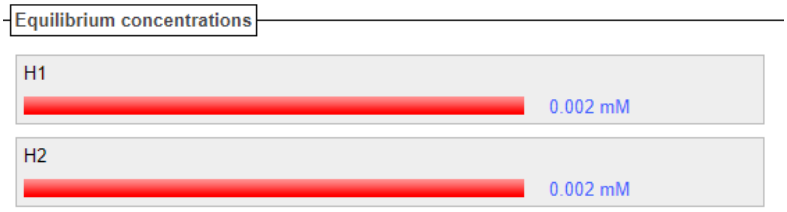
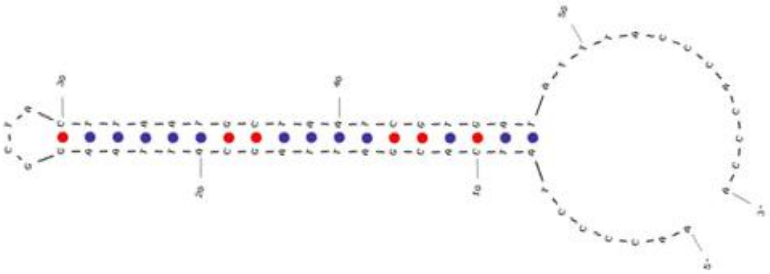
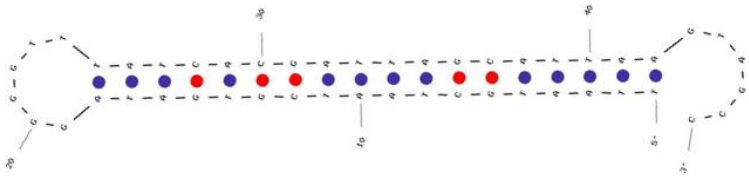


Figure S2 (A) Equilibrium concentration of DNA hairpin probes, H1 and H2, with miR-155. and **(B)** MFE structure of HCR product, presented with probability of base-pairing. **(C)** Equilibrium concentration of DNA hairpin probes, H1 and H2, without miR-155.

Table S1 DNA hairpin structures and their free energy and melting point.

DNA	Structure	ΔG (kcal.mol^{-1})	T_m (°C)
H1		-18.38	67.6
H2		-15.57	61.8

Appendix II: Computational data from Chapter 4

```
#
# design a HCR system
# design material, temperature (C), trials, magnesium [M], sodium [M], dangles
#
material = dna
temperature = 37.0
trials = 10
magnesium = 0.02
sodium = 0.05
dangles = none

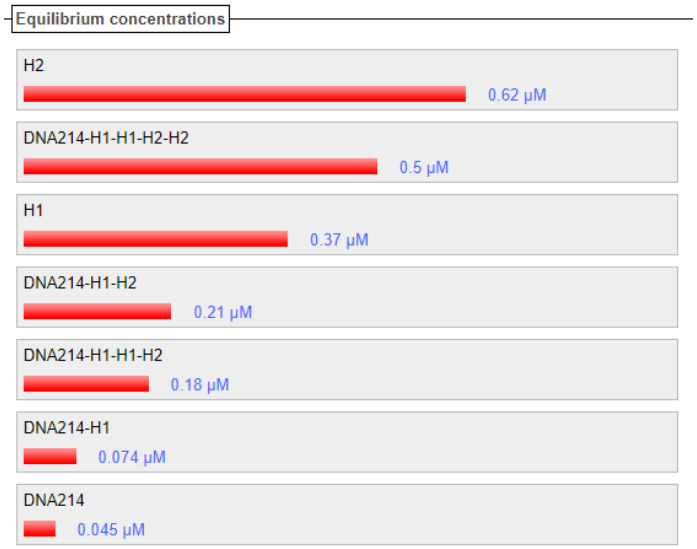
#
# target structures
#
structure H1 = U6 D17 U4 U6
structure H2 = D16 U6 U6
structure DNA214 = U22

#
# sequence domains
#
domain a = ACAGCAGGCACAGACA
domain b = GGCAGT
domain c = C
domain d = N4
domain e = N6

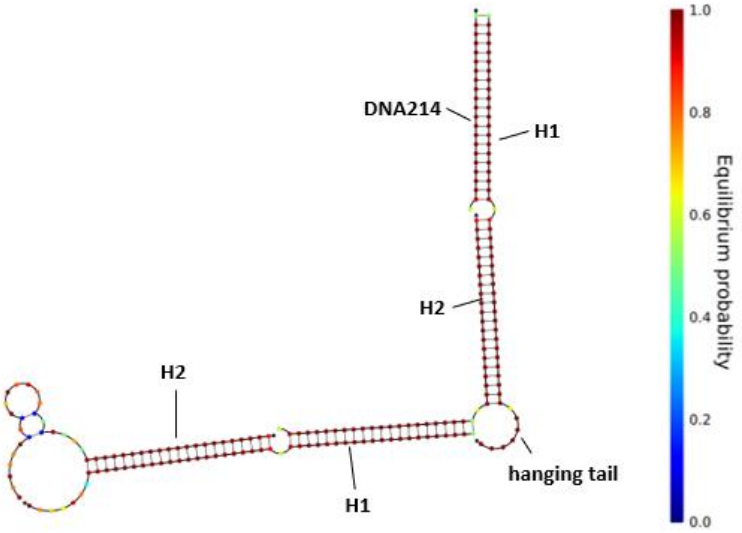
#
# thread sequence domains onto target structures
#
H1.seq = b* a* c d c* a e
H2.seq = a b a* c d* c*
DNA214.seq = a b
```

Figure S1 NUPACK script for the design of DNA hairpins (*i.e.*, H1 and H2) based on target DNA-214 sequence.

A.



B.



C.

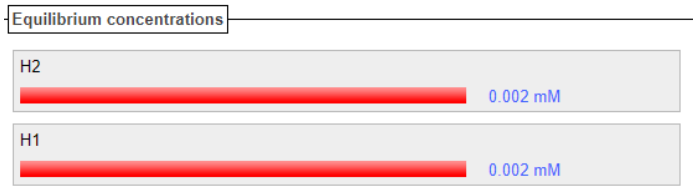
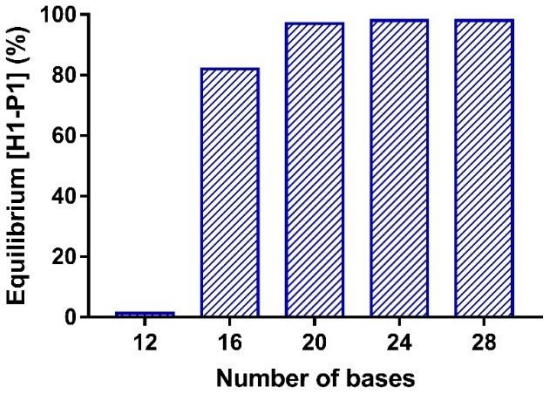
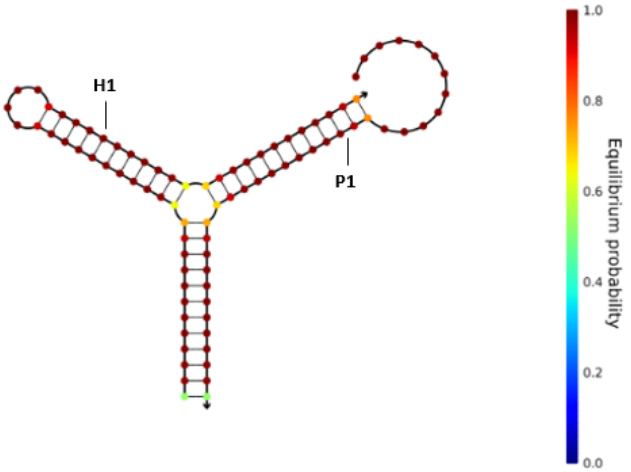


Figure S2 (A) Equilibrium concentration of DNA hairpin probes, H1 and H2, with DNA-214. **(B)** MFE structure of HCR product, presented with the probability of base-pairing. **(C)** Equilibrium concentration of DNA hairpin probes, H1 and H2, without DNA-214.

A.



B.



C.

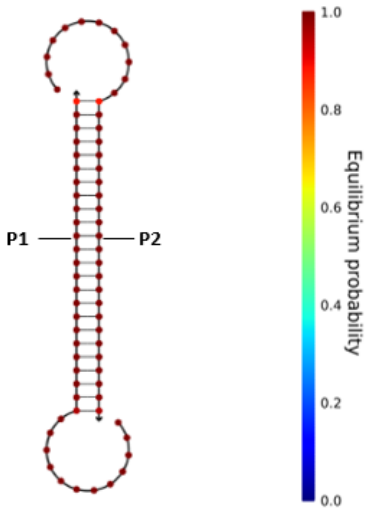
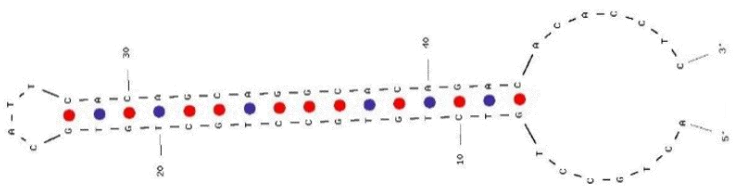
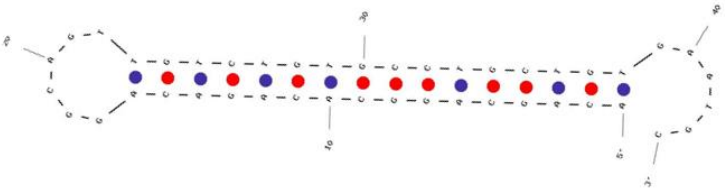


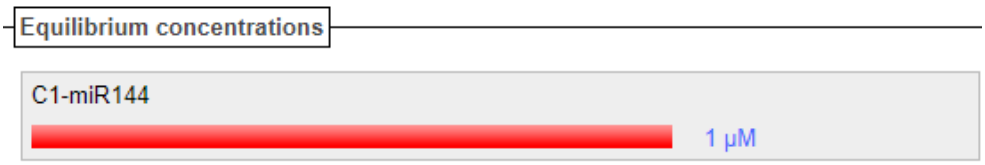
Figure S3 (A) Effect of number of bases on the stability of H1-P1 duplex formation. **(B)** MFE structure of H1-P1 duplex. **(C)** MFE structure of P1-P2 duplex.

Table S1 DNA hairpin structures and their free energy and melting point

DNA	Structure	ΔG (kcal.mol^{-1})	T_m (ºC)
H1		-21.02	77.2
H2		-19.12	76.8

Appendix III: Computational data from Chapter 5

A.



B.

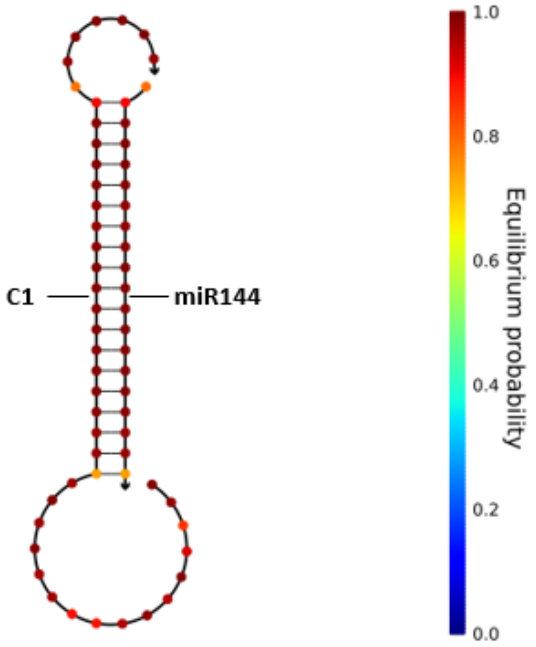
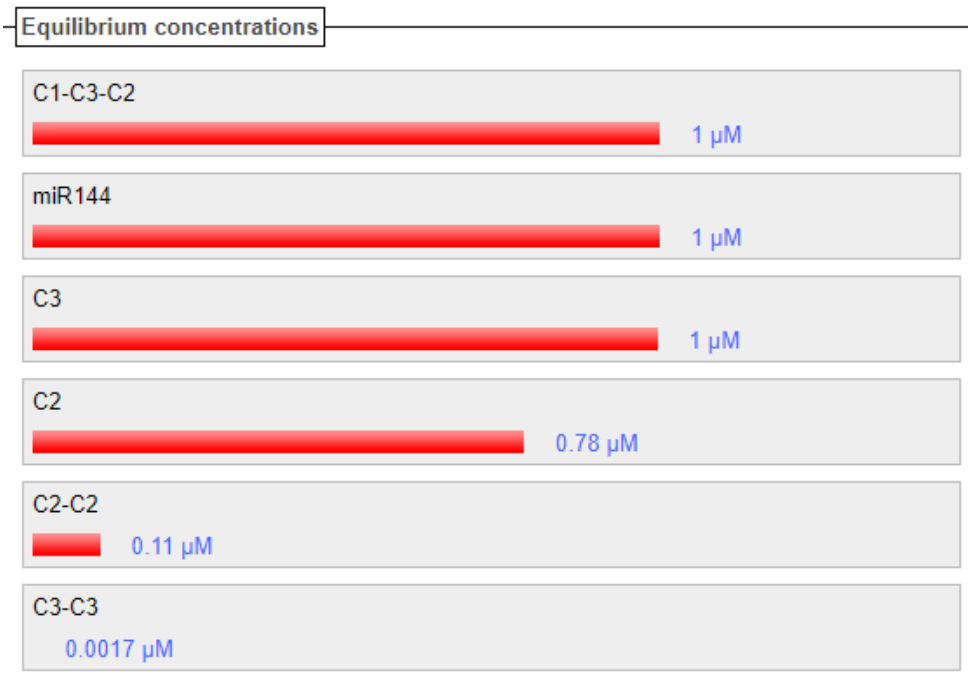


Figure S1 (A) Equilibrium concentration of C1 and miR-144-3p. **(B)** MFE structure of C1-miR-144-3p duplex, presented with the probability of base-pairing.

A.



B.

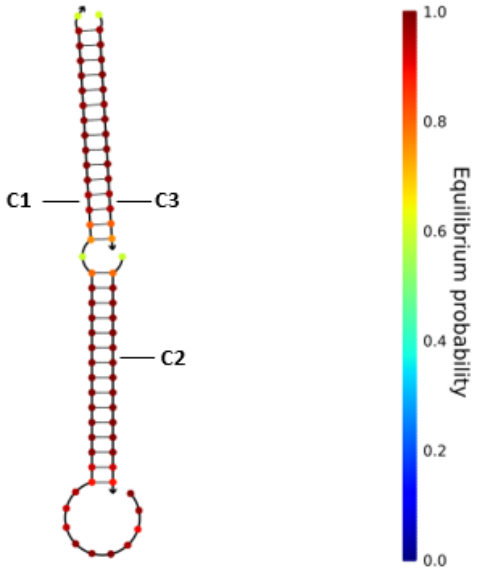


Figure S2 (A) Equilibrium concentration between C1, C2, C3 and miR-144-3p. **(B)** MFE structure of C1-C2-C3 complex, presented with the probability of base-pairing.

```
#
# design a HCR system
# design material, temperature (C), trials, magnesium [M], sodium [M], dangles
#
material = dna
temperature = 37.0
trials = 10
magnesium = 0.001
sodium = 0.1
dangles = none

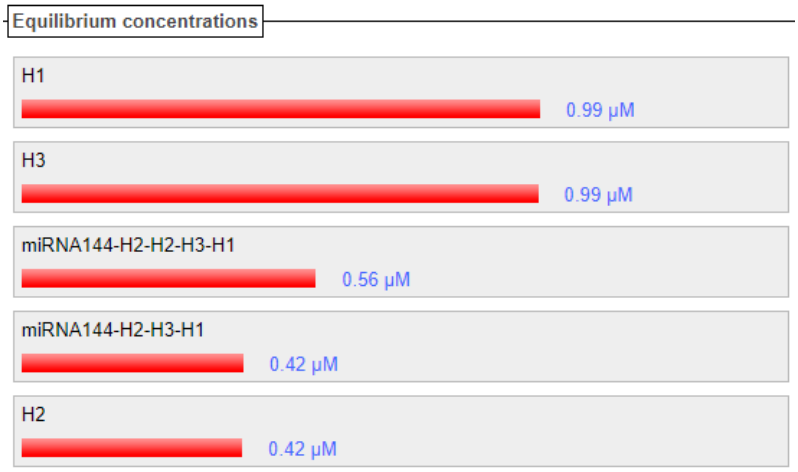
#
# target structures
#
structure H1 = U2 D14 U7 U6
structure H2 = U7 D17 U4 U21
structure H3 = D16 U7 U6
structure miRNA144 = U20

#
# sequence domains
#
domain a = TACAGT
domain b = ATAGATGATGTACT
domain c = AGCGGTG
domain d = N2
domain e = C
domain f = N4
domain g = TTTGCCTTTTGGGGACGGATA

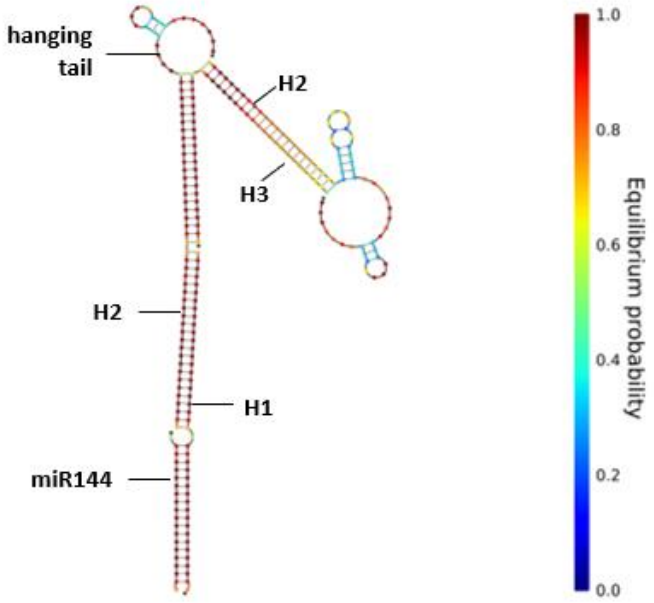
#
# thread sequence domains onto target structures
#
H1.seq = d b c b* a*
H2.seq = c* b* d* e f e* d b g
H3.seq = d b c b* d* e f* e*
miRNA144.seq = a b
```

Figure S3 NUPACK script for the design of DNA hairpins (*i.e.*, H1, H2 and H3) based on target miR-144-3p sequence.

A.



B.



C.

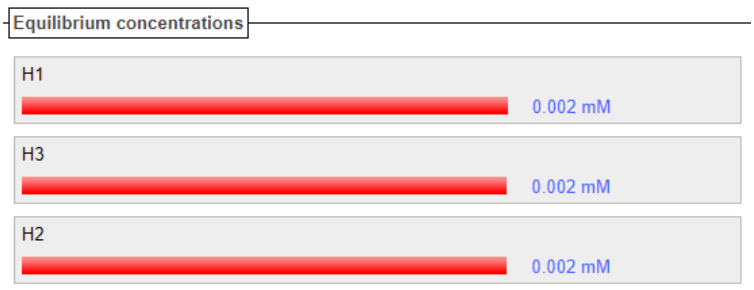
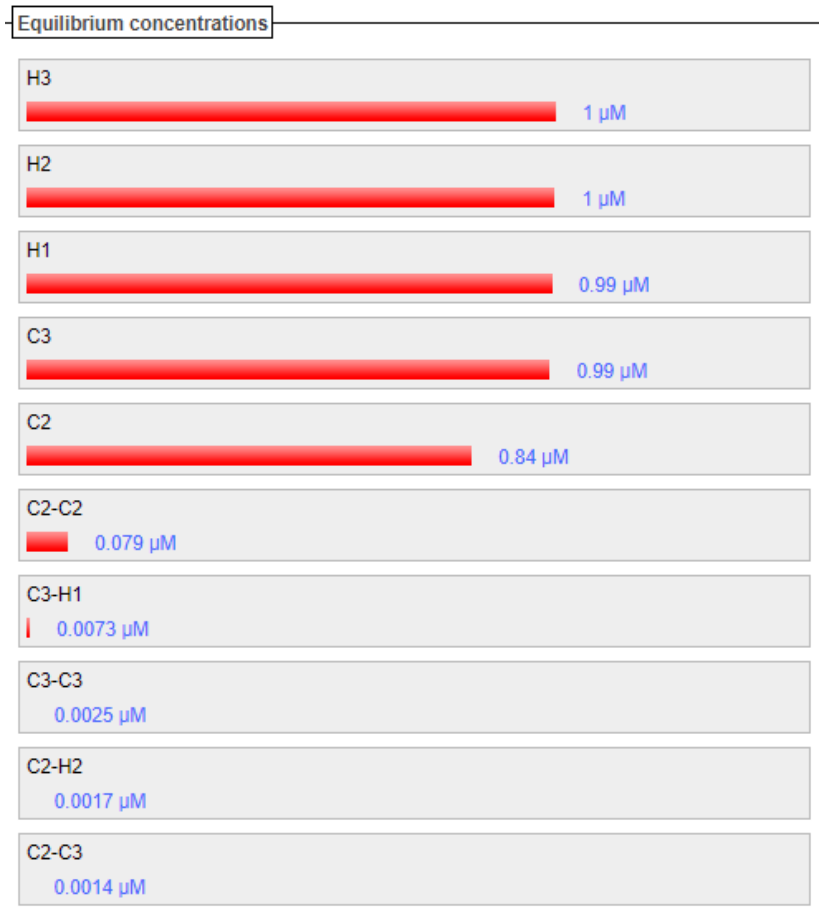


Figure S4 (A) Equilibrium concentration of DNA hairpin probes, H1, H2 and H3, with miR-144-3p. **(B)** MFE structure of HCR product, presented with the probability of base-pairing. **(C)** Equilibrium concentration of DNA hairpin probes, H1, H2 and H3, without miR-144-3p.

A.



B.

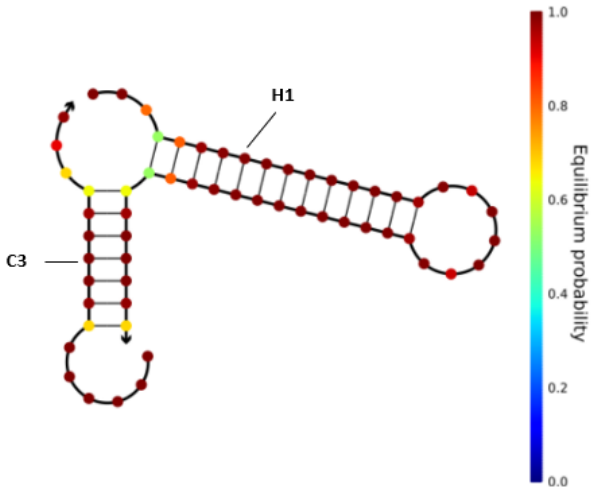
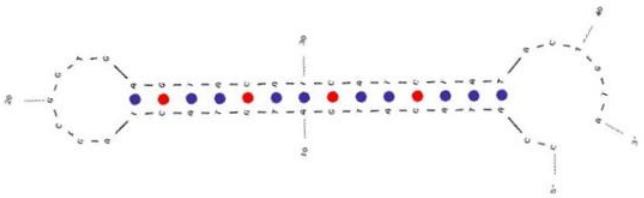
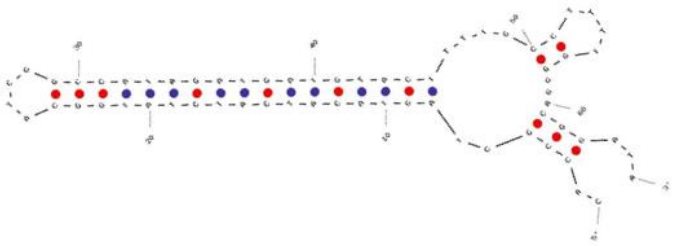
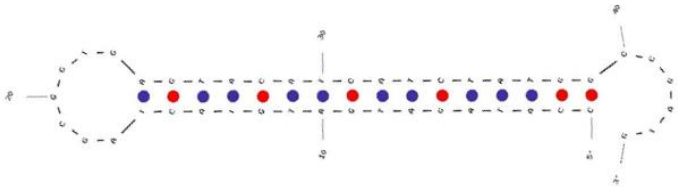


Figure S5 (A) Equilibrium concentration between C2, C3, H1, H2 and H3. **(B)** MFE structure of C3-H1 complex, presented with the probability of base-pairing.

Table S1 DNA hairpin structures and their free energy and melting point.

DNA	Structure	ΔG (kcal.mol^{-1})	T_m (^oC)
H1		-10.69	59.9
H2		-18.71	57.7
H3		-13.49	62.4

Appendix IV: Research outcomes

The following paper has been produced from this research.

Journal paper(s):

Z.W. Wong, J.F. Ng, S.Y. New, Ratiometric Detection of MicroRNA Using Hybridisation Chain Reaction and Fluorogenic Silver Nanoclusters, Chem. Asian J. *16* (2021) 4081–4086. https://doi.org/10.1002/asia.202101145

(Impact factor = 4.568)

(As referred to for **Chapter 3**)

Z.W. Wong, S.Y. New, An enzyme-free turn-on fluorescent strategy for nucleic acid detection based on hybridisation chain reaction and transferable silver nanoclusters. (2022) (manuscript submitted for publication)

(As referred to for **Chapter 4**)

Z.W. Wong, K. Muthoosamy, N.A.H. Mohamed, S.Y. New, A fluorogenic biosensor based on magnetic-assisted hybridisation chain reaction and DNA-templated silver nanoclusters for sensitive microRNA detection. (2022) (manuscript submitted for publication)

(As referred to for **Chapter 5**)

This research has been presented on numerous occasions.

Presentations (*e.g.*, conferences, symposiums, forums, etc.):

2022 Poster presentation - Chemical Nanoscience and Nanotechnology Early Career Researcher Virtual Poster Meeting, 20th June 2022 (virtual).

2021 Poster presentation - Graduate Research Symposium 2021, Scientific Research Today: Borderless, Collaborative, and Innovative, 30th November 2021 (virtual).

Poster presentation - 7th Nano Today Conference, 16th – 18th November 2021 (virtual).

Oral presentation - Bio-Inspired Nanomaterials, Nature Conferences, 15th –

17th November 2021 (virtual).
Awarded: 2021 Travel Grant by Royal Society of Chemistry (RSC), Malaysia Local Section

Poster presentation - 2nd International Online Conference on Polymer Science: Polymers and Nanotechnology for Industry 4.0, 1st – 15th November 2021 (virtual).

Poster presentation - EMBO | EMBL Symposium, Seeing is Believing: Imaging the Molecular Processes of Life, 5th – 8th October 2021 (virtual).
Awarded: EMBO|EMBL Symposia Fellowship by EMBO|EMBL Corporate Partnership Programme

Poster presentation - Norwegian NanoSymposium 2021, 5th – 6th October 2021 (virtual).

Poster presentation - 2nd Commonwealth Chemistry Posters, 30th September – 1st October 2021 (virtual).
Awarded: Poster Prize Winner (Health and Wellbeing) by Commonwealth Chemistry Executive Board

Flash presentation - Early Career Researcher Living Light 2021, 22nd – 23rd September 2021 (virtual).

Poster presentation - UNM Postgraduate Showcase 2021, 8th September 2021 (virtual).

Oral presentation - 1st Malaysia International Conference on Nanotechnology & Catalysis (MICNC) 2021, 1st – 3rd September 2021 (virtual).
Awarded: Best Session Presenter (Nanosensor and Nanosafety) by Catalysis Research Center, Universiti Malaya
Awarded: Researcher Development Grant by RSC

Oral presentation - UNM Pharm/Biomed 6th Annual Postgraduate Research Symposium, Innovating Science: Evolution to Revolution, 26th August 2021 (virtual).
Awarded: First Runner Up (Oral presentation) by University of Nottingham Malaysia

Oral presentation - 37th International Symposium on Microscale Separations and Bioanalysis (e-MSB) 2021, 12th – 15th July 2021 (virtual).

Poster presentation - The Online Nucleic Acids Forum 2021, 9th July 2021

(virtual).

Oral presentation - Monash Initiate 2021 (MINIT): A Virtual Conference, 16th – 17th June 2021 (virtual).

Oral presentation - 4th International Conference on Molecular Biology & Biotechnology (ICMBB) 2021, 1st – 3rd June 2021 (virtual).

Poster presentation - YSN-ASM International Scientific Virtual Conference (ISVC) 2021, 29th March – 1st April 2021 (virtual).

2020 Oral and poster presentation - UNM Postgraduate Research Showcase 2020, 6th October 2020 (virtual).

2019 Poster presentation - UNM-Biomed/AAPS-NUS PharmSci@Asia Symposium, 25th July 2019.